AD/A-000 419

AIRCRAFT PENETRATION OF CLOUDS GENERATED BY NUCLEAR BURSTS

Rayford P. Patrick, et al

Air Force Weapons Laboratory
Kirtland Air Force Base, New Mexico

September 1974

DISTRIBUTED BY:

NTIS
National Technical Information Service
U. S. DEPARTMENT OF COMMERCE

This final report was prepared by the Air Force Weapons Laboratory, Kirtland Air Force Base, New Mexico, under Job Order 88090327. Major Rayford P. Patrick (SAS) was the Laboratory Project Officer-in-Charge.

When US Government drawings, specifications, or other data are used for any purpose other than a definitely related Government procurement operation, the Government thereby incurs no responsibility nor any obligation whatsoever, and the fact that the Government may have formulated, furnished, or in any way supplied the said drawings, specifications, or other data, is not to be regarded by implication or otherwise, as in any manner licensing the holder or any other person or corporation, or conveying any rights or permission to manufacture, use, or sell any patented invention that may in any way be related thereto.

This technical report has been reviewed and is approved for publication.

Rayford P. Patrick

RAYFORD P. PATRICK
Major, USAF
Project Officer

WAYNE L. TYLER
Lt Colonel, USAF
Chief, System S/V Support Branch

CHARLES C. HYRE, JR.
Colonel, USAF
Chief, Analysis Division

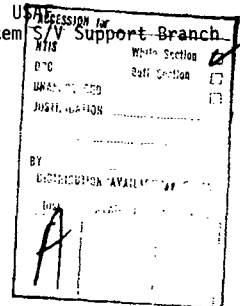

DO NOT RETURN THIS COPY. RETAIN OR DESTROY.

UNCLASSIFIED

SECURITY CLASSIFICATION OF THIS PAGE (When Data Entered)

AD/A-000 419

REPORT DOCUMENTATION PAGE

READ INSTRUCTIONS BEFORE COMPLETING FORM

1. REPORT NUMBER: AFWL-TR-73-82	2. GOVT ACCESSION NO. / 3. RECIPIENT'S CATALOG NUMBER
4. TITLE (and Subtitle): AIRCRAFT PENETRATION OF CLOUDS GENERATED BY NUCLEAR BURSTS	5. TYPE OF REPORT & PERIOD COVERED: Final Report, July 1972 to December 1973
	6. PERFORMING ORG. REPORT NUMBER
7. AUTHOR(s): Rayford P. Patrick, Maj, USAF; George D. Arnett, Capt, USAF; William A. Yingling, Lt Col, USAF	8. CONTRACT OR GRANT NUMBER(s)
9. PERFORMING ORGANIZATION NAME AND ADDRESS: Air Force Weapons Laboratory (SAS), Kirtland Air Force Base, NM 87117	10. PROGRAM ELEMENT, PROJECT, TASK AREA & WORK UNIT NUMBERS: Program Element 62301F, Project 8809
11. CONTROLLING OFFICE NAME AND ADDRESS: Air Force Weapons Laboratory, Kirtland Air Force Base, NM 87117	12. REPORT DATE: September 1974
	13. NUMBER OF PAGES: 280
14. MONITORING AGENCY NAME & ADDRESS (if different from Controlling Office)	15. SECURITY CLASS. (of this report): UNCLASSIFIED
	15a. DECLASSIFICATION/DOWNGRADING SCHEDULE

16. DISTRIBUTION STATEMENT (of this Report)

Approved for public release; distribution unlimited.

17. DISTRIBUTION STATEMENT (of the abstract entered in Block 20, if different from Report)

18. SUPPLEMENTARY NOTES

Reproduced by
NATIONAL TECHNICAL
INFORMATION SERVICE
U S Department of Commerce
Springfield VA 22151

19. KEY WORDS (Continue on reverse side if necessary and identify by block number)

Nuclear radiation	B-1
Aircraft design	Crew Survivability/vulnerability
Dust	Radioactive dust clouds
Filter design	Electronic equipment S/V
Nuclear survivability/vulnerability	Cloud penetration

20. ABSTRACT (Continue on reverse side if necessary and identify by block number)

Aircraft penetrating radioactive dust clouds are exposed to an environment which could prove to be mission crippling. The performances of the crew of the aircraft, the mission critical electronics equipment, and/or the engines could be degraded sufficiently to compromise the mission completion capability of the aircraft. A detailed examination of the hazards associated with cloud penetrations has been performed. It was found that the major hazards to the crew consist of the ionizing doses and dose rates from being (over)

DD FORM 1 JAN 73 1473 EDITION OF 1 NOV 65 IS OBSOLETE

UNCLASSIFIED (280)

SECURITY CLASSIFICATION OF THIS PAGE (When Data Entered)

surrounded by the radioactive cloud and from dust which accumulates in the cockpit during penetration, and the radiation burns of skin in direct contact with the dust. The major hazard to electronics equipment is due to the dose accumulated from dust accumulated in the plenum chambers of black boxes which are cooled by an open cycle process. It is shown that significant protection can be provided for the crew and avionics equipment by the installation of filters. General techniques are presented for selecting filter design criteria for the crew and equipment environment control systems.

PREFACE

Appreciation and thanks are given to Dr. T. Mobley and Mr. H. Murphy of the Air Force Weapons Laboratory for their technical advice.

Portions of Section V of this report were developed concurrently with an article, "Potential Crew Hazards Due to Radioactive Cloud Penetration," which was submitted for publication. This article has been accepted and will be published in a future issue of Aerospace Medicine.

CONTENTS

ILLUSTRATIONS

ILLUSTRATIONS (cont'd)

ILLUSTRATIONS (cont'd)

ILLUSTRATIONS (cont'd)

ILLUSTRATIONS (cont'd)

ILLUSTRATIONS (cont'd)

ILLUSTRATIONS (cont'd)

ILLUSTRATIONS (cont'd)

ABBREVIATIONS AND SYMBOLS

A_{cp}	Cross-sectional flow area of the cockpit, cm^2
$A(t)$	Specific activity function, photons/hour-gram(dust)
$A(r,t)$	Specific activity distribution, photons/hour-gram(dust)-micron
$A_\beta(t)$	Beta particle specific activity, disintegrations/hour-gram(dust)
$A_\beta(r,t)$	Beta particle specific activity distribution, disintegrations/hour-gram(dust)-micron
A_1	Constant
C	Conversion factor, rads(tissue)-cm^2/photon
$CD_{cp}(r)$	Cumulative cockpit dose, rads(tissue)
$CD_f(r)$	Cumulative filter dose, rads(tissue)
C.F.	Correction factor, point to vertical distributed source
C.F.'	Correction factor, point to horizontal distributed source
$CM_{cp}(r)$	Cumulative cockpit mass, grams
$CM_f(r)$	Cumulative filter mass, grams
$C_\beta(r,t)$	Beta particle specific activity distribution, microcuries/gram(dust)-micron
C_μ	Total microcurie dose, microcuries
$\dot{D}_{ae}(t)$	Dose rate from dust on aircraft exterior, rads(tissue)/hour
$D_{ae}(t)$	Dose from dust on aircraft exterior, rads(tissue)
$\dot{D}_c(t)$	Cloud immersion dose rate, rads(tissue)/hour
D_c	Cloud immersion dose, rads(tissue)
$D_c(t)$	Cloud immersion dose, rads(tissue)
D_{cm}	Marginal crew dose, rads(tissue)
$\dot{D}_{cp}(r,t)$	Cockpit dust dose rate distribution, rads(tissue)/hour-micron
$D_{cp}(r)$	Cockpit dust dose distribution, rads(tissue)/micron

IATIONS AND SYMBOLS (cont'd)

$D_{cp}(t)$	Cockpit dust dose function, rads(tissue)
$\dot{D}_c(r,t)$	Cloud immersion dose rate distribution, rads(tissue)/hour-micron
D_{cs}	Crew susceptibility threshold dose, rads(tissue)
D_{em}	Marginal equipment dose, rads(Si)
D_{es}	Equipment susceptibility threshold dose, rads(Si)
$\dot{D}_f(r,t)$	Filter dust dose rate distribution, rads(tissue)/hour-micron
$D_f(r)$	Filter dust dose distribution, rads(tissue)/micron
$\dot{D}_f(t)$	Filter dust dose rate function, rads(tissue)/hour
$D_f(t)$	Filter dust dose function, rads(tissue)
$\dot{DI}(r,t)$	Dust inhalation mass rate distribution, grams/sec-micron
$DI_N(r)$	Nasal dust inhalation mass distribution, grams/micron
$DI_P(r)$	Pulmonary dust inhalation mass distribution, grams/micron
D_N	Dose from dust in nasal cavity, rads(tissue)
D_P	Dose from dust in pulmonary tract, rads(tissue)
$\dot{D}_{pp}$	Dose rate at an electronics piecepact, rads(Si)/hour
$\dot{D}_{SD}$	Dose rate due to cockpit suspended dust, rads(tissue)/hour
$D_T(t)$	Total dose, rads(tissue)
E_D	Relative dose effectiveness
ED_{10}	Effective dose for 10 percent incidence of vomiting
FE(r)	Filter trapping efficiency function
G	Dust mass, grams
ILB_{cm}	Crew member initial lung burden, μci/kg
$\dot{IV}$	Inhaled volume rate, cm^3/sec
K_1	Nondimensionalizing constant, gm(dust)/hour
K_2	Nondimensionalizing constant, gm(dust)/hour
K_3	Nondimensionalizing constant, rads(tissue)/hour

ABBREVIATIONS AND SYMBOLS (cont'd)

K_4	Nondimensionalizing constant, rads(tissue)/hour
K_5	Nondimensionalizing constant, rads(tissue)/hour
K_7	Nondimensionalizing constant, gm(dust)/cm
L	Cockpit flow length, cm
L_f	Weapon loading factor, megatons/kilometer^2
L_{fo}	Baseline weapon loading factor, megatons/kilometer^2
$\dot{M}_{cp}(r,t)$	Cockpit dust mass rate of accumulation distribution, grams(dust)/hour-micron
$M_{cp}(r,t)$	Cockpit dust mass distribution, grams(dust)/micron
$M_{cp}(r)$	Cockpit dust mass distribution, grams(dust)/micron
$M_{cp}(t)$	Cockpit dust mass function, grams(dust)
$\dot{M}_e(t)$	Engine dust mass rate of flow, grams(dust)/hour
$M_e(t)$	Engine dust mass, grams(dust)
$\dot{M}_{e/f}(t)$	Engine/filter dust mass rate of flow, grams(dust)/hour
$M_{e/f}(t)$	Engine/filter dust mass, grams(dust)
$\dot{M}_f(r,t)$	Filter dust mass rate of flow distribution, grams/hour-micron
$M_f(r,t)$	Filter dust mass distribution, grams/micron
$\dot{M}_f(t)$	Filter dust mass rate of flow, grams/hour
$M_f(t)$	Filter dust mass, grams
M_t	Total mass, grams
N	Constant of proportionality
NA(r)	Nasal dust accumulation distribution
$P_s(r)$	Particle settling probability
PT(r)	Pulmonary dust accumulation distribution
R	Cloud radius, kilometers
R_c	Critical settling radius, microns

ABBREVIATIONS AND SYMBOLS (cont'd)

Re	Reynolds number
R(t)	Particle size fallout (Nibbling Mouse) function, microns
TF	Cloud exit time, hours after detonation
TI	Cloud entry time, hours after detonation
T_{mc}	Time of mission completion, hours after detonation
TSF	Time scaling factor
T(t)	Shorthand notation for a functional evaluation at t
TT(t)	Shorthand notation for a functional evaluation at t
V_H	Horizontal velocity, cm/sec
V_s	Settling velocity, cm/sec
$\overline{V}_s$	Critical settling velocity, cm/sec
W	Weapon yield, megatons
a	Length measurement, cm
a_i	Variable, grams(dust)/cm^3
b	Constant
b_1	Cockpit radius, cm
d	Distance measurement, cm
d_4	Distance from nasal cavity to epigastric region, cm
d_5	Distance from pulmonary tract to epigastric region, cm
f(r)	Particle number distribution, particles/cm^3-micron
f(r,t)	Particle number distribution function, particles/cm^3-micron
f_1	Constant
f_2	Constant
g	Length measurement, cm
h	Cockpit height, cm
l	Constant

ABBREVIATIONS AND SYMBOLS (cont'd)

m	Constant
$\dot{m}_{ae}$	Engine air mass rate of flow, gram/hour
$\dot{m}_{af}$	Filter air mass rate of flow, gram/hour
m_i	i^{th} mass element
$m(r)$	Mass per volume distribution, grams/cm^3-micron
n	Constant
p	Radius length, cm
r	Particle radius, microns
r_n	Particle radius defined by $R(t_n)$, microns
S_i	i^{th} distance
t	Time, hours after detonation
t_f	Cloud exit time, hours after detonation
t_i	Cloud entry time, hours after detonation
t_L	Last time dummy variable for numerical integration
t_n	Particular time point used in numerical integration to generate r_n via $r_n = R(t_n)$
x	Cockpit settling distance, cm
y	Plane radius, cm
z	Distance above plane, cm
ΔT	Cloud penetration time, hours
θ	Angle measurement
δ	Activity breakpoint, microns
μ'	Mass attenuation factor
ρ_a	Density of air, grams/cm^3
ρ_{acp}	Density of air in the cockpit, grams/cm^3
$\rho_d(r,t)$	Dust density distribution, grams(dust)/cm^3-micron

ABBREVIATIONS AND SYMBOLS (cont'd)

$\rho_d(r)$	Dust density distribution, grams(dust)/cm^3-micron
$\rho_d(t)$	Dust density function, grams(dust)/cm^3
$\rho_{do}(t)$	Baseline dust density function, grams(dust)/cm^3
ρ_r	Dust particle density, grams(dust)/cm^3
τ	Cockpit crossing time, sec

SECTION I

INTRODUCTION

In the event of a nuclear war, strategic aircraft are subject to accidental or deliberate penetration of the late time (10 minutes or longer after detonation) radioactive dust clouds generated by surface detonations of large-yield nuclear weapons. Because of the presence of numerous clouds from enemy first-strike attacks, the majority of cloud penetrations will occur during the high-altitude, Continental United States (CONUS) exit phase of the strategic mission.

Penetrations of radioactive clouds by manned aircraft pose potential hazards to the mission of the aircraft in three ways. First, the crew of the aircraft is susceptible to ionizing radiation and to direct contact with the radioactive particles. Second, the electronic equipment can be degraded by ionizing radiation. Third, the dust ingested by the engines could cause erosion of the compressor blades and/or other degradation.

Consider first the crew. They are subject to ionizing doses from immersion in the "infinite"* radiating cloud, from dust accumulations on the aircraft exterior, from the dust accumulated in the cockpit, and from dust accumulations elsewhere in the aircraft. Dust accumulations in the interior of the aircraft are due to the ingestion of large amounts of air to cool heavy-duty electronics equipment and to provide cockpit pressurization and air conditioning. Because of the continuous ingestion of outside, contaminated air, the crew is also subjected to direct contact with the radioactive dust and to inhalation of the dust suspended in the air. All of the factors above are potential crew-disabling hazards. Each must be thoroughly investigated to determine the seriousness of its impact on crew performance and to determine corrective actions required to minimize this impact.

Because outside air is used to cool electronic equipment, radioactive dust could be introduced into the innermost parts of the electronics. Although the amount of dust accumulated in any one Line Replaceable Unit (LRU) or "black box" is relatively small, the doses accumulated by susceptible piece parts could be quite large because of the nearness of the dust to piece parts requiring cooling,

*"Infinite" implies a spherical radius such that the majority of photons emitted outside the sphere are absorbed by the atmosphere, i.e., about 3000 meters.

i.e., as near as 1 centimeter. Therefore, ionizing dose is a potential cause of degradation and must be investigated. (In today's electronics, the piece parts are mounted on printed circuit cards which are not cooled directly by the air. The air flows through sealed plenum chambers and carries away heat in the wall, generated by high-power devices. There is no direct contact between the piece parts and the dust, and only ionizing gamma radiation is of concern.)

The potential problems caused by ingestion of the dust into the engine will be addressed only to the extent that the amount and size distribution of the dust will be determined. This information could be used by engine design and test engineers to determine whether or not a problem exists. Detailed investigation of the effects of the ingested dust on engine performance is not within the scope of this report.

The first stage of the investigation contained in this report is the determination of the cloud characteristics of interest and the formulation of simple engineering models which approximate the behavior of the cloud with time. Filter design criteria are then discussed. (These are the inputs needed by a designer to design and locate the filter in the aircraft.) Techniques necessary to select a set of filter design criteria are presented. Next a detailed examination of the cockpit dust accumulation, the effects of the cockpit dust on the crew, and the application of the filter selection techniques to choose the optimum cockpit filter are presented. A similar examination dealing with the electronics LRUs is then presented.

In the detailed analyses, maximum effort was expended to make the results general and applicable to any mission, threat, aircraft, and electronics equipment. The results are generally presented in nondimensional form where the nondimensionalizing constants are functions of the mission, threat, etc. However, the calculations of the dust and dose accumulations in the cockpit depend on specific cockpit size and geometry. Therefore, these results are presented for a four to six man cockpit, representative of a manned bomber, transport, tanker, and other large aircraft. If cockpits or cabins cannot be reasonably represented by this model, the analysis must be reaccomplished with a more suitable model. For example, the model and results for the cockpit presented herein may not be adequately representative of fighter cockpits, or large pressurized cargo areas of transports.

SECTION II

SYNOPSIS OF CLOUD CHARACTERISTICS

1. DUST DENSITY FOR BASELINE THREATS

To analyze the problems associated with an aircraft penetrating the high-altitude, dusty, radioactive clouds associated with surface detonations of nuclear weapons, one must first postulate a reasonable threat. In this work, the starting point is the results obtained by Whitaker (ref. 1), who postulated two separate situations. The first was a single surface burst of a 4-megaton nuclear weapon. The second was massive simultaneous surface detonations of four hundred 5-megaton weapons distributed uniformly over a 200 x 200-kilometer surface. The first threat may be likened to an attack on a single hard target. The second may be likened to a first strike attack on USAF missile fields. Based on output of complex dust computer codes and his years of study of nuclear dust clouds, Whitaker determined dust densities of the cloud as a function of time and the spatial extent of the clouds associated with the above threats.

Several factors should be understood at the onset which bear directly on the relation of the dust environment to specific mission and threat dependent variables. First, surface bursts maximize the dust environments and for this reason they are emphasized here. Second, attention is restricted to the dust environments at late times, i.e., aircraft cloud entry 10 minutes or more after the burst. This restriction is primarily based on the practical consideration that at early times the aircraft crew would be more concerned with the immediate hazards of encountering large solid particles (centimeter to meter range) and in interactions with severe burst-induced turbulence. Third, at these late times the major part of the burst-induced turbulence has subsided, very large particles have fallen out, and the temperature of the cloud is relatively close to ambient. Therefore, the 10-minute point marks the end of hydrodynamic motion and the beginning of a phase which may be considered pure fallout in a comparatively static atmosphere. The dust cloud is generally localized around the burst point and has a relatively homogeneous spatial density distribution as a result of

prior mixing. Finally, the effects of any spatial density gradients which exist within the cloud are assumed to be of little importance to the aircraft because integral effects (e.g., total mass collected and associated doses), rather than instantaneous effects, are more important in this analysis.

According to Whitaker, at 10 minutes after detonation, the cloud size* has stabilized. For a zero wind situation, the cloud size based on Whitaker's work and Glasstone (ref. 2) can be approximated by

$$R = 5.7W^{0.4} \tag{1}$$

where R is the cloud radius for $t \geq 10$ minutes after detonation in kilometers and W is the yield of the weapon in megatons.

The dust density obtained by Whitaker for the single 4-megaton detonation can be approximated for times less than 10 hours after detonation by the expression

$$\rho_d(t) = 4.33 \times 10^{-8}\left(t^{-1.6} + 1.31t^{-0.3}\right) \tag{2}$$

where ρ_d is the dust density in grams (dust) per cm^3 and t is in hours after detonation.

The dust density corresponding to the multiburst case can be approximated for times less than 10 hours after detonation by the expression

$$\rho_d(t) = 1.73 \times 10^{-7}\left(t^{-1.6} + 1.31t^{-0.3}\right) \tag{3}$$

It is noted that the above dust density functions are based on the result of detailed calculations by comprehensive computer codes which include fallout as a parameter.

In general, the dust density is a function of the number, type, yield, height of burst, time of detonation, spatial distribution, etc., of the weapons as well as environmental factors such as the composition of the earth's surface under the burst points and the atmospheric conditions in the vicinity of the burst points. In this analysis, worst-case factors have been chosen to arrive

*Cloud is assumed cylindrical.

at the distributions above. These assumptions include zero wind, representative soil conditions, dry temperate atmosphere, and 1 megaton of dust aloft per megaton yield at 10 minutes after detonation. The densities above were obtained based on these assumptions.

2. DUST DENSITY FOR A GENERAL THREAT

The dust densities above are based on specific threats. To support a general analysis addressing other threats, a general dust density is required. To realize this objective, a weapon loading factor, L_f, was originated. This factor is defined as

$$L_f = \frac{\text{TOTAL MEGATONS OF WEAPON(S)}}{\text{AREA OF DUST CLOUD IN km}^2} \tag{4}$$

This factor is an indication of the intensity of the attack and is related to the dust density because of the assumption that 1 megaton of dust is aloft at 10 minutes after detonation per megaton of yield.

Consider now the single, 4-megaton weapon detonation as a baseline load factor, L_{f_o}.

$$L_{f_o} = \frac{4}{\pi R^2} \tag{5}$$

where

$$R = 5.7(4)^{0.4} \tag{6}$$

Therefore,

$$L_{f_o} = 0.0125 \frac{\text{MT}}{\text{km}^2} \tag{7}$$

The general dust density can be expressed in the form

$$\rho_d(t) = \frac{L_f}{L_{f_o}} \rho_{d_o}(t) \tag{8}$$

or, using equations (2) and (7), this expression reduces to

$$\rho_d(t) = 3.46 \times 10^{-6} L_f \left(t^{-1.6} + 1.31t^{-0.3}\right) \quad (9)$$

As a check of this expression, consider the multiburst situation. The weapon loading factor is

$$L_f = \frac{400 \times 5}{200 \times 200} \quad (10)$$

$$L_f = 0.05 \frac{MT}{km^2} \quad (11)$$

The dust density is

$$\rho_d(t) = 3.46 \times 10^{-6} (0.05)\left(t^{-1.6} + 1.31t^{-0.3}\right) \quad (12)$$

or

$$\rho_d(t) = 1.73 \times 10^{-7} \left(t^{-1.6} + 1.31\ t^{-0.3}\right) \quad (13)$$

which is identical to the result previously obtained by Whitaker.

The dust density for any given threat then can be determined by first calculation of the weapon loading factor and substituting into the general expression. It is emphasized again that this entire development is pertinent only for surface detonations and megaton size weapons.

3. DUST CLOUD ACTIVITY

Now that the dust density is determined, the specific activity must be investigated. It is assumed that fission fragments are generated at a rate of 3×10^{26} fission fragments per megaton (i.e., 100 percent fission yield) and are uniformly distributed over the same volume as the dust cloud at 10 minutes after detonation (ref. 2). Using the average decay relation of radioactive debris from Glasstone (ref. 2) and Whitaker's 10-minute result, the following relation is obtained.

$$A(t) = 4.22 \times 10^{12}\ t^{-1.2}\ \frac{\text{photons}}{\text{hour-gram(dust)}} \quad (14)$$

where t is in hours after detonation.

It is noted that since the yield is assumed to be 100 percent fission, neutron activation of surface materials is not a significant factor in the cloud radioactivity. If a significant portion of the yield is fusion, then fewer fission products will be generated. However, because of the higher energy neutrons released from the fusion process, neutron activation of surface materials can be significant. Therefore, in general, the cloud's radioactivity is not a simple function of the yield as is assumed in this work, but is quite complex. However, the 100 percent fission yield assumption should yield results which provide an upper bound on the actual results.

SECTION III

COMPARISON OF DUST CLOUD MODEL RESULTS

1. DUST CLOUD MODELS

The expressions for the dust densities and specific activities developed in the previous section were used in the development of three cloud models, which approximate the actual cloud behavior. These cloud models were used in a perfect filter* analysis of an aircraft environmental control system. In this section, the various cloud models developed will be discussed briefly, and the results of the perfect filter analysis for each model will be compared. Based on this comparison, one dust cloud model will be chosen as the baseline model to be used in the subsequent detailed analyses.

The first dust cloud model developed was the Uniform Fallout Model, described in detail in appendix A. This model is a first-order approximation to the actual dust cloud. It takes fallout into account, but in a rather simple fashion. The dust cloud in this model may be considered to consist of dust particles uniform in size and activity. Therefore, the governing equations are relatively simple and easy to use, but are not functions of particle size. An obvious disadvantage to this model then is that it would not furnish the filter designer a trapped mass distribution as a function of particle size. Because of the lack of particle size dependency, the results may also not be realistic.

The second model developed was the Improved Fallout Model (appendix B). In this model, particle size was taken into account both in the relation for the dust density and the specific activity. The density distribution was obtained through the consideration of a number-distribution function based on a typical soil at the burst point. The activity as a function of particle size was assumed to be proportional to the particle volume for very small particles and to the

---

*A perfect filter is defined to be a filter which traps, or collects, all dust particles which enter the environmental control system, regardless of the size of the particles.

particle surface area for larger particles. This assumption is based on the consideration that small particles are predominately condensed bomb debris, whereas larger particles are composed of an inert core of soil covered with a surface coating of weapon debris. The specific activity (particle activity/ particle mass) is a function of particle size and time after detonation (to account for the radioactive decay of the fission fragments). Fallout is modeled after Stokes Law which states that for small particles, the fallout velocity is proportional to the square of the particle size. This model is a great deal more representative of the actual cloud behavior but is still a homogeneous cloud model, i.e., no variation in cloud parameters with altitude or range from the point of detonation.

The third and last model developed (appendix C) was the Zero Fallout Model. This model represents a limit case where there is no fallout and is useful in this report only as an extreme worst-case standard of comparison. The only time dependence in this model is the radioactive decay of the fission products. The dust density and the mass rate of flow to the filter are constant during cloud penetration. The use of this crude model in a penetration analysis would lead to gross overdesign of the filter and is presented only as a limit case and as a standard of comparison.

It is noted that the detailed results from all cloud models in appendixes A through C are nondimensional. The nondimensionalizing constants, K_1 through K_5, (defined in equation (A-44)) take into account specific threat, aircraft, mission profile, distance from source (when applicable), and photon energy.

It is also noted that the aircraft is assumed to enter the cloud at some cloud entry time, TI, and exit the cloud at a time, TF where TF = TI + ΔT, and ΔT is the penetration duration.

2. PERFECT FILTER RESULTS

A major objective of this report is to provide results which can be used to set aircraft filtration requirements. Because of the necessity to provide adequate protection to the crew and electronic equipment, and the cost and weight restraints on any aircraft filter design, the filter must provide protection against any reasonable worst-case cloud penetration, but must not be grossly overdesigned. The cloud model then must be capable of supporting the design criteria selection and must produce realistic results.

The two models which will be investigated as candidates to support the penetration analyses are the Uniform Fallout Model and the Improved Fallout Model. It is apparent at first glance that the Zero Fallout Model would predict results leading to gross overdesign of the filter and is not a candidate.

Consider the dust mass trapped by a perfect filter during penetrations of clouds modeled by the two candidates. The total mass trapped as a function of time is identical. However, the Improved Fallout Model has the capability also of predicting the particle size distribution of the trapped mass. This added capability is significant and would provide a designer with more information to aid in the filter design.

The most significant differences in the two candidate models are in the dose and dose rate predictions. Figures 1 and 2 depict the cloud immersion dose rates and doses respectively as a function of time for the two candidate models with the Zero Fallout Model results shown as a standard. The Uniform Fallout Model dose rate decreases with time at early times at a significantly higher rate than the Improved Fallout Model. This difference is caused by the differences in the cloud models. The particle sizes and associated activities in the Uniform Fallout Model are all equal. Therefore, fallout equally affects the dust density and the cloud activity. The dust density and the specific activity of the dust in the Improved Fallout Model are dependent on the particle size. The larger particles are less radioactive per unit mass than the small ones. Early fallout is associated with the large particles which have relatively lower activities. The smaller, more radioactive particles remain aloft. Therefore, the dose rate decrease with time in the early phases of the cloud is less, although the overall dust density behavior with time is identical. At later times, the Uniform Fallout Model dose rates results tend to level out, while the Improved Model results tend to decrease at a greater rate. This difference again is attributable to the same model parameter differences. In the Improved Fallout Model, the smaller, more radioactive particles are now falling out of the cloud taking with them relatively greater amounts of the radioactive debris.

The cloud immersion doses for TI = 10 minutes as depicted in figure 2 also reflect major differences, as would be expected since the dose is merely an integral over time of the dose rate. The Improved Fallout Model dose results are considerably larger in value, because the smaller, more radioactive particles remain aloft and cause more dose to be accumulated for a given mass of dust.

The doses, for TI = 10 minutes and ΔT = 120 minutes, due to the trapped filter duse are depicted in figure 3. In this case also, the doses predicted using the Improved Fallout Model are higher than those predicted by the Uniform Fallout Model. This again is directly attributable to the presence of the smaller particles which are trapped.

In summary, the total masses collected by a perfect filter are the same in both models. The cloud dust density as a function of time is also the same. The Improved Fallout Model provides additional information about the size distribution of the trapped mass. The dose rates and the doses predicted by the Improved Fallout Model are larger than those predicted by the Uniform Fallout Model, but are still significantly lower than the limiting results from the Zero Fallout Model.

3. SELECTION OF MODEL FOR ANALYSIS

The Improved Fallout Model is chosen to support the aircraft penetration analyses for the following reasons:

a. More detailed results may be obtained, i.e., trapped mass and filter dose as functions of particle size.

b. The model more closely approximates the actual cloud behavior.

c. The dose results predicted by the use of the Uniform Fallout Model are not conservative, and could result in underdesign of the filter, which could compromise the aircraft mission.

In view of these considerations, all further analyses will be based on the Improved Fallout Model of the radioactive dust clouds.

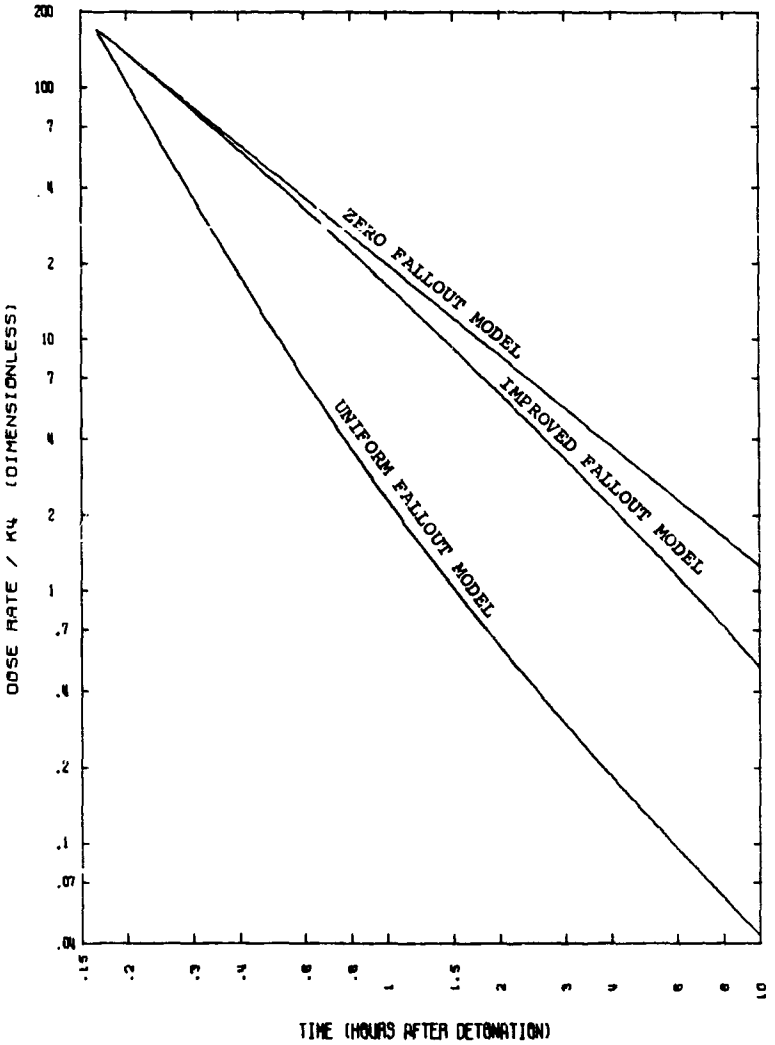

Figure 1. Model Comparison, Cloud Immersion Dose Rate

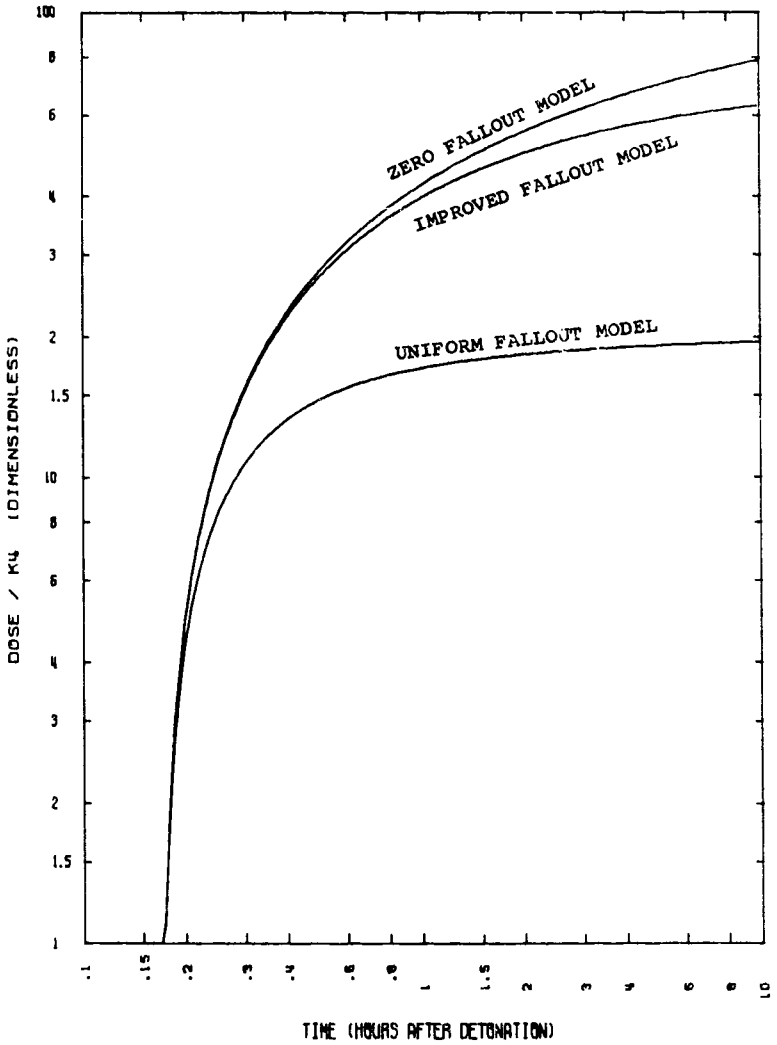

Figure 2. Model Comparison, Cloud Immersion Dose

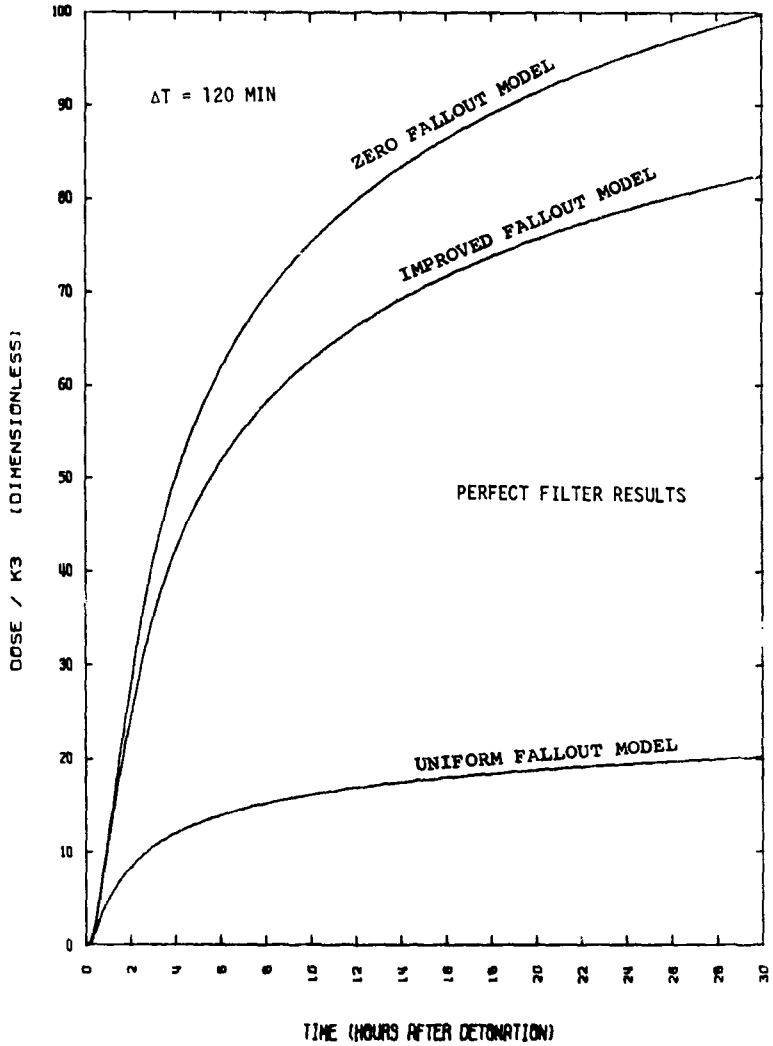

Figure 3. Model Comparison, Filter Dust Dose, TI = 10 Minutes

SECTION IV

FILTER DESIGN CONSIDERATIONS

The primary purpose of filters in the environmental control system (ECS) of an aircraft during a general war mission is to minimize the ionizing dose accumulated by the crew and electronic equipment during radioactive cloud penetrations. This section presents (1) the filter criteria required by a designer to design a filter and position it in the aircraft; (2) the procedures necessary to arrive at this set of criteria by a planner; and (3) the procedure for adapting the perfect filter model presented in appendix B to a real filter. In general, the protection required by the crew differs from that required by the electronic equipment. Therefore, the filter design criteria would differ.

1. DISCUSSION OF POINT DESIGN CRITERIA

The starting point of a filter design criteria selection process is an operational analysis based on aircraft basing plans, mission routings, mission profiles, time lines, threats, etc. The end result of this analysis would be the determination of a Point Design Condition, which effectively means the fixing of the parameters TI, TF, L_f, and aircraft altitude. (For a given analysis, the aircraft parameters of interest would also be known.) One major constraint is placed on this result. The cloud immersion ionizing dose accumulated for the Point Design Condition must not exceed the susceptibility threshold levels of the crew and electronics. Filters cannot alleviate these doses, and if they are exceeded, the mission is in jeopardy. In fact, there must be some margin between the cloud immersion dose and the susceptibility thresholds to give some flexibility in the filter criteria choice. For example, if no margin is allowed, the filter effectiveness and the filter location required to provide the necessary protection may be completely unrealistic and unattainable.

If the Point Design Condition is not realistic in view of the above limitation, then an iteration is necessary, with constraints on some of the operational variables, so that an acceptable Point Design Condition is obtained. This report

will not dwell any further upon the selection of the Point Design Condition because it is out of the scope of this work. From this point on, it is assumed that the Point Design Condition is a known input. The remaining criteria selection process, however, will be examined in detail.

2. FILTER DESIGN CRITERIA

To design a filter and locate it in an aircraft, a designer must be provided the following criteria:

a. Filter trapping efficiency.

b. Total mass of dust trapped by the filter.

c. Mass distribution of the trapped dust as a function of particle size.

d. Minimum separation distances from the filter to the crew and electronic equipment.

The filter trapping efficiency is defined as

$$FE(r) = \frac{\text{dust of radius r trapped in the filter}}{\text{total dust of radius r entering the filter}} \qquad (15)$$

All the dust which is not trapped by the filter could enter the cockpit or the plenum chambers of the electronic equipment and become a source of radioactivity which could adversely affect the mission completion capability of the aircraft.

The total mass of dust trapped is required for filter sizing, while the mass distribution is required to support the possible necessity to stage the filter. For example, the filter may be a two-stage design. The first stage may trap large particles and the second stage may trap small ones. The minimum spacing criteria would provide the designer with the input necessary to develop an envelope of satisfactory filter locations. This envelope would be coordinated with other designers to determine filter locations consistent with other functional requirements.

Selection of the filter criteria is based exclusively upon the marginal ionizing dose which may be accumulated by the crew and the electronic equipment due to all sources except cloud immersion. The differences between the cloud immersion dose (which in the proper units, i.e., rads(tissue) or rads(Si), is

equally applicable to both the crew and the electronics) and the susceptibility thresholds of the crew and electronics are the basis for the filter design criteria selection.

Based on available information, the effective dose for a 10-percent incidence of vomiting (ED_{10}) in man is about 70 rads(tissue) mid-epigastric dose (ref. 3). This dose converts to about 100 rads(tissue) incident dose which is appropriate to the work at hand. Above this level, nausea, vomiting, and other performance degrading responses appear in an increasing number of irradiated humans. The electronic equipment susceptibility thresholds are equipment dependent. For existing equipment, the values are the thresholds of damage/upset of the equipment to ionizing dose and are obtained through an assessment of the equipment. Much equipment presently under development has a total ionizing dose requirement laid upon it by the responsible Program Office. This requirement may be used as the susceptibility threshold in this case. Otherwise, more detailed analysis of the equipment must be accomplished.

At this point, it is assumed that the Point Design Condition, which yields the cloud immersion dose, D_c, and the crew and equipment susceptibility threshold doses (D_{cs} and D_{es}) are known. The marginal crew dose, D_{cm}, and the marginal equipment dose, D_{cm}, are

$$D_{cm} = D_{cs} - D_c \tag{16}$$

$$D_{em} = D_{es} - D_c \tag{17}$$

These doses are the constraints placed on the crew and the electronic equipment filter criteria selection process. In other words, the total dose due to the trapped dust in the filters, the dust accumulated in the cockpit and avionics equipment, and the dust on the aircraft exterior must not exceed the marginal dose levels.

All crew doses from equipment not open-cycle, air-cooled, or equipment more than several meters from the crew may be neglected in the crew filter criteria selection. In general, for today's streamlined, high-speed aircraft, the amount of dust accumulated on the aircraft exterior is minimal and may be neglected. Because of the generally lower vulnerability of the equipment than the crew, the

only significant dose to consider in the equipment filter criteria selection is that due to dust trapped in its own interior. This dust would accumulate primarily in the cooling plenum chamber, which may be only centimeters away from the susceptible devices being cooled. Unless the equipment is located immediately adjacent to a filter with a relatively large amount of trapped dust, the plenum chamber dose will far exceed all other sources. For crew members, the only significant dose contributions that will be considered here are the doses due to cloud immersion, the dust trapped in the filters, and dust deposited in the cockpit. For electronics, the only significant dose contributions are due to dust deposited in equipment which are cooled by an open-cycle cooling system and possibly due to dust deposited in nearby filters.

3. REAL FILTERS VERSUS PERFECT FILTERS

The analysis presented in appendix B is based on the use of a perfect filter in the environmental control system. A perfect filter is defined as one which traps all dust entering the filter regardless of particle size, i.e., FE(r) = 1.0. The results of this perfect filter analysis were used in the previous section to compare results of the different cloud models. As will be shown later, these results are also very useful in a real filter analysis. Of course, no real filter can trap all input dust particles.

Modification of the perfect filter analysis to make it suitable for a real filter is straightforward. Start with the equations for the mass rate of flow of dust and the mass of dust from appendix B (i.e., equations B-27, B-28, and B-29) and rewrite them to include the filter trapping efficiency.

$$\frac{\dot{M}_f(r,t)}{K_2} = 9.9 \times 10^{-2}\ FE(r)\ r^{-0.5} \qquad 0.1\mu \le r \le R(t) \qquad (18)$$

$$\frac{M_f(r,t)}{K_2} = 9.9 \times 10^{-2}\ FE(r)\ r^{-0.5}(t-t_i) \qquad 0.1\mu \le r \le R(t) \qquad (19)$$

$$\frac{M_f(r,t)}{K_2} = 9.9 \times 10^{-2}\ FE(r_n)\ r_n^{-0.5}(t_n-t_i) \qquad R(t) \le r_n \le R(t_i) \qquad (20)$$

where $t_i \le t_n \le t$, and $r_n = R(t_n)$.

From this point, the technique used to determine expressions for the mass and dose accumulated in the filter is identical to that used in appendix B (where effectively the filter efficiency (FE) was 1) except that the factor FE(r) must be included in all operations upon the equations. For any given FE(r) the same technique, which consists of a mixture of analytical and numerical integration, is used to obtain mass/dose results for the dust trapped in the filter.

For simple filter efficiency functions, a simpler graphical technique to obtai this result is appropriate. This technique involves using the perfect filte results of appendix B. For example, if

$$FE(r) = 0 \qquad 0.1\mu \leq r \leq 10\mu \tag{21}$$

$$FE(r) = 1.0 \qquad r \geq 10\mu$$

use the perfect filter mass/dose distributions for $r \geq 10\mu$, which shows the mass/dose accumulated for a given TI, and ΔT, as a function of particle radius. The total mass/dose is obtained from the cumulative results by subtracting the value at 10μ from the value at $10^4\mu$. More detailed examples are presented in reference 4.

SECTION V

COCKPIT ANALYSIS

1. POTENTIAL CREW HAZARDS FROM COCKPIT DUST

In section IV, a general procedure which led to the determination of the filter design criteria was described. One of the key elements in the selection of the filter criteria was the dose due to the dust not trapped by the environmental control system (ECS) filter. This dust enters the cockpit and is a potential hazard to the crew. This section presents in detail the determination of the ionizing crew dose resulting from the dust entering the cockpit. In addition, the effects on the crew due to inhalation of the airborne particles and to skin contact with these particles are investigated. For the purposes of illustration, a Point Design Condition and a set of aircraft parameters will be assumed and the appropriate filter criteria will be selected. The assumed conditions were chosen deliberately not only to show how the criteria can be obtained, but also to represent a realistic set of conditions for today's cargo or bomber aircraft so that this example may be directly applicable to the majority of filter criteria selections in the Air Force today.

There are essentially four concerns associated with the dust particles which are passed by the filter. The first is the consequence of the airborne dust in the cockpit. It is a source of ionizing dose. The second concern is the dust which settles out in the cockpit. It is also a source of ionizing dose. The third is the consequence of crew inhalation of the airborne dust particles. The fourth concern is the direct contact of the radioactive dust particles with the skin of the crew. To scope the problems associated with cockpit ingested dust, zero filtration is assumed for the cockpit ECS.

2. DUST SUSPENDED IN COCKPIT AIR

The dust suspended in the air in the cockpit will be examined first. This ionizing dose source is assumed to be pertinent only during the actual penetration. The air flow through the cockpit is assumed to be sufficient to ensure that the dust density inside is the same as that outside, corrected by the cockpit pressurization factor, ρ_{acp}/ρ_a. It is also assumed that the dust is

uniformly suspended and that the cockpit can be approximated by a sphere of 1 meter radius. The dose rate at the center of the sphere then due to the suspended dust is

$$\dot{D}_{SD} = \int_0^{100cm} \frac{\rho d(r,t)\ A(r,t)\ C\{1 - FE(r)\}\ \frac{\rho_{acp}}{\rho_a} e^{-\mu' b_1}\ 4\rho b_1^2 db_1}{4\pi b_1^2} \qquad (23)$$

or

$$\dot{D}_{SD}(r,t) = \frac{C\ \rho_{acp}\ \rho_d(r,t)\ A(r,t)\ \{1 - FE(r)\}}{\rho_a\ \mu'} \left[1 - e^{-100\mu'}\right] \qquad (24)$$

Since μ' is approximately 10^{-5} cm^{-1}, the factor in the brackets is very small and results in a very small dose rate. Because 1-MeV photons are assumed, the constant $C = 4.88 \times 10^{-10}\ \frac{rads(tis)}{photon/cm^2}$. The dose was calculated for the worst case, i.e., TI = 10 minutes, ΔT = 2 hours, and FE = 0, and found to be on the order of 1 rad(tissue). Therefore, this source of ionizing dose is negligible in comparison to the other sources.

3. DUST ACCUMULATED IN COCKPIT

The second source of ionizing radiation is due to the dust particles which settle out in the cockpit and remain in the cockpit throughout the mission. In addition, those particles which settle on the crew members' clothing and nearby surfaces, because of their nearness and the $1/d^2$ nature of the phenomenon, can contribute substantially to the total ionizing dose to the crew members. Thus, it is important to determine the amount of dust settled out in the cockpit, to determine its distribution relative to the crew member, and to determine its contribution to the total ionizing dose accumulated by the crew.

To obtain meaningful results, the actual cockpit, which is geometrically very complex, must be approximated by a model which is more tractable to analysis. The cockpit is modeled by a square box with inlet ducts on one side and outlet ducts on the opposite side. The inlet and outlet velocities are assumed to be uniform and on the order of the uniform velocity of air across the box. It is also assumed that no settling occurs in the ducting between the filter and the

inlet duct to the cockpit. From a mass flow continuity equation and cockpit dimension consideration, we can calculate a horizontal velocity of the air flowing through the cockpit. Neglecting any slippage of the dust with respect to the air, the horizontal velocity of the dust is identical to that of the air mass. This horizontal velocity of the dust through the cockpit can be written as

$$V_H = \frac{\dot{M}_{af}}{\rho_{acp} A_{cp} 3600} \tag{25}$$

where

ρ_{acp} = air density inside the cockpit

A_{cp} = cross-sectional flow area of the cockpit

Superimposed on the dust particles is the previously introduced settling velocity, V_S (appendix B, equation (B-2)), which is a function of particle size. The time required for a dust particle to cross the cockpit is

$$\tau = \frac{L}{V_H} \tag{26}$$

where L is the length of the cockpit in the direction of the flow. During this same time a particle will fall a distance of

$$x = V_S \tau = \frac{V_S L}{V_H} \tag{27}$$

If a particle has a settling velocity V_S such that its vertical distance of fall, x, is equal to or greater than the cockpit height h, then it will be collected in the cockpit. Defining a critical settling velocity, $\overline{V}$, as

$$\overline{V}_S = \frac{h}{L} V_H \tag{28}$$

any particle with a settling velocity, V_S, greater than or equal to $\overline{V}_S$ will be collected.

Since it was assumed that the initial spatial distribution of particles is uniform in the vertical direction, the probability of a particle with $V_S < \overline{V}_S$ settling in the cockpit will be a linear function of its settling velocity. For example, if a particle has $V_S = 1/2\ \overline{V}_S$, it will only fall a distance $x = h/2$ in the time it takes the particles to move through the cockpit. Thus, the particles with this settling velocity which are initially in the lower half of the cockpit will be collected and those in the upper half will not have sufficient residence time to reach the cockpit floor.

Defining $P_S(r)$ as the probability of a particle settling yields

$$P_S(r) = 1 \quad \text{for } V_S \geq \overline{V}_S \tag{29}$$

$$P_S(r) = \frac{V_S}{\overline{V}_S} \quad \text{for } V_S < \overline{V}_S \tag{30}$$

This probability can be related to particle size r in microns, because V_S is related to particle size through Stokes Law.

Associated with the critical settling velocity, $\overline{V}_S$, is a critical particle size, R_c, given by

$$R_c = \left(\frac{\overline{V}_S}{0.024}\right)^{1/2} = \left(\frac{h\ \dot{m}_{af}}{L\ A_{cp}\ \rho_{cp}\ 86.4}\right)^{1/2} \tag{31}$$

and the related probabilities of a particle settling in the cockpit can be given by

$$P_S(r) = 1.0 \quad \text{for } r \geq R_c \tag{32}$$

$$P_S(r) = \frac{86.4\ V_{cp}\ \rho_{cp} r^2}{h\ \dot{m}_{af}} \quad \text{for } r < R_c \tag{33}$$

where the cockpit volume is given by $V_{cp} = L\ A_{cp}$. It is noted here that the actual cockpit volume should be used in this expression, if it is known. The cockpit height can be chosen as the maximum height if more conservative results are wanted, or the effective height, which is the actual volume divided by the horizontal cross-section area of the cockpit.

It is noted that $P_S(r)$ is a "filter efficiency" of the cockpit. Therefore, the equations for the mass rate and mass of the dust accumulating in the cockpit can be expressed in the following manner:

$$\frac{\dot{M}_{cp}(r,t)}{K_2} = 9.9 \times 10^{-2}[1\text{-}FE(r)]\ P_S(r)r^{-0.5} \qquad 1\mu \le r \le R(t) \quad (34)$$

$$\frac{M_{cp}(r,t)}{K_2} = 9.9 \times 10^{-2}[1\text{-}FE(r)]\ P_S(r)r^{-0.5}(t\text{-}t_i) \qquad 1\mu \le r \le R(t) \quad (35)$$

$$\frac{M_{cp}(r,t)}{K_2} = 9.9 \times 10^{-2}[1\text{-}FE(r_n)]\ P_S(r_n)r_n^{-0.5}(t_n\text{-}t_i) \quad R(t) \le r_n \le R(t_i) \quad (36)$$

where $\dot{M}_{cp}(r,t)$ is the rate at which the dust settles in the cockpit, $M_{cp}(r,t)$ is the mass of dust accumulated in the cockpit, and [1 - FE(r)] accounts for the dust collected by the air conditioning in-line filter. A more expanded development of the equations for mass deposition in the cockpit is found in appendix D.

Calculation of the dose rates and doses for this situation is not as straightforward as the calculation associated with the dust trapped in the filter. The dust settles out uniformly over the entire cockpit and is not concentrated at a single point. Therefore, to obtain dose results, some simplifying assumptions are made. Any one crew member would be subject to varying amounts of dose from each dust particle, depending upon its distance from the crew member.

From a crew dose contribution viewpoint, the effectiveness of an element of mass, m_i, located some distance s_i from the crew member is proportional to m_i/s_i^2. A relative dose effectiveness, E_D, is defined for any mass distribution as

$$E_D = \frac{\sum_i \frac{m_i}{s_i^2}}{M_t} = \sum_i \frac{m_i}{M_t\, s_i^2} \quad (37)$$

If the entire mass, M_t, were located at a distance of 1 meter from the crew member, E_D would be one. Thus, to apply the results (at 1 meter) to other situations, multiply them by the relative dose effectiveness, E_D, determined for the dust distribution of interest.

In this work, the spatial dust distribution assumes that 98 percent of the dust is located at an effective distance of 1 meter (the approximate distance from the critical mid-epigastric region of the seated crew member to the cockpit floor or to equipment consoles) and that 2 percent of the dust is located at an effective distance of 10 centimeters (to account for the dust deposited on clothing and nearby surfaces).* These percentages were estimated from horizontal surface area considerations in a typical four-man cockpit and result in a relative dose effectiveness of about three. This value has been used in the cockpit dose calculations in this report. (The cockpit dose results for other dust distribution models can be obtained by dividing the calculated dose (at 1 meter) by three, and multiplying by the relative dose effectiveness for the dust distribution of interest.) A complete mathematical development of the cockpit dose is presented in appendix D. Note that the dose equations are developed based on the assumption that no filter at all is installed. Therefore, all the dust enters the cockpit and FE(r) = 0. This case is called the imperfect filter analysis and is a limit case, just as the perfect filter analysis of appendix B was a limit case in the other extreme. It will be shown later in this section that these two limit cases can be used to great advantage in the filter criteria selection process and in an evaluation of existing filters.

For the purposes of illustration, it is assumed that the cockpit effective height is 2 meters, the cockpit volume is 1.83×10^7 cm^3, and the mass rate of flow of air to the cockpit is 1.24×10^6 grams per hour. These parameters should be representative of the cockpit for a crew of four to six for most existing bomber and cargo type aircraft. The values of these parameters must be known

*This rather crude distribution was used because it is impossible a priori with no knowledge of the specific cockpit geometry and equipment location to determine the exact distribution. This distribution, however, should be a reasonable representation (on the conservative side, deliberately). The equipment in military aircraft is arranged on consoles within easy reach of the crew. Dust accumulations on these surfaces are probably 1 meter or less from the crew member.

or assumed in order to calculate the critical radius of the dust particles. For these values $R_c \approx 20\mu$. The cockpit temperature is assumed to be 75°F, the cockpit altitude to be 10,000 feet, and the aircraft altitude to be 30,000 feet.

The calculations of the dust mass distribution were made according to the equations in appendix D, and the results are presented in figures D1 through D9. Each curve provides, for a particular cloud entry time, the dust mass distribution function as a function of particle size for various penetration durations, i.e., 2, 5, 10, 15, 30, 60, and 120 minutes. The entry times presented range from 10 minutes to 5 hours.

The results show that for $r > R_c = 20\mu$, all particles are collected and, in this range of r, the results are identical to the perfect filter results. For $r < 20\mu$, there is a marked difference, demonstrating the fact that small particles tend to be carried through and out of the cockpit without settling out.

The next series of figures (appendix D, figures D10 through D18) displays the cumulative dust mass collected in the cockpit. The cumulative mass is defined as the contribution to the cockpit mass attributable to all particles of size less than or equal to r. These figures present this cumulative mass as a function of particle size for a particular cloud-entry time and with penetration duration as a parameter. The same ranges of entry times and penetration durations are used. Observe that since the small particles tend to be carried out of the cockpit with the air, the cumulative mass is small for small particles. The effect of fallout can also be observed, particularly at late times, because the lines of constant penetration become horizontal in the larger particle size range, indicating that no particles of these sizes are present.

The cumulative mass evaluated at r = 10,000 microns is equal to the total mass deposited in the cockpit for any given TI and ΔT. Figure D19 depicts this total mass accumulation as a function of time after cloud entry. A comparison of figure D10 and the perfect filter results for the same TI given by figure B33 (adjusted by the same K_2, equation 59) shows that an appreciable number of small particles are not retained in the cockpit. This difference is entirely due to the fact that the smaller particles are ejected from the cockpit with the air.

Since the smaller particles have higher specific activities, and the cockpit is less efficient in collecting these "hottest" particles, one might expect that the cockpit dose for a given TI and ΔT would be less than the perfect filter

dose (at 1 meter). However, the filter dust represents a localized source of radioactivity, whereas the settled dust in the cockpit is distributed over horizontal surfaces within the cockpit and on the crew members. Because of the nearness of some of these particles to the crew member, the particles effectiveness from a dose standpoint is greatly enhanced. Therefore, it is difficult to state a priori which dose would be greater.

The cockpit dose results, which are obtained from analytical/numerical integration of the equations developed in appendix D, are presented in three series of graphs. The cloud entry times and the penetration durations were deliberately chosen to coincide with those values used in the perfect filter analysis in appendix B. The first series of figures (figures D20 through D28) presents the cockpit dust dose distribution as a function of particle size for a particular cloud-entry time and with penetration duration as a parameter. The second series (figures D29 through D37) presents the cumulative cockpit dose, i.e., the cumulative dose due to all particles which have the size r or less, as a function of r for a particular cloud entry time and with penetration duration as a parameter. The third series (figures D38 through D46) presents the total cockpit dose due to all the dust mass which has settled in the cockpit as a function of penetration duration for a particular cloud entry time. The pertinent results may be scaled to mission lengths other than the one presented by techniques identical to the ones discussed in appendix B.

It is apparent from these results that the ionizing dose from dust accumulated in the cockpit for the no-filter case is significant and must be accounted for in any survivability or vulnerability study.

4. INHALATION OF AIRBORNE DUST IN COCKPIT

The above discussion investigated the ionizing dose which the crew member would accumulate from the dust ingested into the cockpit. This dose is a result of gamma radiation only. The next concern deals with the inhalation of the airborne dust particles. Most modern aircraft have a requirement for a "shirt-sleeve" cockpit environment. A shirt-sleeve environment means that the crew member would be comfortable in the cockpit with normal flight clothing. Temperature and pressure are maintained such that no special equipment or clothing is required for crew comfort. For the purposes of this work, it is assumed that

no gloves are worn and that the crew member is breathing cockpit air. Therefore, during penetration of the cloud, the crew member will inhale the airborne dust and retain some portion of it in his body. This retained dust is a source of gamma and beta radiation.

The total dust accumulated in the respiratory system of a crew member by breathing air which is contaminated with dust will now be estimated. From reference 5, the fraction of particles of radius r accumulated in the nasal and pulmonary regions may be approximated by the following relations.

$$NA(r) = -9.241 + 9.585\ r^{1/2} - 52.52\ r^{1/3} + 52.57\ r^{1/4} \tag{38}$$

$$PT(r) = 8.785e^{-1.4r} - 18.65e^{-2r} + 10.48e^{-2.7r} \tag{39}$$

The above functions are "filter efficiencies" of the nasal cavity and the pulmonary tract, respectively. For a man at rest,

$$\text{Inhaled volume/time} = (\text{respiration/min})(\text{tidal volume}) \tag{40}$$

$$I\dot{V} = (15)(1000)\ \frac{cm^3}{min} \tag{41}$$

$$I\dot{V} = 250\ \frac{cm^3}{sec} \tag{42}$$

The total mass of dust inhaled per second is

$$D\dot{I}(r,t) = I\dot{V}\ \rho_d(r,t)\ \frac{\rho_{cp}}{\rho_a} \tag{43}$$

Therefore,

$$DI(r,t) = \int_t I\dot{V}\ \rho_d(r,t)\ \frac{\rho_{cp}}{\rho_a}\ dt \tag{44}$$

The total dust trapped in the nasal and the pulmonary tracts then as a function of size is

$$DI_N(r) = \int_t I\dot{V}\, \rho_d(r,t)\, \frac{\rho_{cp}}{\rho_a}\, NA(r)dt \qquad \text{Nasal} \tag{45}$$

$$DI_p(r) = \int_t I\dot{V}\, \rho_d(r,t)\, \frac{\rho_{cp}}{\rho_a}\, PT(r)dt \qquad \text{Pulmonary} \tag{46}$$

Here, assume that the crew ionizing dose due to suspended particles in the respiratory system is negligible and that the only potential dose contributor is the dust trapped in the body. The "effective" whole body dose (due to gamma radiation) associated with the dust trapped in the nasal and pulmonary tracts can be approximated by the equations

$$D_N = \int_r \int_t \frac{DI_N(r,t)\, A(r,t)dtdr}{4\pi d_4^{\,2}} \tag{47}$$

$$D_p = \int_r \int_t \frac{DI_p(r,t)\, A(r,t)dtdr}{4\pi d_5^{\,2}} \tag{48}$$

where D_N and D_p are the equivalent doses associated with the nasal cavity and the pulmonary tract and d_4 and d_5 are effective distances from these dust accumulations to the epigastric region. These doses are determined in this manner because there is evidence to suggest that radiation impinging the epigastric region causes nausea and other symptoms which tend to cause performance degradation on a short term basis (ref. 3). The doses calculated previously were incident doses. The incident dose is related to the mid-body and whole-body dose by the relation

$$\text{Whole-body dose} \approx 0.667 \times \text{Incident dose} \tag{49}$$

Performing the indicated operations for the worst case, i.e., TI = 10 minutes and ΔT = 120 minutes, yields a total equivalent incident ionizing dose of 0.357 rad(tissue). This dose is negligible in relation to the other doses.

The inhaled and retained dust also produces physiological damage to the tissue of the respiratory system. This damage is due to the beta particles associated with the contaminated dust retained in the body. The alpha particle emission associated with the fission products rapidly decreases with time after detonation so that even at 10 minutes after detonation, the alpha particle emission is negligible. For this first cut approximation, it is assumed that the gamma ray is the result of a disintegration of a fission product. This same disintegration produces a beta particle, which in the previous discussions was neglected because it is so rapidly absorbed by the atmosphere. For this analysis, however, the beta is quite important because the radioactive material is in direct contact with tissue and can cause damage to the tissue. The specific activity derived in appendix B and in section II then is appropriate to this situation

$$A_\beta(t) = (4.22 \times 10^{12})t^{-1.2} \tag{50}$$

where A_β is in beta particles per hour-gram(dust). In terms of particle size

$$A_\beta(r,t) = 11.83\ A_1\ t^{-1.2} \qquad 0.1_\mu \leq r \leq 20\mu \tag{51}$$

$$A_\beta(r,t) = \frac{236.55\ A_1\ t^{-1.2}}{r} \qquad 20_\mu \leq r \leq 10_\mu^4 \tag{52}$$

where A_1 is defined in appendix A.

In discussing tissue damage due to beta radiation, different units are used, i.e., the microcurie. Since each beta particle is assumed to be the result of a disintegration,

$$C_\beta = \frac{A_\beta\left(\frac{1}{3600}\right)}{(3.7 \times 10^{10})(10^{-6})} \tag{53}$$

with the unit equation

$$C_\beta = \frac{\frac{\text{disintegrations}}{\text{hour-gram(dust)}} \cdot \frac{\text{hour}}{\text{seconds}}}{\frac{\text{disintegrations/second}}{\text{curie}} \quad \frac{\text{curie}}{\text{microcurie}}} \tag{54}$$

where C_β has the units of microcuries per gram of dust, and 3.7×10^{10} disintegrations/second is the standard definition of a curie. Therefore,

$$C_\beta(r,t) = 3.75 \times 10^5 \, t^{-1.2} \qquad 0.1\mu \leq r \leq 20\mu \tag{55}$$

$$C_\beta(r,t) = \frac{7.49 \times 10^6 \, t^{-1.2}}{r} \qquad 20\mu \leq r \leq 10^4\mu \tag{56}$$

The total number of microcuries associated with the dust which is inhaled and retained by a crew member can now be determined.

Although there is a relatively small amount of information available in the literature about humans inhaling radioactive material either as a result of exposure to fallout or as a result of incidents involving other radioactive material, the conclusions which can be drawn from this information are limited. The reason for this limitation is that little was known and/or recorded about the precise amount inhaled, the activities of the inhaled material, etc.. Therefore, for the purposes of this analysis, the human data are of little value as a standard for comparison.

Because of the impreciseness associated with human data, other areas were explored and it was found that some excellent experimental work has been done by the Lovelace Foundation, Albuquerque, New Mexico (ref. 5). Carefully controlled experiments to determine the effects on dogs of inhalation of various radioactive aerosals have been conducted. All of the experiments were tightly controlled. The dogs were observed closely, and the physiological effects were noted by professionals. Therefore, these experiments are valuable to the present work. The dog used was the Beagle, which is smaller than a man and, of course, is not identical. However, the results were presented in terms of Initial Lung Burdens (ILB) of radioactive material, which has units of microcurie/kg (body weight). The body weight of a warm-blooded mammal is representative of its vital lung capacity because the lungs furnish oxygen to tissue, and

the more tissue to be supplied, the larger the lungs required. Therefore, it is assumed that the Initial Lung Burden which can be calculated for a crew member is correlateable (at least approximately) to the Beagle results and some conclusions can be drawn about the effect of the inhaled dust on the human.

The Beagle study of most significance here is the one (ref. 6) wherein a radioactive isotope in fused clay was inhaled. The isotope has a relatively short half life, and is a beta emitter. These properties, as well as the fact that fused clay was used as a carrier, are similar to the properties of the radioactive particles generated by surface detonations of nuclear weapons. The Initial Lung Burdens of the dogs varied from 80 to 5200 μCi/kg and the associated lung doses from 1200 to 55,000 rads. The clinical signs observed in the dogs that died were those typical of severe pulmonary injury and included progressive increases in the respiratory rate, abnormal lung sounds, terminal cyanosis of mucous membranes and increased density of the lungs on radiograph examination.

Although the nature of the clinical signs did not differ markedly, the time of onset of the symptoms and the times of death varied considerably with the Initial Lung Burden. The dogs with high ILBs can be classified into three groups. The first group of four dogs had ILBs of 2600 to 5200 μCi/kg and lung doses of 32,000 to 55,000 rads(tissue). Symptoms were first observed at 7 to 10 days after exposure with deaths at 7.5 to 47 days after exposure. The second group of 18 dogs had ILBs of 850 to 2400 μCi/kg and lung doses of 11,000 to 29,000 rads(tissue). Symptoms were first observed at 3 to 4 weeks after exposure with a median survival time of 85 days after exposure. The third group of 17 dogs had ILBs of 590 to 760 μCi/kg and lung doses of 7300 to 9400 rads. Initial symptoms were observed at 6 to 8 weeks with a median survival time of 185 days after exposure. Dogs with ILBs of 80 to 460 μCi/kg and lung doses of 990 to 5700 rads(tissue) showed no detectable clinical symptoms up to 735 days after inhalation exposure. In this experiment, no potential performance degradation was assessed. Only clinical observations were made.

In order to compare ILBs for the human case to the above experiment, one must calculate the total microcuries trapped in the lungs of a crew member, and divide by a body weight. The total amount of microcuries, C_μ, associated with the dust trapped in the pulmonary system is

$$C_u = \int_r \int_t (I\dot{V})\, \rho_d(r,t)\, \frac{\rho_{acp}}{\rho_a}\, PT(r)\, C_\beta(r,t)\,dt\,dr \qquad (57)$$

Assume that an average crew member's body weight is 80 kg. Therefore, the crew member's Initial Lung Burden, ILB_{cm}, in μCi/kg, is

$$ILB_{cm} = \frac{C_u}{80} \qquad (58)$$

Performing the calculation yields (for a TI of 10 minutes, a ΔT of 120 minutes, the same mission, and aircraft parameters used previously) an extremely worst case ILB for the crew member of 325 μCi/kg. This level is relatively benign when compared to the Beagle levels above. Therefore, because this level is low, it can be predicted with reasonable confidence that a crew member would experience little or no performance degradation over the duration of the mission due to physiological damage caused by the inhaled dust. (Although long-term effects may be significant, here only the time associated with "bombs on target" is pertinent.)

As noted above, the actual physical damage should not cause performance degradation on a short-term basis. However, the psychological effects could be significant. An individual's performance could be degraded because of the emotional reaction to the awareness of the potential hazard of inhalation of the particles. Therefore, it is recommended that a warning system be incorporated in the aircraft to notify the crew that the aircraft is in a radioactive cloud. (Note that a warning system, and not a dosimeter, is recommended. The dosimeter readings themselves could cause psychological problems.) Upon initiation of the warning, the crew would don oxygen masks with 100 percent oxygen for the duration of the penetration. This simple precautionary action would reduce the possibility of inhalation of the particles and alleviate the uneasiness associated with the inhaling of the radioactive particles. This precautionary measure is recommended even if a cockpit ECS filter is installed because no filter can completely remove all the dust particles suspended in the ingested air.

5. EXPOSURE OF BARE SKIN TO THE RADIOACTIVE DUST

Because of the large number of variables associated with this potential hazard, precise calculations of the skin dose are impossible. For example, the crew member is constantly in motion, may wipe hands on clothing, and may or may not be perspiring. All these factors and more affect the results of a skin dose calculation. However, an upper bound for the dose may be estimated. This upper bound consists of estimating the skin dose by assuming all of the dust which would settle on that piece of skin is retained on the skin for some period of time. Bare skin is also assumed, i.e., no clothing covering the skin at the point of exposure.

Probably the main region of concern in the skin would be the dermis, or corium. (It is protected by the outer layer of skin, the epidermis, which varies from 0.07 to 0.12 mm over most of the body.) The corium is 2 to 4 mm thick and contains numerous nerve endings (ref. 7). Beta-radiation penetrating the corium could cause damage which would be sensed by the nerve endings and could result in severe pain to the crew member. Since the epidermis is about 0.1 mm thick, it absorbs all beta particles with energies less than about 200 keV and, therefore, provides some degree of protection to the sensitive corium. Beta particles whose energies range between 200 keV and 700 keV are absorbed in the corium, and beta particles with energies in excess of 700 keV pass through the corium. (Assuming that the skin has the same properties as water, the graphs in reference 8 were used as the basis for these statements.) As a worst case, it is assumed that all the beta particles emitted by the radioactive dust which settle onto the skin possess energies in excess of 700 keV. Although this assumption is somewhat conservative, study of the energies of beta particles emitted by typical decaying fission products indicate that the majority of the beta particles are quite energetic. Therefore, this assumption is not totally unrealistic.

From reference 7 it is noted that the energy loss of a beta particle impinging on any substance is approximately 2 MeV/gm/cm^2. Therefore, the conversion constant from beta particles per centimeter^2 to rads (tissue), C_S, is

$$C_S = \frac{2 \frac{\text{MeV}}{\text{gm/cm}^2/\beta} \cdot 1.6 \times 10^{-6} \frac{\text{ergs}}{\text{MeV}}}{100 \frac{\text{ergs}}{\text{gm}} / \text{rads(tissue)}}$$

$$C_S = 3.2 \times 10^{-8} \frac{\text{rads(tissue)}}{\beta/\text{cm}^2} \tag{59}$$

If it is now assumed that each photon generated by a disintegration is accompanied by a beta particle, then

$$A(r,t) = A_\beta(r,t) \tag{60}$$

where A_β is the specific activity of the radioactive dust in β/gm(dust)-hour and $A(r,t)$ is defined in section II. It is now assumed that the dust settles out on the exposed skin in a uniform manner and that half of the beta particles released by the layer of disintegrating fission products penetrate the skin in a normal direction. The other half escapes in the opposite direction and is not of concern. The approximate skin dose then is

$$D_S(r,t) = \int_t \dot{D}_S(r,t)\, dt \tag{61}$$

$$D_S(r,t) = \int_t \frac{C_S\, M_{cp}(r,t)\, A_\beta(r,t)}{2}\, dt \tag{62}$$

It is noted that this expression differs only by a constant from the dose from dust accumulated in the cockpit, i.e., equation (21). In other words

$$\frac{D_S(r,t)}{K_3'} = \frac{D_{cp}(r,t)}{K_3} \tag{63}$$

where

$$K_3 = \frac{C\, A_1 \, [illegible]\, a_i}{4\pi d^2 \, [illegible]_\alpha}$$

$$K_3' = \frac{C_S A_1 \dot{m}_{af} a_i}{\rho_a (2)(3) A_{cp}'}$$

where the factor of 2 in the denominator of K_3' accounts for the assumption that only half of the beta particles penetrate the skin, the factor of 3 is associated with the assumed cockpit dust distribution and is not appropriate for the skin dose calculation. The factor A_{cp}' is the area of the horizontal portion of the cockpit, and a_i and A_1 are constants.

Performing the indicated operations yields the relation

$$D_S(r,t) = 15.0\ D_{cp}(r,t) \tag{64}$$

Therefore, the skin dose results may be obtained from figures D-20 through D-47 simply by multiplying these results by 15.0. Note that the skin dose results are quite significant even for rather short penetration durations.

The severity, time of appearance, and duration of skin response as a function of radiation depends on a complex interaction of many factors, e.g., dose rate, anatomical region exposed, area of skin irradiated, presence of other irritants (e.g., clothing chafing the irradiated area), energy of impinging beta particles, and depth of penetration into the skin (see reference 3 for a more detailed discussion). However, for the case assumed above, i.e., beta particles with energies in excess of 700 keV, the surface dose required to produce recognizable transepidermal injury is about 2000 rads(tissue).* Therefore, unprotected skin in a cockpit which is supplied with unfiltered air during cloud penetrations of relatively short durations could be a performance crippling factor. Some degree of protection would be afforded the crew member by wearing gloves and a helmet during the mission. However, reliance on protective clothing alone would violate the cockpit "shirt-sleeve" environment requirement.

*This is the dose required for 50 percent of the human population to experience visible skin damage. The human susceptibility threshold is probably lower, i.e., on the order of 800 to 1000 rads (tissue).

6. EXAMPLE COCKPIT FILTER SELECTION

In the filter criteria selection process, the perfect filter results of appendix B are used. To use these results, the nondimensionalizing constants, K_2 through K_4 must be determined. The altitude, the aircraft characteristics, i.e., cockpit size, mass flow rates of air to the cockpit, etc., have been assumed earlier in this section. Now assume that the threat corresponds to the massive multiburst situation, so that L_f is fixed.

The pertinent constants (equations (A-44)) then are determined to be

$$K_2 = 480.76 \frac{\text{gm(dust)}}{\text{hr}} \tag{65}$$

$$K_3 = 7.878 \frac{\text{rads(tissue)}}{\text{hr}} \tag{66}$$

$$K_4 = 12.724 \frac{\text{rads(tissue)}}{\text{hr}} \tag{67}$$

In the following discussion, the values obtained for the perfect filter cases are the values read off the ordinate of the particular graph multiplied by the pertinent constant.

Now that a cockpit deposition model has been developed, and the primary short-term concern associated with the dust which enters the cockpit has been determined to be the ionizing crew dose from the nearby dust accumulations, filter design criteria can be chosen. This selection procedure is based solely upon the necessity to protect the crew from excessive accumulation of ionizing dose.

It is assumed for the purpose of this exercise that the Point Design Condition has been fixed and leads to the case of TI = 30 minutes and ΔT = 10 minutes. From the cloud immersion dose results (figure B-61), the cloud immersion dose is 47 rads(tissue). Since it was stated earlier that the ED_{10} for vomiting was 100 rads(tissue) incident, there is a margin of 53 rads. In other words, the total crew dose from the cockpit dust and the filter dust must not exceed 53 rads. It is assumed that all other sources of ionizing dose due to cloud penetration are vanishingly small.

To alleviate all potential hazards from the cockpit dust, 23 rads(tissue) are chosen as the marginal cockpit dust dose, and 30 rads(tissue) as the marginal filter dose. Going to figure D31 and choosing ΔT = 10 minutes, it is found that the 23 rads(tissue) limit corresponds to a particle size of 18 microns. Therefore, the filter trapping efficiency must be

$$FE(r) = 1.0 \qquad r \geq 18\mu \tag{68}$$

$$FE(r) = 0.0 \qquad r < 18\mu \tag{69}$$

Now go to figure B35, which is the perfect filter dose (at 1 meter). The dose for TI = 30 minutes and ΔT = 10 minutes is 71 rads(tissue). However, the particles smaller than 18 microns are passed. The dose associated with particles 18 micron and smaller is 35 rads. Therefore, the total filter dose is 71 - 35 = 36 rads(tissue) at 1 meter. Therefore, to attenuate this dose to the marginal 30 rads(tissue), the filter must be located at a distance greater than 1 meter from the crew member. The distance, d, corresponding to the 30 rads(tissue) is

$$\frac{36}{d^2} = 30 \tag{70}$$

$$d = 1.2 \text{ m} \tag{71}$$

Therefore, the filter must be located at least 1.2 meters away from the nearest crew member.

The only remaining part of the design criteria needed is the total mass, and its distribution with size, trapped by the filter. To obtain this information go to figures B7 and B16. From figure B7 the mass distribution is obtained by recalling that all particles less than 18 microns are passed. The remainder of the particles are trapped. Therefore, the mass distribution is represented by the ΔT = 10 minute curve with the distribution function below 18 microns set identically to zero. The total mass trapped by the filter can be obtained from figure B16. Read the mass collected for the ΔT = 10 minute curve corresponding to r = 10,000μ, which is 326 grams. Subtract from this value the mass corresponding to r = 18μ, which is 72 grams. The result, 254 gm, is the total mass accumulated by the filter.

Therefore, it is apparent that given the Point Design Condition, which is based on an operational analysis, it is quite straightforward to choose filter design criteria which provides the crew necessary protection from the radioactive dust. This design criteria may be specified to a designer, who can design the filter and locate it in the aircraft without any knowledge of nuclear survivability/vulnerability (S/V) or nuclear environments.

This method may also be used to evaluate existing filters. The only difference would be that the trapping efficiency is now fixed and the associated cockpit dose is not variable, but also fixed. The filter dose then fixes the minimum distance to the crew. The filter mass as dictated by the filter efficiency can be determined and compared to the capacity of the existing filter.

SECTION VI

ELECTRONIC EQUIPMENT FILTER ANALYSIS

1. GENERAL CONSIDERATION

In the previous section, a detailed analysis was presented which resulted in design criteria for the cockpit environmental control system filter. Earlier it was stated that separate filters would probably be required for the cockpit and the electronic equipment because of different filtration requirements. Therefore, it is necessary now to investigate the electronic equipment protection requirements and to select an appropriate set of filter design criteria.

In one respect, the electronic equipment analysis is simpler than the cockpit analysis. There are no biological considerations other than ensuring that the crew does not accumulate excessive dose from the dust trapped in each line replaceable unit (LRU)(a self-contained "black box"). Generally, the amount of dust trapped is relatively small and the LRUs are located in equipment bays considerable distances away from the aircrew. Therefore, the effects on the crew generally are negligible. However, in another respect, the analysis is more complex. Each LRU in the aircraft has a potentially different power requirement and dissipation. Therefore, each could require a different amount of cooling air and each could have a different plenum chamber geometry. Therefore, the analysis must consider each LRU independently. The filter design criteria then would be that necessary to provide the protection required by the most susceptable LRU.

2. PRELIMINARY ANALYTICAL CONSIDERATIONS

Since the number of LRUs in a modern aircraft is quite large, some initial considerations to reduce the number to be analyzed are in order. First, only those LRUs which are mission critical need be considered. Line replaceable units are mission critical if their operations are necessary to the successful completion of the mission. Second, only those LRUs which are air cooled by open cycle flow techniques must be considered. Much of the equipment,* such as

*Only cloud immersion doses are pertinent to these LRUs.

controls and displays, and other low heat dissipation LRUs, do not require special cooling. Other LRUs are cooled by a closed cycle, or a regenerative cooling technique. This type of cooling technique reuses the same working fluid, air, Freon, etc. This fluid is forced through the LRUs, through a heat exchanger to remove excess heat, and then back through the LRUs. Therefore, little or no outside air is introduced into the LRUs. The open cycle cooling technique uses engine bleed air, cools it, forces it through the LRUs, and then ejects it overboard. Therefore, there is a continuous flow of outside air through the LRUs which results in dust deposition in the plenum chamber. Third, only those LRUs using components which are susceptible to total ionizing doses need be considered. For example, those LRUs based on vacuum tube technology will not be affected by total dose accumulations. Only the latest state-of-the-art semiconductor components such as metal oxide semiconductors (MOS) devices are susceptible.

3. LINE REPLACEABLE UNIT ANALYSIS

After the list of LRUs requiring analysis has been reduced to a minimum, the remaining LRUs must be analyzed. The first step in this analysis is the development of a dust deposition model for the LRU plenum chamber. The basic mechanism of deposition is the same for the LRU as it was for the cockpit. Therefore, the same model will be used. The critical particle size, R_c (defined in equation (31)) is of particular importance. This parameter is a function of the plenum chamber geometry and the mass rate of flow of the cooling air. Both these variables could vary from LRU to LRU and must be considered in each LRU analysis.

The approach taken at this point is to obtain general results which can be applied to any specific LRU. Recall that in the cockpit analysis a representative example was presented as an illustration. The critical particle size was 20 microns. The LRU critical particle size, however, may vary considerably from LRU to LRU. Therefore, the LRU critical particle size is an important parameter in the general results.

To be precise, the same type graphical results presented in the cockpit deposition analysis should be presented here for each and every critical particle size. However, presentation of these results would require thousands of graphs. Therefore, another approach will be investigated. In the cockpit analysis, the margin between the crew susceptibility threshold and the immersion dose was tens

of rads(tissue). Here the margin between the LRU susceptibility and the immersion dose is generally thousands of rads(Si). (It should be noted that rads(Si) = 0.922 rad(tissue) for the assumed 1 meV photons.) In this analysis, extreme precision and accuracy are not so critical. Therefore, a simplified approach will be described which yields general, slightly conservative results, and which can be simply applied to any LRU.

The equations which were developed in appendix D for the cockpit are appropriate to this analysis if the cockpit critical particle size of 20 microns is replaced by the general parameter R_c and all of the constants are divided by 3 to account for the magnification factor, E_D, used earlier in the cockpit analysis. For any given R_c these equations were analytically/numerically integrated using the Air Force Weapons Laboratory (AFWL) CDC 6600. The results of interest in this simplified approach are the total mass of dust collected in the LRU and the total dose, at 1 meter, associated with the total mass which accumulates over the mission. In other words, in this analysis the distributions of the mass and dose with respect to particle size are not of interest. The total mass collected can be used to determine the volume taken up by the dust in the plenum chamber to support plenum chamber clogging investigations. The total dose will be used to establish the total dose incident on susceptible piece parts in the LRU.

It is apparent that the integration of the equations for each R_c yields a single data point. Numerous values of R_c must be chosen so that the results are comprehensive enough to support general LRU analysis. These operations have been performed and the results are presented in figures 4 through 21. Each figure represents a single different cloud entry time and each curve on each figure represents a single different penetration duration. The ordinate is the nondimensional mass or dose used in appendix B and the abscissa is the critical particle size. The dose curves are 30-hours-after-detonation cases. The doses for other times can be obtained by use of the time scaling factor discussed in appendix B. It is noted that each point on these curves corresponds to the area under mass and dose distributions similar to those presented in the cockpit analysis section.

The doses, at-1-meter, are now available. However, these doses were determined based on an assumed point source of radioactivity. The dust which settles out in a plenum chamber is not a point source. It is distributed as a planar

source. Therefore, the point source results must be modified to take this difference into account. A plenum chamber model will be introduced which simplifies the complex plenum chamber geometry, and from which a correction factor can be devised. It is assumed that the dust trapped is uniformly distributed over a circular area, equal to the plenum chamber area. Its radius is Y centimeters. The susceptible piece part is located a distance of Z centimeters above the center of the plane. If the activity of the dust is A photons/cm^2-sec. and only a distance attenuation is appropriate, the dose rate $\dot{D}_{pp}$ at the piece part is

$$\dot{D}_{pp} \sim \int_0^Y \frac{A\, 2\pi\, Y\, dY}{4\pi\left(\sqrt{Z^2 + Y^2}\right)^2} = \frac{A}{2}\left\{1/2\, \ln\left[1 + \left(\frac{Y}{Z}\right)^2\right]\right\} \tag{72}$$

if

$$\left(\frac{Y}{Z}\right)^2 >> 1$$

$$\dot{D}_{pp} \sim \frac{A}{4} \ln \left(\frac{Y}{Z}\right)^2$$

For a point source located directly beneath the piece part, the dose rate is

$$\dot{D}_{pp} \sim \frac{A}{4}\left(\frac{Y}{Z}\right)^2 \tag{73}$$

The correction factor to convert point source results to planar source results is

$$C.F. = \frac{\ln \left(\frac{Y}{Z}\right)^2}{\left(\frac{Y}{Z}\right)^2} \tag{74}$$

For any LRU, then, the first step is to determine the critical particle size, and the pertinent nondimensionalizing constant. From the figures presented earlier, a dose at 1 meter is obtained. This dose is converted to the dose (still point source) at the piece part by multiplying by the factor $10^4/Z^2$.

This dose is then multiplied by the correction factor shown previously. This dose, then, is the dose which is accumulated by the piece part of a particular LRU for a given TI, ΔT, etc. This dose determination is done for all the potentially susceptible piece parts of the LRU in question. This dose for each mission-critical piece part is added to the immersion dose, and all other doses (including any possible dose resulting from exposure to prompt radiation during the mission). This total dose is compared to the total dose susceptibility threshold of the piece part (which is assumed known). If the dose level is below the susceptibility threshold for each mission-critical piece part, then the LRU is not vulnerable and no filter is required to protect the LRU from total dose effects from the accumulated dose. If this result exceeds the threshold susceptibility for any one mission-critical piece part, the LRU is vulnerable and protection is required in the form of a filter.

This analysis is repeated for each mission-critical LRU. The most vulnerable of the LRUs will drive the filter selection. At this point, the difference or margin between the susceptibility threshold level and the accumulated dose level is known and is the key element in the filter criteria selection. This margin is related to the amount of dust which must be trapped by a filter. Since in this analysis mass and dust distributions are not available, the approach used in the cockpit filter criteria selection is not appropriate. A different procedure will be used.

If the curves depicting the mass and dose distribution with particle size for the cockpit analysis are recalled, it is apparent that the LRU and cockpit act as perfect filters for particles whose sizes are larger than the critical particle size, R_c. Therefore, the perfect filter results of appendix B with the appropriate constant (the constant in this case must be based on the mass rate of flow of air to the LRU), can be used to determine the necessary filter trapping efficiency. The procedure is to convert the dose margin to point source (at-1-meter) results by going through the conversion procedure described above in reverse. The result will be subtracted from the dose result on the pertinent accumulated dose curve at the 10,000-micron point on the ordinate. This result corresponds to some particle size. The filter must trap all particles larger than this size to provide the required protection. This fixes the filter efficiency.

The trapping efficiency of the filter is now known. The dust mass and the dust mass distribution of the filter now can be found from the perfect filter results of appendix B in the same manner as was done in the cockpit analysis section. Note that the nondimensional constant in this case must be based on the total mass rate of flow of the cooling air through the filter to the entire electronic equipment payload, not just to the single LRU.

3. EXAMPLE LINE REPLACEABLE UNIT ANALYSIS

An example LRU will now be considered as an illustration to clarify the technique. A case of TI = 30 minutes, ΔT = 30 minutes will be considered. It is assumed that the LRU of interest is the critical one in the aircraft, based on preliminary analysis of the type described previously. This example was chosen to represent a typical LRU of one of today's aircraft. Its physical configuration is presented in figure 22. It is assumed that it requires a mass rate of flow of 2 lbm (air)/minute. Thus from equation (A-44), $K_3' = 0.305$, where 2 lbm (air)/minute (converted to grams/hour) replaces $\dot{m}_{af}$ in the K_3 equation, and the LRU dimensions replace the cockpit dimensions. The constant has been multiplied by 0.922 to convert it to rads(Si). Applying the LRU parameters to equation (31), the critical particle size, R_c is 36μ. From figure 15, the dose for 36μ at 1 meter from a point source is 30.5 rads(Si). For this LRU, Z = 2 cm and Y = 8 cm. Therefore, the dose from figure 15 is multiplied by the factor $10^4/Z^2$ to correct for the difference in at-1-meter and actual distance calculations. Next multiply by the correction factor, C.F. = 0.1733 (equation (68)) to account for the fact that it is a distributed source and not a point source. The total dose then which impinges on the susceptible component is 1320 rads(Si). It is assumed that the piece part has a susceptibility threshold of 820 rads(Si). Therefore, the margin of 500 rads(Si) must be collected by the filter.

Now to determine the filter requirements, divide the margin dose of 500 rads(Si) by the two correction factors above, resulting in an at-1-meter point source dose of 1.15 rads(Si). If this is now divided by K_3', the result is 3.77, which has been converted back to rads(tissue) and then nondimensionalized. This value can now be used directly on the perfect filter graphs in appendix B. In this case, go to figures B-35 and B-44. The value, on the figures at r = 10,000 microns for ΔT = 30 minutes, is 24. Subtracting, 24 - 3.77, results in a level

of 20.23. On figure B-35 for ΔT = 30 minutes, this level occurs at a particle size of 60 microns. Therefore, the filter efficiency must be 1 for particles 60 microns or larger, i.e., the filter must trap all particles larger than 60 microns. The filter dust distribution then can be obtained from figure B-7, using a K_2 based on the total mass rate of flow required for all electronics. Only the portion of the distribution above 60 microns is pertinent. The remainder is passed by the filter. The total dust mass in the filter can be obtained from figure B-16, the dose distribution from figure B-26 and the total dose accumulated in the filter from figure B-35 in a similar manner.

4. FILTER LOCATION

There is one remaining aspect of the problem which must be considered in this section. How close to the filter (either the electronic equipment or the cockpit filter) may susceptible electronic equipment be located? The answer to this question would delineate a "forbidden region" in the volume adjacent to the filter in which no susceptible electronics may be located. This volume would be a strong function of the equipment susceptibility and how much dose it accumulates from other sources.

Consider now a filter which has trapped a considerable amount of dust during the cloud penetration. The filter dose at-1-meter assuming a point source of radiation is known from previous considerations. However, for nearby electronic equipment, the dust distribution does not "look like" a point source, but rather a distributed source, because the filter element is assumed to be a plane perpendicular to the flow through the filter. Therefore, a correction factor similar to the one developed previously for the LRU plenum chamber is needed. (It is noted that the geometry chosen here is only applicable for a planar-element filter. Some filters have other geometries, e.g., cylindrical filter elements, and must be considered separately, but in a similar manner.)

This geometry is indicated in figure 23 with the appropriate distances shown. The piece part is located at the point PP. The filter element is represented by the circle of radius d, which has a uniform dust distribution and specific activity A in photons/cm^2-sec. The differential area pdpdθ is located at point DA. The dose rate at the piece part is

$$\dot{D}_{pp} = 2 \int_0^d \int_0^{\pi} \frac{A\, p\, d\theta\, dp}{4\pi g^2} \tag{75}$$

where

$$g^2 = (a + d)^2 - 2p(a + d)\cos\theta + p^2 \tag{76}$$

Performing the indicated operations, $\dot{D}_{pp}$ is obtained

$$\dot{D}_{pp} = \frac{A}{4} \ln \frac{(a + d)^2}{a(a + 2d)} \tag{77}$$

for the dose rate at the piece part due to the distributed dust. If all the dose were concentrated at the center of the filter element, the dose rate at the piece part would be

$$\dot{D}_{pp} = \frac{A}{4} \frac{d^2}{(a + d)^2} \tag{78}$$

Therefore, the correction factor for this situation is

$$C.F.' = \frac{(a + d)^2}{d^2} \ln \frac{(a + d)^2}{a(a + 2d)} \tag{79}$$

The dose results from the previous work must first be corrected for the actual distance from the filter element to the piece part location, or any location of interest, and then corrected by the correction factor above. Using this procedure, contours of constant dose, or isorads, may be determined. The equipment must not be located such that its threshold susceptibility is exceeded, i.e., inside the pertinent isorad. Generally, this forbidden region is relatively small, i.e., on the order of inches away from the filter, because of the rapid fall-off of dose rate with distance away from the filter and the relatively high thresholds of the equipment. However, this forbidden region must be a consideration in equipment and filter location planning.

The determination of the distance which the filter must be located away from the crew is much simpler. Generally, this distance is at least a meter or greater and at this distance the point source approximation is reasonably accurate. Only very near the filter must the correction factor above be used.

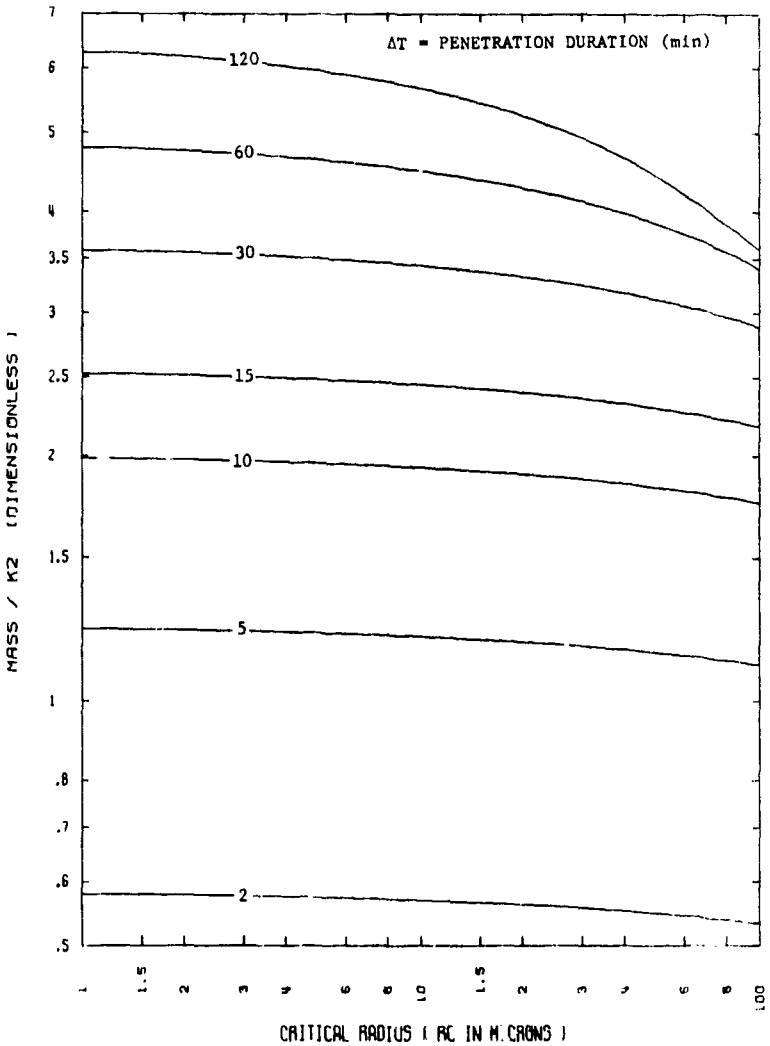

Figure 4. Total LRU Chamber Mass versus Critical Radius, TI = 10 Minutes

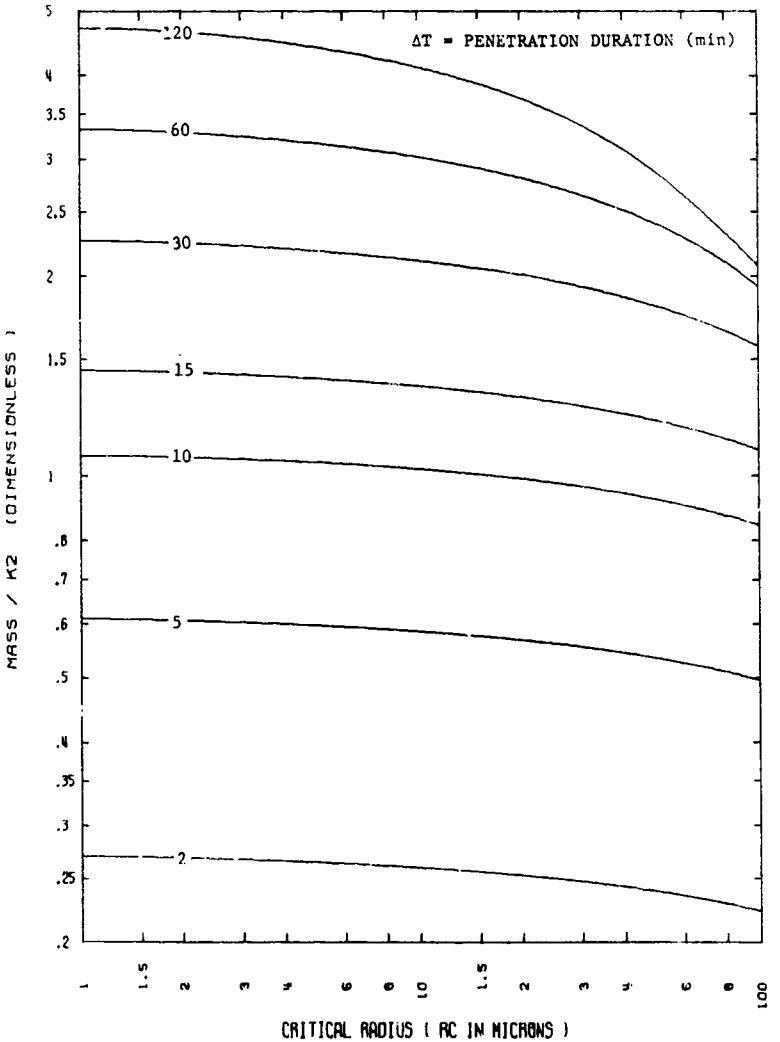

Figure 5. Total LRU Chamber Mass versus Critical Radius, TI = 18 Minutes

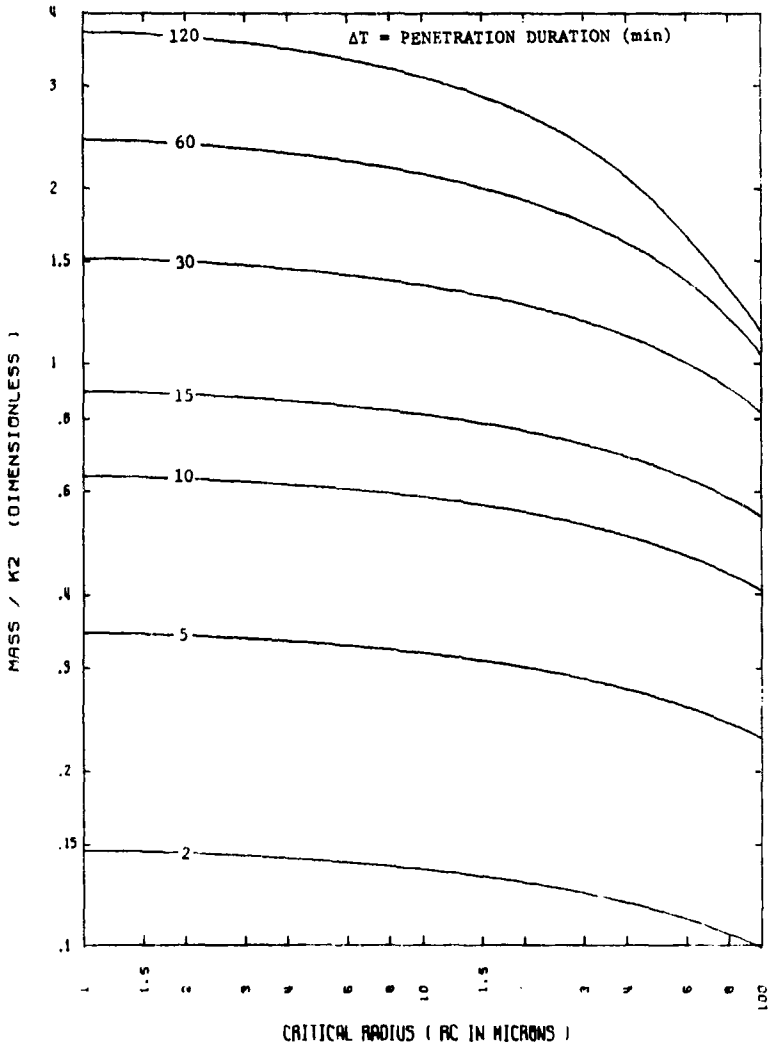

Figure 6. Total LRU Chamber Mass versus Critical Radius, TI = 30 Minutes

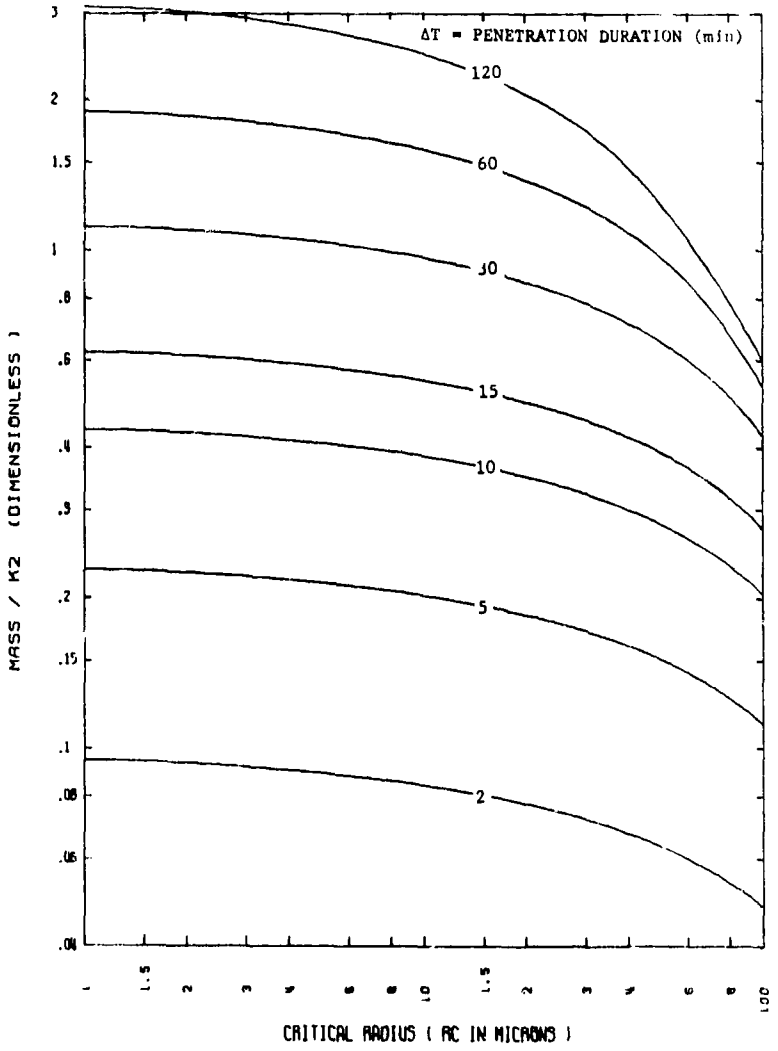

Figure 7. Total LRU Chamber Mass versus Critical Radius, TI = 45 Minutes

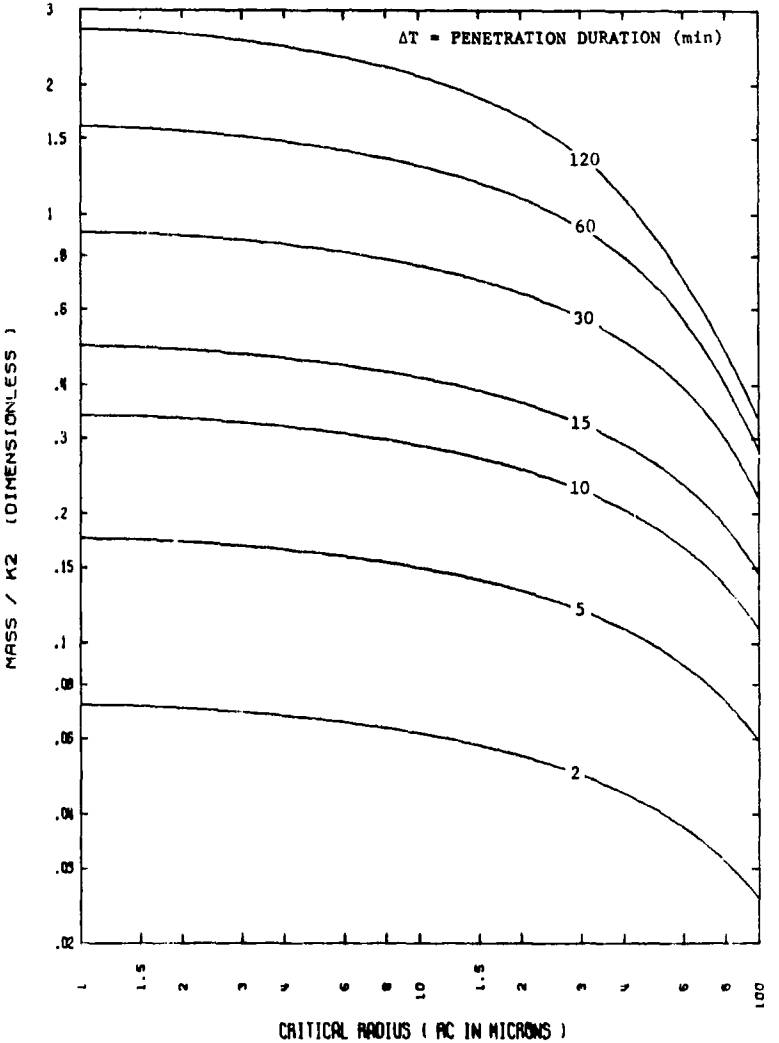

Figure 8. Total LRU Chamber Mass versus Critical Radius, TI = 1 Hour

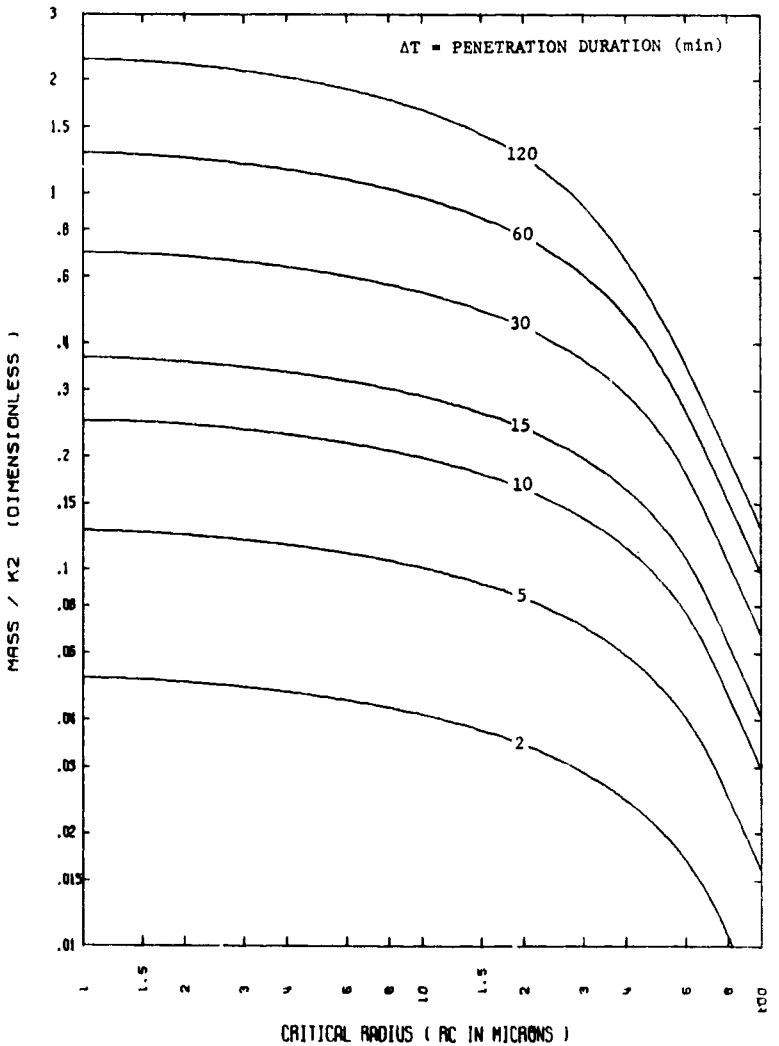

Figure 9. Total LRU Chamber Mass versus Critical Radius, TI = 1.5 Hours

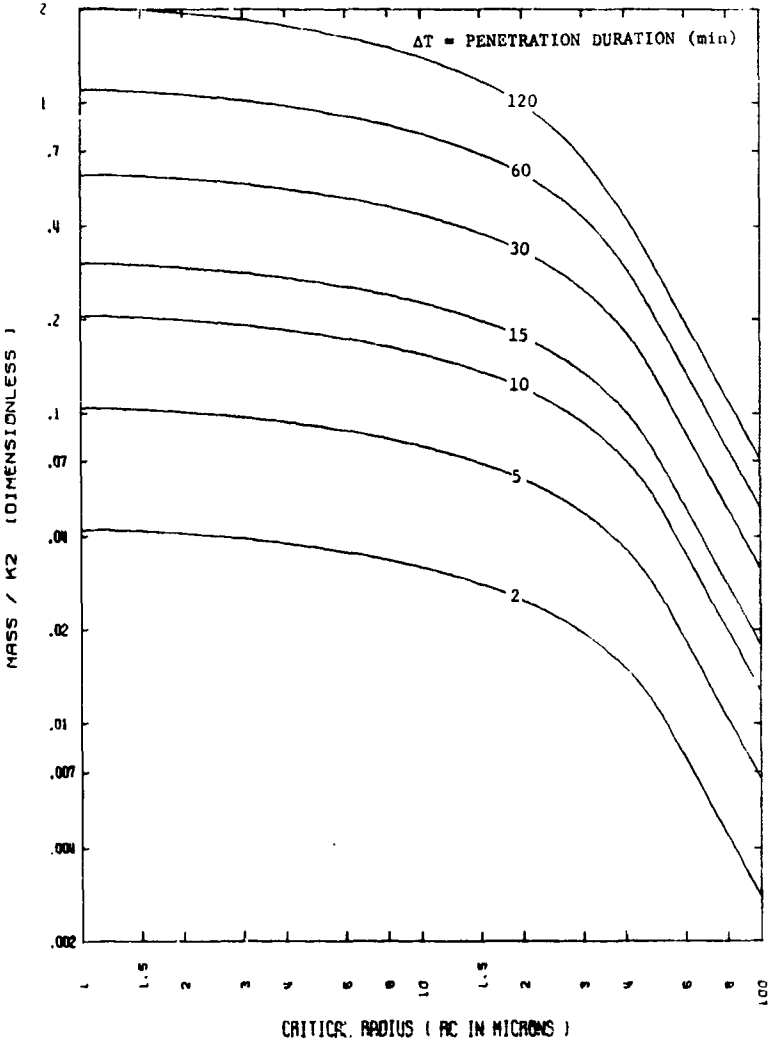

Figure 10. Total LRU Chamber Mass versus Critical Radius, TI = 2 Hours

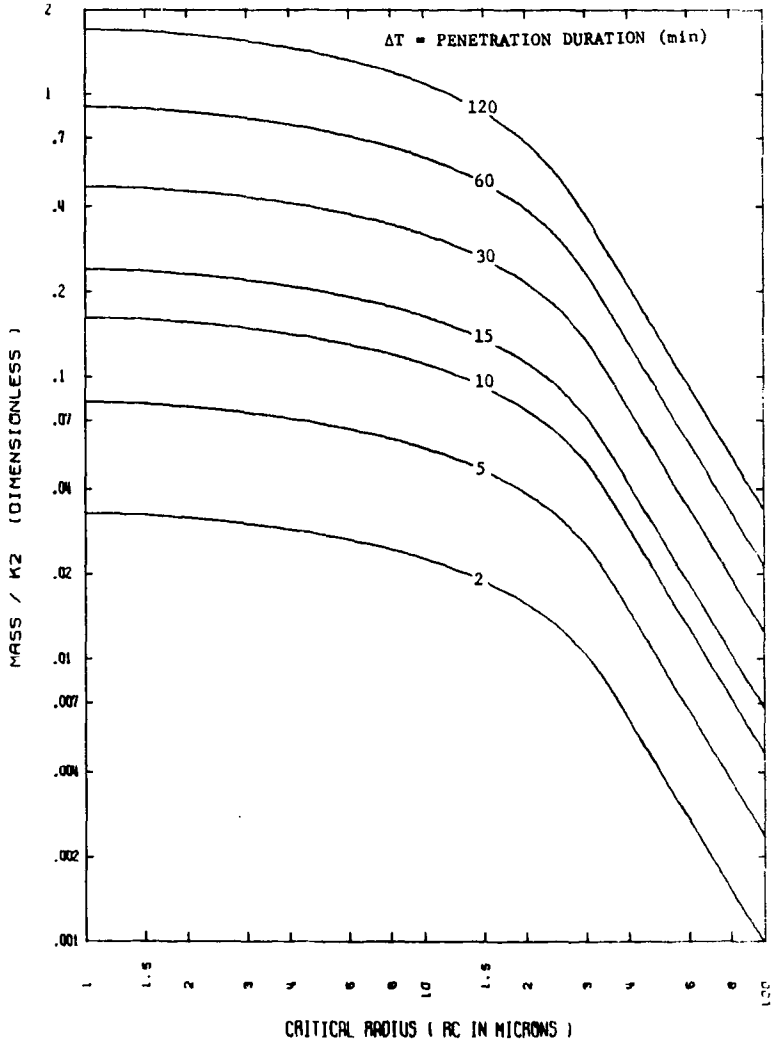

Figure 11. Total LRU Chamber Mass versus Critical Radius, TI = 3 Hours

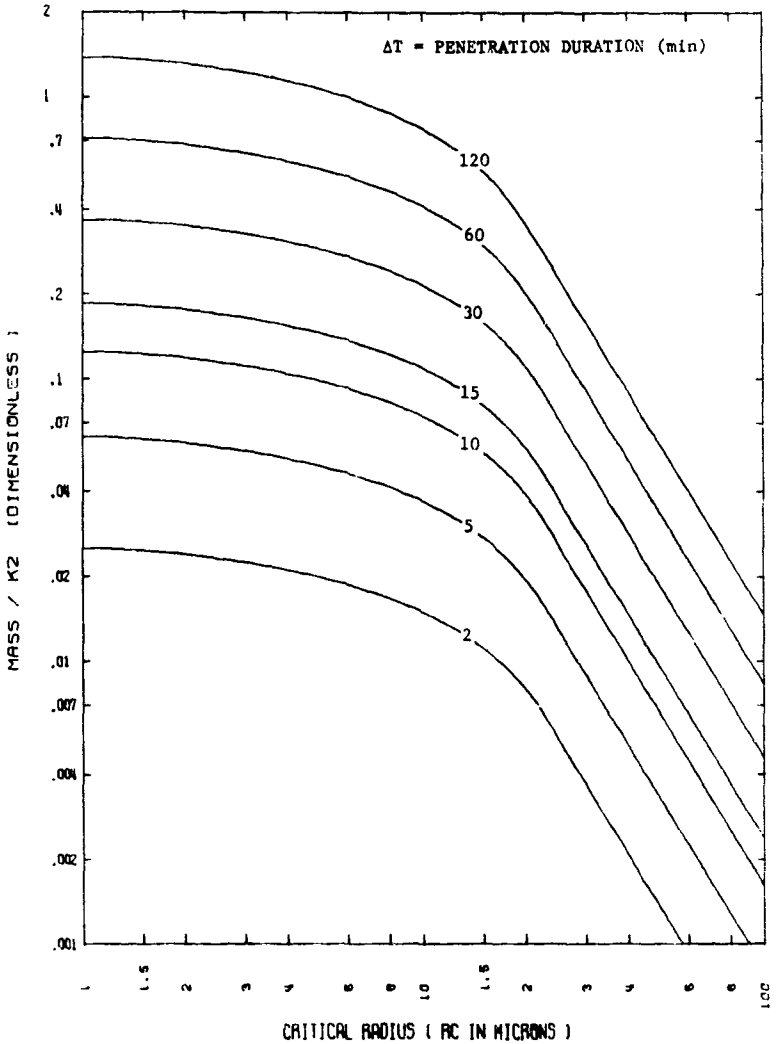

Figure 12. Total LRU Chamber Mass versus Critical Radius, TI = 5 Hours

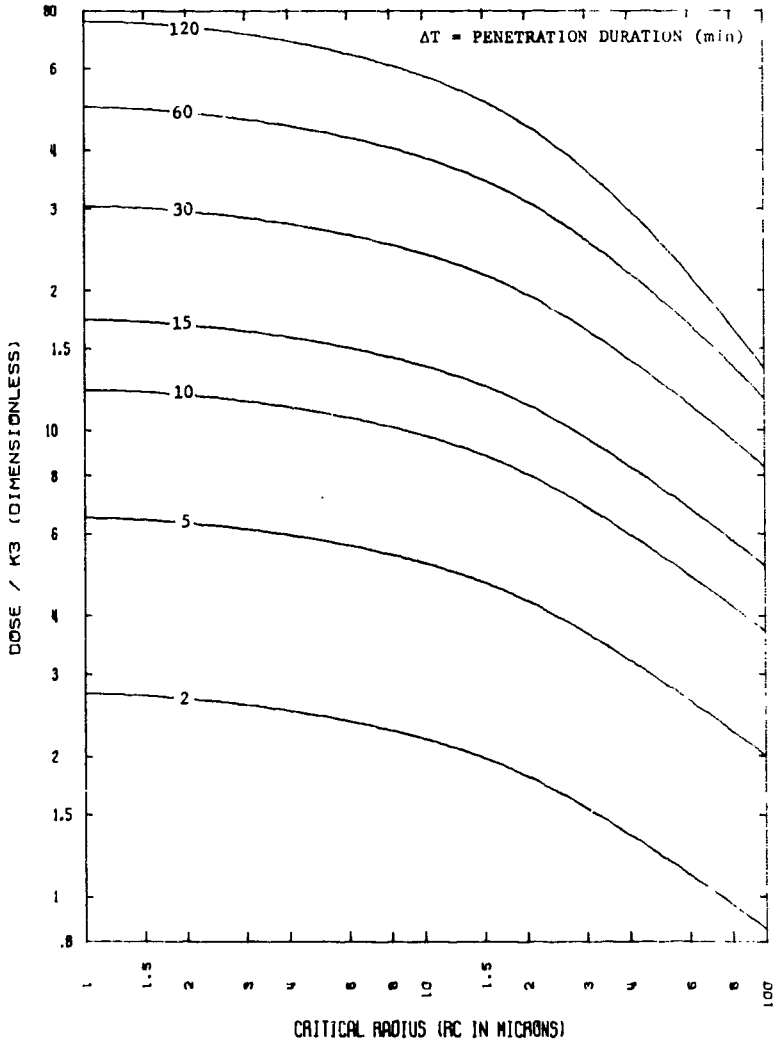

Figure 13. Total LRU Chamber Dose versus Critical Radius, TI = 10 Minutes

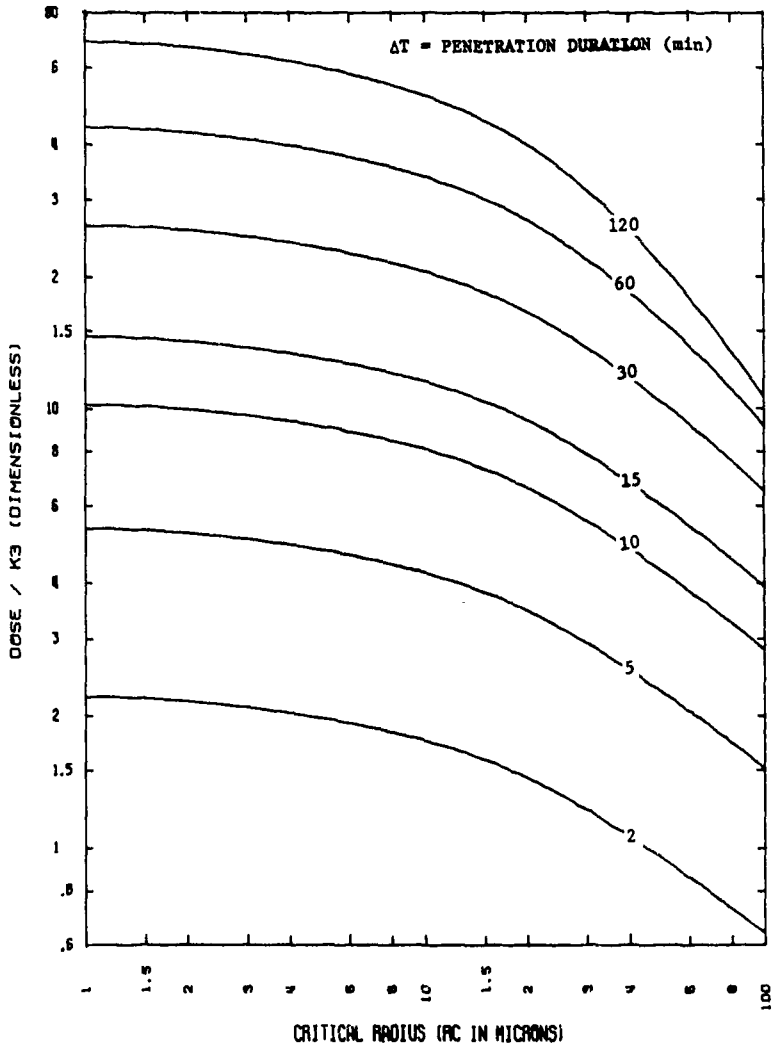

Figure 14. Total LRU Chamber Dose versus Critical Radius, TI = 18 Minutes

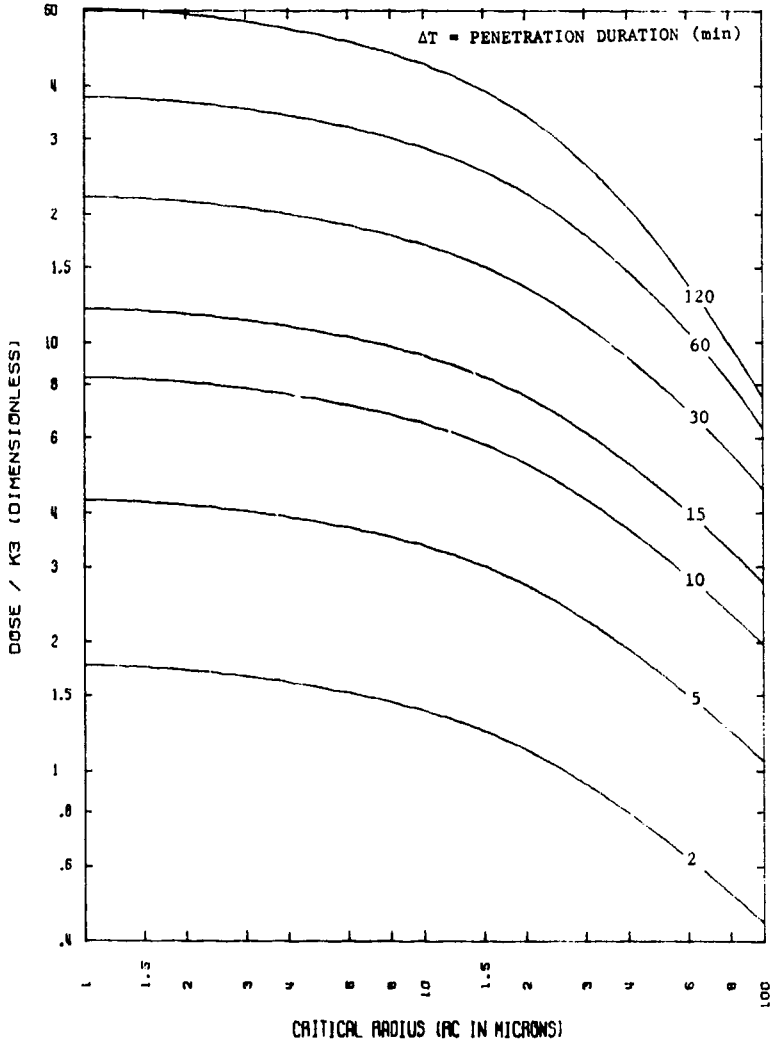

Figure 15. Total LRU Chamber Dose versus Critical Radius, TI = 30 Minutes

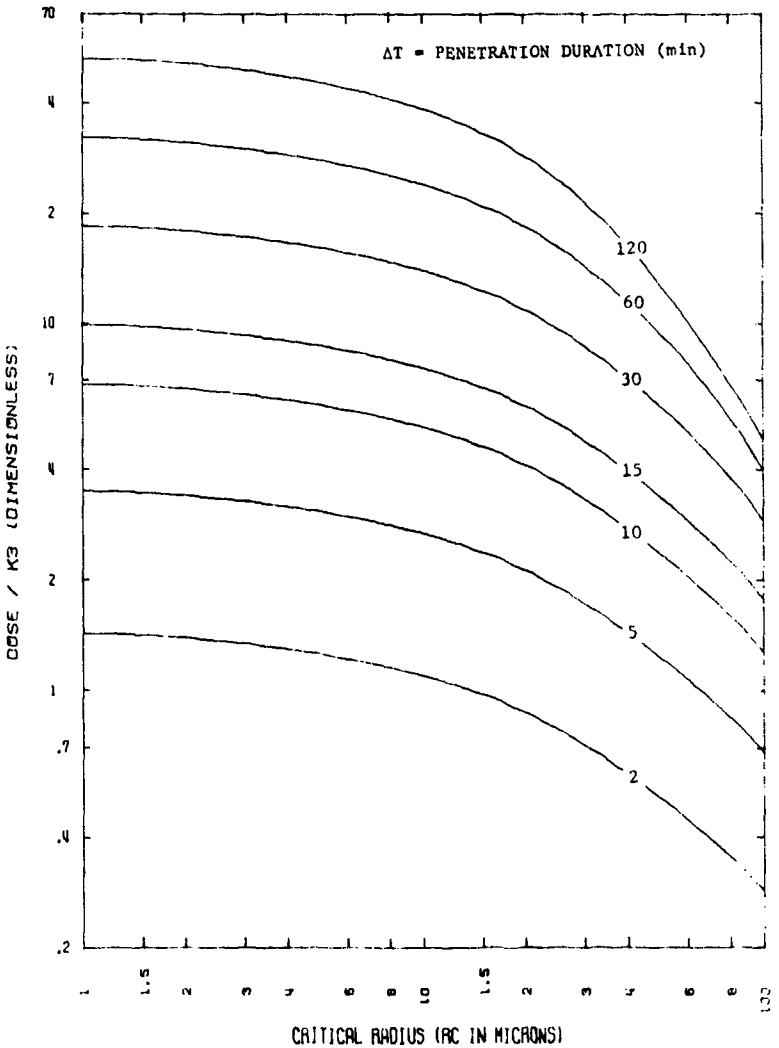

Figure 16. Total LRU Chamber Dose versus Critical Radius, TI = 45 Minutes

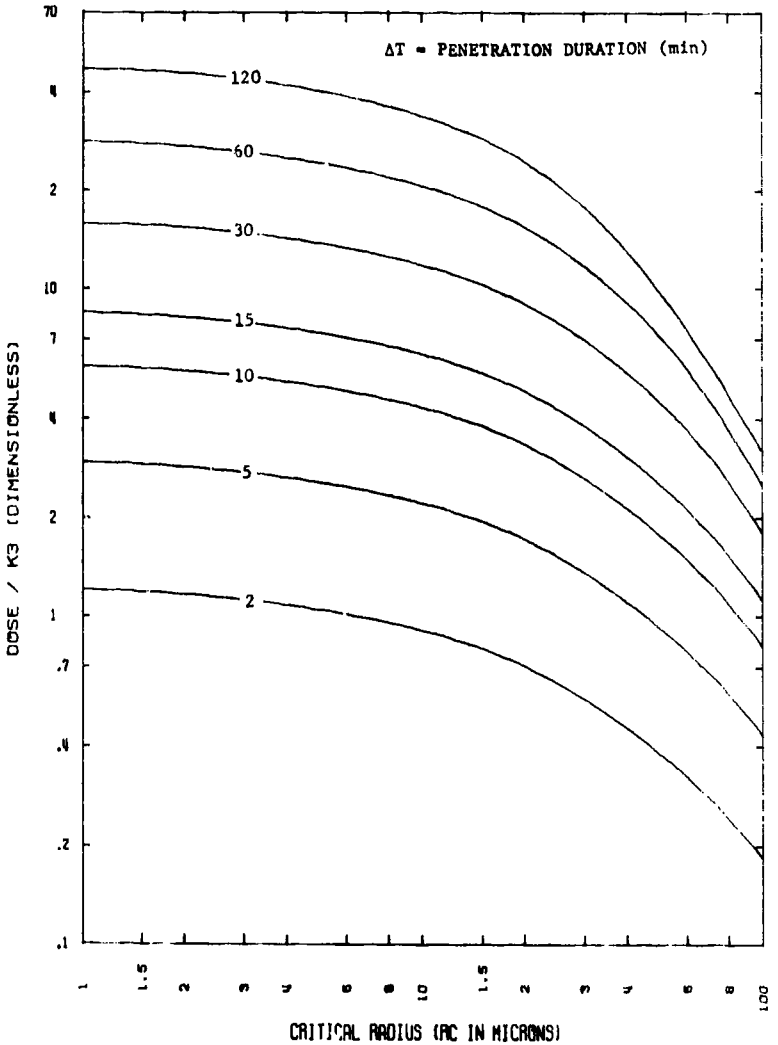

Figure 17. Total LRU Chamber Dose versus Critical Radius, TI = 1 Hour

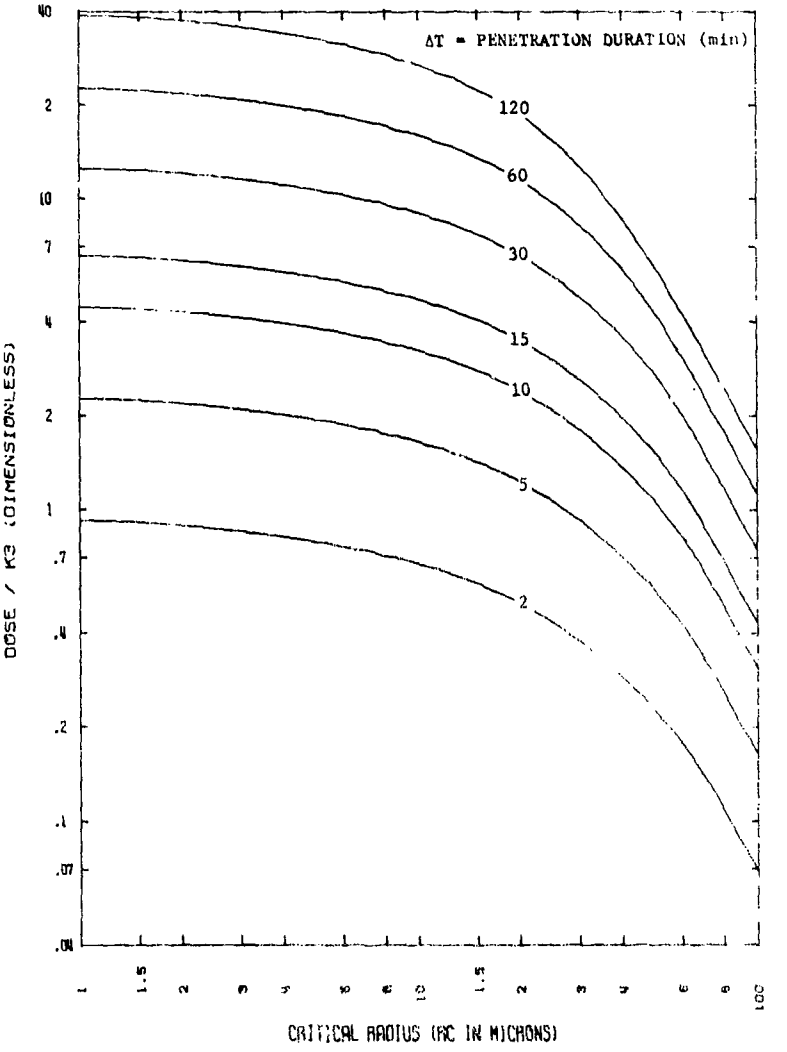

Figure 18. Total LRU Chamber Dose versus Critical Radius, TI = 1.5 Hours

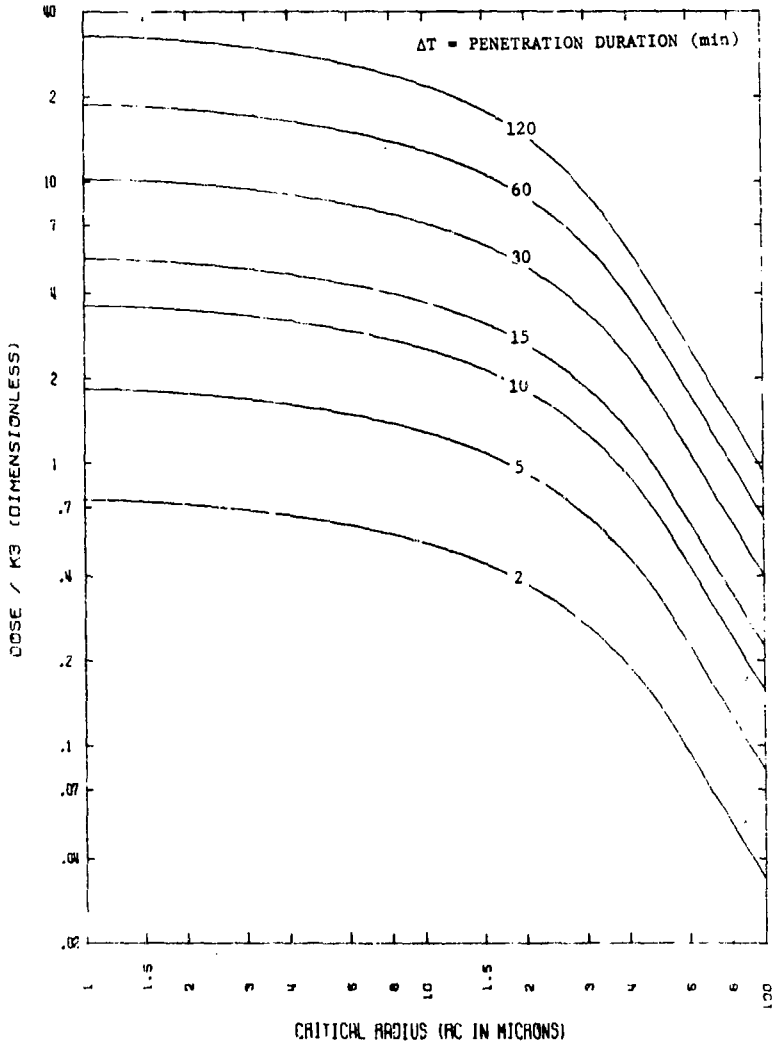

Figure 19. Total LRU Chamber Dose versus Critical Radius, TI = 2 Hours

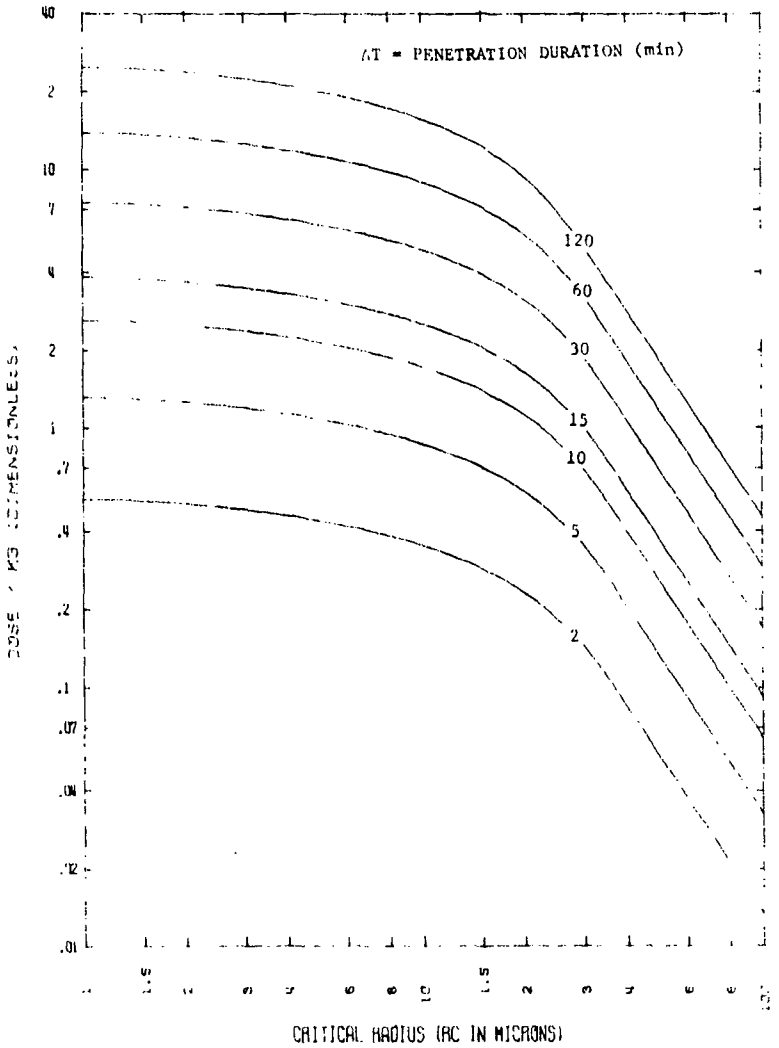

Figure 20. Total LRU Chamber Dose versus Critical Radius, TI = 3 Hours

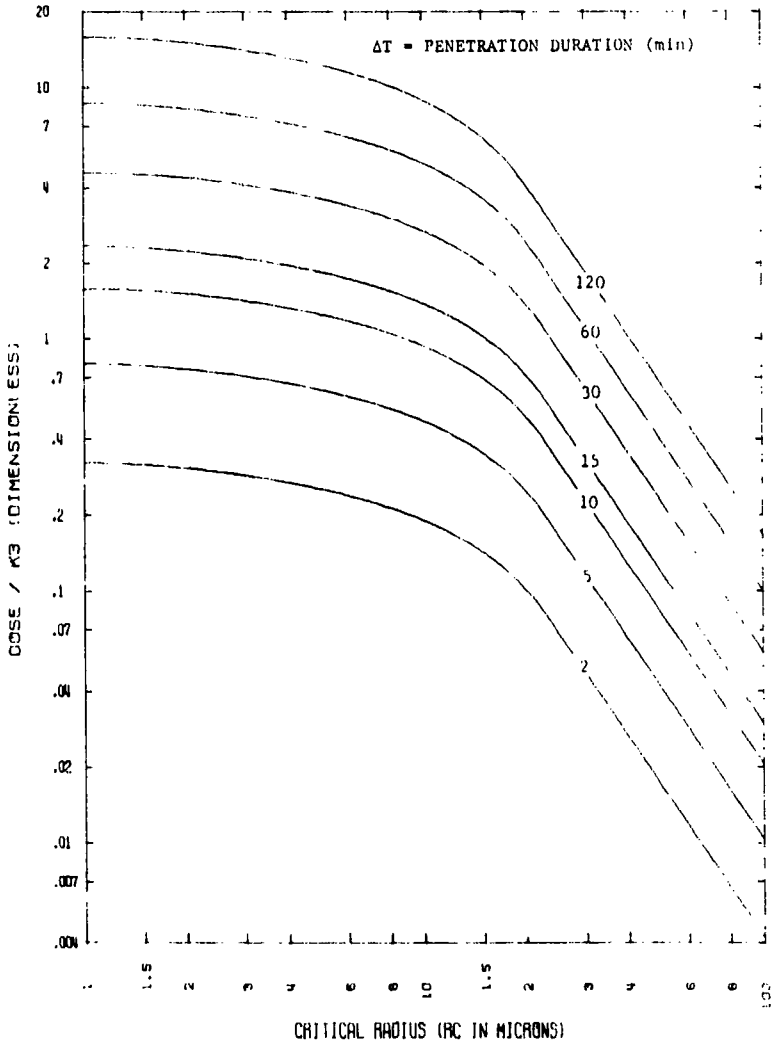

Figure 21. Total LkU Chamber Dose versus Critical Radius, TI = 5 Hours

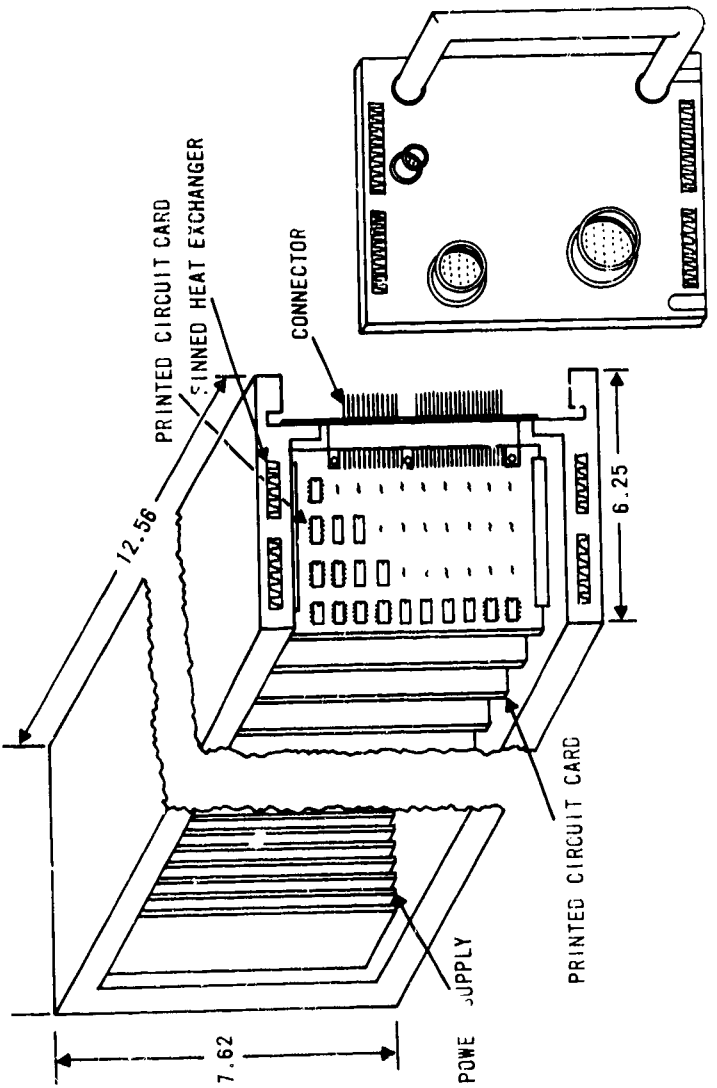

Figure 22. Typical Aircraft LRU

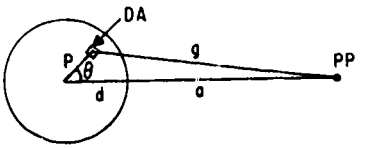

Figure 23. Planar Distributed Source

SECTION VII

MISCELLANEOUS CONSIDERATIONS

The major thrust of this work is toward the protection required by the crew and the electronic equipment from the contaminated dust ingested into the aircraft via the environmental control system. These problems were addressed in detail in the preceding sections. This section will briefly address the aircraft engines and the dose due to dust accumulated on the aircraft exterior.

1. ENGINE INGESTION OF DUST

The air flow through the engines is much larger than the air flow to the environmental control system. Therefore, much greater masses of dust will be ingested. However, because the engine interior is streamlined to offer low flow resistance, little of the ingested dust will be accumulated. There is no problem of the engine being a source of radiation due to trapped dust. The only significant potential problem is that the large amounts of dust ingested could erode the compressor-and-turbine rotor and stator blades, and cause unacceptable damage.

It is beyond the scope of this work to investigate any potential damage caused by the dust. All that will be done is to present the technique of determining the total mass and the mass distribution with particle size of the dust ingested by the engines during the cloud penetrations. It is hoped that this information could be used by engine design and test engineers to ensure that the mission completion capability of the engine is not compromised by cloud penetrations.

Since the engine traps little or no dust, all of the dust which is ingested flows through and out of the engine. Recall that the perfect filter analysis in appendix B determined all of the dust which entered the filter and it was assumed to trap it all. Therefore, the perfect filter results of appendix B are pertinent to the engine. However, in this case, the results merely show what has passed through the engine during the penetration and not what was trapped.

The total mass ingested by the engine during a penetration can be obtained by figure B-23 of appendix B with the constant (K_1) based on the total mass rate of flow of air through the engine. The mass distribution of the dust as a function of particle size can be obtained from figures B-5 through B-22.

2. DUST ACCUMULATED ON THE AIRCRAFT EXTERIOR

The dose due to the mass of dust trapped on the aircraft exterior is addressed briefly in appendix A. Generally, this dose is relatively small and will not affect either the crew or the electronic equipment. The primary interest to date in this dust is related to the recovery of the aircraft by maintenance personnel after a mission involving a penetration of a radioactive dust cloud. Washing the aircraft and other decontamination techniques should minimize the hazard due to external dust accumulations. However, the main problem in recovery will be changing the filters and LRUs with open-cycle cooling. These problems should be addressed and recovery techniques formulated to minimize the hazard to ground crews.

SECTION VIII

CONCLUSIONS

The purpose of this report was to investigate the penetratior of a radioactive cloud by a manned aircraft. The concerns associated with such a penetration are three: the crew, the electronic equipment, and the engines. If any of the thre· experience significant performance degradation, the strategic mission of the aircraft could be in jeopardy. Because detailed quantitative results are extremely system dependent, specific conclusions about the effects of cloud penetration on crew members, electronics, and engines cannot be drawn. However, some general observations can be made.

1. The cloud immersion dose is accumulated equally by the crew and the electronic equipment during cloud penetration. The only feasible action to reduce this dose is to avoid the cloud. Shielding to attenuate this cloud immersion radiation is impractical because of the great weight of material required to provide any appreciable attenuation.

2. In addition to the cloud immersion dose, the crew could be subjected to potentially severe hazards associated with the dust ingested into the cockpit by the environmental control system (ECS). Although these hazards, particularly the ionizing dose accumulations from dust accumulated in the cockpit and skin burns from the beta radiation associated with the radioactive dust, can be reduced considerably by the installation of a suitable filter in the ECS.

3. Although precise filter criteria for the cockpit ECS filter are the end product of a detailed analysis and are system and threat dependent, study of the cockpit dose results in appendix D reveals that filters which trap all particles in excess of 6 to 8 microns in radius would provide good protection to the crew. This capability is well within the present state of the art in filter design.

4. Although the ionizing dose accumulated by piece parts in electronic equipment is system and threat dependent, it is observed that the critical particle size, R_c, for typical plenum chamber geometrics and mass flow rates of cooling air, is relatively large, i.e., 50 microns or larger. Because fallout rapidly depletes the cloud of large particles and the plenum chambers of

representative line replaceable units trap relatively large particles, the amount of dust accumulated in the plenum chambers is relatively small. Therefore, the piece-part ionizing dose accumulation is probably relatively low. Therefore, alleviation of this potential mission crippler should be relatively straightforward.

This report has shown that cloud penetration by manned aircraft could result in unacceptable performance degradation. Strategic aircraft should be subjected to detailed analyses to determine potential vulnerabilities and the corrective actions necessary to reduce these vulnerabilities.

APPENDIX A

UNIFORM FALLOUT MODEL

This appendix develops a preliminary model using the cloud dust density and specific activity functions which were presented in section II. The relationships from section II are independent of particle size. This model may be viewed as a first order approximation. Because particle size is not a consideration, the dust cloud effectively may be modeled by a cloud consisting of dust particles which are uniform in size and activity. This model does take fallout into account, but in a rather simplified fashion.

For the purposes of this development, the dust density and specific activity functions are written in the form developed directly by curve fitting Whitaker's data (section II).

$$\rho_d(t) = a_i\left(t^{-m} + bt^{-n}\right) \tag{A-1}$$

$$A(t) = A_1 t^{-\ell} \tag{A-2}$$

where

$$a_i = 3.46 \times 10^{-6}\ L_f\ \text{gms(dust)/cm}^3$$

$$\ell = 1.2$$

$$m = 1.6$$

$$n = 0.3$$

$$b = 1.313$$

$$A_1 = 4.22 \times 10^{12}\ \frac{\text{photons}}{\text{gm(dust)-hour}}$$

1. DUST INGESTION BY THE ENGINES

The mass rate of flow of air through the engines is given by $\dot{m}_{ae}$ grams (air) per hour and is constant for a given engine and flight condition of the aircraft.

The air drawn through the engines contains dust in the ratio $\rho_d(t)/\rho_a$ grams of dust per gram of air. The mass rate of flow of dust through the engines $\dot{M}_e(t)$ in grams per hour is given by the relation

$$\dot{M}_e(t) = \dot{m}_{ae} \frac{\rho_d(t)}{\rho_a} = \frac{\dot{m}_{ae}\, a_i}{\rho_a} \left(t^{-m} + bt^{-n}\right) \qquad t_i \le t \le t_f \qquad \text{(A-3)}$$

$$\dot{M}_e(t) = 0 \qquad \text{all other } t \qquad \text{(A-4)}$$

For some purposes, such as considerations of the effect of engine lifetime after dust ingestion, one may be interested in the total mass of dust ingested by the engines during a cloud penetration. This can be obtained by integration of the above equation.

$$M_e(t) = 0 \qquad t < t_i \qquad \text{(A-5)}$$

$$M_e(t) = \frac{\dot{m}_{ae}\, a_i}{\rho_a} \left[\frac{t_i^{1-m} - t^{1-m}}{m-1} + b\left(\frac{t^{1-n} - t_i^{1-n}}{1-n}\right)\right] \qquad t_i \le t \le t_f \qquad \text{(A-6)}$$

$$M_e(t) = \frac{\dot{m}_{ae}\, a_i}{\rho_a} \left[\frac{t_i^{1-m} - t_f^{1-m}}{m-1} + b\left(\frac{t_f^{1-n} - t_i^{1-n}}{1-n}\right)\right] \qquad t \ge t_f \qquad \text{(A-7)}$$

2. DUST ACCUMULATION IN AIR CONDITIONING FILTERS

Also of concern to this analysis is the mass of dust collected by a perfect filter in the bleed air line from the engines which supplied air to the crew compartment/electronics. The accumulation of radioactive dust in the filter is a source of radiation which contributes to the dose received by the aircrew members and electronic equipment.

If one assumes that the trapped dust is a point source of radioactivity and neglects any shielding, one can calculate the dose rate and dose at some distance, d_1 centimeters, from the filter. This distance represents the distance to the crewmember/electronic equipment from the filter.

The mass of dust ($M_f(t)$) trapped by the filter can be calculated, assuming 100 percent filter trapping efficiency, in a manner similar to the one used above. This relation is given by the following:

$$M_f(t) = 0 \qquad t \le t_i \qquad \text{(A-8)}$$

$$M_f(t) = \frac{\dot{m}_{af}\, a_i}{\rho_a}\left[\frac{t_i^{1-m} - t^{1-m}}{m-1} + b\left(\frac{t^{1-n} - t_i^{1-n}}{1-n}\right)\right] \qquad t_i \le t \le t_f \qquad \text{(A-9)}$$

$$M_f(t) = \frac{\dot{m}_{af}\, a_i}{\rho_a}\left[\frac{t_i^{1-m} - t_f^{1-m}}{m-1} + b\left(\frac{t_f^{1-n} - t_i^{1-n}}{1-n}\right)\right] \qquad t \ge t_f \qquad \text{(A-10)}$$

The product $M_f(t)\, A(t)$ is the effective source strength of the filter trapped dust. The dose rate measured at a distance d centimeters away from the source is

$$\dot{D}_f(t) = \frac{C\, M_f(t)\, A(t)}{4\pi d^2} \qquad \text{(A-11)}$$

where C is a conversion factor with units of rads(tissue) centimeter^2/photon. The dose rate due to the dust trapped in the filter then is given by

$$\dot{D}_f(t) = 0 \qquad t \le t_i \qquad \text{(A-12)}$$

$$\dot{D}_f(t) = \frac{C\, A_1\, \dot{m}_{af}\, a_i}{4\pi d^2\, \rho_a}\left[\frac{t_i^{1-m} - t^{1-m}}{m-1} + b\left(\frac{t^{1-n} - t_i^{1-n}}{1-n}\right)\right] t^{-\ell} \qquad t_i \le t \le t_f \qquad \text{(A-13)}$$

$$\dot{D}_f(t) = \frac{C\, A_1\, \dot{m}_{af}\, a_i}{4\pi d^2\, \rho_a}\left[\frac{t_i^{1-m} - t_f^{1-m}}{m-1} + b\left(\frac{t_f^{1-n} - t_i^{1-n}}{1-n}\right)\right] t^{-\ell} \qquad t \ge t_f \qquad \text{(A-14)}$$

The total dose accumulated by time t due to the filter dust is obtained by integration of the dose rate.

$$D_f(t) = 0 \qquad t \leq t_i \qquad \text{(A-15)}$$

$$D_f(t) = K_3\left[\frac{t_i^{1-m}}{(m-1)(\ell-1)}\left(t_i^{1-\ell} - t^{1-\ell}\right) + \frac{t^{2-m-\ell} - t_i^{2-m-\ell}}{(m-1)(m+\ell-2)}\right.$$

$$\left. + \frac{b\left(t^{2-n-\ell} - t_i^{2-n-\ell}\right)}{(1-n)(2-n-\ell)} + \frac{b\, t_i^{1-n}\left(t^{-\ell+1} - t_i^{-\ell+1}\right)}{(1-n)(\ell-1)}\right]$$

$$t_i \leq t \leq t_f \qquad \text{(A-16)}$$

$$D_f(t) = K_3\left\{\frac{t_i^{1-m}}{(m-1)(\ell-1)}\left(t_i^{1-\ell} - t_f^{1-\ell}\right) + \frac{t_f^{2-m-\ell} - t_i^{2-m-\ell}}{(m-1)(m+\ell-2)}\right.$$

$$+ \frac{b\left(t_f^{2-n-\ell} - t_i^{2-n-\ell}\right)}{(1-n)(2-n-\ell)} + \frac{b\, t_i^{1-n}\left(t_f^{1-\ell} - t_i^{1-\ell}\right)}{(1-n)(\ell-1)}$$

$$\left. + \left[\frac{\left(t_i^{1-m} - t_f^{1-m}\right)}{m-1} + \frac{b\left(t_f^{1-n} - t_i^{1-n}\right)}{1-n}\right]\frac{\left(t_f^{-\ell+1} - t^{-\ell+1}\right)}{\ell-1}\right\}$$

$$t \geq t_f \qquad \text{(A-17)}$$

where

$$K_3 = \frac{C\, A_1\, \dot{m}_{af}\, a_i}{4\pi d^2\, \rho_a} \qquad \text{(A-18)}$$

3. DOSE DUE TO CLOUD RADIOACTIVITY

Another primary source of dose to the crew results from the integrated effect of the dose from the radioactive debris surrounding the aircraft as it passes through the cloud. It is assumed that the cloud is an infinite, homegeneous mixture with a distributed source of radiation of strength given by the product of the dust density, and the specific activity A(t). For simplicity, consider the aircraft to be adequately represented by a sphere of radius R centimeters and neglect any shielding effect of aircraft structure. For any source point at a distance d > R from the center of the sphere, the rate at which photons are emitted from a volume element dV is given by ρ_d A(t) dV. Since the source is assumed isotropic in nature ρ_d A(t) dV/$4\pi d^2$ is the fluence at the center of the sphere from the volume element. One must also account for atmospheric attenuation of these photons which requires a factor of exp $\left(-(\mu'/\rho_a)\rho_a d\right)$ where μ'/ρ_a is the mass attenuation coefficient for the photons of interest. To convert from photons per centimeter^2 to dose units use the conversion constant C, which is a function of the energy level of the photons. The total dose rate due to all volume elements is given by

$$\dot{D}_c(t) = \int_R^\infty \frac{C\,\rho_d(t)\,A(t)\,e^{-\left(\frac{\mu'}{\rho}\right)\rho d}\,4\pi d^2\,dd}{4\pi d^2} \qquad \text{(A-19)}$$

or

$$\dot{D}_c(t) = \frac{C\,\rho_d(t)\,A(t)}{\mu}\,e^{-\mu' R} \qquad \text{(A-20)}$$

since

$$\mu \sim 10^{-5},\ R \sim 10^2 \text{ cm, and } e^{-\mu' R} \sim 1$$

therefore,

$$\dot{D}_c(t) = \frac{C\,\rho_d(t)\,A(t)}{\mu'} \qquad \text{(A-21)}$$

Substituting, the equation becomes

$$\dot{D}_c(t) = \frac{c}{\mu'} A_1 \, t^{-\ell} \, a_i \left[t^{-m} + b t^{-n} \right] \qquad t_i \le t \le t_f \qquad \text{(A-22)}$$

$$\dot{D}_c(t) = 0 \qquad \text{all other } t \qquad \text{(A-23)}$$

The total dose accumulated at time, t, is given by

$$D_c(t) = \int_{t_i}^{t} \dot{D}_c(t) \, dt$$

Performing the indicated integration

$$D_c(t) = 0 \qquad t \le t_i \qquad \text{(A-24)}$$

$$D_c(t) = \frac{c}{\mu'} A_1 \, a_i \left[\frac{1}{m+\ell-1} \left(t_i^{\,1-(m+\ell)} - t^{1-(m+\ell)} \right) + \frac{b}{n+\ell-1} \left(t_i^{\,1-(n+\ell)} - t^{1-(n+\ell)} \right) \right] \qquad t_i \le t \le t_f \qquad \text{(A-25)}$$

$$D_c(t) = \frac{c \, A_1 \, a_i}{\mu'} \left[\frac{1}{m+\ell-1} \left(t_i^{\,1-(m+\ell)} - t_f^{\,1-(m+\ell)} \right) + \frac{b}{n+\ell-1} \left(t_i^{\,1-(n+\ell)} - t_f^{\,1-(n+\ell)} \right) \right] \qquad t \ge t_f \qquad \text{(A-26)}$$

4. DOSE DUE TO EXTERNAL ACCUMULATION OF DUST

If radioactive dust is accumulated on the skin of the aircraft or in crevices and discontinuities caused by joints in the external structure, it would also contribute to the radiation dose received by the crew/electronic equipment.

Since the dose from this source would be inversely proportional to the square of the distance from the source point to the crew member/electronic equipment, it would appear reasonable to consider only the dust accumulated in the near vicinity of the crew member/electronic equipment. For example, in determining the dose to the pilot, one would restrict his attention to the accumulation of dust in the cockpit/crew station area.

If one could reasonably estimate the amount of dust accumulated in the pilot's vicinity as G grams at an effective distance of d centimeters one could estimate the dose due to the source.* To be conservative one might assume that all of this dust was accumulated at the time of entry, t_i, into the radiation cloud and remained there during the remainder of the mission.

Then the dose rate at position R from this source would be given by

$$\dot{D}_{ae}(t) = \frac{GCA(t)}{4\pi d^2} \tag{A-27}$$

or

$$\dot{D}_{ae}(t) = \frac{GCA_1}{4\pi d^2} t^{-\ell} \qquad t \geq t_i \tag{A-28}$$

The integrated dose then is

$$D_{ae}(t) = 0 \qquad t \leq t_i \tag{A-29}$$

$$D_{ae}(t) = \frac{GCA_1}{4\pi d^2}\left(\frac{t_i^{-\ell+1} - t^{-\ell+1}}{\ell - 1}\right) \qquad t \geq t_i \tag{A-30}$$

This area has been investigated experimentally and analytically by several researchers. No attempt will be made here to correlate the experimental findings with this rather crude first cut analysis. Future effort in this area is needed. However, in this work this dose is much less critical than the filter and cloud doses, and has been presented briefly only for the purposes of completeness.

5. TOTAL DOSE

The total radiation dose due to penetration of the cloud then is the sum of individual doses.

---

*As a "first cut" at the accumulation of dust on the aircraft exterior, one could measure or estimate the volume of all the cracks, crevices, etc., and the volume of surface accumulation, which would be a function of the boundary layer thickness. If then the dust density in the cracks, etc., is known or assumed, a total mass can be approximated.

$$D_T(t) = D_f(t) + D_c(t) + D_{ae}(t) \qquad \text{(A-31)}$$

6. SPECIFIC RESULTS

Substituting the values for the cloud parameters, i.e., m, n, ℓ, and b, into the equations developed previously, and grouping the remaining constants, the following equations are obtained.

$$\frac{\dot{M}_{e/f}(t)}{K_{1/2}} = t^{-1.6} + 1.313\ t^{-0.3} \qquad t_i \le t \le t_f \qquad \text{(A-32)}$$

$$\frac{M_{e/f}(t)}{K_{1/2}} = \frac{\left(t_i^{-0.6} - t^{-0.6}\right)}{0.6} + \frac{1.313}{0.7}\left(t^{0.7} - t_i^{0.7}\right) \qquad t_i \le t \le t_f \qquad \text{(A-33)}$$

$$\frac{M_{e/f}(t)}{K_{1/2}} = \frac{\left(t_i^{-0.6} - t_f^{-0.6}\right)}{0.6} + \frac{1.313}{0.7}\left(t_f^{0.7} - t_i^{0.7}\right) \qquad t \ge t_f \qquad \text{(A-34)}$$

$$\frac{\dot{D}_f(t)}{K_3} = \left[\frac{1}{0.6}\left(t_i^{-0.6} - t^{-0.6}\right) + \frac{1.313}{0.7}\left(t^{0.7} - t_i^{0.7}\right)\right] t^{-1.2} \qquad t_i \le t \le t \qquad \text{(A-35)}$$

$$\frac{\dot{D}_f(t)}{K_3} = \left[\frac{1}{0.6}\left(t_i^{-0.6} - t_f^{-0.6}\right) + \frac{1.313}{0.7}\left(t_f^{0.7} - t_i^{0.7}\right)\right] t^{-1.2} \qquad t \ge t_f \qquad \text{(A-36)}$$

$$\frac{D_f(t)}{K_3} = 6.25\ t_i^{-0.8} + 2.083\ t^{-0.8} + 3.751\ t^{0.5} + 9.379\ t_i^{0.7}\ t^{-0.2} - 8.33\ t_i^{-0.6}\ t^{-0.2} - 13.13\ t_i^{0.5} \qquad t_i \le t \le t_f \qquad \text{(A-37)}$$

$$\frac{D_f(t)}{K_3} = 6.25\ t_i^{-0.8} + 13.13\ t_f^{0.5} - 6.25\ t_f^{-0.8} - 13.13\ t_i^{0.5} + \left(9.379\ t_i^{0.7} + 8.333\ t_f^{-0.6} - 8.333\ t_i^{-0.6} - 9.379\ t_f^{0.7}\right) t^{-0.2} \qquad t \geq t_f \quad \text{(A-38)}$$

$$\frac{\dot{D}_c(t)}{K_4} = \left(t^{-1.6} + 1.313\ t^{-0.3}\right) t^{-1.2} \qquad t_i \leq t \leq t_f \quad \text{(A-39)}$$

$$\frac{D_c(t)}{K_4} = \frac{1}{1.8}\left(t_i^{-1.8} - t^{-1.8}\right) + \frac{1.313}{0.5}\left(t_i^{-0.5} - t^{-1.5}\right) \qquad t_i \leq t \leq t_f \quad \text{(A-40)}$$

$$\frac{D_c(t)}{K_4} = \frac{1}{1.8}\left(t_i^{-1.8} - t_f^{-1.8}\right) + \frac{1.313}{0.5}\left(t_i^{-0.5} - t_f^{-0.5}\right) \qquad t \geq t_f \quad \text{(A-41)}$$

$$\frac{\dot{D}_{ae}(t)}{K_5} = t^{-1.2} \qquad t \geq t_i \quad \text{(A-42)}$$

$$\frac{D_{ae}(t)}{K_5} = 5\left(t_i^{-0.2} - t^{-0.2}\right) \qquad t \geq t_i \quad \text{(A-43)}$$

where

$$K_1 = \frac{\dot{m}_{ae}\ a_i}{\rho_a}\ \frac{\text{gm(dust)}}{\text{hr}}$$

$$K_2 = \frac{\dot{m}_{af}\ a_i}{\rho_a}\ \frac{\text{gm(dust)}}{\text{hr}}$$

$$K_3 = \frac{C\ A_1\ \dot{m}_{af}\ a_i}{4\pi d^2\ \rho_a}\ \frac{\text{rads(tissue)}}{\text{hr}}$$

$$K_4 = \frac{C\, A_1\, a_i}{\mu'} \quad \frac{\text{rads(tissue)}}{\text{hr}}$$

$$K_5 = \frac{GCA_1}{4\pi d^2} \quad \frac{\text{rads(tissue)}}{\text{hr}} \qquad \text{(A-44)}$$

Note that the expression for the amount of dust ingested into the engine is functionally identical to the expression for the amount of dust trapped by the perfect filter. The only difference is in the constant, i.e., K_1 corresponds to the dust ingested by the engines and K_2 to the dust trapped by the filter. Therefore, these two equations were combined in equations A-32 through A-34.

7. GRAPHICAL RESULTS

These equations are all completely analytical and easy to solve for any given set of input parameters. Representative results have been obtained and are shown in figures A1 through A10. The ordinate in each case is the independent variable of interest nondimensionalized by the pertinent constant, i.e., K_1, K_2, K_3, K_4, or K_5. These results then are general. For a specific aircraft, threat, and mission profile, the constants can be determined and the specific results can be determined.

Figure A1 depicts the mass rate of flow of the dust to the engines or the filter. Fallout of the dust in the cloud is reflected in this figure through the decrease with time of the mass rate of flow of the dust. For a no-fallout situation, the mass rate of flow of dust would be constant. Therefore, fallout is a significant factor in this development. Figure A2 depicts the total mass ingested by the engines/trapped by the filter for two cloud entry times (TI), 10 minutes and 60 minutes after detonation. The total mass ingested/trapped as a result of a particular penetration duration (ΔT) is read from the ordinate at an exit time of $TF = TI + \Delta T$, for the curve corresponding to the proper TI.

Figures A3 and A4 depict the dose rates (at 1 meter) due to the dust trapped in the filter. Figure A3 corresponds to a TI of 10 minutes and figure A4 a TI of 60 minutes. Each figure depicts a family of curves corresponding to penetration durations of 2, 5, 10, 15, 30, 45, 60, 120, 300, and 600 minutes. The rapid decrease in the dose rates with time is due to two factors, the fallout

of the dust particles from the cloud, and the decrease in photon emission due to the normal decay process. Note that the dose rate does not go to zero after exit from the cloud because the dust trapped in the filter remains in the filter after cloud exit and is a source of ionizing dose.

Figures A5 and A6 depict the ionizing dose (at 1 meter) due to the dust trapped in the filter for cloud entry times of 10 and 60 minutes after detonation, respectively. The curves in the figure correspond to the same penetration durations given previously. Note that the dose rate and dose results are presented for a distance from the filter of 1 meter. These results can be related to other distances by multiplying the results by the factor $(1 \text{ meter})^2/(\text{distance in meters})^2$. Figure A7 depicts the dose rate due to the aircraft being immersed in the cloud. (The crew and all aircraft components are exposed equally to the photons emitted from the cloud, because the shielding provided by the aircraft is negligible.)

Figure A8 depicts the dose accumulated by the crew due to cloud immersion for TIs of 10 and 60 minutes after detonation. The dose accumulation is read by choosing the curve corresponding to the TI of interest, determining the cloud exit time, $TF = TI + \Delta T$, and reading the dose from the ordinate. Figure A9 depicts the dose rate (at 1 meter) per gram of dust accumulated on the aircraft exterior. Figure A10 depicts the dose (at 1 meter) per gram of dust accumulated on the aircraft exterior for TIs of 10 and 60 minutes after detonation.

This model is simple, easy to use, and its associated equations are completely analytical. For any given set of input parameters, i.e., Ks, TI, and ΔT, results can be obtained with only a slide rule. However, this model does not realistically represent the actual radioactive dust environment and its behavior with the time and may not yield realistic results.

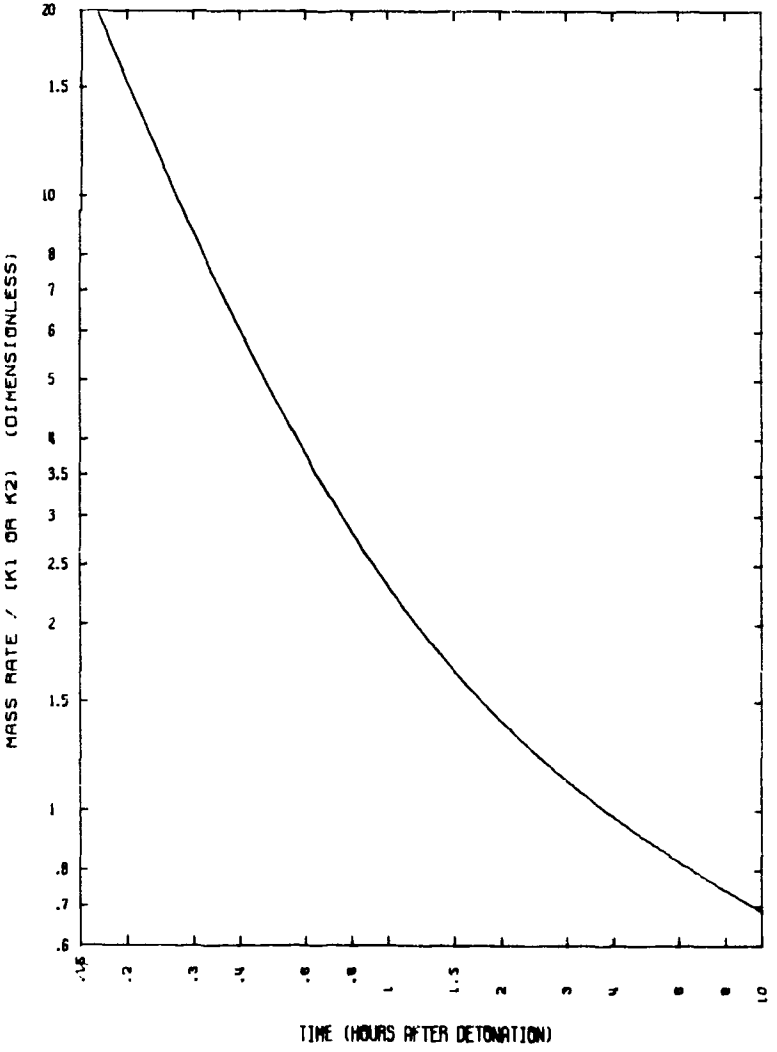

Figure A1. Mass Rate of Flow of Dust to Engines or Filter

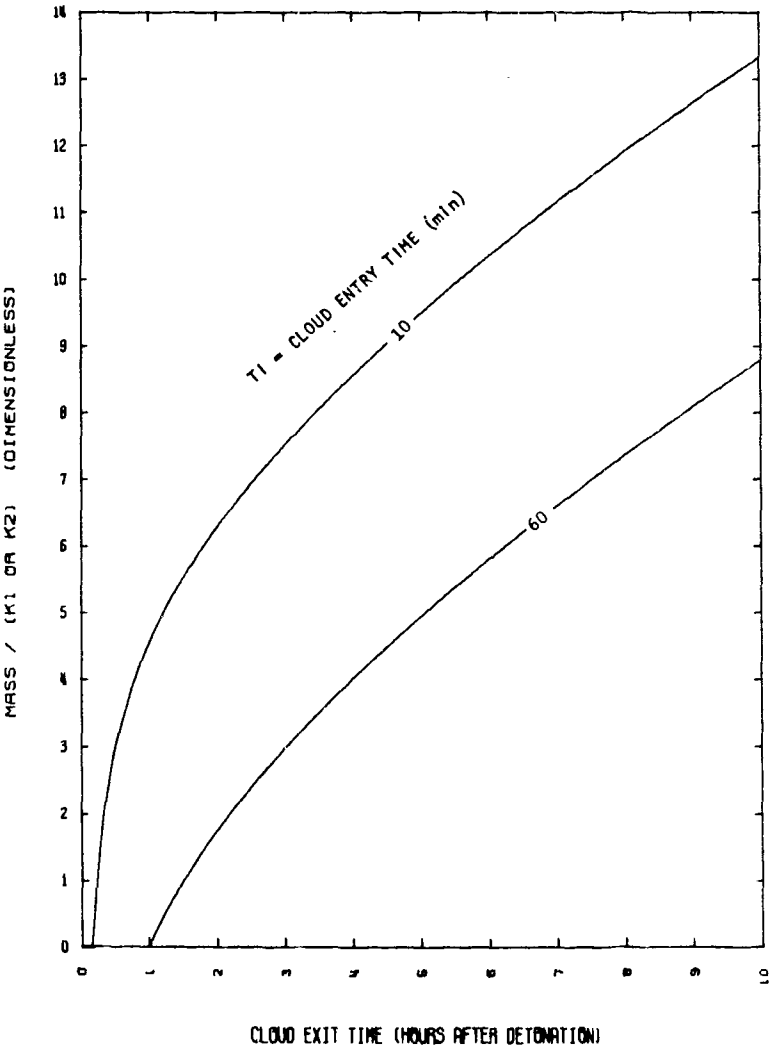

Figure A2. Filter/Engine Dust Mass as a Function of Time

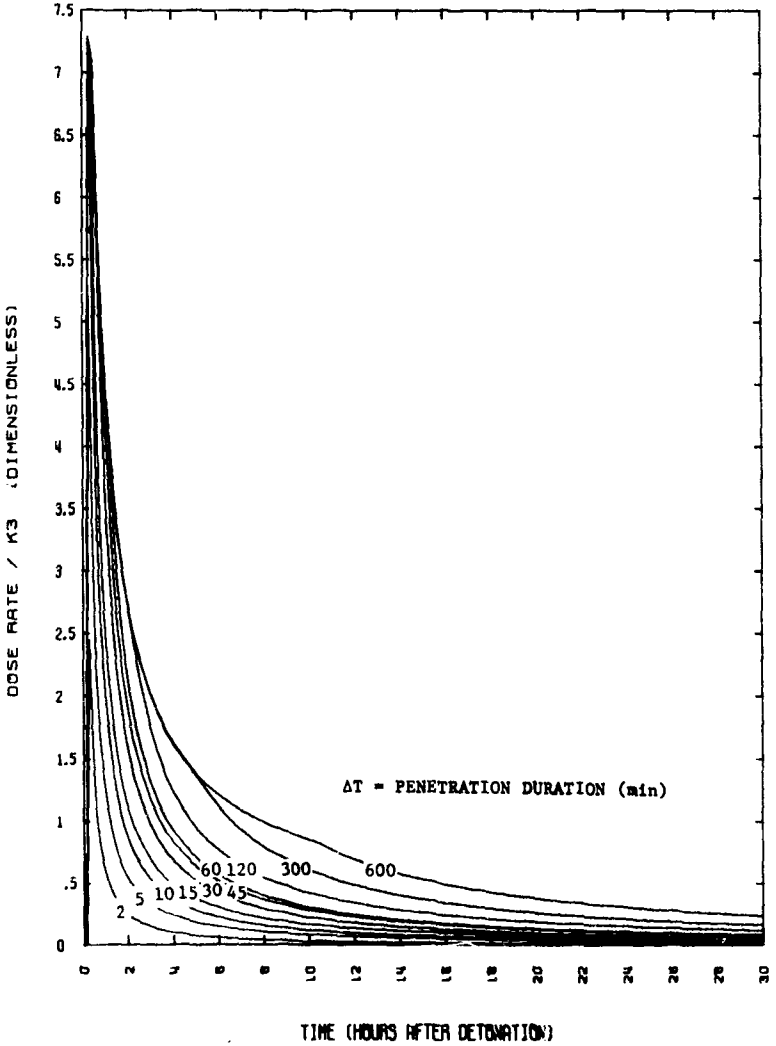

Figure A3. Dose Rate from Dust in Filter, TI = 10 Minutes

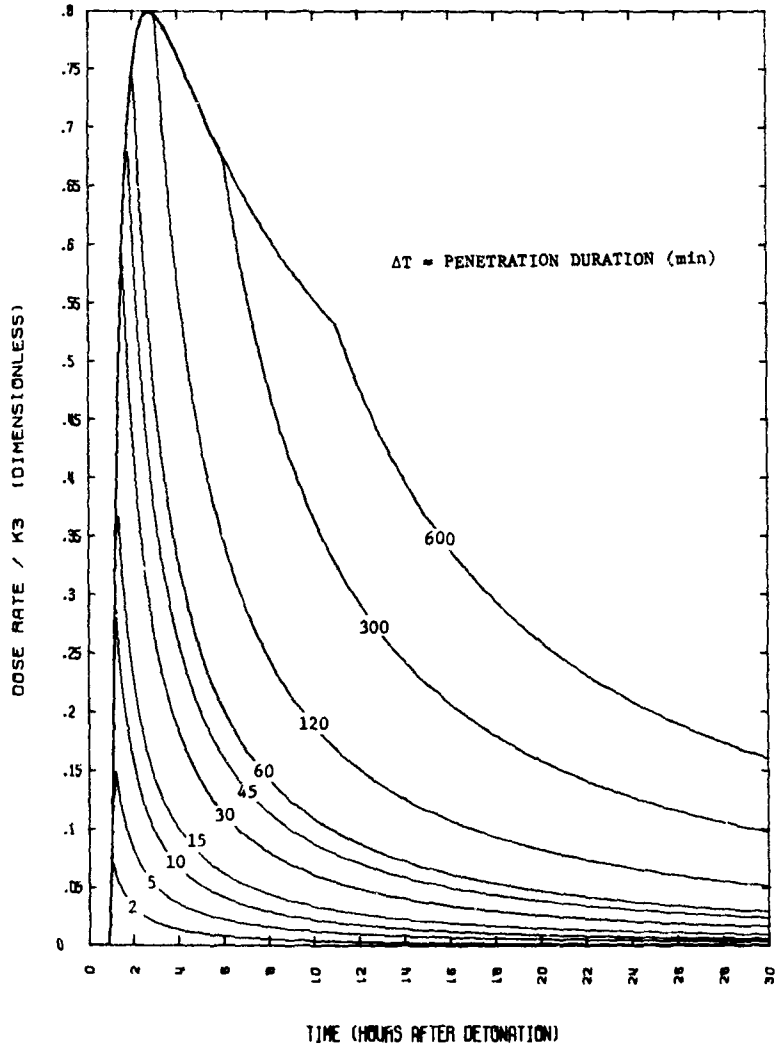

Figure A4. Dose Rate from Dust in Filter, TI = 1 Hour

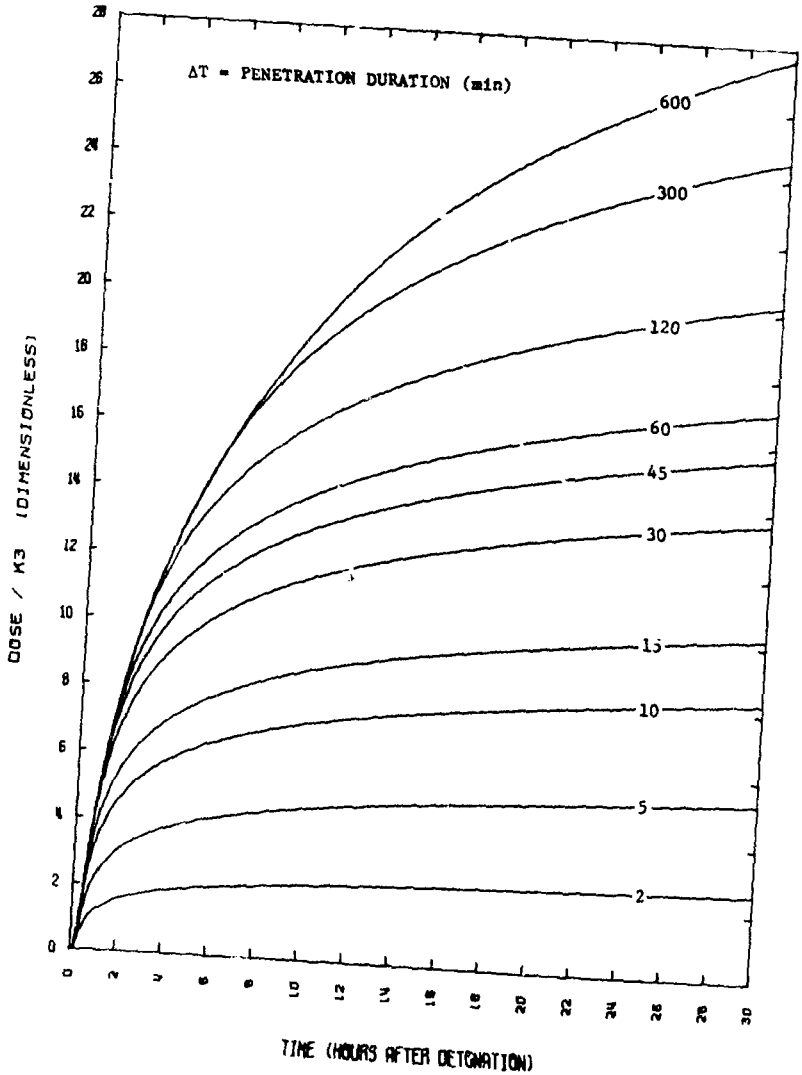

Figure A5. Radiation Dose from Dust in Filter, TI = 10 Minutes

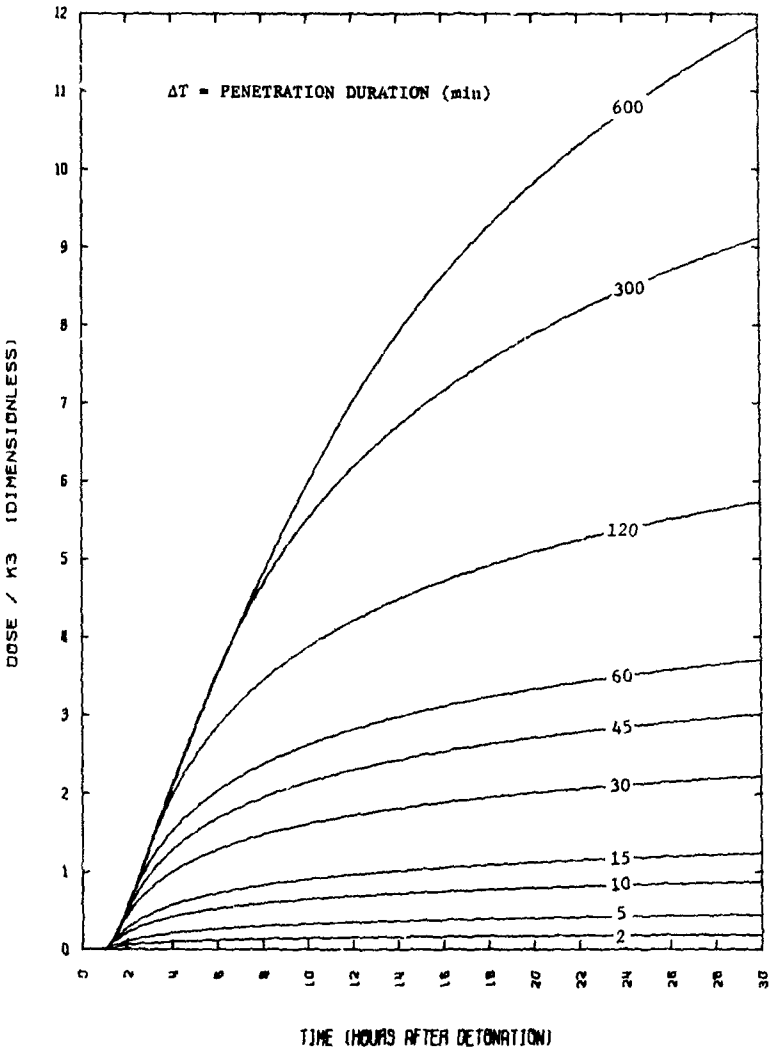

Figure A6. Radiation Dose from Dust in Filter, TI = 1 Hour

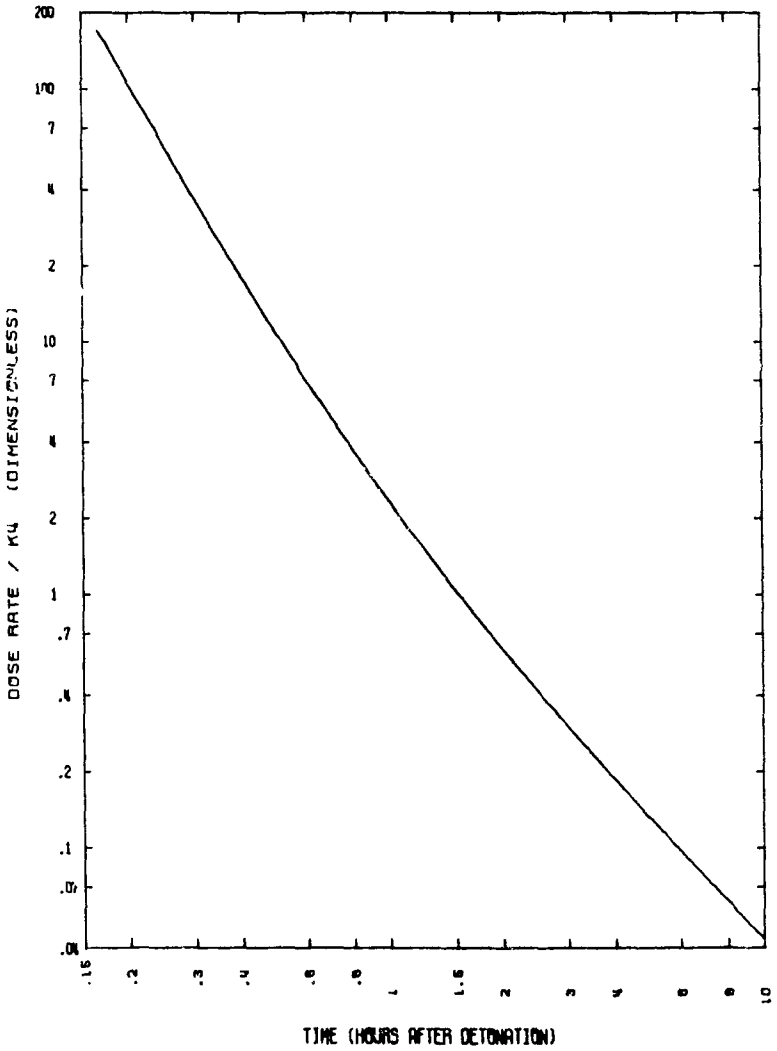

Figure A7. Cloud Immersion Dose Rate

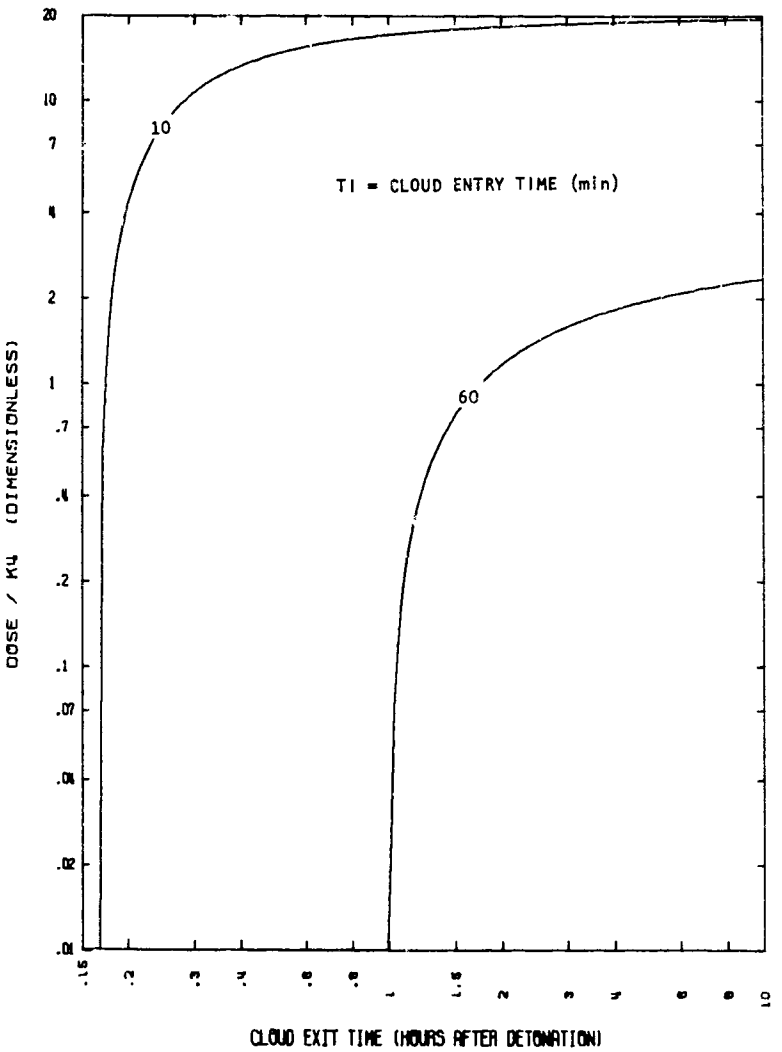

Figure A8. Cloud Immersion Dose

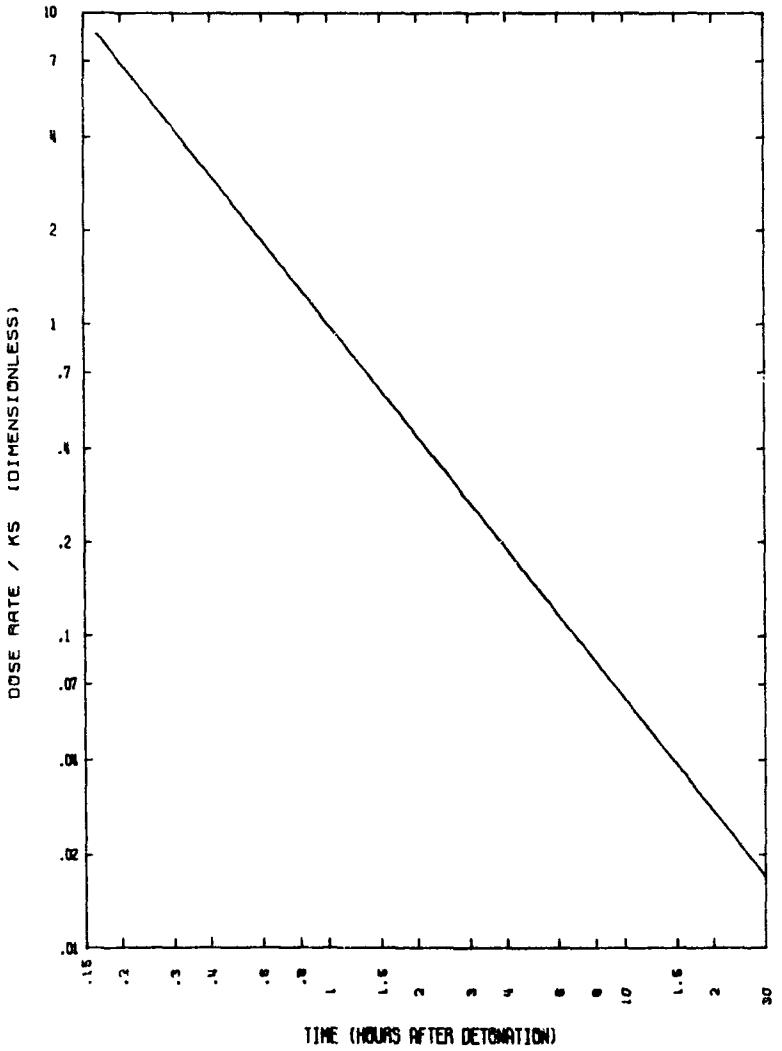

Figure A9. Dose Rate from Dust on Aircraft Exterior

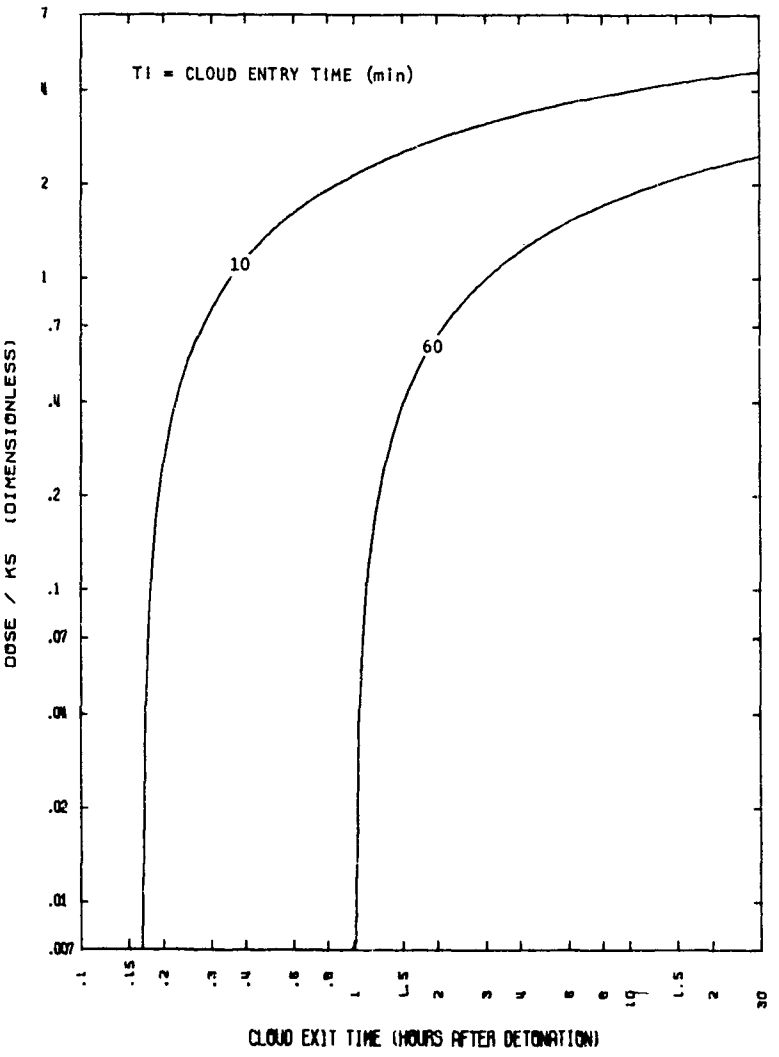

Figure A10. Radiation Dose from Dust on Aircraft Exterior

APPENDIX B

IMPROVED FALLOUT MODEL

In the previous appendix, a first cut, simple dust cloud model was developed. Because this model does not account for dependence of the results on particle size, the predicted results will not support additional detailed analyses. The lack of particle size dependence, in particular, handicaps the filter trapping analysis. For these reasons, it was decided to develop a more realistic model. This model and its predicted results will be investigated to determine if its more realistic results (compared to the Uniform Fallout Model) offset the added complexity of the model and associated equations. Although the equations associated with this approach appear to be rather complicated, in reality, they are relatively simple and straightforward. Relatively simple numerical techniques are employed to solve them using only a minute or so of computer time, rather than the hours required for the complex dust environment codes.

It is well known that very small particles, i.e., $r < 1\mu$, tend to remain suspended in the atmosphere almost indefinitely (ref. 9). One method of ultimate removal is by their being used as precipitation centers for water vapor and falling out with rain or other precipitation. The point is that they do not fall out, at least over the time period of interest. The settling velocity of very small particles is expressed in Stokes (ref. 10) as

$$V_s = 1.2 \times 10^5 \rho_r r_c^2 \qquad (B\text{-}1)$$

where V_s is the settling velocity in cm/sec, ρ_r is the density of the particle in gm/cm^3 and r_c the particle radius in centimeters. Substituting in the value of ρ_r for a representative soil, $\rho_r = 2$ gm/cm^3 and converting the radius to microns, then

$$V_s = 0.024\ r^2 \qquad (B\text{-}2)$$

where r is the particle radius in microns. The equation was derived with the assumption that the Reynold's Number based on the particle diameter and settling

velocity was very small, i.e.,

$$Re = \frac{2 \times \text{radius} \times V_s}{\nu_{air}} << 1 \qquad \text{(B-3)}$$

where ν_{air} is the viscosity of air. The relation is very accurate for the range of particle radius from 1 micron to 50 microns (ref. 9). Although Stoke's Law was derived for Re << 1, it has been found experimentally that there is good agreement between the theory and experiment up to RE ~ 1, where divergence begins, but agreement is still adequate up to RE ~ 10 (ref. 11). Therefore, the settling velocity concept is reasonably accurate up to a particle radius of about $10^3\mu$.* Based on review of available literature, the initial particle size distribution was assumed to be

$$f \sim r^{-3.5} \qquad \text{(B-4)}$$

with cutoffs at r = 0.1μ at the lower end and r = 10,000μ at the upper end. These cutoffs were based on intuition sharpened by study of available information. The upper limit was suggested by Whitaker's work (ref. 1) and the lower based on consideration of possible condensation patterns after a detonation. The assumption is made that

$$f(r) = N\, r^{-3.5} \qquad \text{(B-5)}$$

where f(r) is the total number of particles with radius r in a cubic centimeter, and N is the constant of porportionality. Then the mass per cubic centimeter of all the particles with radius r is

$$\rho_d(r) = \frac{m(r)}{cm^3} = \rho_r \frac{4}{3}\pi r^3 \; N\, r^{-3.5}$$

$$\rho_d(r) = \frac{4}{3}\rho_r N \pi r^{-0.5} \qquad \text{(B-6)}$$

*Although this concept breaks down for particle sizes greater than $10^3\mu$, equation (B-2) was used in the numerical integrations used to calculate the results in this appendix. Therefore, the results associated with particle sizes in excess of 1000μ are somewhat inaccurate.

where ρ_r is the density of each solid particle (assumed to be 2 gm/cm^3) and ρ_d is the standard dust density distribution (equation (3) in section II).

It has been shown that the larger particles tend to fall out faster than the small particles (ref. 9). It is assumed that all particles with the largest radius fall out before any of the next smaller radius. This is referred to as the "nibbling mouse" assumption, because the only change to the number distribution or the density with time is the disappearing end point. The end point can be envisioned to be in the process of being eaten by a mouse nibbling the curve at a "rate," R(t). Figures B1 and B2 show the number distribution and the density with cutoffs noted. These curves were obtained by fixing the constants involved in the following way. The following relation is forced to hold.

$$\rho_d(t) = \int_{0.1}^{R(t)} \rho_d(r)\, dr \qquad \text{(B-7)}$$

where ρ_d is defined by equation (3) in section II. Note that the time dependence of the density distribution with r enters only through the upper limit of the integral. The value of R(t) at 10 minutes (or 0.167 hour) is defined to be 10^4 microns. The above relation evaluated at 10 minutes after detonation fixes the value of the constant N. Therefore,

$$f(r,t) = 1.2 \times 10^{10}\, a_i\, r^{-3.5} \qquad 0.1 \le r \le R(t) \qquad \text{(B-8)}$$

$$\rho_d(r,t) = 9.9 \times 10^{-2}\, a_i\, r^{-0.5} = 9.9 \times 10^{-2}\, K_7\, r^{-0.5} \qquad 0.1 \le r \le R(t) \qquad \text{(B-9)}$$

where $K_7 = a_i$ gm(dust)/cm^3, a nondimensionalizing constant. Recall that

$$\rho_d(t) = 9.9 \times 10^{-2}\, a_i \int_{0.1}^{R(t)} r^{-0.5}\, dr$$

or

$$\rho_d(t) = 0.2\, a_i \left[R(t)^{0.5} - 0.316\right] \qquad \text{(B-10)}$$

To determine R(t) note that equation (B-10) must hold for all t. Therefore,

$$a_i \left(t^{-1.6} + 1.313\ t^{-0.3}\right) = 0.2\ a_i \left[R(t)^{1/2} - 0.316\right] \qquad \text{(B-11)}$$

which results in

$$R(t) = \left[5.04 \left(t^{-1.6} + 1.313\ t^{-0.3}\right) + 0.316\right]^2 \qquad \text{(B-12)}$$

The density distribution function is completely defined as a function of particle size and time; the specific activity must now be determined. It appears reasonable to assume that the activity of the smaller particles is proportional to the entire particle mass which is predominately condensed bomb debris, and that of larger particles is proportional to the mass of the surface coating on the particle which is condensed bomb debris. If this assumption is made then the specific activity per particle is given by

$$A_{particle} \sim r^3 \qquad 0.1 \leq r \leq \delta \qquad \text{(B-13)}$$

$$A_{particle} \sim r^2 \qquad \delta \leq r \leq 10^4 \qquad \text{(B-14)}$$

where δ is the somewhat arbitrary boundary (assumed from hereon to be 20μ) separating the region where particles are assumed to be composed entirely of condensed debris and the region where particles are assumed to be coated with bomb debris.

Relating the activity to the mass of each particle, then

$$A(r,t) = f_1\ t^{-1.2} \qquad 0.1 \leq r \leq \delta \qquad \text{(B-15)}$$

$$A(r,t) = f_2\ r^{-1}\ t^{-1.2} \qquad \delta \leq r \leq 10^4 \qquad \text{(B-16)}$$

Making use of the condition that at $r = \delta$,

$$A(r,t)_{r \to \delta^-} = A(r,t)_{r \to \delta^+} \qquad \text{(B-17)}$$

This results in the relation

$$f_2 = f_1 \delta \qquad \text{(B-18)}$$

To evaluate the constant, one other condition is needed. The condition chosen was based on the physical situation. It is assumed that the 10 minute conditions in all the fallout models considered are identical. Therefore, the total number of fission fragments, the photons per unit area of an immersed body, and the dose rates for both cases are equal at 10 minutes after detonation. For the Uniform Fallout Model,

$$\dot{D}_c(t) = \frac{C}{\mu'} \rho_d(t)\, A(t) \tag{B-19}$$

For the Improved Fallout Model

$$\dot{D}_c(t) = \frac{C}{\mu'}\left[\int_{0.1}^{\delta} \rho_d(r)\, A(r,t)\, dr + \int_{\delta}^{R(t)} \rho_d(r)\, A(r,t)\, dr\right] \tag{B-20}$$

and it was assumed that

$$\dot{D}_{c\ \text{improved}}(0.167) = \dot{D}_{c\ \text{uniform}}(0.167) \tag{B-21}$$

Performing the necessary operations and simplifying, the following is obtained.

$$f_1 = \frac{99.684_1}{2d^{0.5} - 0.01\ \delta - 0.316} = 11.83\ A_1 \tag{B-22}$$

$$f_2 = \delta\, a = 236.55\ A_1 \tag{B-23}$$

where A_1 is defined in appendix A and $\delta = 20\mu$. Therefore,

$$A(r,t) = 11.83\ A_1\ t^{-1.2} \qquad 0.1 \le r \le 20\mu \tag{B-24}$$

$$A(r,t) = \frac{236.55\ A_1\ t^{-1.2}}{r} \qquad 20\mu \le r \le 10^4\mu \tag{B-25}$$

Note that the specific activity is applicable from r = 0.1 to r = 10^4 for all t. The "nibbling mouse" is not applied to the activity because the activity is per gm of dust.

The cloud parameters are now defined and using the same assumptions mentioned earlier, i.e., zero wind, etc., the mass rate, mass dose rate, and dose calculations performed earlier are repeated using the newly derived cloud characteristics, which are now particle size dependent.

The mass trapped in the filter as a function of time and particle size is determined assuming that all the dust is trapped by the filter.

$$\dot{M}_f(r,t) = \frac{\dot{m}_{af}}{\rho_s} \rho_d(r,t) \tag{B-26}$$

or

$$\frac{\dot{M}_f(r,t)}{K_2} = 9.946 \times 10^{-2}\, r^{-0.5} \qquad 0.1\mu \le r \le R(t) \tag{B-27}$$

where K_2 is the same as defined in equation (A-44) in appendix A.

The total mass trapped is the integral over time of the above relation.

$$\frac{M_f(r,t)}{K_2} = 9.946 \times 10^{-2}\, r^{-0.5}\,(t - t_i) \qquad 0.1\mu \le r \le R(t) \tag{B-28}$$

$$\frac{M_f(r,t)}{K_2} = 9.946 \times 10^{-2}\, r_n^{-0.5}\,(t_n - t_i) \qquad R(t) \le r_n \le R(t_i) \tag{B-29}$$

where $t_i \le t_n \le t$, and $r_n = R(t_n)$. Equation (B-29) is handled with numerical techniques for plotting purposes.

This combination of analytical and numerical techniques is necessary because of the "nibbling mouse." Figure B3 is representative of the mass rate of flow of dust into the filter, $\dot{M}_f(r,t)$. Note that it is a simple prism with the "nibbling mouse" eating away at the edge. Figure B4 is a representation of the mass of dust collected in the filter. This three-dimensional figure is considerably more complex than the previous figure. "Slices" of three-dimensional figure B4 for various (t_i, t_f) sets are presented in figures B5 through B13.

This $\dot{M}_f(r,t)$ equation set can be integrated over r and then evaluated at t_f to give an equation set, which represents the cumulative mass (CM_f) as a function of r, for some (t_i, t_f).

$$\frac{CM_f(r)}{K_2} = 0.1989 \left(r^{0.5} - 0.3162\right)(t_f - t_i) \qquad 0.1 \leq r \leq R(t_f) \quad \text{(B-30)}$$

$$\frac{CM_f(r)}{K_2} = 0.1989 \left[R(t_f)^{0.5} - 0.3162\right] (t_f - t_i) + 9.946 \times 10^{-2} \sum_{R(t_f)}^{R(t_i)} r_n^{-0.5}(t_n - t_i)\Delta r \qquad R(t_f) \leq r_n \leq R(t_i) \quad \text{(B-31)}$$

Note that the second equation must be integrated numerically. These results are presented in figures B14 through B22. Figure B23 presents the total mass collected by the filter as a function of time after weapon detonation for the TIs of interest. The total mass results in this figure are identical to the results in figure A2 in appendix A.

These results may be used to directly determine the total mass (and its size distribution) ingested by the engine in the same manner as discussed in the Uniform Fallout Model Analysis.

Now consider the dose rate and dose which are associated with the dust trapped in the filter. This dust acts as a source of photons which could affect the crew/electronic equipment. The dose rate can be written as

$$\dot{D}_f(r,t) = \frac{C}{4\pi d^2} M_f(r,t)\, A(r,t) \quad \text{(B-32)}$$

Substituting, the following set of equations is obtained.

$t_i \leq t \leq t_f$

$$\frac{\dot{D}_f(r,t)}{K_3} = 1.176\, r^{-0.5}\, (t - t_i)\, t^{-1.2} \qquad 0.1 \leq r \leq 20 \quad \text{(B-33)}$$

$$\frac{\dot{D}_f(r,t)}{K_3} = 23.52\, r^{-1.5}\, (t - t_i)\, t^{-1.2} \qquad 20 \leq r \leq R(t) \quad \text{(B-34)}$$

$$\frac{\dot{D}_f(r,t)}{K_3} = 23.52\, r_n^{-1.5}\, (t_n - t_i)\, t^{-1.2} \qquad R(t) \leq r_n \leq R(t_i) \quad \text{(B-35)}$$

$t \geq t_f$

$$\frac{\dot{D}_f(r,t)}{K_3} = 1.176\ r^{-0.5}\ (t_f - t_i)\ t^{-1.2} \qquad 0.1 \leq r \leq 20 \qquad \text{(B-36)}$$

$$\frac{\dot{D}_f(r,t)}{K_3} = 23.52\ r^{-1.5}\ (t_f - t_i)\ t^{-1.2} \qquad 20 \leq r \leq R(t_f) \qquad \text{(B-37)}$$

$$\frac{\dot{D}_f(r,t)}{K_3} = 23.52\ r_n^{-1.5}\ (t_n - t_i)\ t^{-1.2} \qquad R(t_f) \leq r_n \leq R(t_i) \qquad \text{(B-38)}$$

From these, the dose distribution as a function of size r for a (t_i, t_f) set can be obtained by integrating over t. The distribution can be determined at any time after detonation. The time of most interest here is the time of mission completion (T_{mc}). The complete set of equations for $T_{mc} > t_f$ and $R(t_f) > 20\mu$ is

$0.1 \leq r \leq 20$

$$\frac{D_f(r)}{K_3} = 5.88\ r^{-0.5} \left[1.25\ \left(t_f^{0.8} - t_i^{0.8}\right) + T_{mc}^{-0.2}\ (t_i - t_f)\right] \qquad \text{(B-39)}$$

$20 \leq r \leq R(t_f)$

$$\frac{D_f(r)}{K_3} = 117.6\ r^{-1.5} \left[1.25\ \left(t_f^{0.8} - t_i^{0.8}\right) + T_{mc}^{-0.2}\ (t_i - t_f)\right] \qquad \text{(B-40)}$$

$R(t_f) \leq r_n \leq R(t_i)$

$$\frac{D_f(r)}{K_3} = 117.6\ r_n^{-1.5} \left[1.25\ \left(t_n^{0.8} - t_i^{0.8}\right) + T_{mc}^{-0.2}\ (t_i - t_n)\right] \qquad \text{(B-41)}$$

where $r_n = R(t_n)$ and $t_i \leq t_n \leq t_f$.

If $R(t_f) < 20\mu$, then the above set of equations becomes

$0.1 \leq r \leq R(t_f)$

$$\frac{D_f(r)}{K_3} = 5.88\, r^{-0.5} \left[1.25\left(t_f^{0.8} - t_i^{0.8}\right) + T_{mc}^{-0.2}\,(t_i - t_f)\right] \qquad \text{(B-42)}$$

$R(t_f) \leq r \leq 20$

$$\frac{D_f(r)}{K_3} = 5.88\, r_n^{-0.5} \left[1.25\left(t_n^{0.8} - t_i^{0.8}\right) + T_{mc}^{-0.2}\,(t_i - t_n)\right] \qquad \text{(B-43)}$$

$20 \leq r \leq R(t_i)$

$$\frac{D_f(r)}{K_3} = 117.6\, r_n^{-1.5} \left[1.25\left(t_n^{0.8} - t_i^{0.8}\right) + T_{mc}^{-0.2}\,(t_i - t_n)\right] \qquad \text{(B-44)}$$

These equations are plotted in figures B24 through B32.

Integrating this set over r gives a cumulative-dose-as-a-function-of-r set of equations. Note that again numerical integration must be used in parts of the evaluation. For $R(t_f) \geq 20\mu$,

$0.1 \leq r \leq 20$

$$\frac{CD_{f_1}(r)}{K_3} = 11.76 \left[1.25\left(t_f^{0.8} - t_i^{0.8}\right) + T_{mc}^{-0.2}\,(t_i - t_f)\right]\left(r^{0.5} - 0.316\right) \qquad \text{(B-45)}$$

$20 \leq r \leq R(t_f)$

$$\frac{CD_{f_2}(r)}{K_3} = \frac{CD_{f_1}(20)}{K_3} + 235.7 \left[1.25\left(t_f^{0.8} - t_i^{0.8}\right) + T_{mc}^{-0.2}\,(t_i - t_f)\right]\left[0.2236 - r^{-0.5}\right] \qquad \text{(B-46)}$$

$R(t_f) \leq r_n \leq R(t_i)$

$$\frac{CD_{f_3}(r)}{K_3} = \frac{CD_{f_2}\left(R(t_f)\right)}{K_3} + 117.6 \sum_{R(t_f)}^{R(t_i)} \left[1.25 \left(t_n^{0.8} - t_i^{0.8}\right) + T_{mc}^{-0.2} (t_i - t_n)\right] r_n^{-1.5} \Delta r \qquad \text{(B-47)}$$

where $r_n = R(t_n)$ and $t_i \leq t_n \leq t_f$.

If $R(t_f) \leq 20\mu$, the preceding set of equations becomes

$0.1 \leq r \leq R(t_f)$

$$\frac{CD_{f_1}(r)}{K_3} = 11.76 \left[1.25 \left(t_f^{0.8} - t_i^{0.8}\right) + T_{mc}^{-0.2} (t_i - t_f)\right] (r^{0.5} - 0.316) \qquad \text{(B-48)}$$

$R(t_f) \leq r \leq 20$

$$\frac{CD_{f_2}(r)}{K_3} \quad \frac{CD_{f_1}\left(R(t_f)\right)}{K_3} + 5.88 \sum_{R(t_f)}^{20} \left[1.25 \left(t_n^{0.8} - t_i^{0.8}\right) + T_{mc}^{-0.2} (t_i - t_n)\right] r_n^{-0.5} \Delta r \qquad \text{(B-49)}$$

$20\mu \leq r \leq R(t_i)$

$$\frac{CD_{f_3}(r)}{K_3} \quad \frac{CD_{f_2}(20)}{K_3} + 117.6 \sum_{20}^{R(t_i)} \left[1.25 \left(t_n^{0.8} - t_i^{0.8}\right) + T_{mc}^{-0.2} (t_i - t_n)\right] r_n^{-1.5} \Delta r \qquad \text{(B-50)}$$

where $r_n = R(t_n)$ and $t_i \leq t_n \leq t_f$. These equations are plotted in figures B33 through B41 in semilog scaling for better accuracy at the higher dose levels and figures B42 through B50 in log-log scaling for better accuracy for the lower dose levels.

Another useful set of equations can be determined by taking equations (B-33) through (B-38) and integrating out the size dependence to obtain the dose as a function of time. Again a numerical technique must be used, and $r_n = R(t_n)$ with $t_i \leq t_n \leq t_f$. For $t_i \leq t \leq t_f$ and if $R(t) \geq 20\mu$

$$\frac{D_{f_1}(t)}{K_3} = \left(101.46 - 235.27\, R(t)^{-0.5}\right)\left(0.25\, t^{0.8} - 1.25\, t_i^{0.8} + t_i t^{-0.2}\right) + 117.6\left(t_i^{-0.2} - t^{-0.2}\right)\sum_{R(t)}^{R(t_i)} r_n^{-1.5}\,(t_n - t_i)\,\Delta r \qquad \text{(B-51)}$$

if $R(t) < 20\mu$

$$\frac{D_{f_2}(t)}{K_3} = \left(11.76\, R(t)^{0.5} - 3.7185\right)\left(0.25\, t^{0.8} - 1.25\, t_i^{0.8} + t_i t^{-0.2}\right) + \left(t_i^{-0.2} - t^{-0.2}\right)\left[5.88 \sum_{R(t)}^{20} r_n^{-0.5}\,(t_n - t_i)\,\Delta r + 117.6 \sum_{20}^{R(t_i)} r_n^{-1.5}\,(t_n - t_i)\,\Delta r\right] \qquad \text{(B-52)}$$

For times after t_f, i.e., $t > t_f$, the equations become, for $R(t_f) > 20\mu$,

$$\frac{D_f(t)}{K_3} = \left(t_f^{-0.2} - t^{-0.2}\right)\left[(t_f - t_i)\left(101.46 - 235.27\, R(t_f)^{-0.5}\right) + 117.6 \sum_{R(t_f)}^{R(t_i)} r_n^{-1.5}\,(t_n - t_i)\,\Delta r\right] + \frac{D_{f_1}(t_f)}{K_3} \qquad \text{(B-53)}$$

If $R(t_f) < 20\mu$, this set of equations becomes

$$\frac{D_f(t)}{K_3} = \left(t_f^{-0.2} - t^{-0.2}\right)\left[(t_f - t_i)\left(11.76\, R(t_f)^{0.5} - 3.7185\right) + 5.88 \sum_{R(t_f)}^{20} r_n^{-0.5}\,(t_n - t_i)\,\Delta r + 117.6 \sum_{20}^{R(t_i)} r_n^{-1.5}\,(t_n - t_i)\,\Delta r\right] + \frac{D_{f_2}(t_f)}{K_3} \qquad \text{(B-54)}$$

The filter dose as a function of time is plotted for several TI and TF combinations in figures B51 through B59.

The dose rate in a cloud is

$$\dot{D}_c(r,t) = \frac{C}{\mu'} \rho_d(r,t)\ A(r,t) \qquad \text{(B-55)}$$

or

$$\frac{\dot{D}_c(r,t)}{K_4} = 1.176\ r^{-0.5}\ t^{-1.2} \qquad 0.1\mu \leq r \leq 20 \qquad \text{(B-56)}$$

$$\frac{\dot{D}_c(r,t)}{K_4} = 23.527\ r^{-1.5}\ t^{-1.2} \qquad 20 \leq r \leq R(t) \qquad \text{(B-57)}$$

Integrating over r

$$\frac{\dot{D}_c(t)}{K_4} = 47.054\ t^{-1.2} \left(0.4314 - R(t)^{-0.5}\right) \qquad \text{(B-58)}$$

The dose then is

$$\frac{D_c(t)}{K_4} = 47.054 \left[2.157 \left(t_i^{-0.2} - t^{-0.2}\right) - \sum_{t_i}^{t} R(t)^{-0.5}\ t^{-1.2}\ \Delta t \right] \qquad \text{(B-59)}$$

The dose rate and the dose are presented in figures B60 and B61.

In all these relations the summation symbol indicates numerical integration, and the integral symbol analytical integration. Extensive checks of the numerical techniques used were made to ensure reasonable accuracy. Comparing figures B33 and B51, it is seen that the two different approaches yield results at t = 30 hours very close in value, i.e., to about 1 percent.

It is noted again that these results are applicable for the 100-percent efficient filter.

GRAPHICAL RESULTS

The equations associated with this model are considerably more complex than those associated with the simpler Uniform Fallout Model, and dictate the use of numerical techniques to obtain numerical results. Therefore, extensive graphical results are presented to support accurate interpolation. This model is more realistic than the Uniform Fallout Model, but could be further refined by inclusion of the dependence of the dust density on altitude as a function of time and the use of a better, more mathematically precise number distribution, i.e., refine the "nibbling mouse" assumption. The above refinements might provide more accurate results, but the increase in accuracy would probably not be significant.

The graphical results themselves will now be discussed to illustrate their use. Recall that the filter used in this development was a perfect filter. It collects all ingested dust particles for the penetration Δl. When the aircraft exits the cloud at TF = TI + ΔT, no more particles are collected. The trapped mass distribution results are shown in figures B5 through B13. Each graph presents the dust mass collected by the filter as a function of particle size for a particular TI and with penetration duration, ΔT, as a parameter. Each graph considers ΔTs of 2, 5, 10, 15, 30, 60, 120, and 300 minutes. These figures are for cloud entry times ranging from 10 minutes to 5 hours after weapon detonation, which should cover the range of interest for most analyses. Particle size distributions range from 0.1 micron to 10,000 microns radius. A comparison of figure B5 for a cloud entry time of 10 minutes with figure B13 for a cloud entry time of 5 hours shows the appreciable effect of fallout on the results. At TI = 10 minutes a sizable portion of the mass consists of particles with r > 10 microns; whereas, for TI = 5 hours all of these particles have fallen out prior to aircraft entry, and thus no particles in this size range are collected by the filter.

The second series of perfect filter graphs, figures B14 through B22, presents the cumulative mass collected by the filter for a particular TI, as a function of particle size and in terms of the same range of parameters ΔT. Cumulative mass $CM_f(r)$, means the dust mass collected by the filter represented by dust particles which have sizes less than or equal to r. If $M_f(r)$ represents the dust

mass distribution function for the filter as a function of particle size r for a TI, ΔT case, then

$$CM_f(r) = \int_0^r M_f(r)\, dr \qquad \text{(B-60)}$$

Figures B14 through B22 present these results for cloud entry times ranging from 10 minutes to 5 hours. To further clarify the meaning of these figures, consider for a moment figure B14. This figure gives the cumulative mass collected by the filter as a function of particle size for a cloud entry time of TI = 10 minutes. For illustration purposes select a penetration duration of ΔT = 30 minutes, then focus on the question of how much dust will be collected which has particle sizes ranging up to 50 microns. Entering the abscissa at 50 microns and moving up to the curve corresponding to ΔT = 30 minutes, a result of 0.67 K_2 grams is obtained from the ordinate. Similarly 2.2 K_2 grams of dust particles with sizes up to 500 microns have been collected by the perfect filter for the the same entry time of 10 minutes and penetration duration of 30 minutes.

The cumulative mass collected for particle sizes up to 10,000 microns represents the total mass collected by the filter since this represents the upper limit of particle sizes considered in the analysis. Figure B23 presents the total mass collected by the perfect filter as a function of time after weapon detonation with cloud entry time as a parameter. Results for cloud entry times of 10, 18, 30, 45, 60, 90, 120, 180, and 300 minutes are included in this figure. As an example of the utility of this figure consider the following: How many grams of dust would be collected by a perfect filter in the aircraft environmental control system if it entered the cloud at TI = 30 minutes and exited the cloud after a penetration duration ΔT = 30 minutes? In this example, note that the aircraft exits the cloud at TF = TI + ΔT = 60 minutes = 1 hour after weapon detonation. Enter the abscissa at TF = 1 hour and move up to the parametric curve for TI = 30 minutes and read from the ordinate the fact that 1.6 K_2 grams of dust have been collected by the filter. The total mass of dust collected is an extremely strong function of cloud entry time, which again attests to the fact that fallout effects are significant in the analysis.

Curves pertaining to the filter dust mass distribution function, cumulative mass, and total mass collected by the filter are in themselves useful from a filter design standpoint. However, another major factor must be considered.

The dust particles collected by the filter are a source of radioactivity which is carried with the aircraft and contributes dose to the crew/electronics in the vicinity of the filter. Dose calculations from this source have been made and are based upon several assumptions. The filter is assumed to be a point source of radioactivity emitting gamma rays with an average energy of 1 MeV. The resultant dose calculated corresponds to a dose "at-1-meter" so that a simple correction factor of $(1 \text{ meter}/d \text{ meters})^2$ can be applied to the results to correct for actual separation distance of crew/electronics from the filter.

The product of the mass distribution function and the specific activity distribution function is involved in the filter dose calculations. In addition, after the aircraft exits from the cloud, the dust previously collected continues to contribute to the dose until the mission is completed. Thus, to present the results, a particular time after weapon detonation must be selected as a baseline, and in this work the dose data are presented at a time of 30 hours after weapon detonation. These results can be scaled to other times, as will be demonstrated.

Figures B24 through B32 present the resultant perfect filter dose distribution function as a function of particle size and with penetration duration as a parameter for a particular cloud entry time, TI. The penetration durations presented on each figure are 2, 5, 10, 15, 30, 60, 120, and 300 minutes, and each separate curve presents results for a particular cloud entry time in the range from 10 minutes to 5 hours. Again the effects of fallout can be easily observed by a comparison of early and late cloud entry data, for there is no dose contribution from large particle sizes for late cloud entry time. Although not as noticeable, it can be also observed that the exponential radioactive decay law has been included in the analysis, figures B33 through B50.

The next series of figures presents data on the cumulative filter dose at 30 hours after weapon detonation as a function of particle size. Figures B33 through B41 use semi-log scaling and figures B42 through B50 use log-log scaling. These sets of graphs depict the same data and both are presented to facilitate the accurate interpretation of the numerical values. The term cumulative filter dose is defined as that portion of the total dose attributable to all particles collected which have sizes less than or equal to r. These figures present this cumulative dose for cloud entry times from 10 minutes to 5 hours, and in each

figure results are presented over the range of penetration durations of 2, 5, 10, 15, 30, 60, and 120 minutes. As an example of the use of these curves consider the following question: For a cloud entry time of 10 minutes and a penetration duration of 15 minutes, how much of the "at-1-meter" filter dose collected during the 30 hours after weapon detonation is attributable to particles with particle sizes of 10 microns radius or less? In figure B33 enter the abscissa at 10 microns, move up to the parametric curve for a 15-minute penetration duration, and read the filter dose of 6.5 K_3 rads(tissue). The dose attributable to all particles for these same conditions is 19 K_3 rads(tissue) so that the particles with size of 10 microns or less contribute approximately one-third of the total dose. From figure B41, for later entry times, i.e., 5 hours, and for the same 15-minute penetration duration, the smaller particles with $r \leq 10$ microns contribute 1.8 K_3 rads(tissue) out of 2.7 K_3 rads(tissue). Figures B51 through B59, for the perfect filter case, provide the total dose "at-1-meter" due to all particles collected by the filter as a function of time after weapon detonation and with penetration duration as a parameter. In these figures results are presented for penetration durations ranging from 2 minutes to 120 minutes, and each figure is for a particular entry time in the range from 10 minutes to 5 hours. For the baseline case of TI = 30 minutes and ΔT = 30 minutes, note from figure B53 that 24 K_3 rads(tissue) would be accumulated by a crew member located "at-1-meter" from the filter at 30 hours after weapon detonation due to dust collected by the filter.

This set of figures, figures B51 through B59, for the perfect filter case also provides the basis for scaling the previous dose results (i.e., figures B24 through B50) which were presented at 30 hours after weapon detonation to earlier times. A time-scaling factor (TSF) can be obtained from this series of curves and used to scale the 30-hour results to the particular time of interest. The time-scaling factor is defined as

$$TSF = \frac{D(t)}{D_f(30 \text{ hours})} \qquad \text{(B-61)}$$

where $D_f(t)$ is the filter dose at time t after detonation ($t_f \leq t \leq 30$ hours), and $D_f(30 \text{ hours})$ is the filter dose at t = 30 hours. Both doses are obtained from the appropriate figure (figures B51 through B59) for a particular case

of interest (defined by a particular TI and ΔT). To obtain the filter dust dose distribution function or the cumulative filter dose at some time other than 30 hours, multiply the ordinate of the appropriate figure by the time-scaling factor.

To further clarify the use of the time-scaling factor, consider the following example. Assume that the aircraft lifts off at midnight and at 0600 it enters a radioactive dust cloud resulting from the baseline massive multiburst dust environment. Assume further that the weapons were detonated at 0530. Thus, the aircraft cloud entry time is 30 minutes after detonation. Assume also that at 0630 the aircraft exits the cloud. Thus, the penetration duration ΔT = 30 minutes and cloud exit time is TF = TI + ΔT = 60 minutes after weapon detonation. Assume finally that the aircraft completes its mission and lands at a base at 1200 hours. The landing time corresponds to a time of t = 6.5 hours after weapon detonation. From figure B53, D_f(30 hours) = 24 K_3 rads(tissue) and $D_f(t)$ = D_f(6.5 hours) = 16 K_3 rads(tissue). The 16 K_3 rads(tissue) is the filter dose (at-1-meter) which would be accumulated by the crew. The time-scaling function (TSF) is 16 K_3/24 K_3 = 0.67. The 6.5-hour dose distribution as a function of particle size and the 6.5-hour cumulative dose as a function of particle size are obtained by scaling the 30-hour results in figures B26, B35, and B44 by the time-scale factor, 0.67.

Since crew response to radiation is dependent upon the dose rate as well as the dose received, figures B62 through B70 are included. These filter dust rate graphs are nondimensionalized by K_3 and are given for the same TI, ΔT cases as the filter dust dose graphs.

Also of interest is the specific activity distribution function, equations (B-24) and (B-25), which is shown graphically in figure B71.

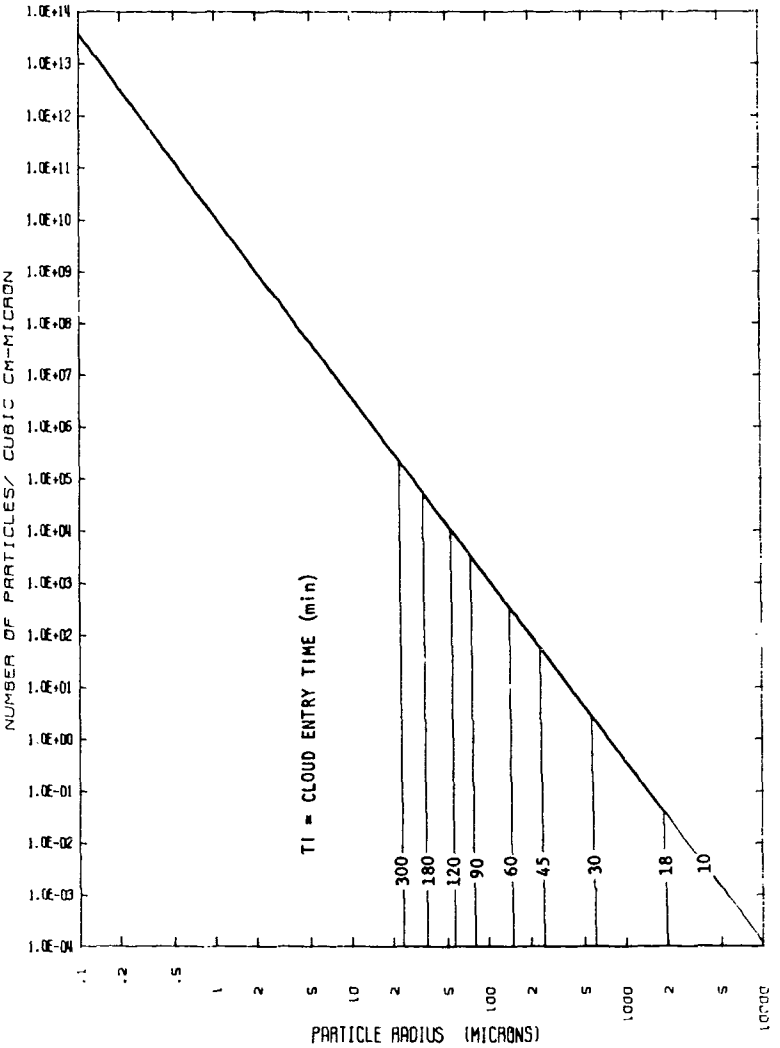

Figure B1. Particle Size Distribution Function

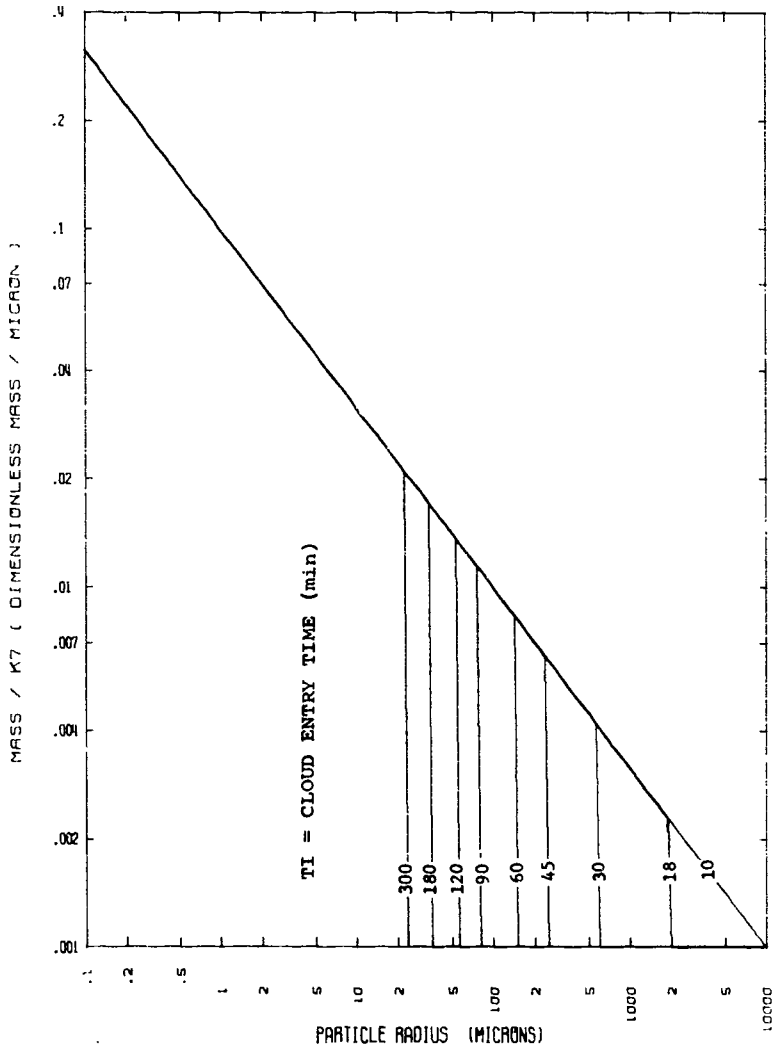

Figure B2. Particle Mass Distribution Function

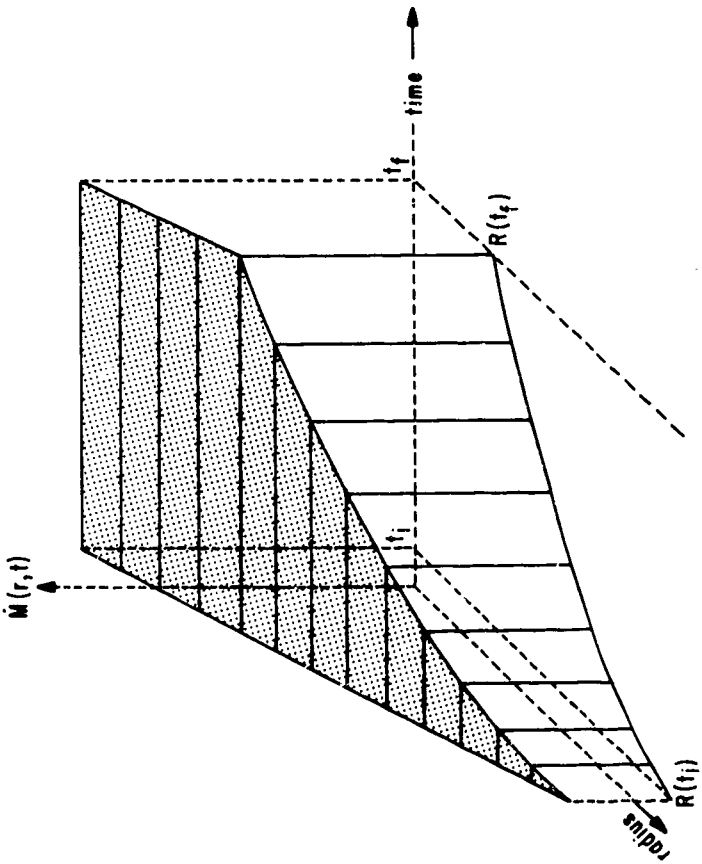

Figure B3. Mass Rate of Dust into Filter versus Time and Size

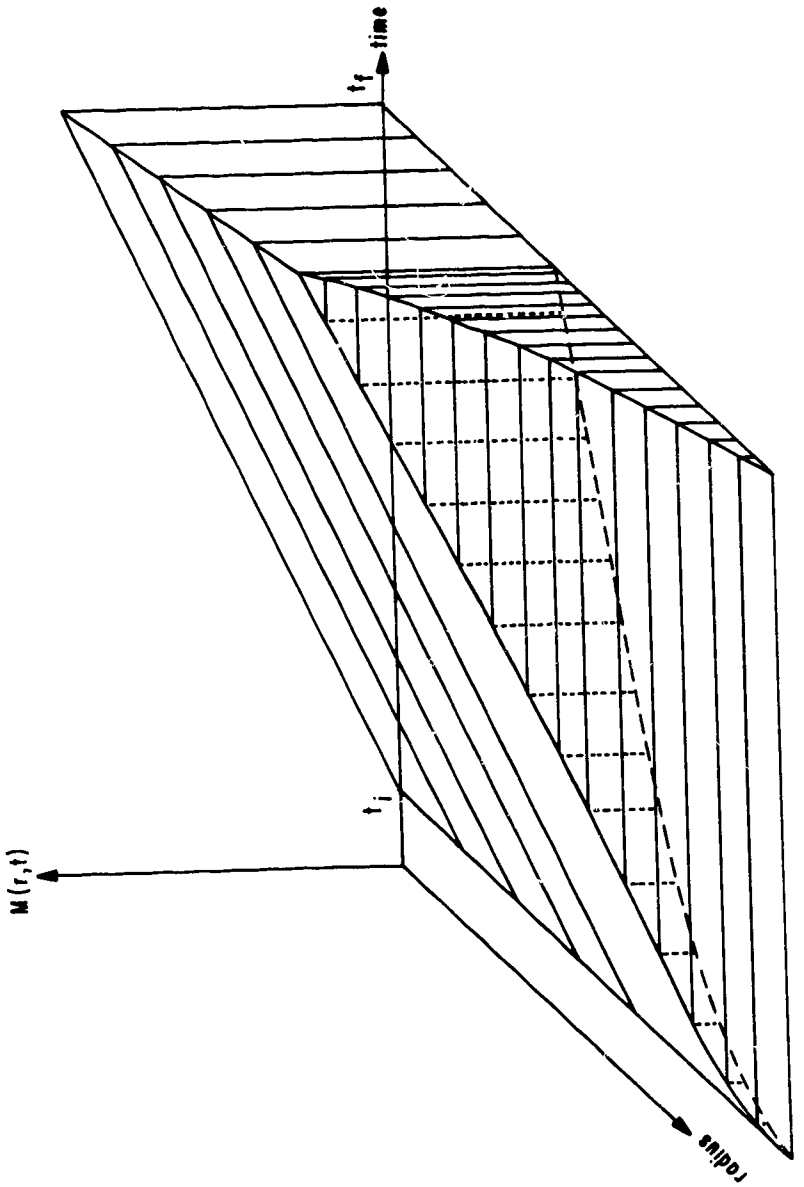

Figure B4. Mass of Dust Accumulated in the Filter versus Time and Size

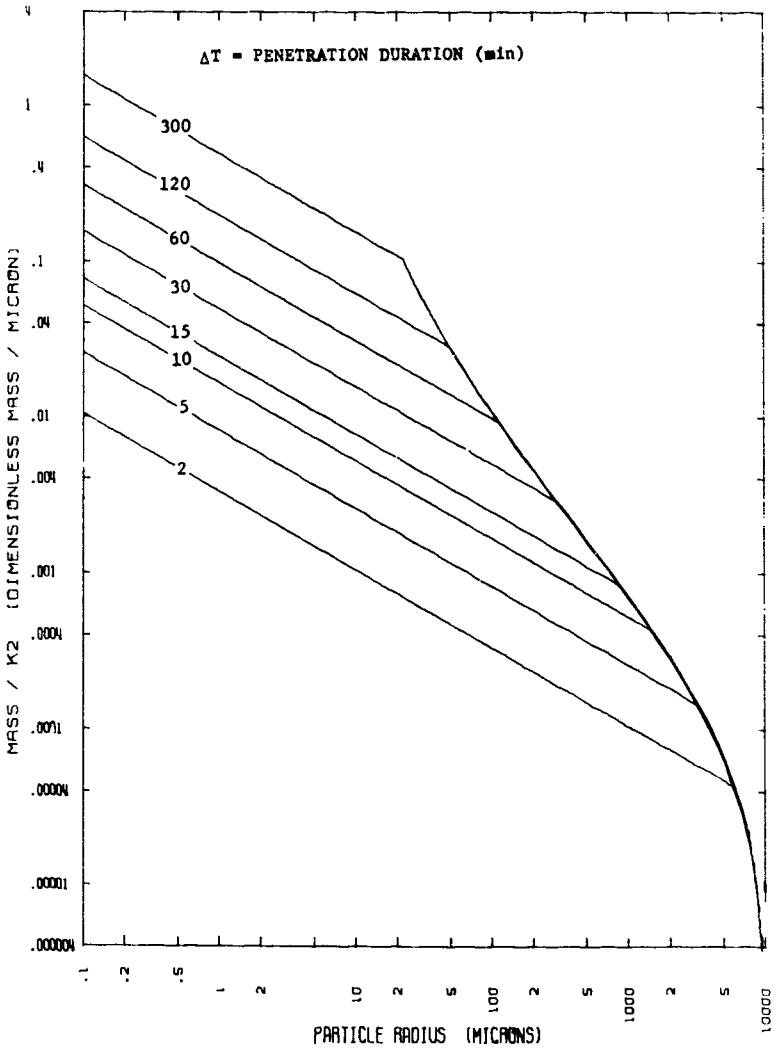

Figure B5. Perfect Filter Mass Distribution Function, TI = 10 Minutes

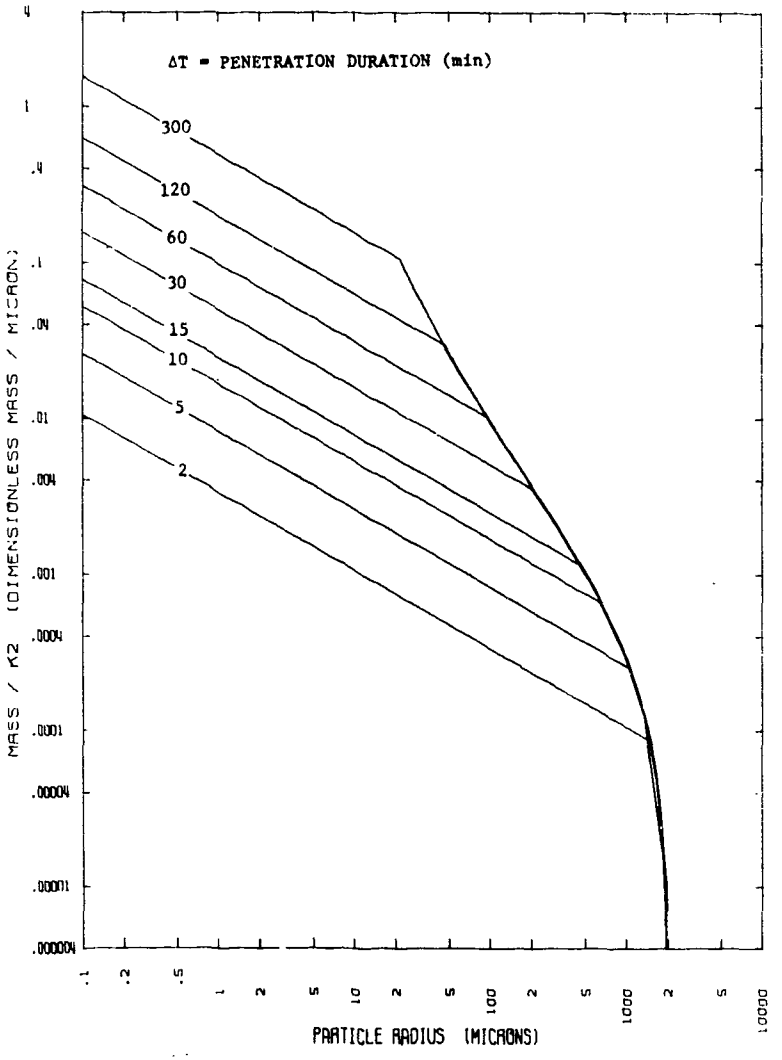

Figure B6. Perfect Filter Mass Distribution Function, TI = 18 Minutes

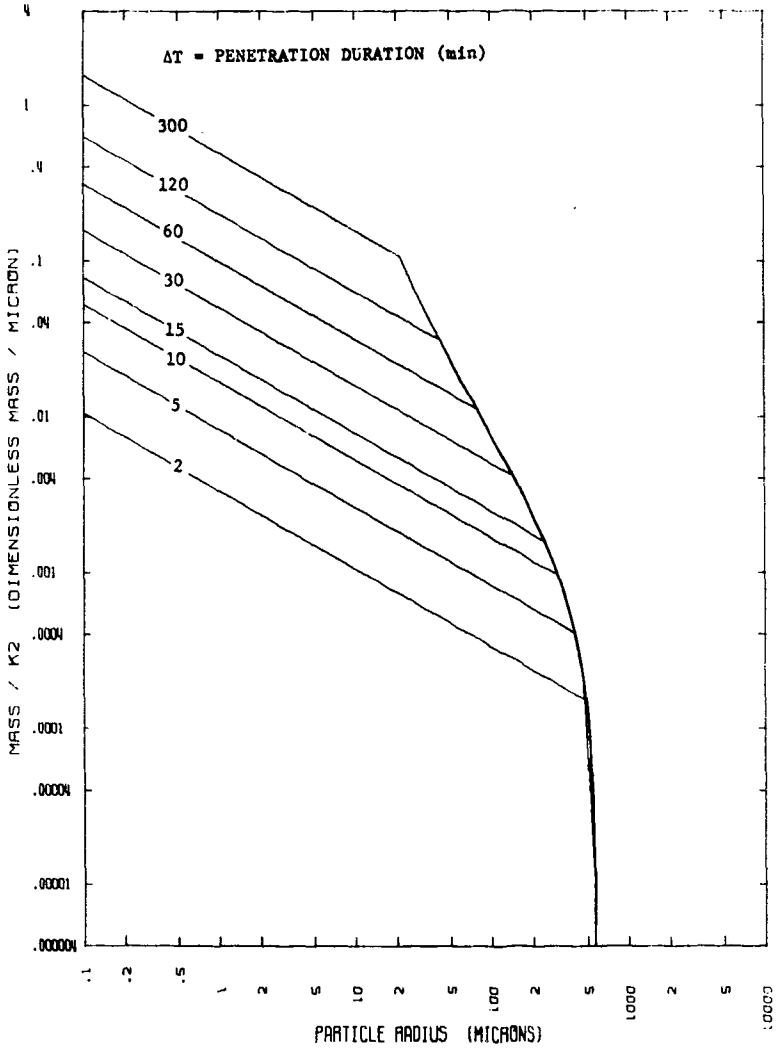

Figure B7. Perfect Filter Mass Distribution Function, TI = 30 Minutes

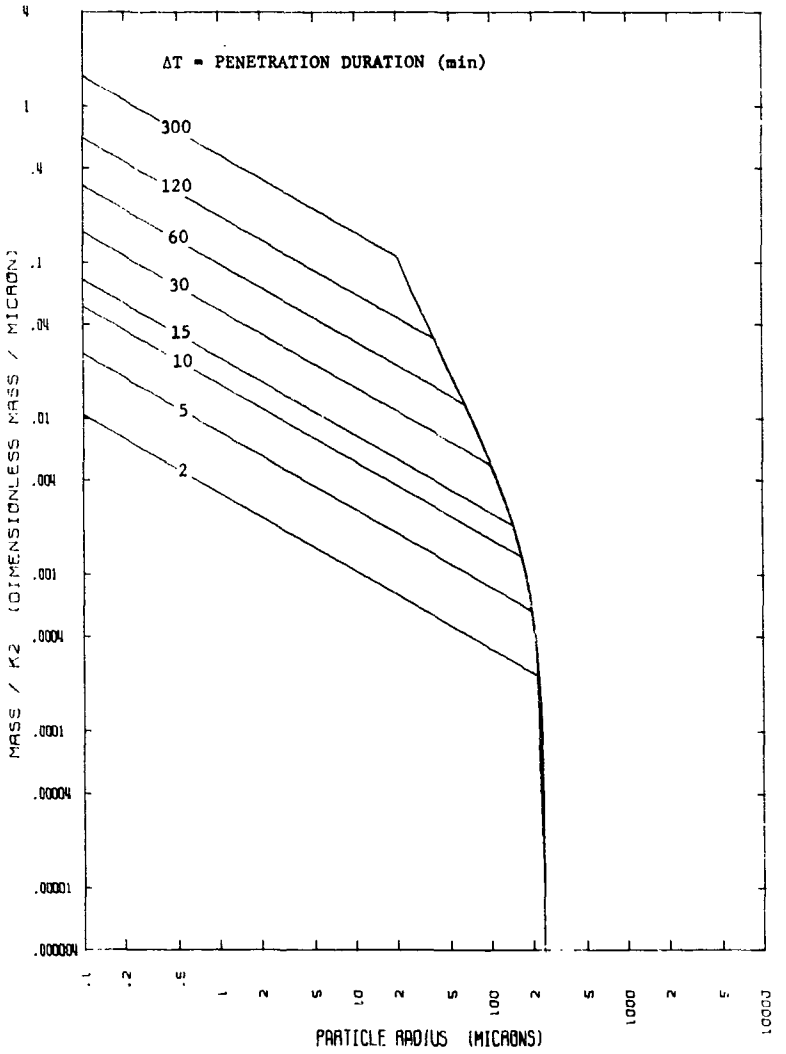

Figure B8. Perfect Filter Mass Distribution Function, TI = 45 Minutes

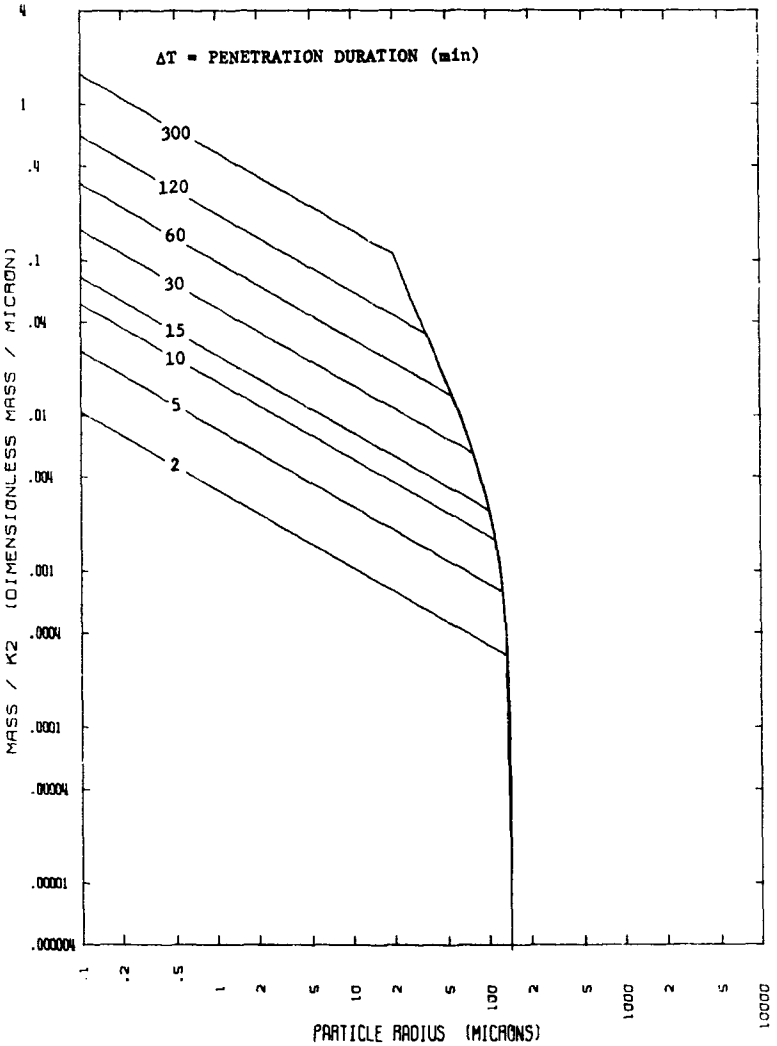

Figure B9. Perfect Filter Mass Distribution Function, TI = 1 Hour

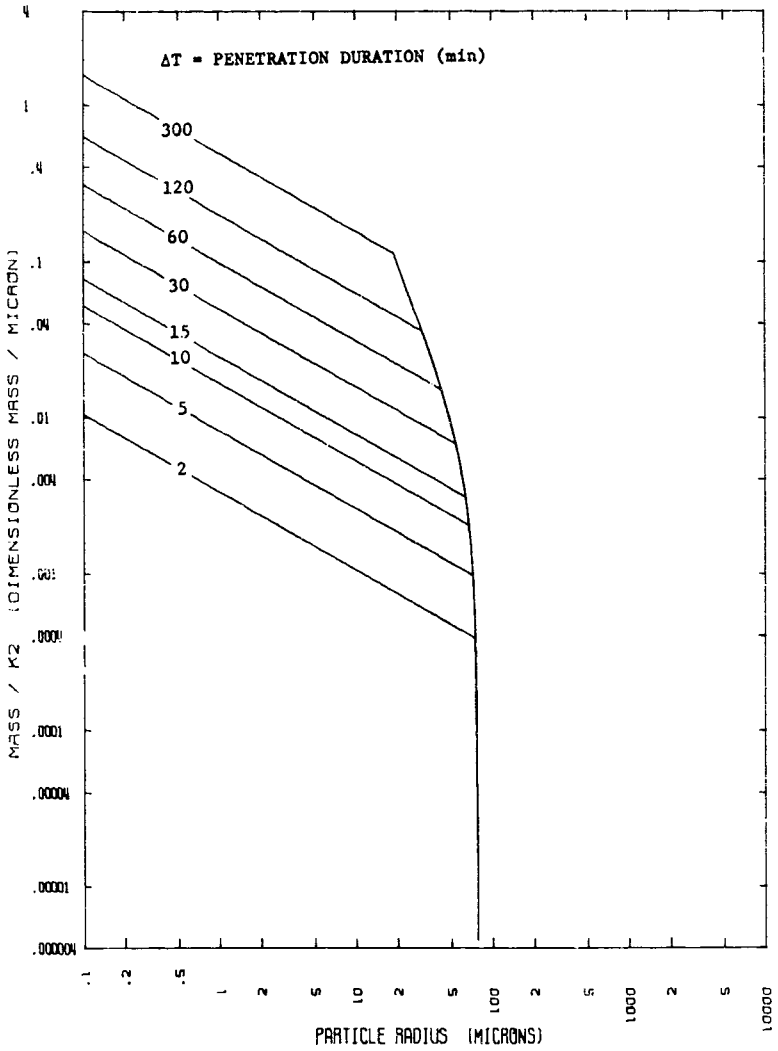

Figure B10. Perfect Filter Mass Distribution Function, TI = 1.5 Hours

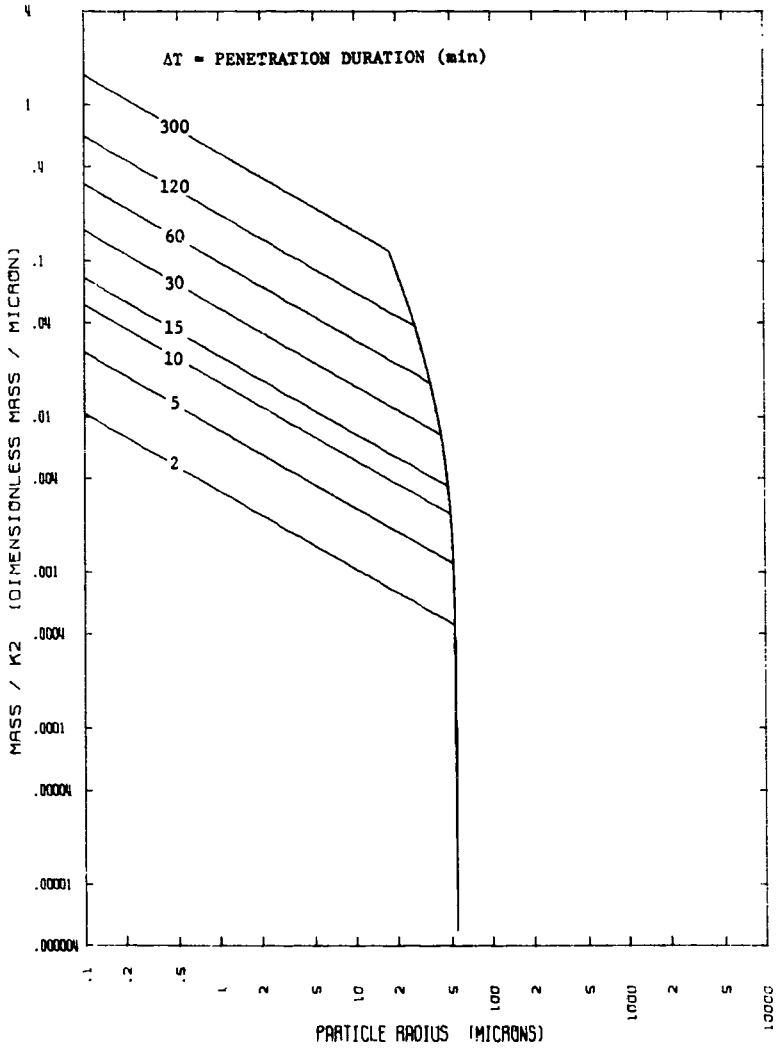

Figure B11. Perfect Filter Mass Distribution Function, TI = 2 Hours

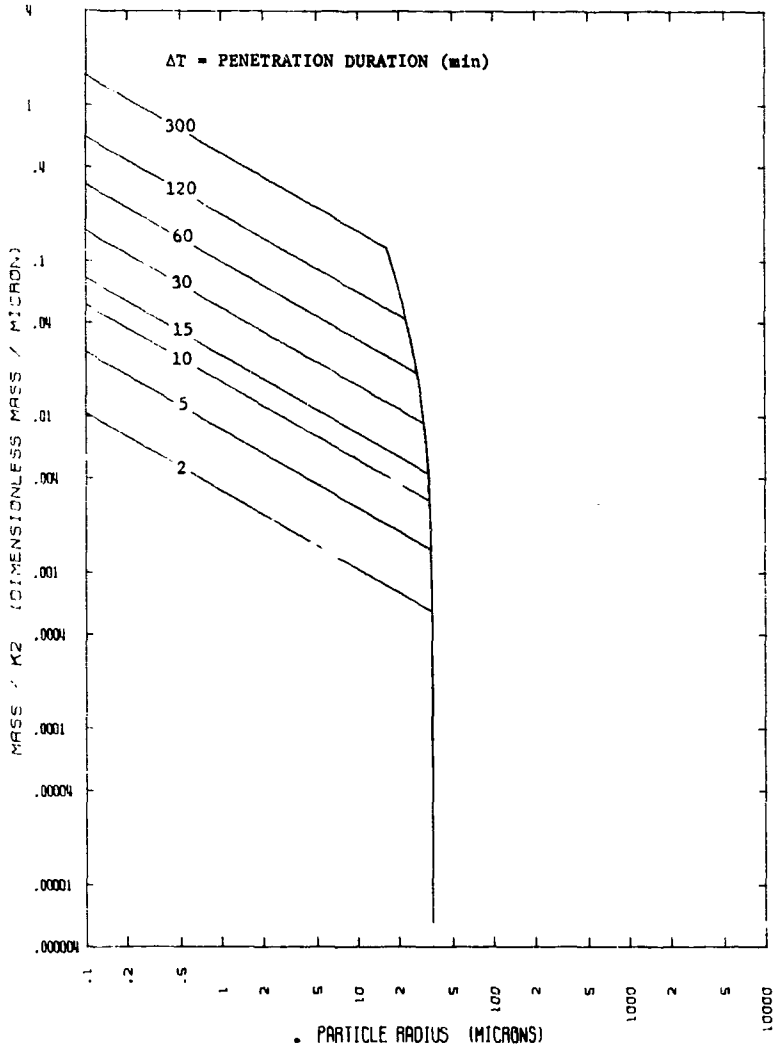

Figure B12. Perfect Filter Mass Distribution Function, TI = 3 Hours

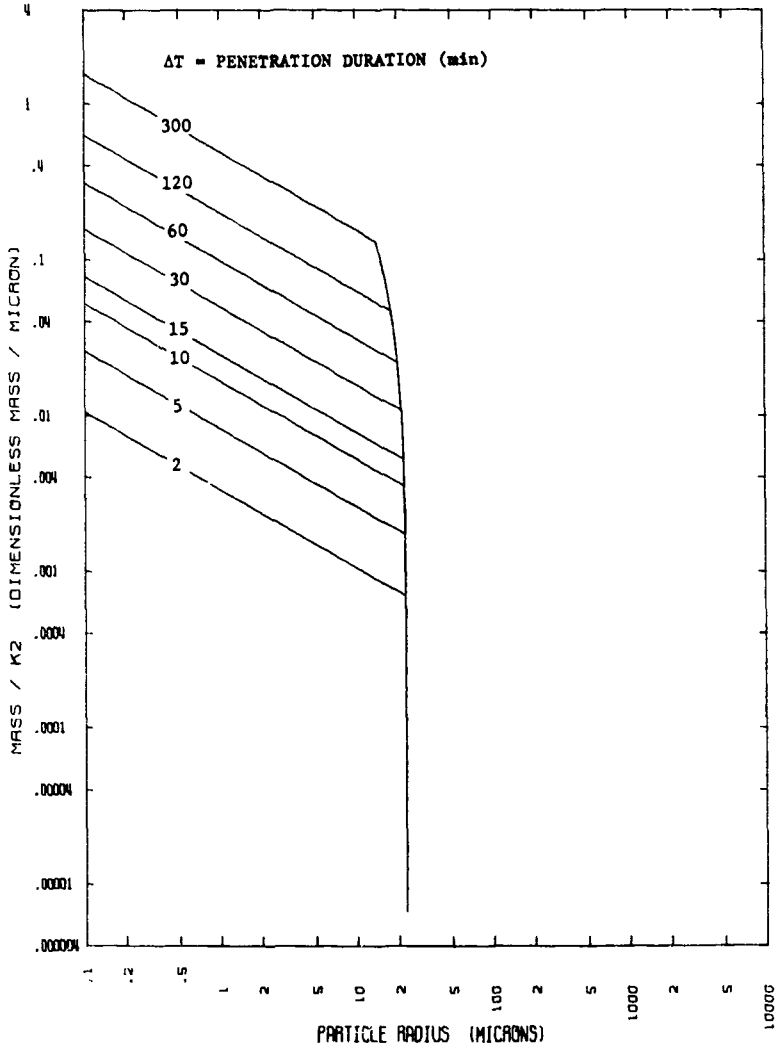

Figure B13. Perfect Filter Mass Distribution Function, TI = 5 Hours

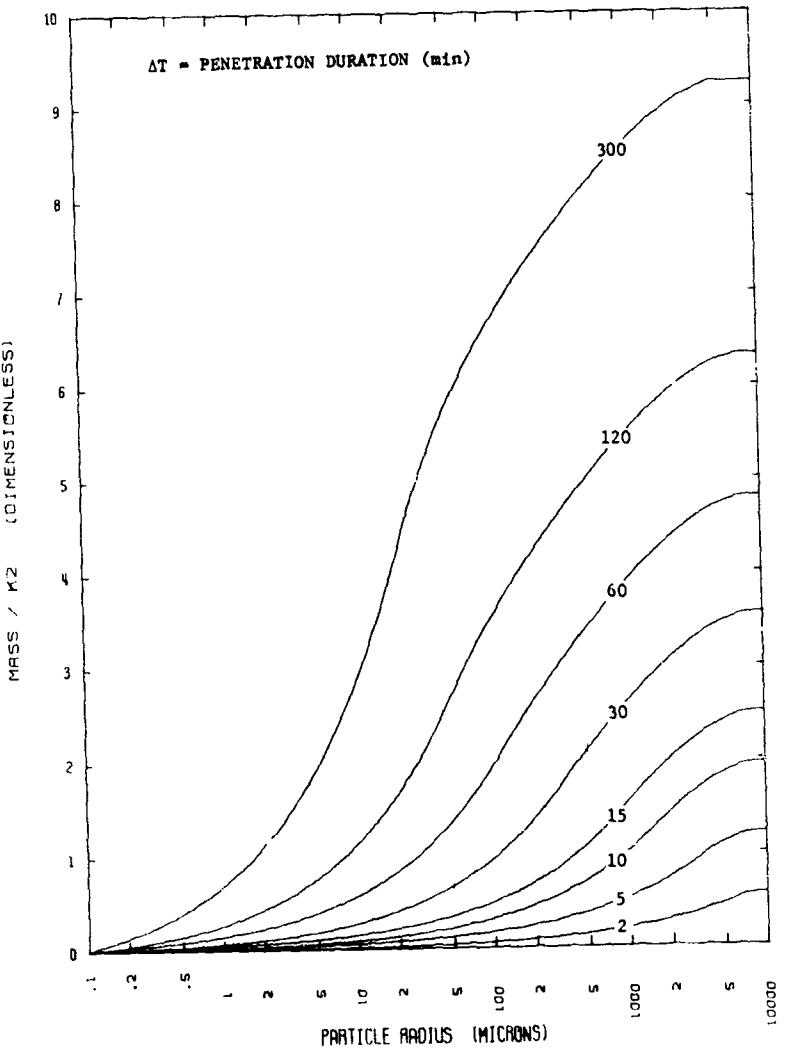

Figure B14. Cumulative Mass as a Function of Size, TI = 10 Minutes

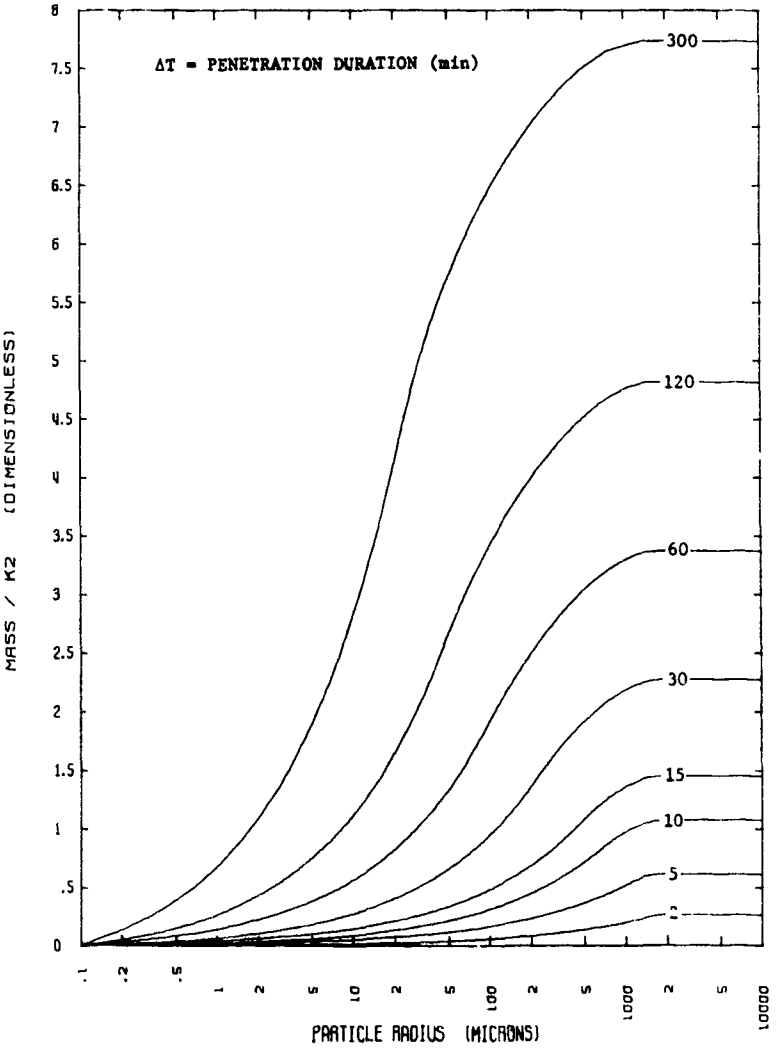

Figure B15. Cumulative Mass as a Function of Size, TI = 18 Minutes

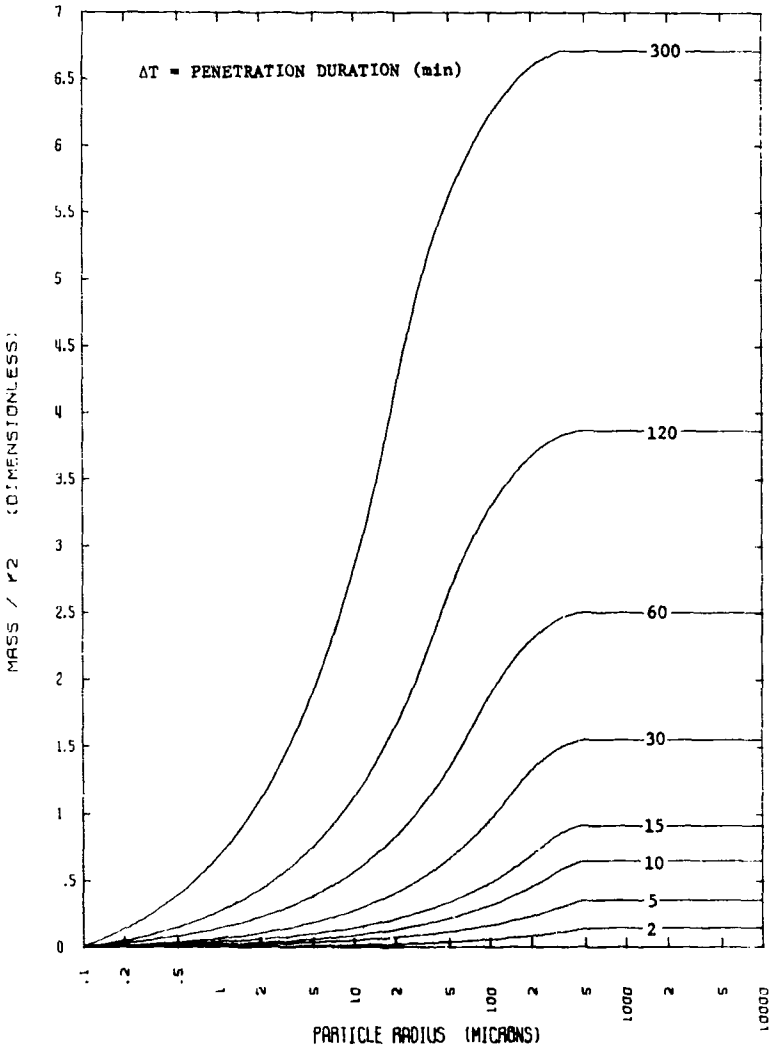

Figure B16. Cumulative Mass as a Function of Size, TI = 30 Minutes

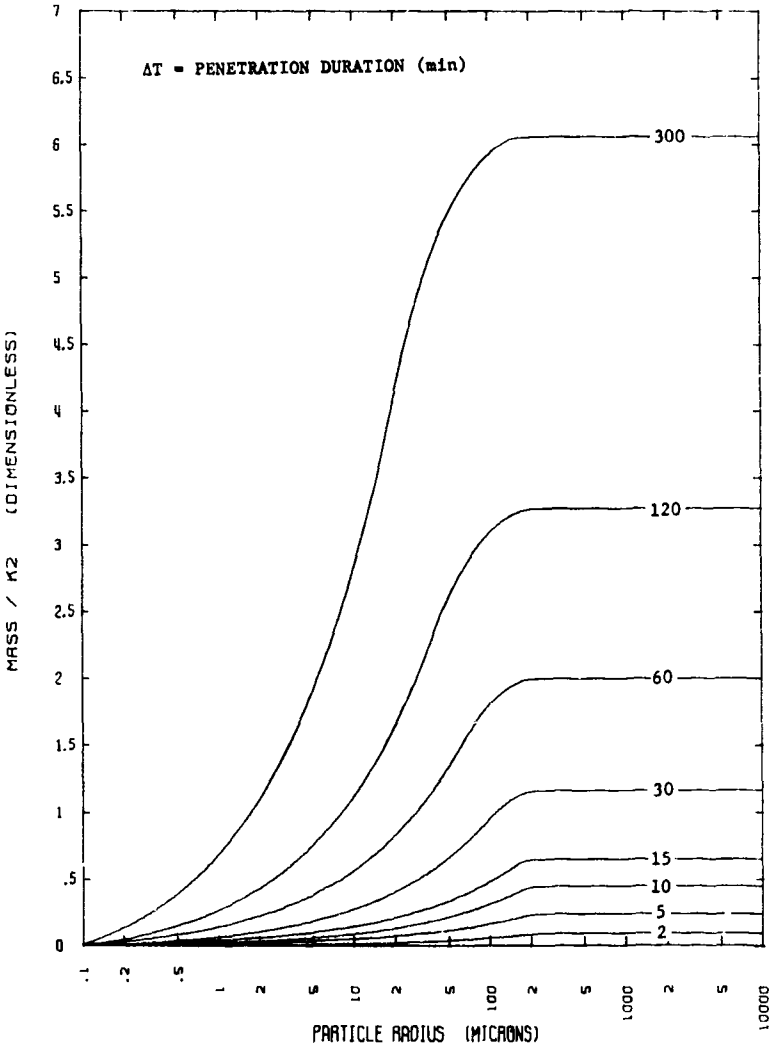

Figure B17. Cumulative Mass as a Function of Size, TI = 45 Minutes

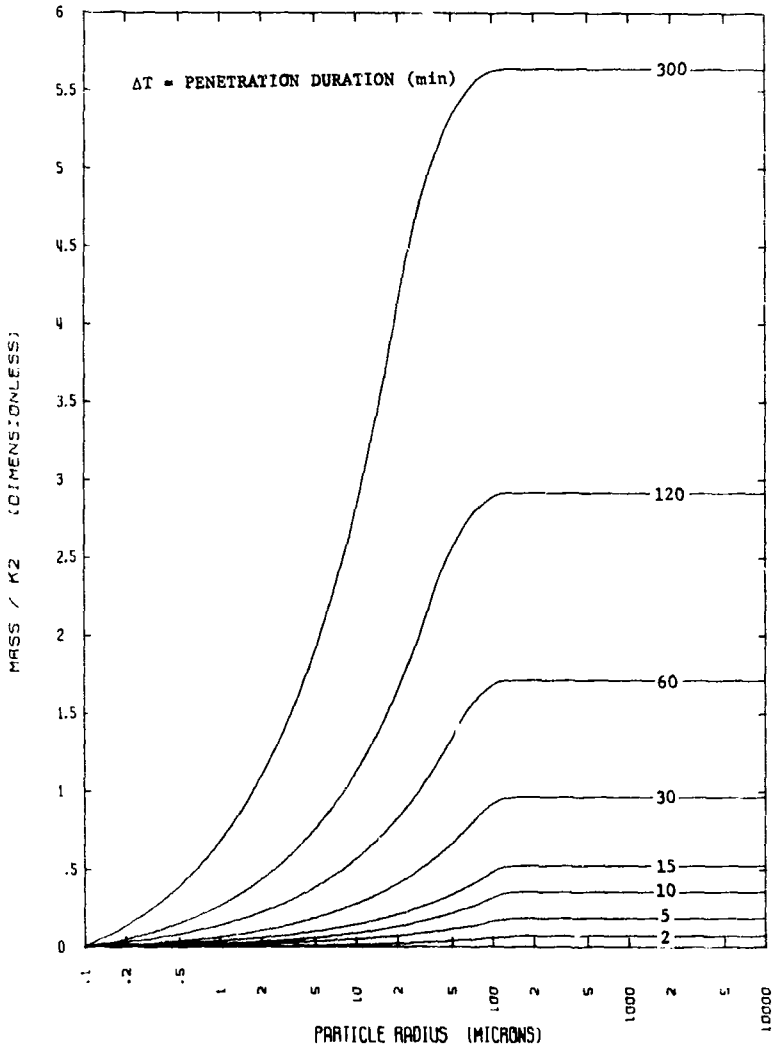

Figure B18. Cumulative Mass as a Function of Size, TI 1 Hour

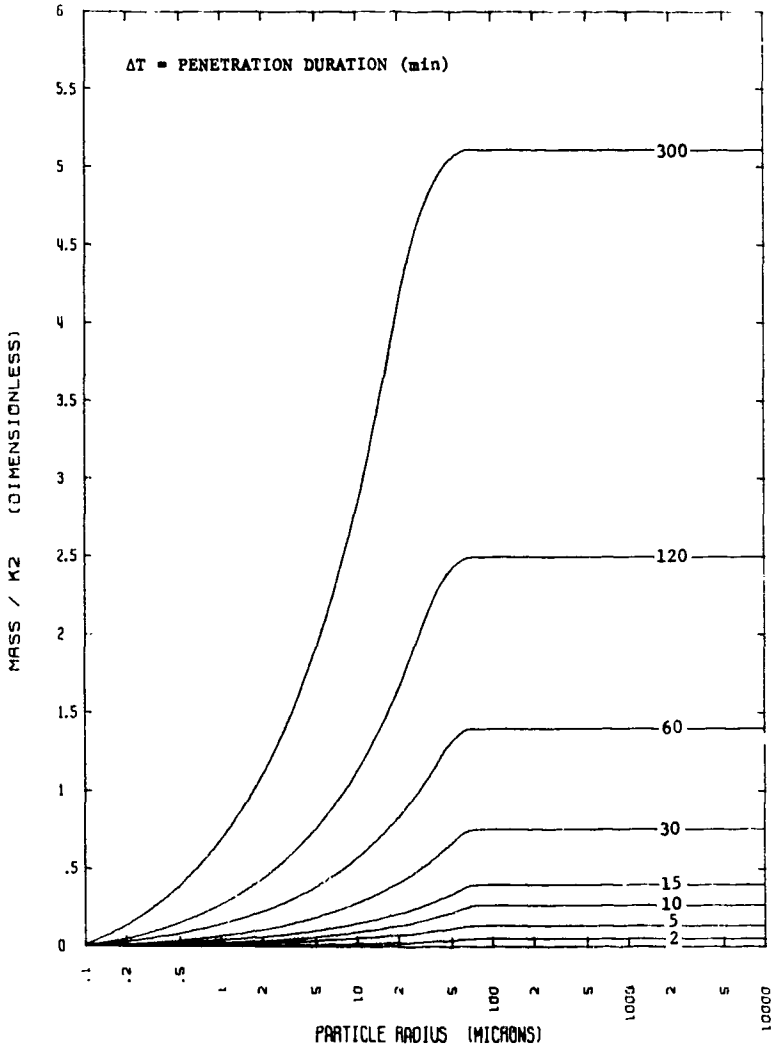

Figure B19. Cumulative Mass as a Function of Size, TI = 1.5 Hours

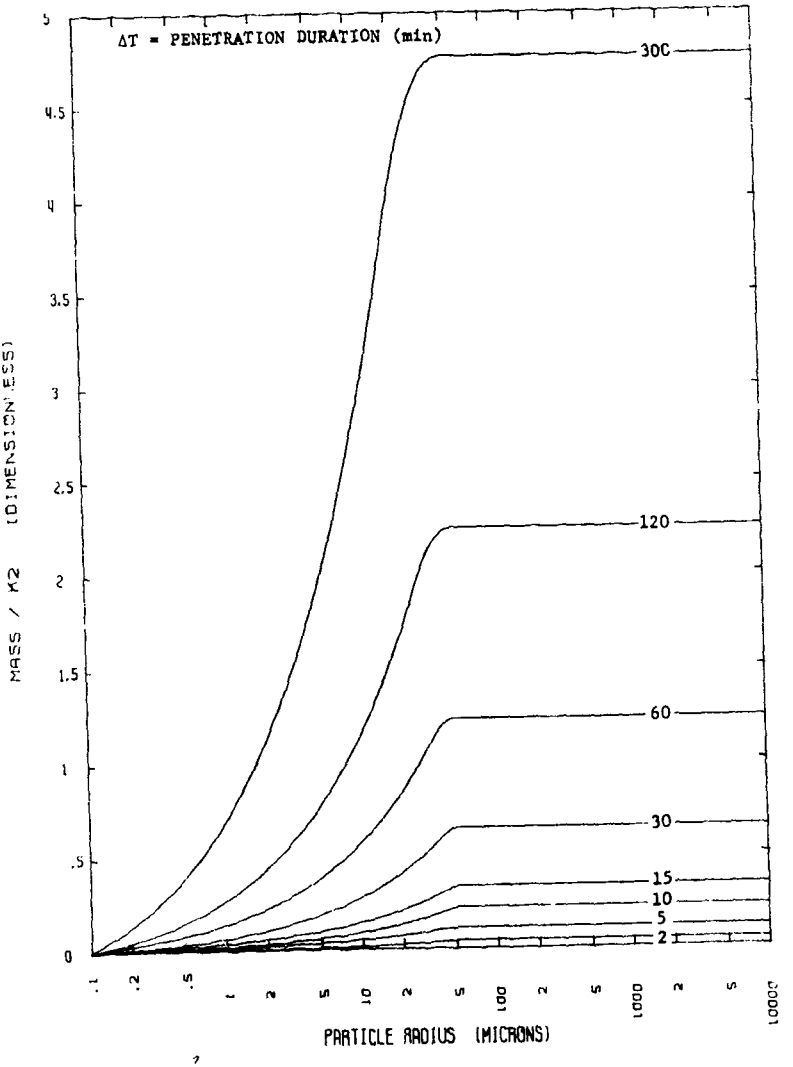

Figure B20. Cumulative Mass as a Function of Size, TI = 2 Hours

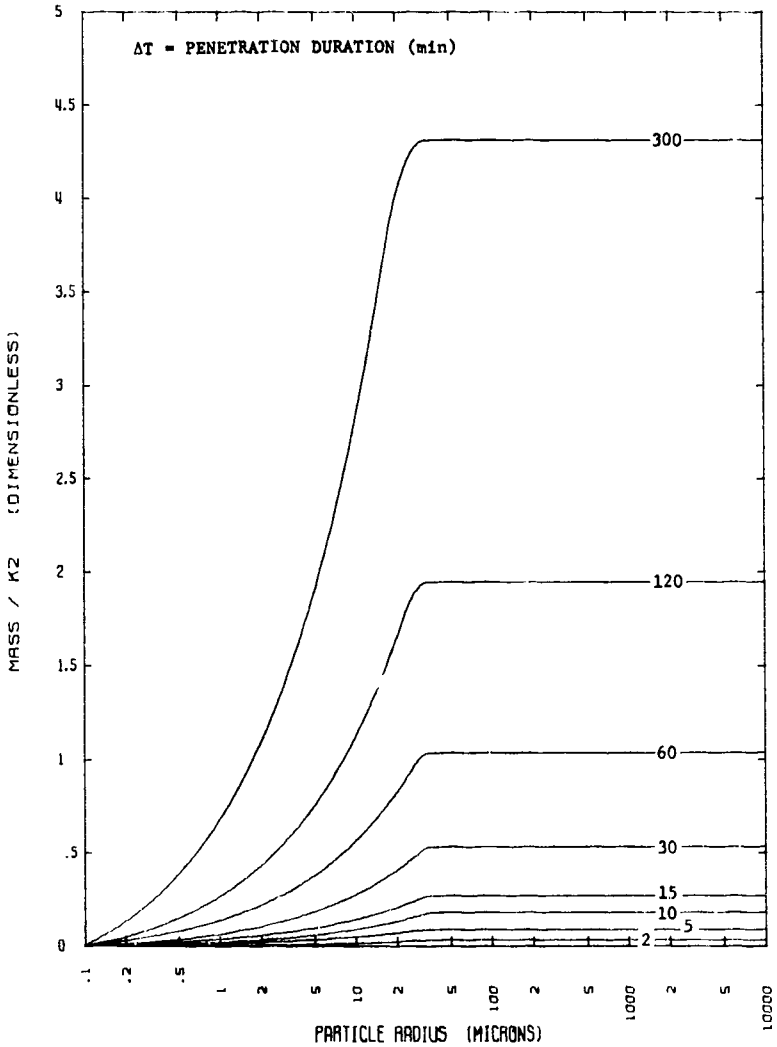

Figure B21. Cumulative Mass as a Function of Size, TI = 3 Hours

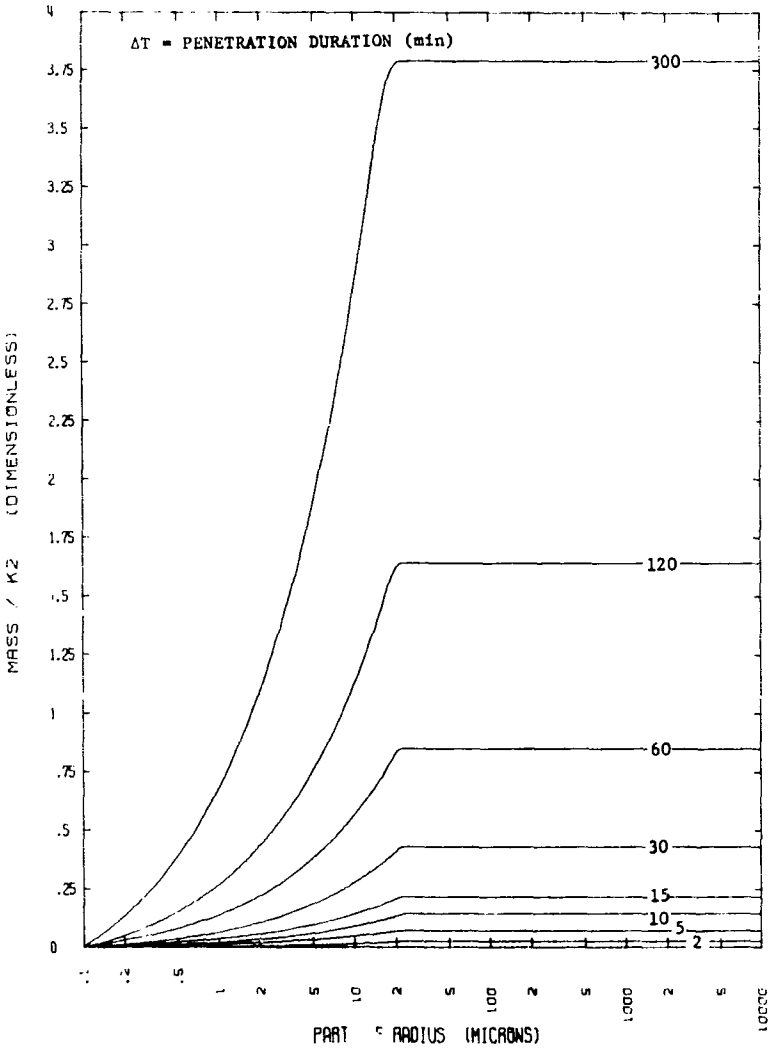

Figure B22. Cumulative Mass as a Function of Size, TI = 5 Hours

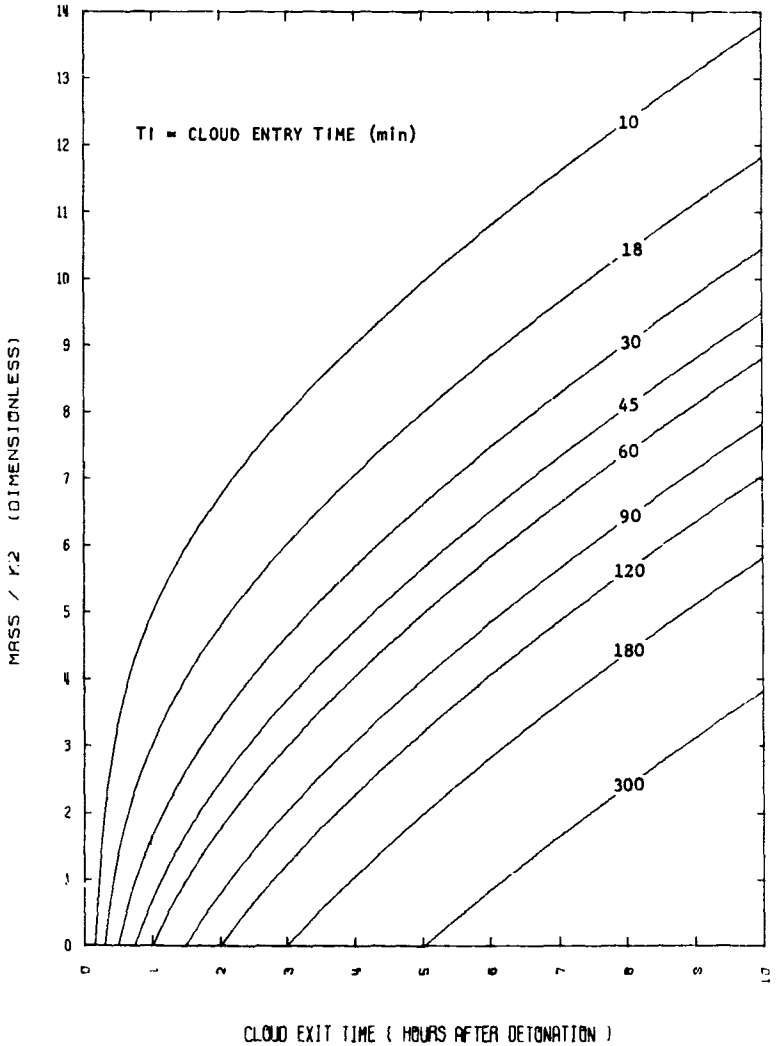

Figure B23. Filter Dust Mass as a Function of Time

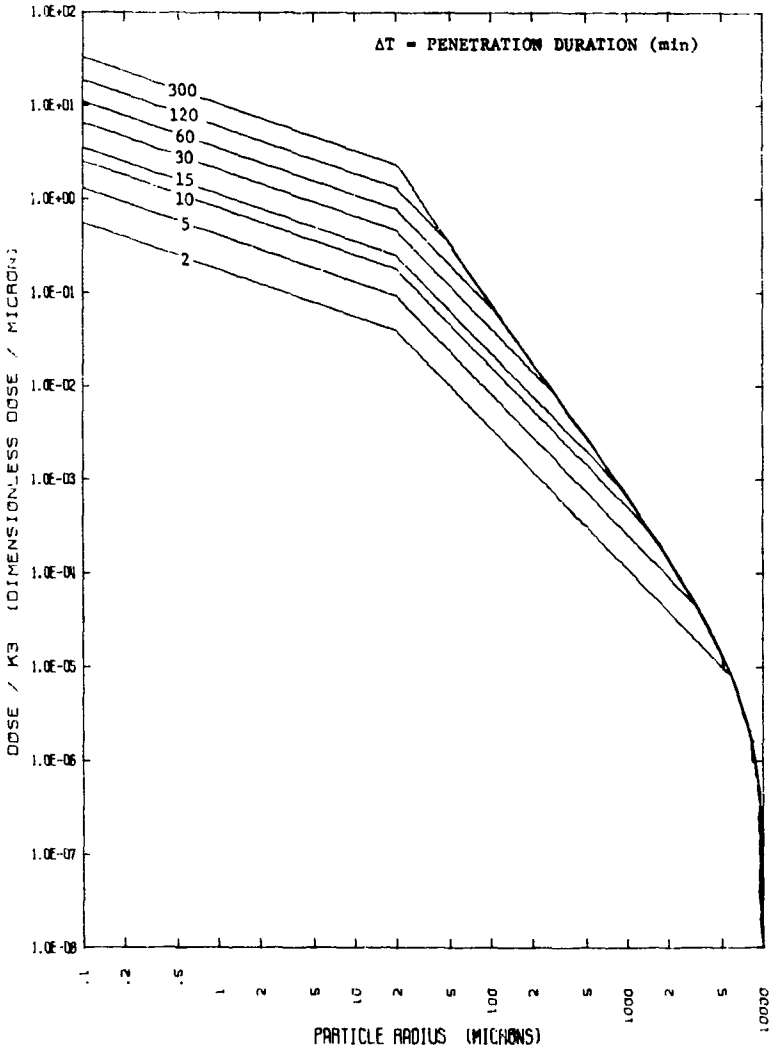

Figure B24. Dose from Filter Dust at 30 Hours, TI = 10 Minutes

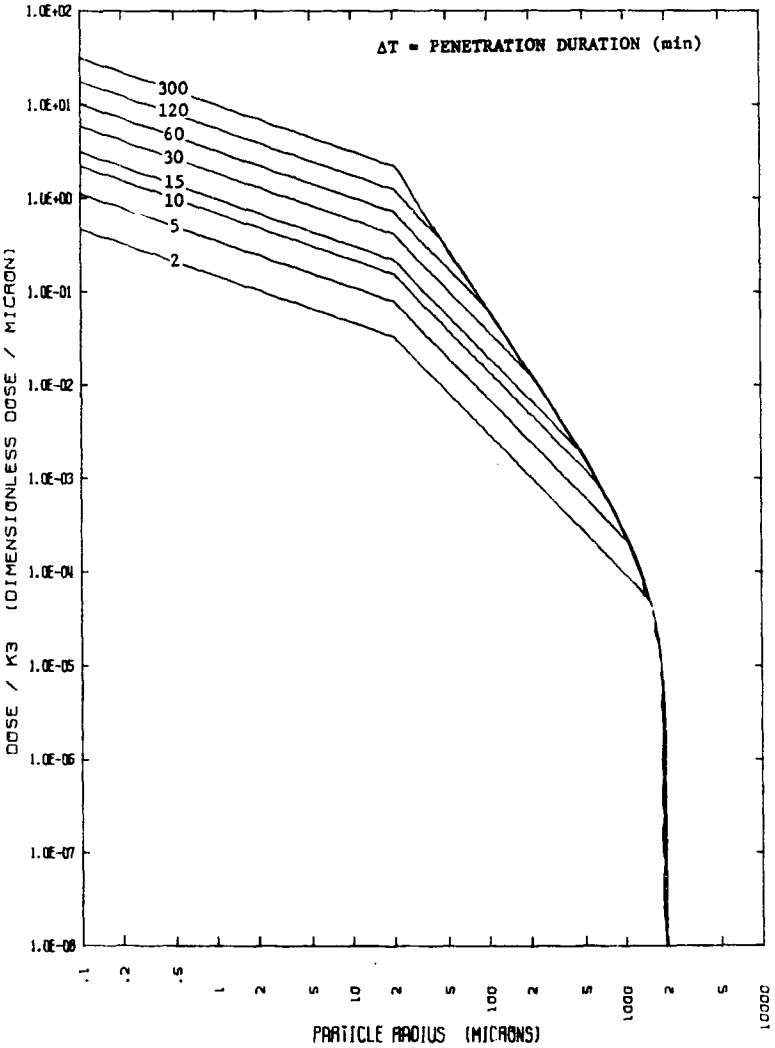

Figure B25. Dose from Filter Dust at 30 Hours, TI = 18 Minutes

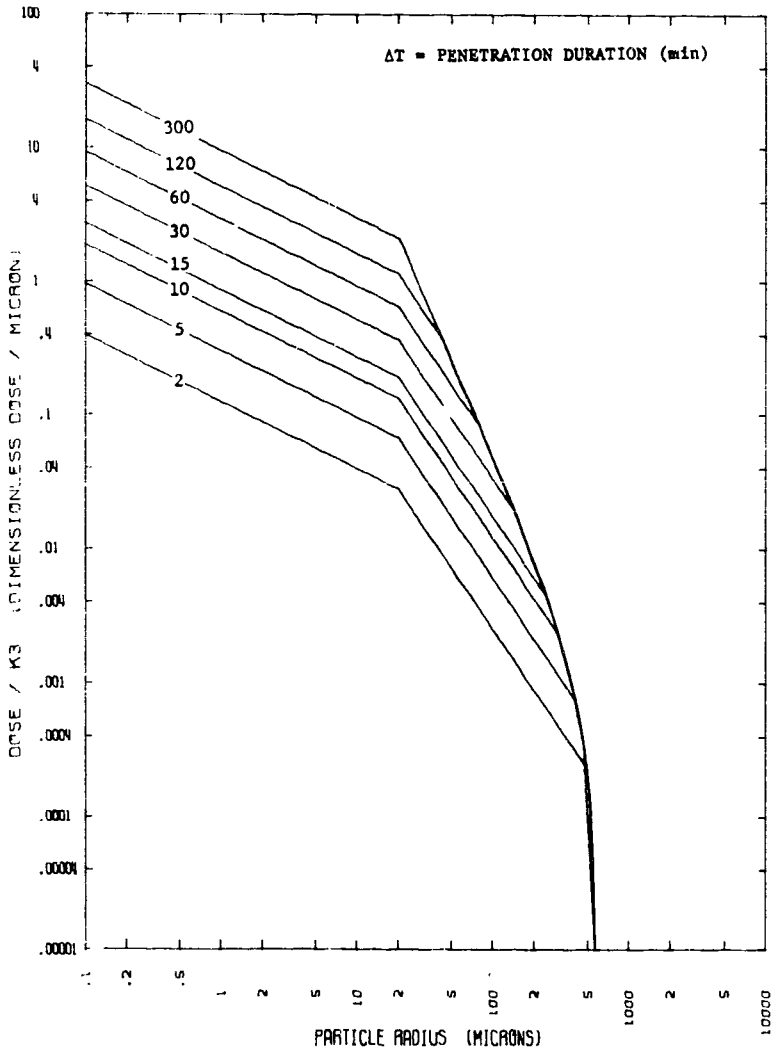

Figure B26. Dose from Filter Dust at 30 Hours, TI = 30 Minutes

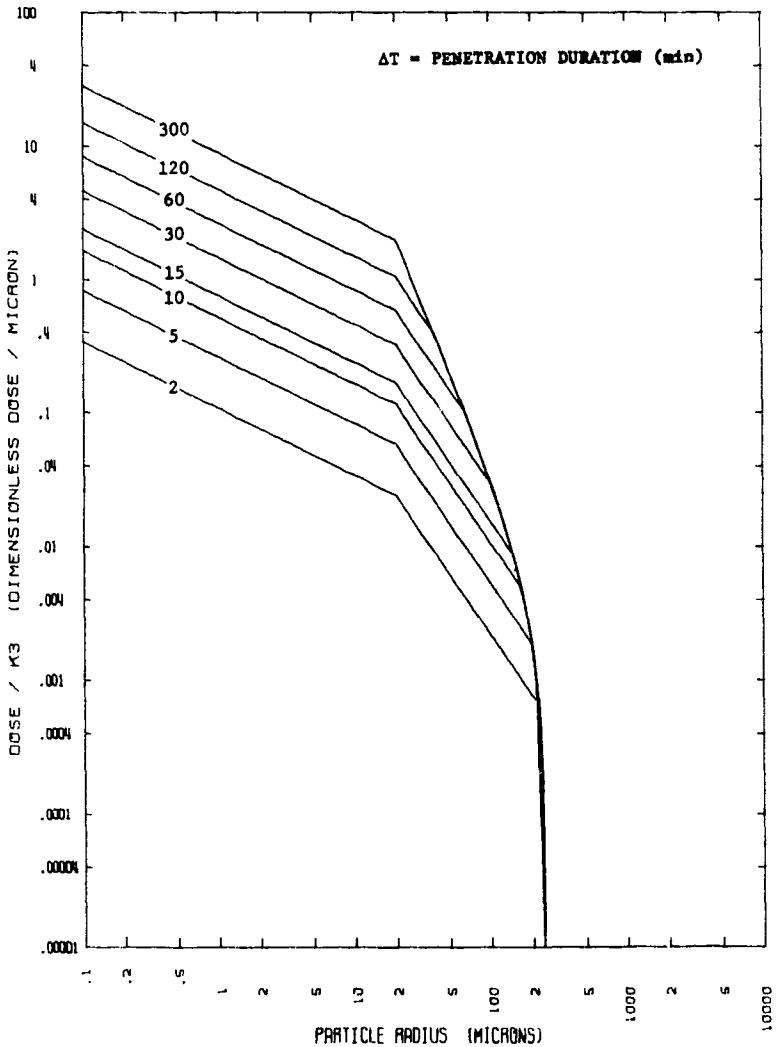

Figure B27. Dose from Filter Dust at 30 Hours, TI = 45 Minutes

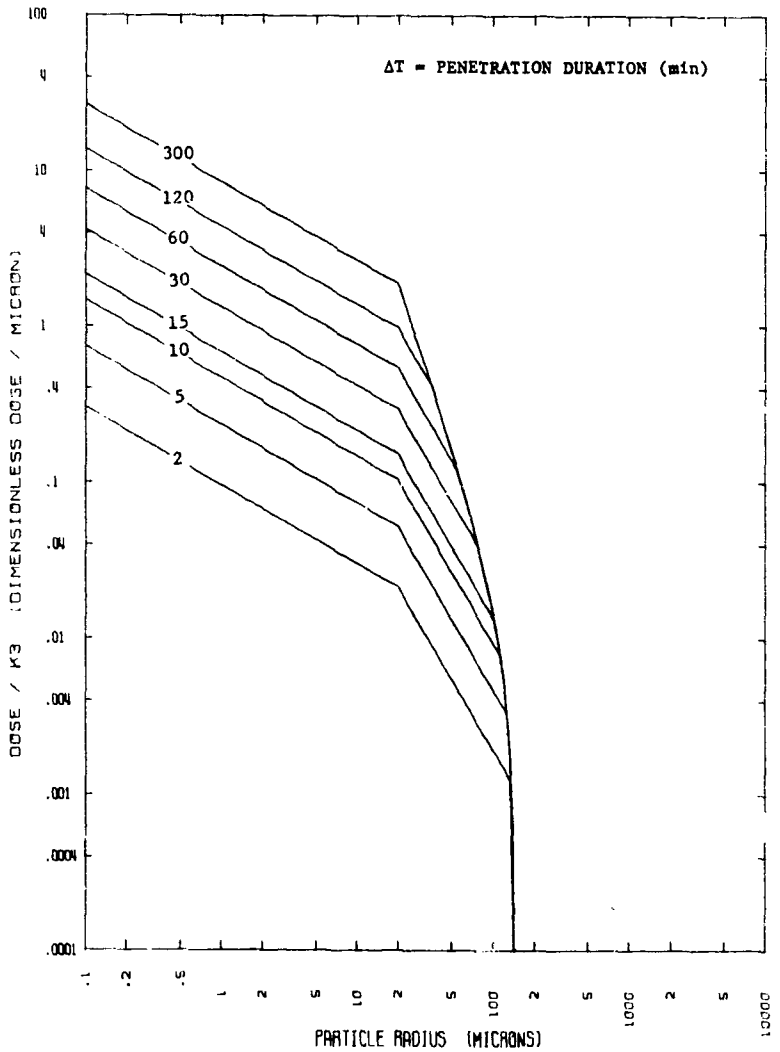

Figure B28. Dose from Filter Dust at 30 Hours, TI = 1 Hour

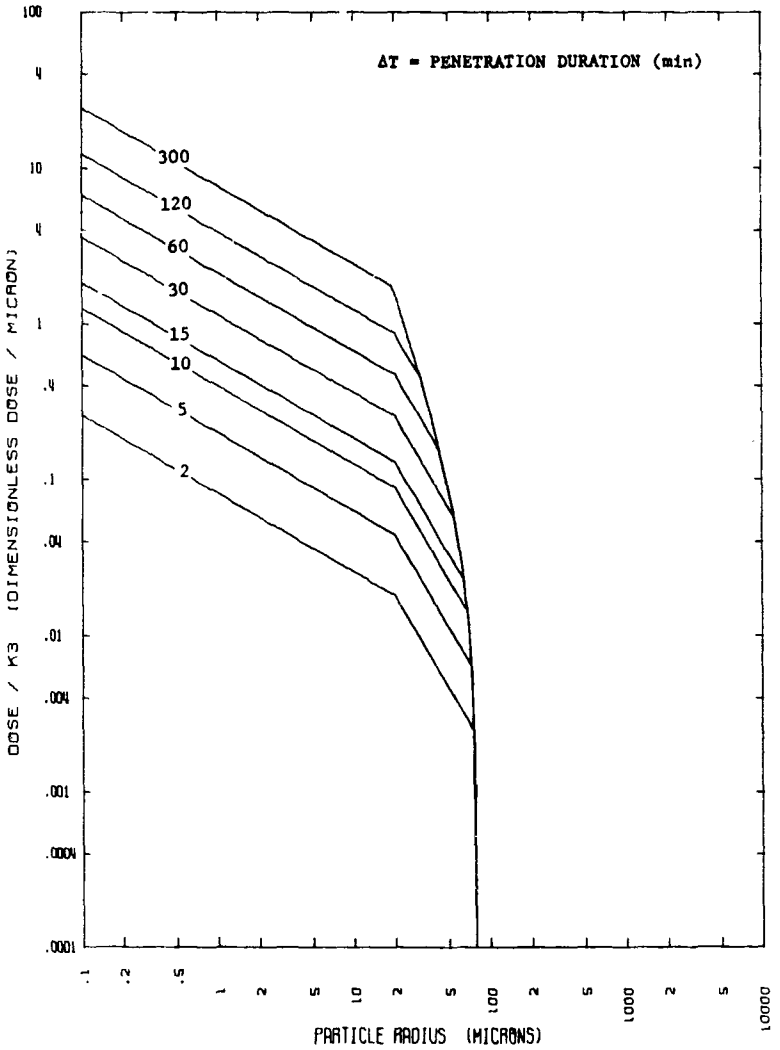

Figure 829. Dose from Filter Dust at 30 Hours, TI = 1.5 Hours

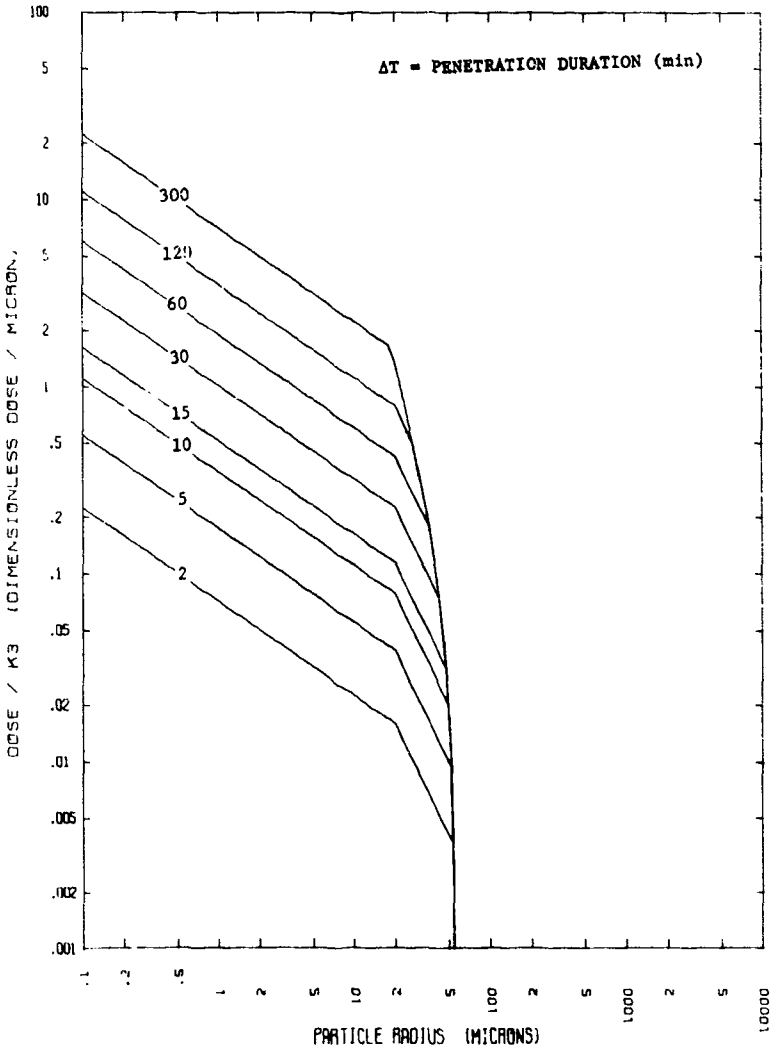

Figure B30. Dose from Filter Dust at 30 Hours, TI = 2 Hours

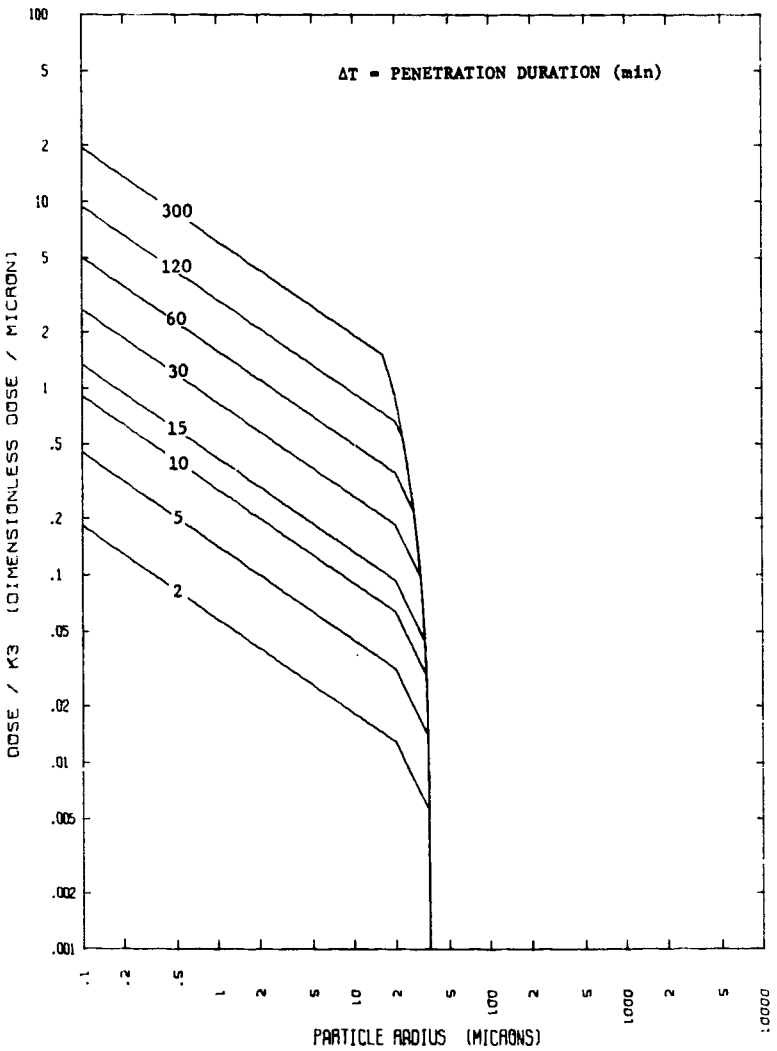

Figure B31. Dose from Filter Dust at 30 Hours, TI = 3 Hours

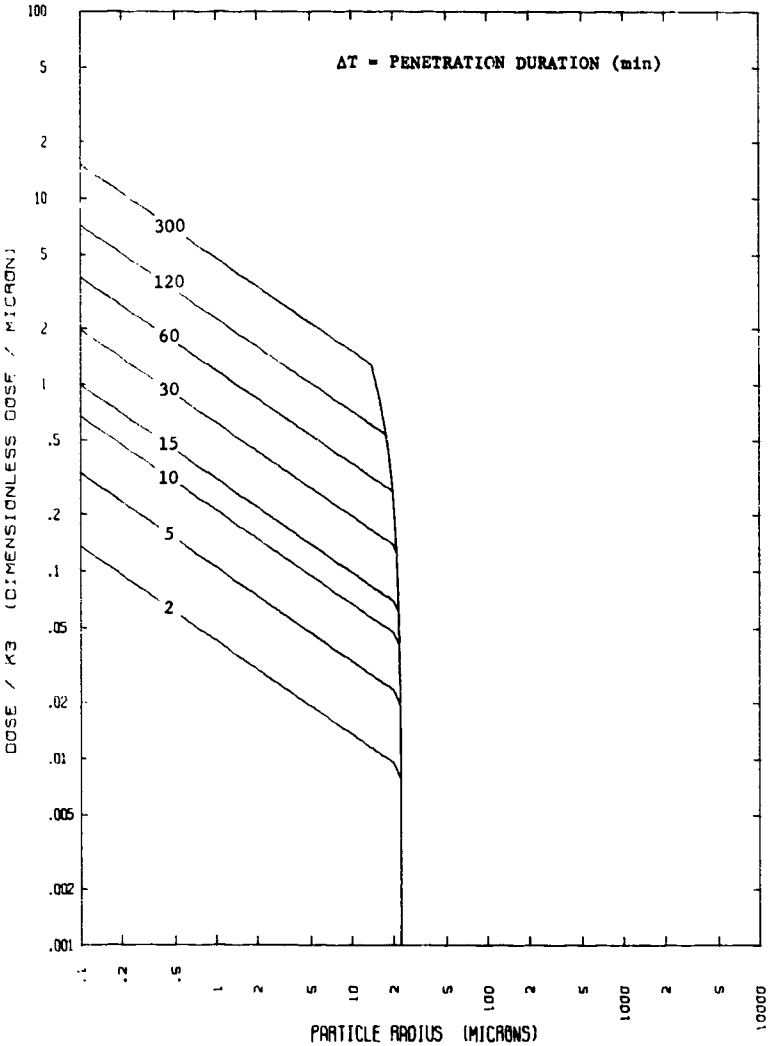

Figure B32. Dose from Filter Dust at 30 Hours, TI = 5 Hours

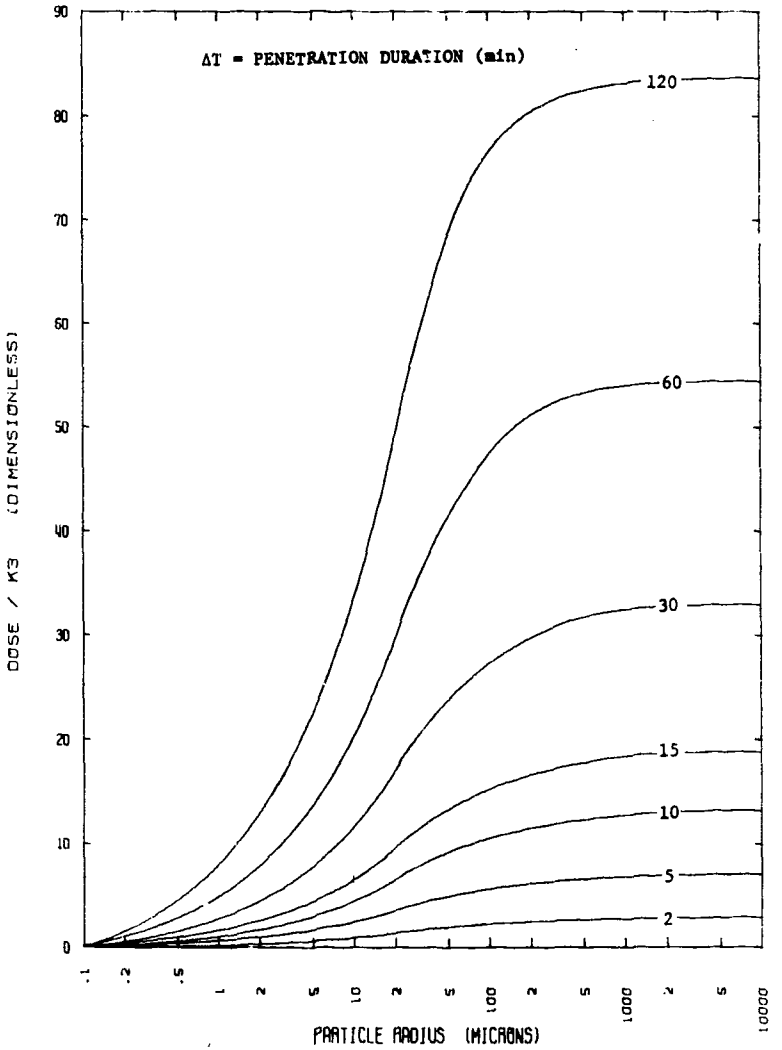

Figure B33. Cumulative Filter Dose at 30 Hours, TI = 10 Minutes

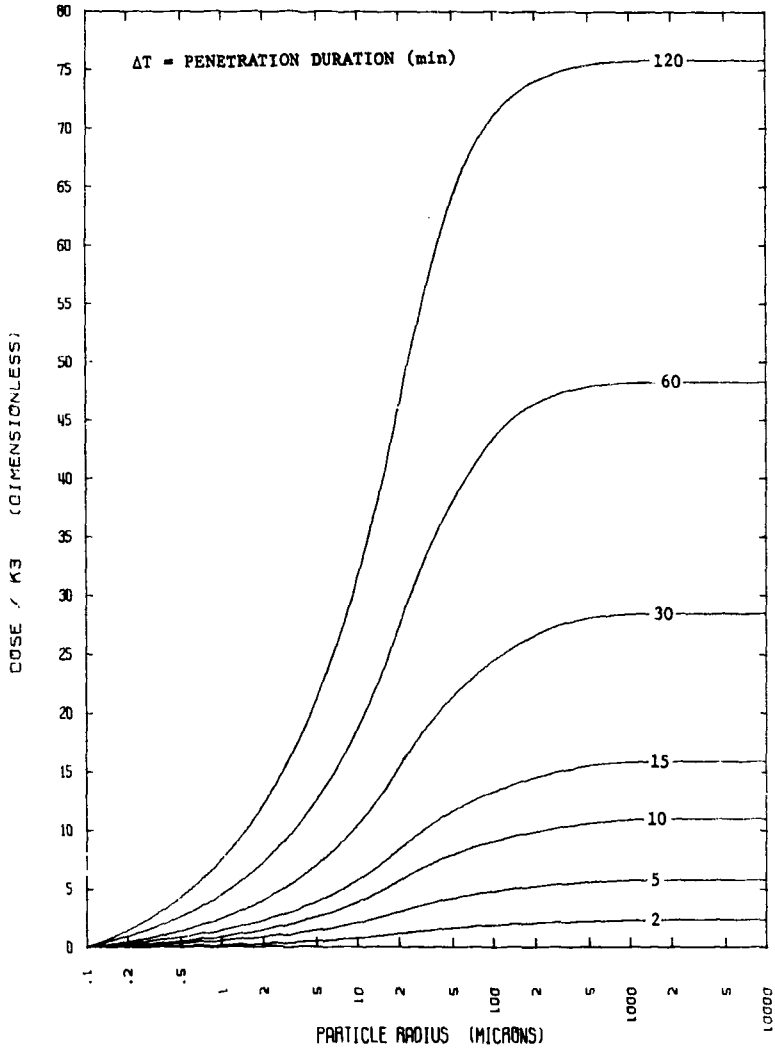

Figure B34. Cumulative Filter Dose at 30 Hours, TI = 18 Minutes

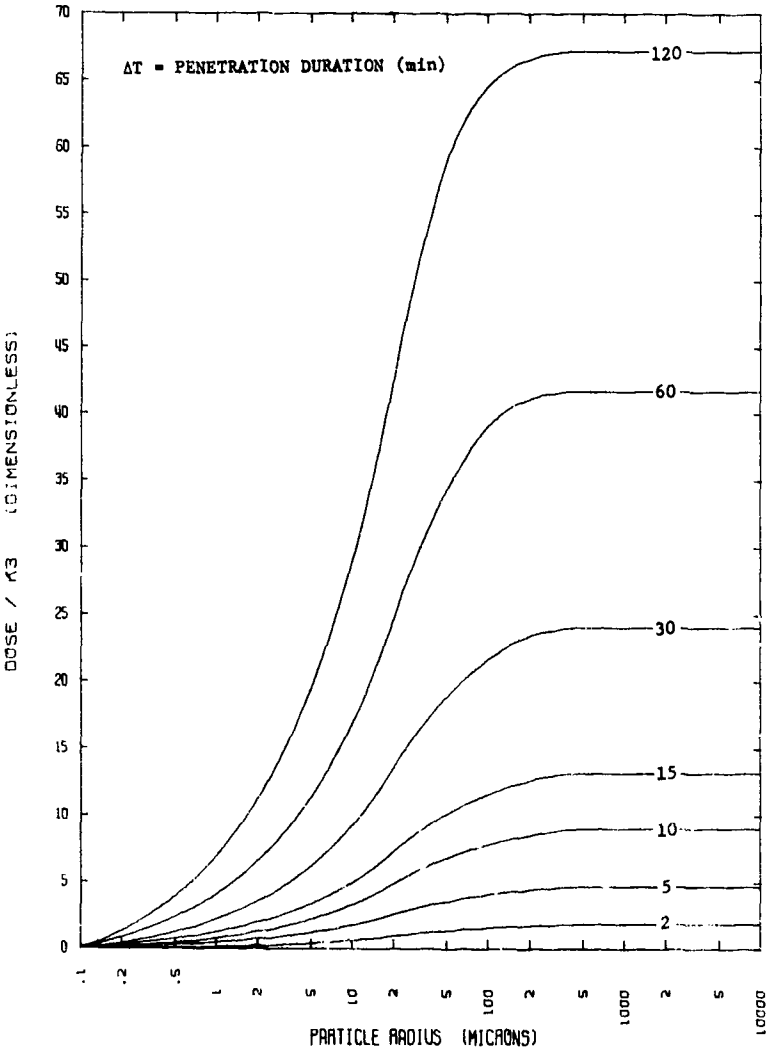

Figure B35. Cumulative Filter Dose at 30 Hours, TI = 30 Minutes

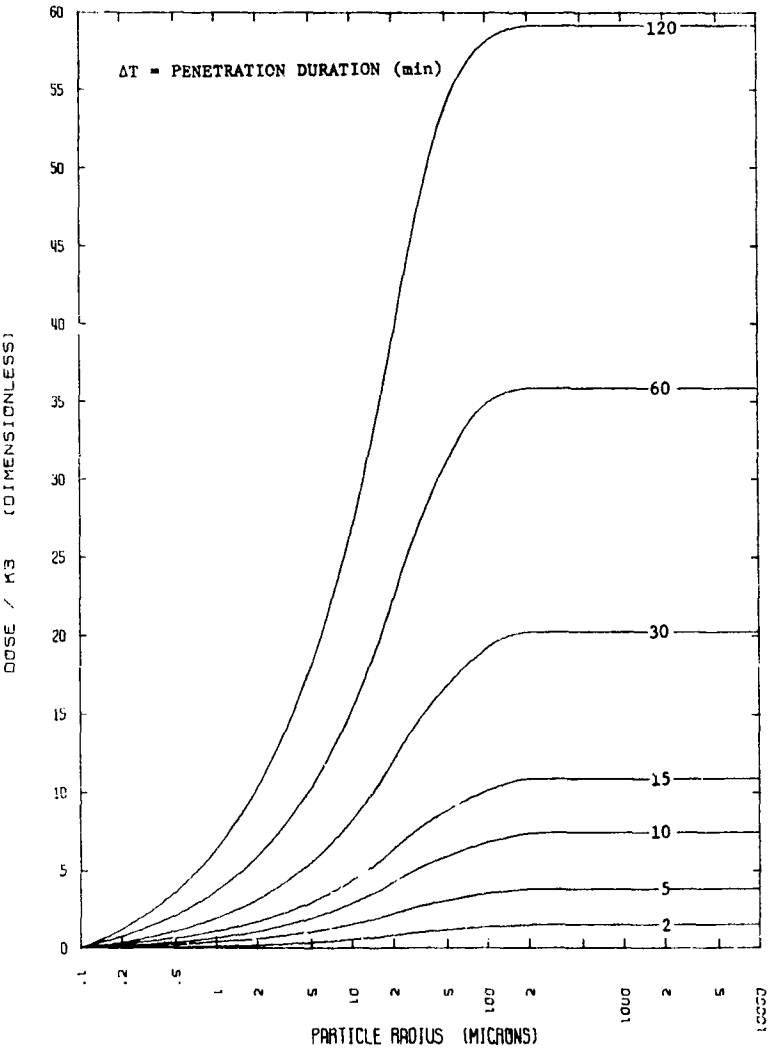

Figure B36. Cumulative Filter Dose at 30 Hours, TI = 45 Minutes

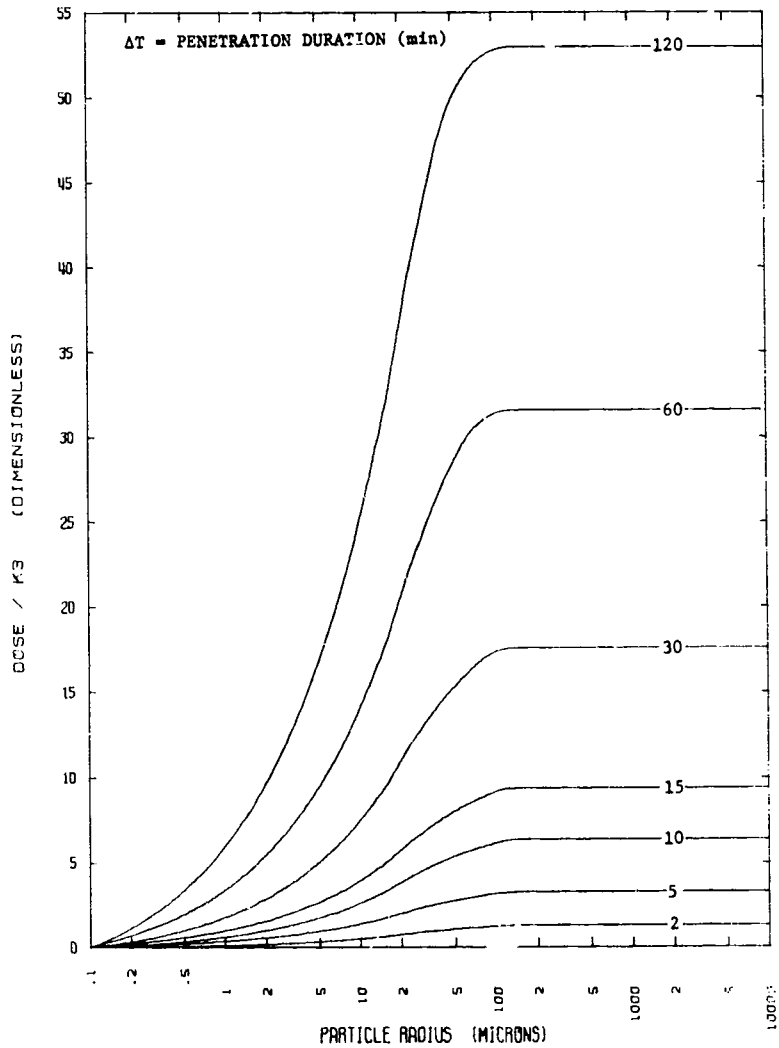

Figure B37. Cumulative Filter Dose at 30 Hours, TI = 1 Hour

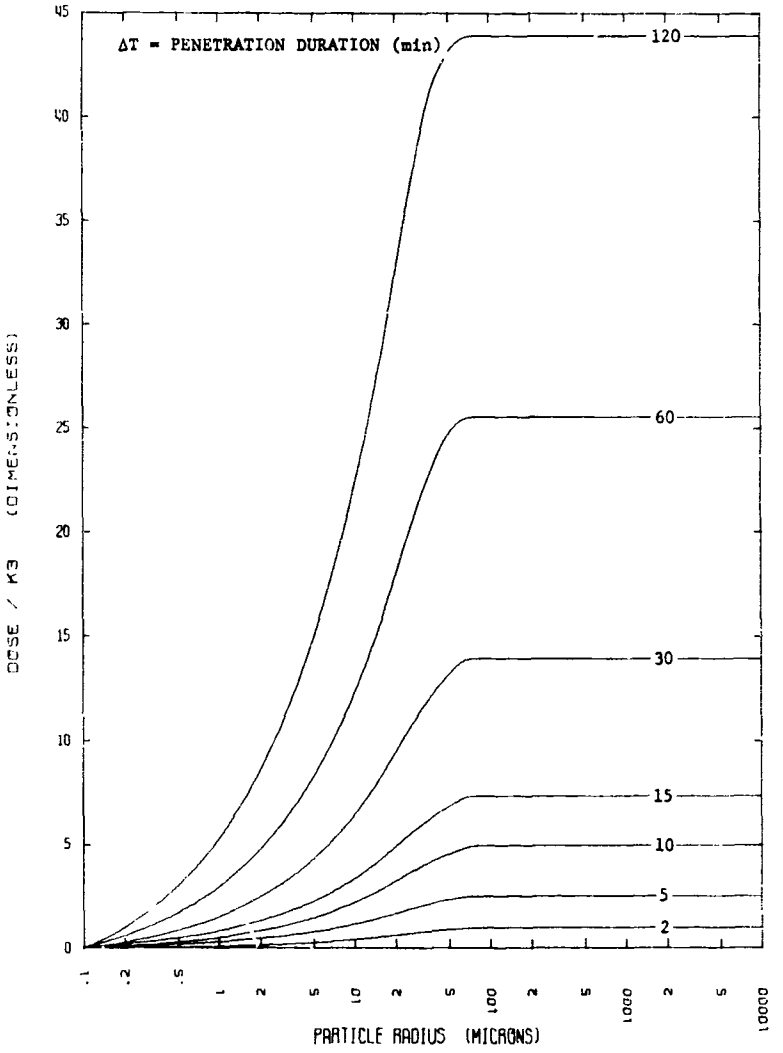

Figure B38. Cumulative Filter Dose at 30 Hours, TI = 1.5 Hours

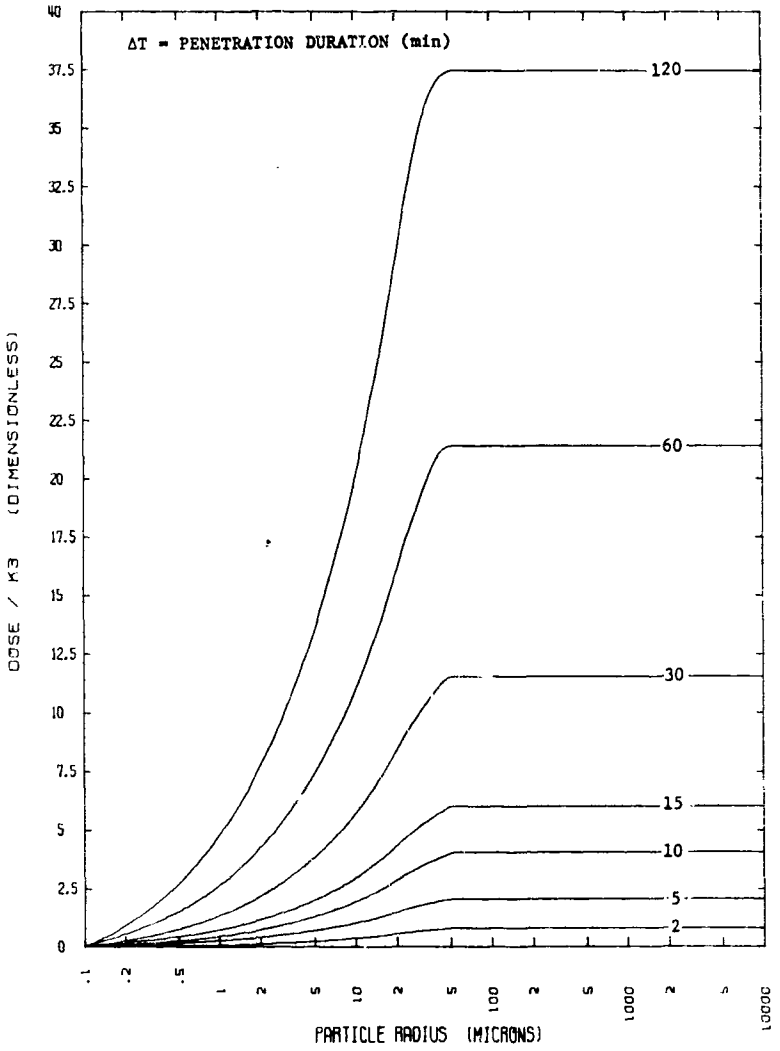

Figure B39. Cumulative Filter Dose at 30 Hours, TI = 2 Hours

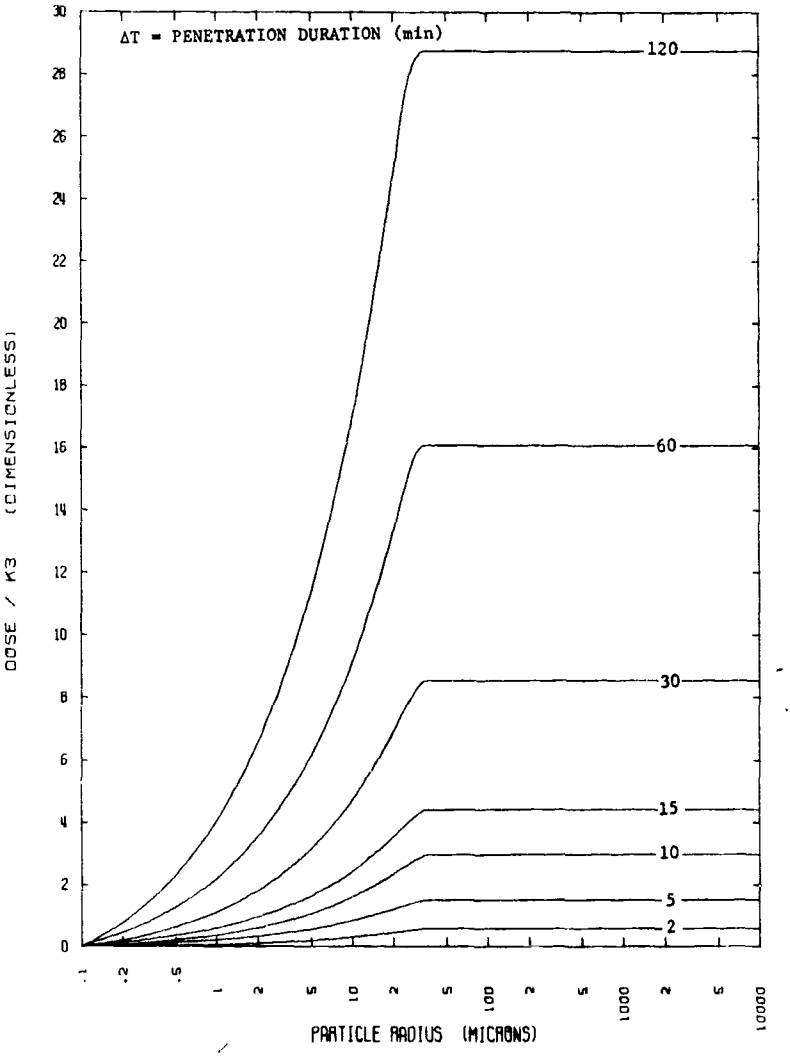

Figure B40. Cumulative Filter Dose at 30 Hours, TI = 3 Hours

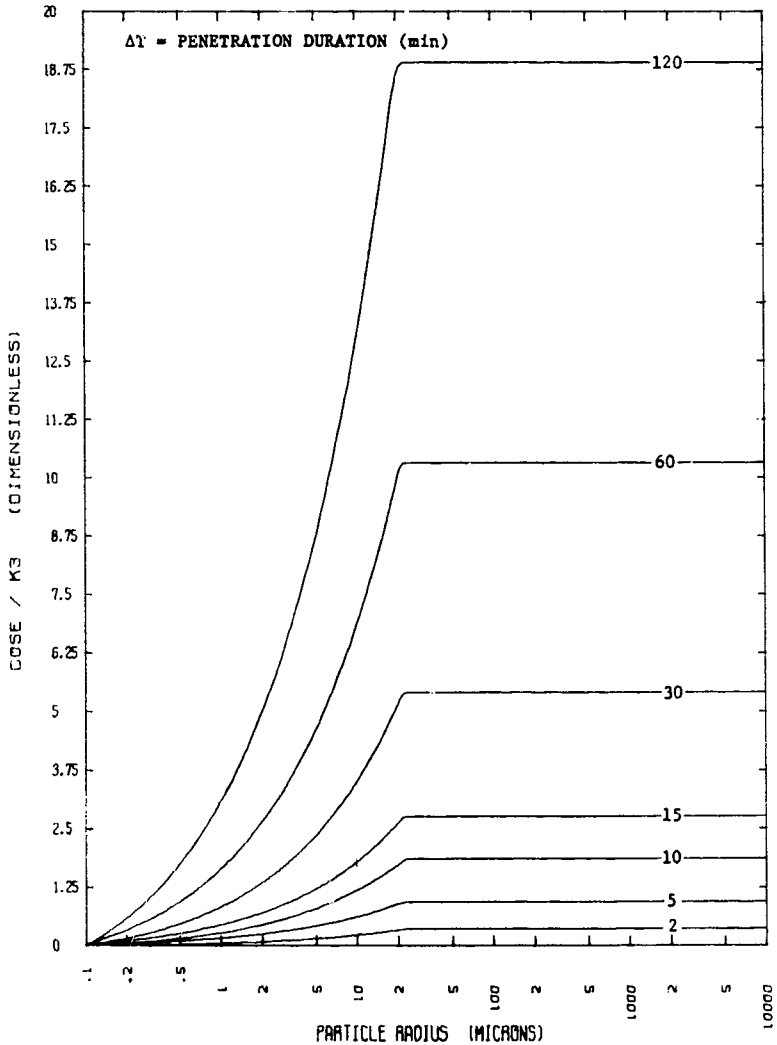

Figure B41. Cumulative Filter Dose at 30 Hours, TI = 5 Hours

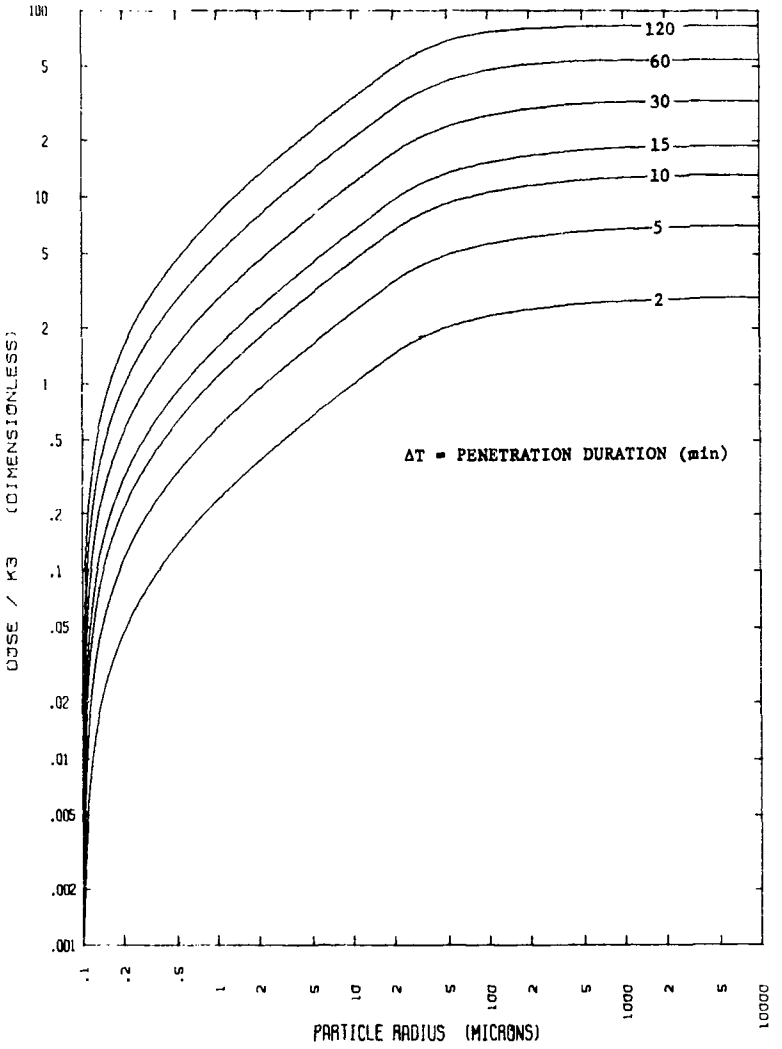

Figure B42. Cumulative Filter Dose at 30 Hours, TI = 10 Minutes

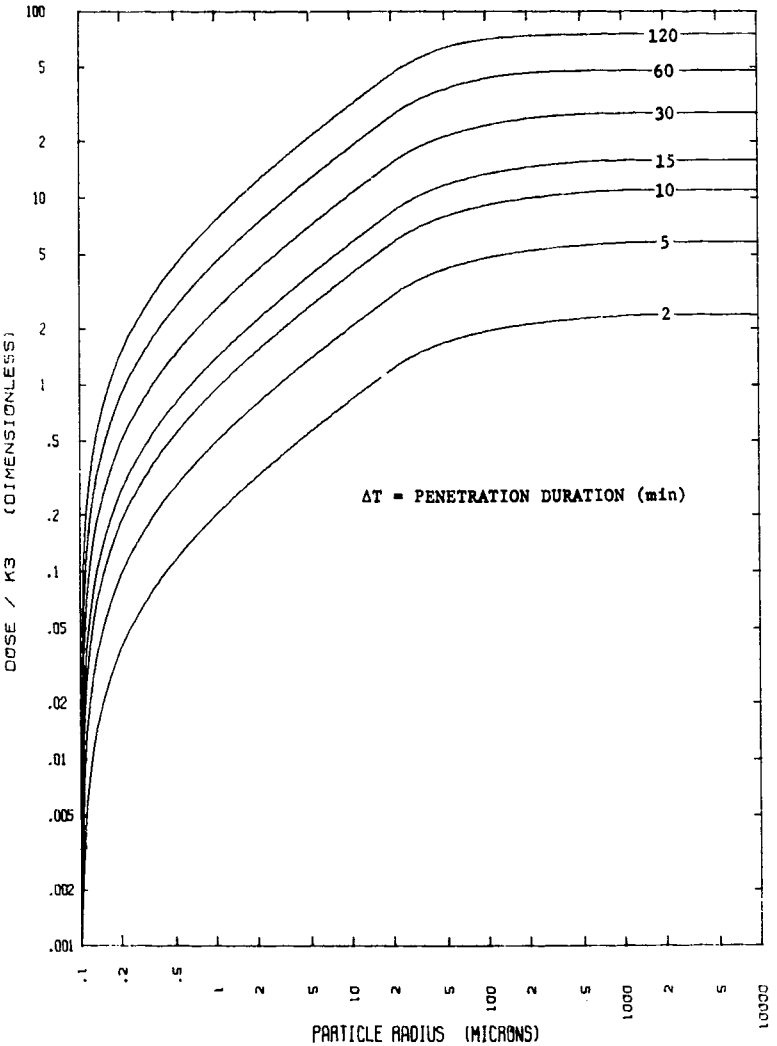

Figure B43. Cumulative Filter Dose at 30 Hours, TI = 18 Minutes

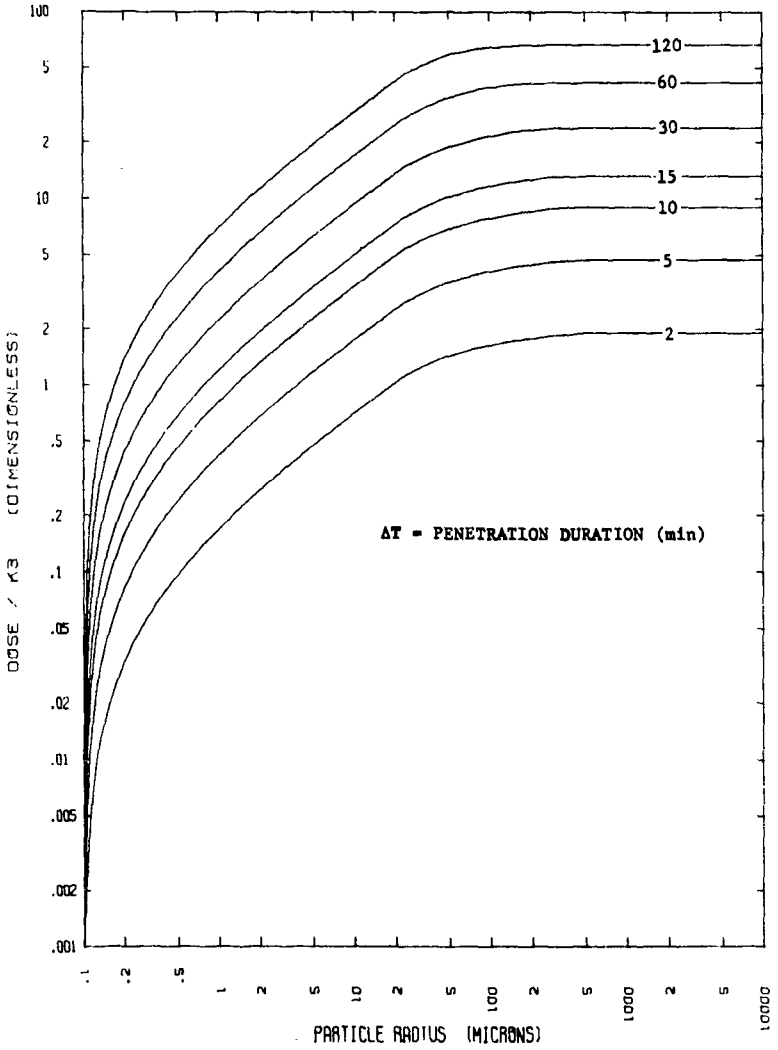

Figure B44. Cumulative Filter Dose at 30 Hours, TI = 30 Minutes

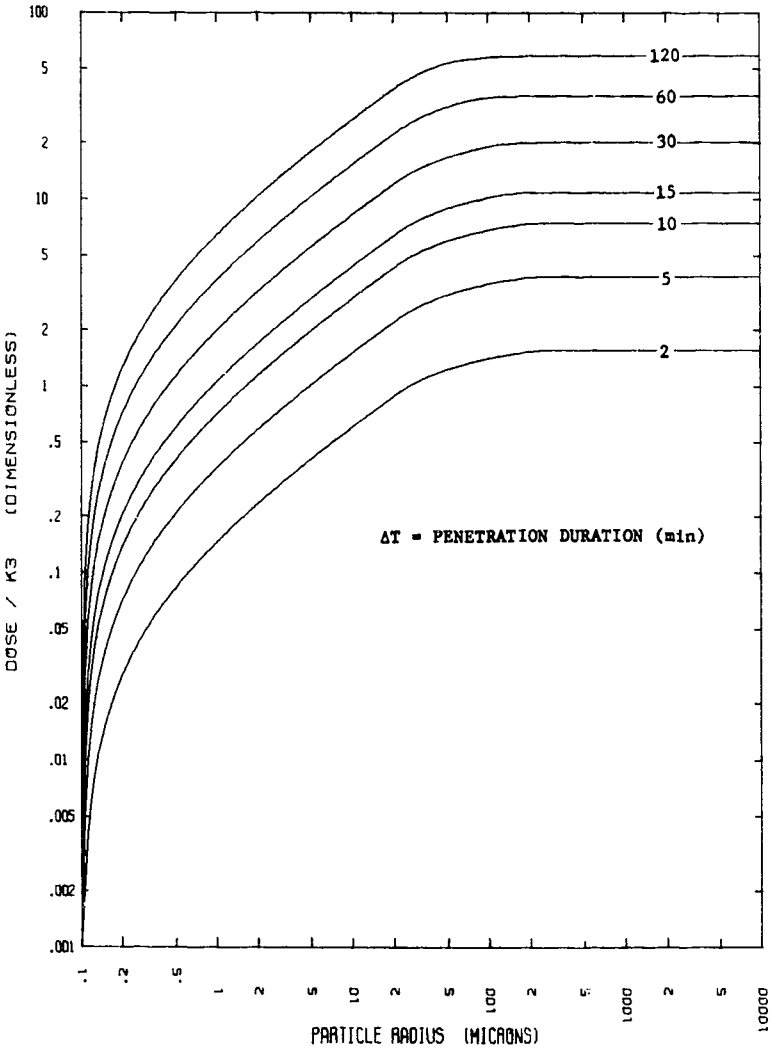

Figure B45. Cumulative Filter Dose at 30 Hours, TI = 45 Minutes

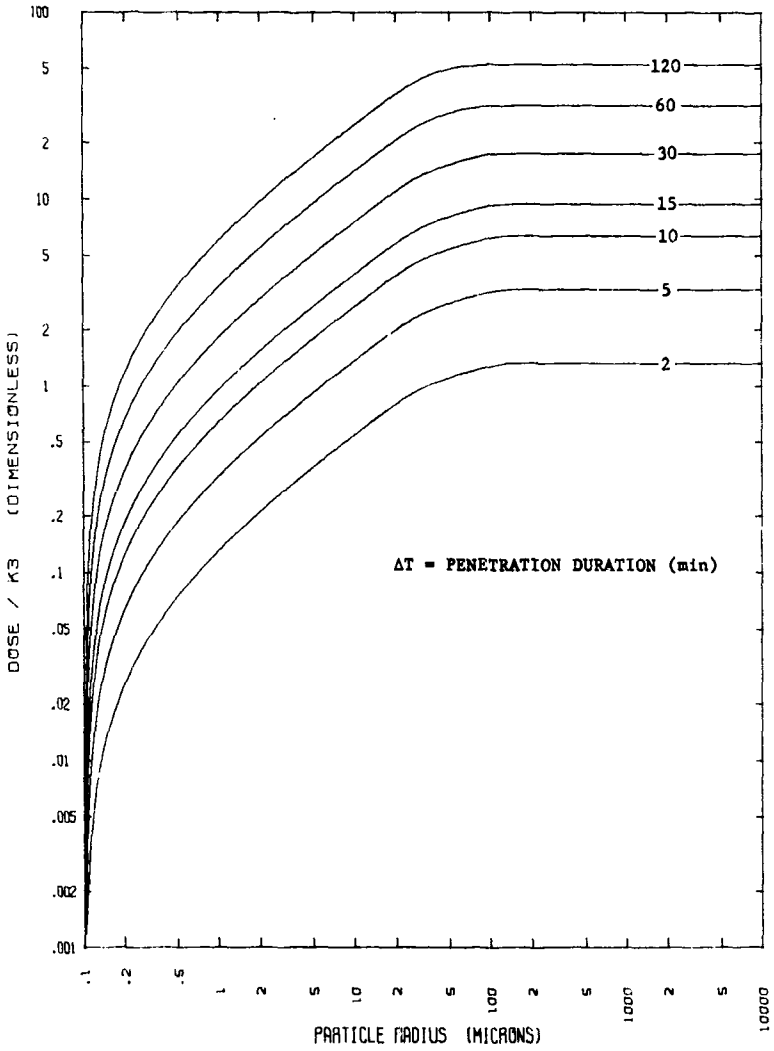

Figure B46. Cumulative Filter Dose at 30 Hours, TI = 1 Hour

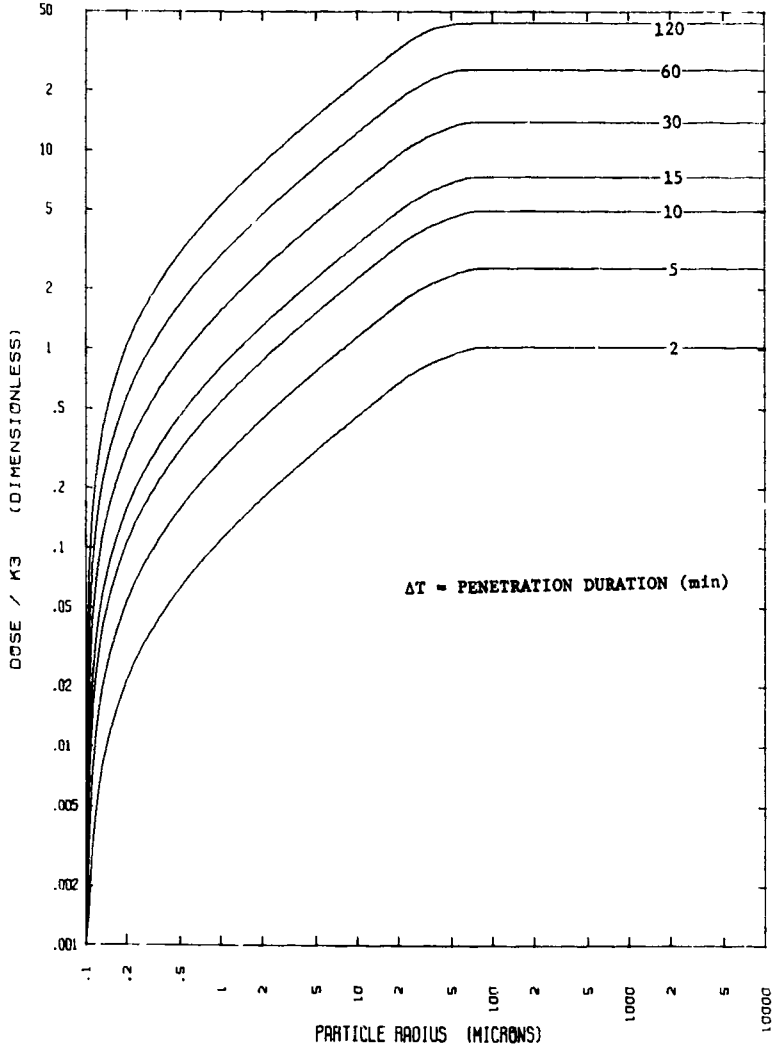

Figure B47. Cumulative Filter Dose at 30 Hours, TI = 1.5 Hours

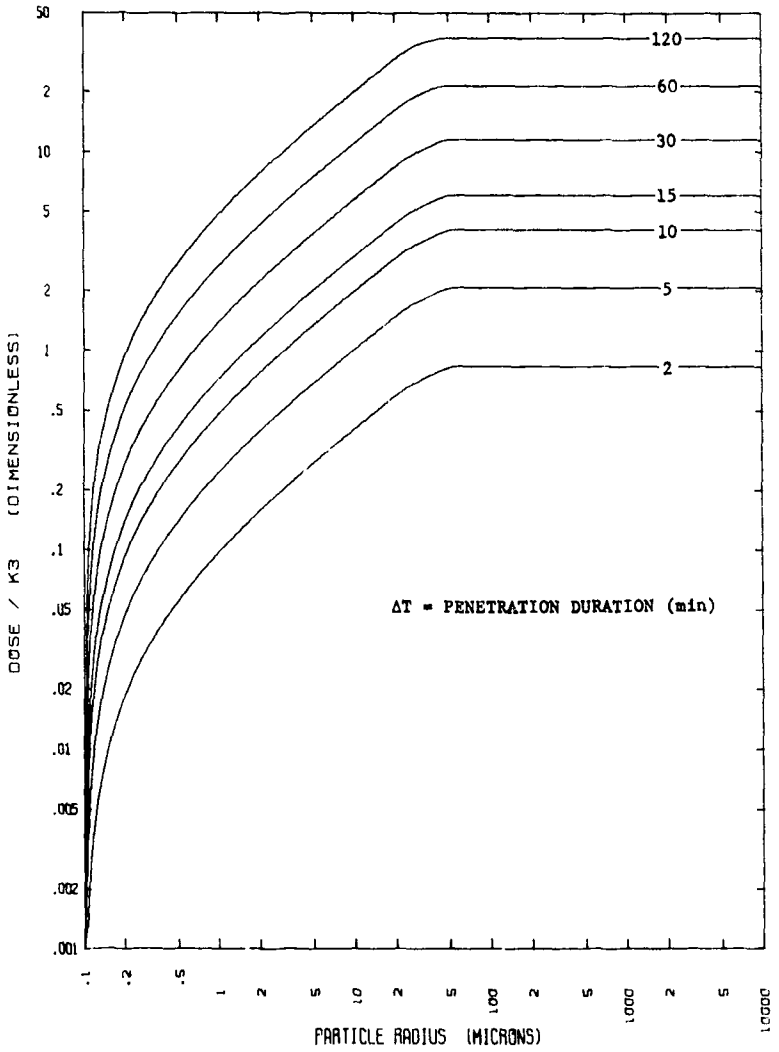

Figure B48. Cumulative Filter Dose at 30 Hours, TI = 2 Hours

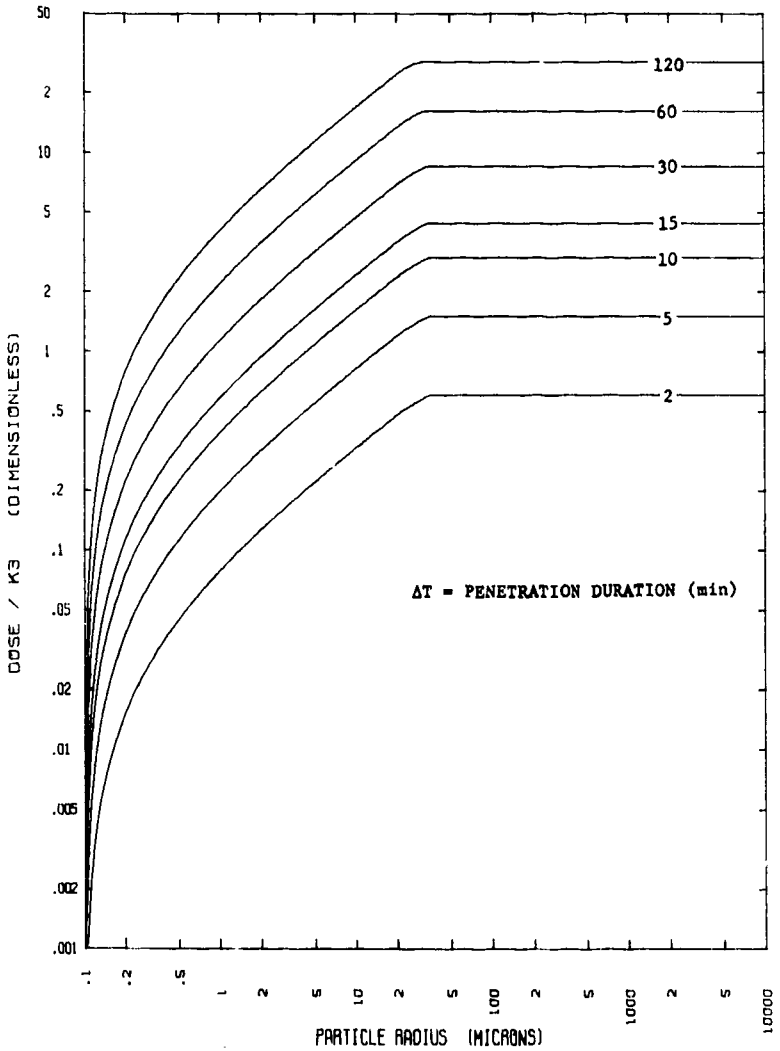

Figure B49. Cumulative Filter Dose at 30 Hours, TI = 3 Hours

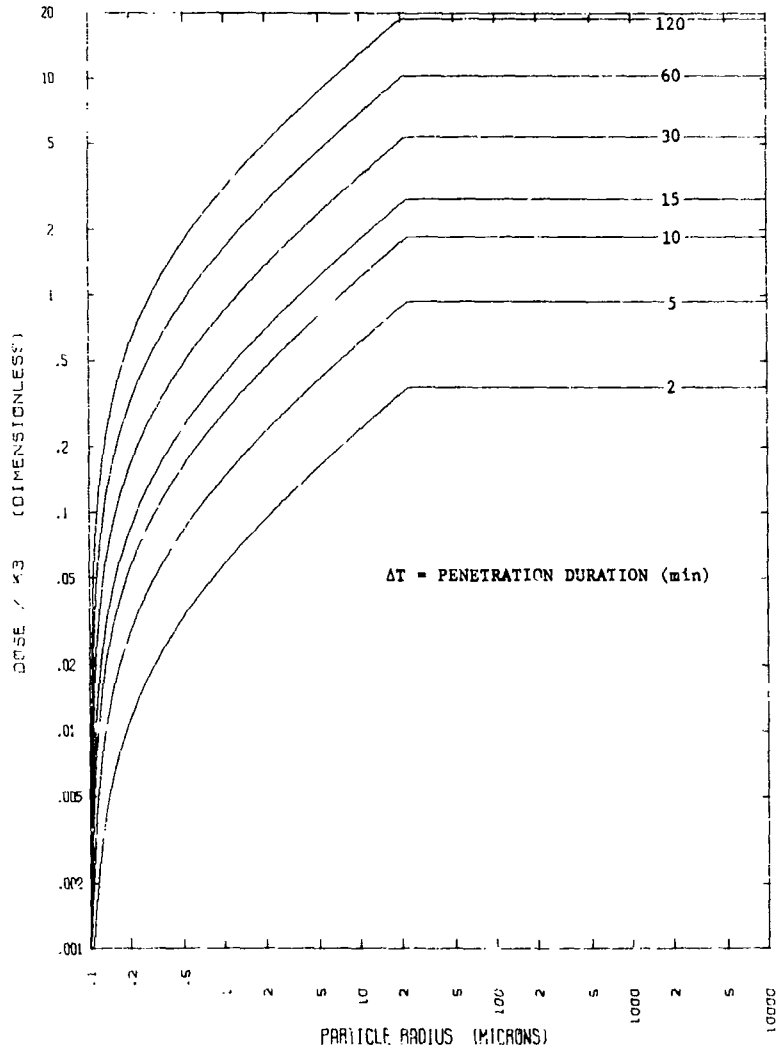

Figure B50. Cumulative Filter Dose at 30 Hours, TI = 5 Hours

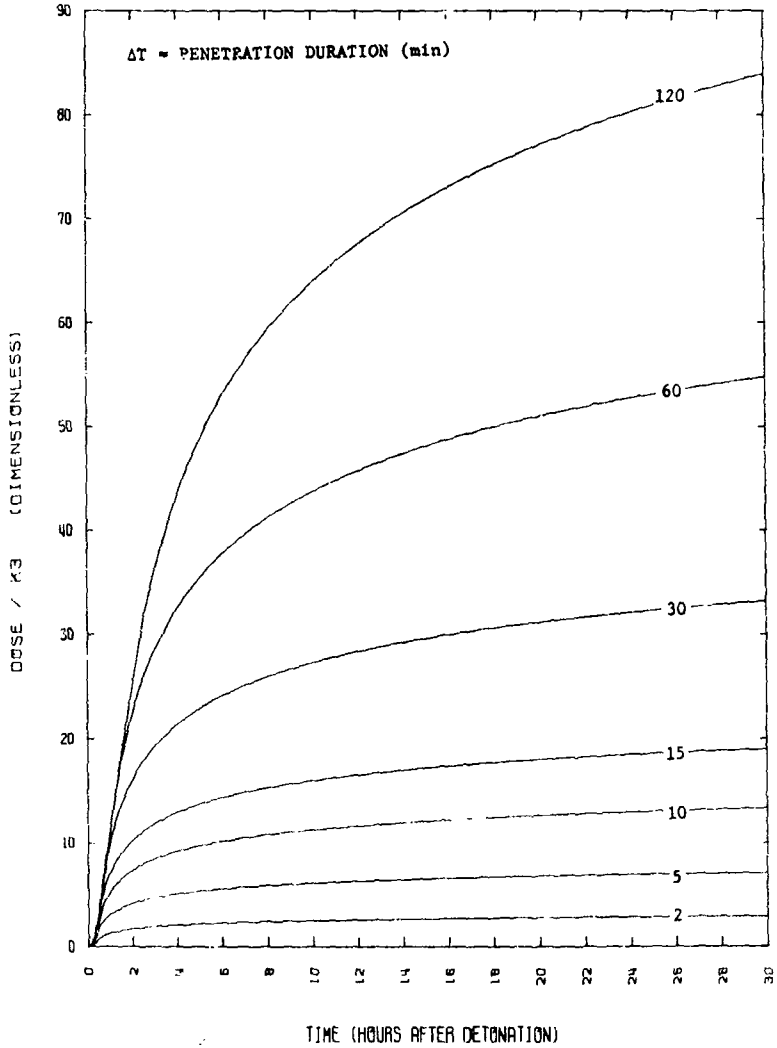

Figure 151. Filter Dose as a Function of Time, TI = 10 Minutes

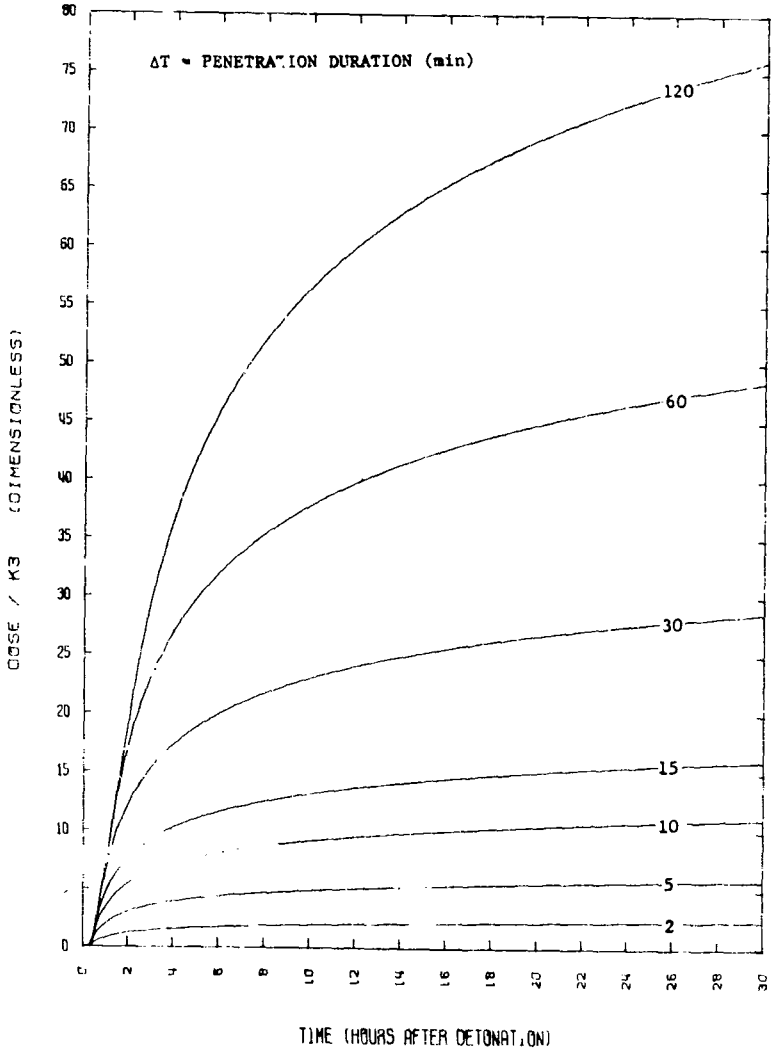

Figure B52. Filter Dose as a Function of Time, TI = 18 Minutes

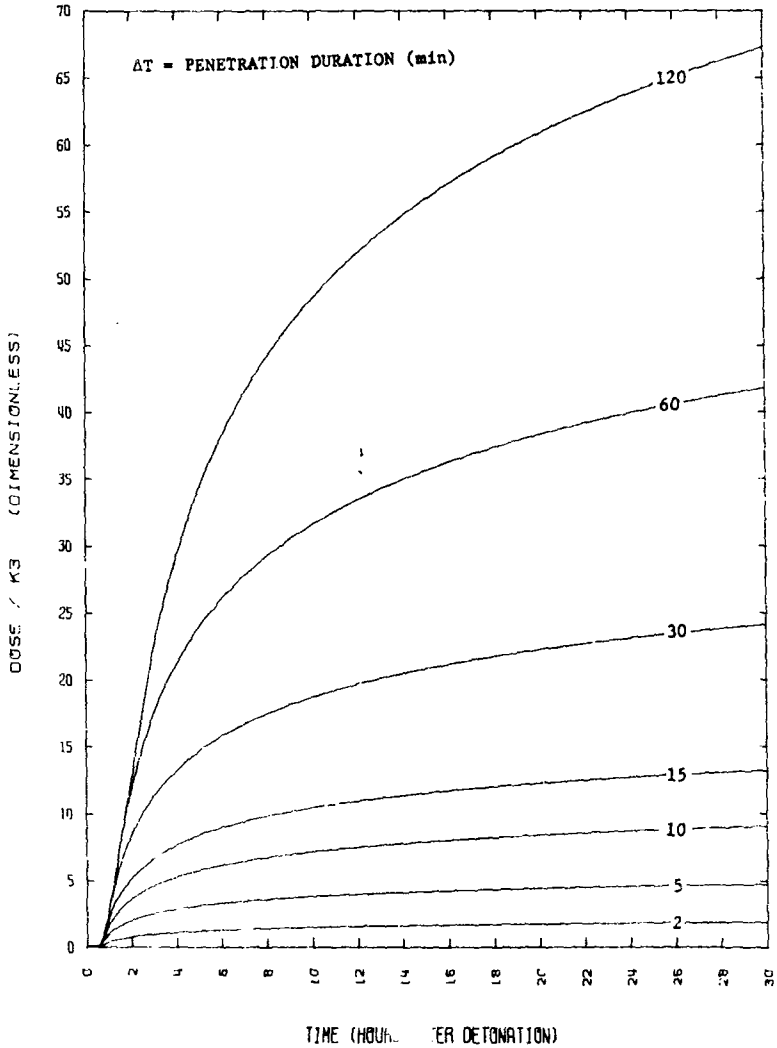

Figure B53. Filter Dose as a Function of Time, TI = 30 Minutes

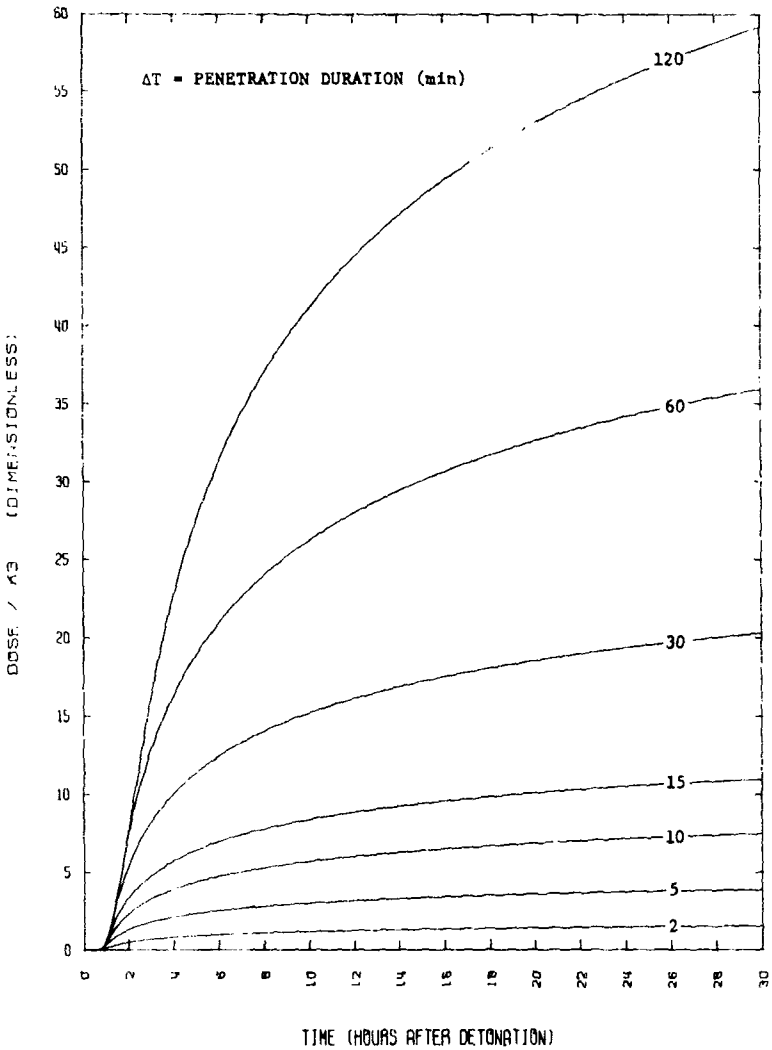

Figure B54. Filter Dose as a Function of Time, TI = 45 Minutes

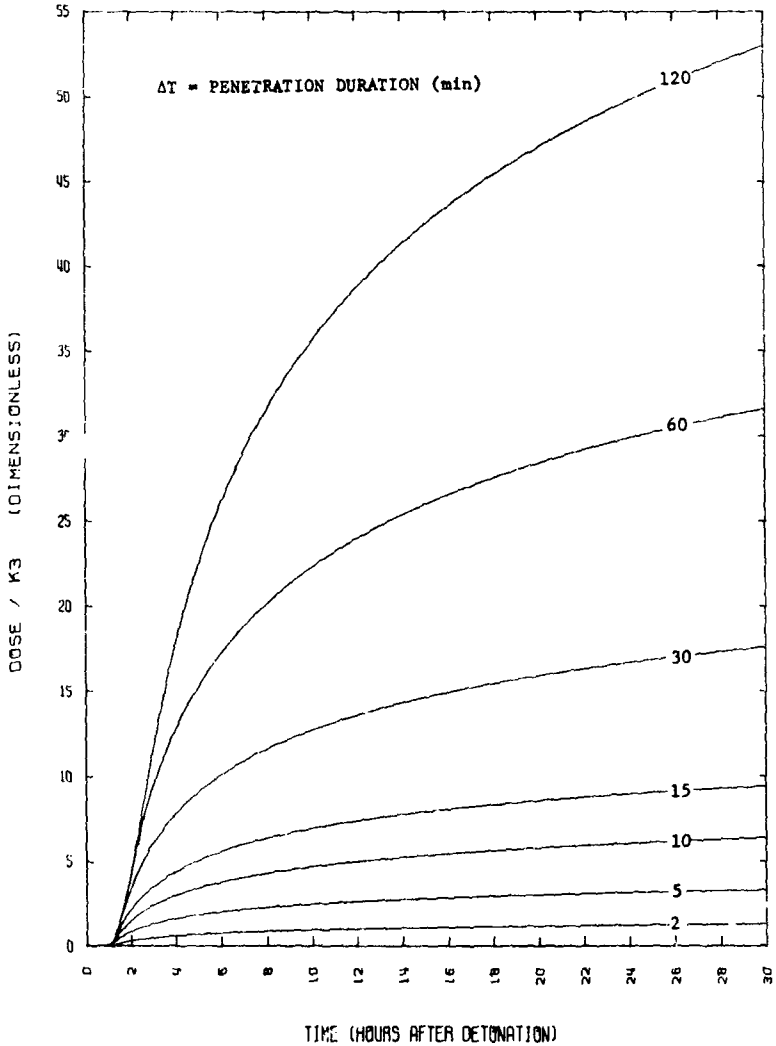

Figure B55. Filter Dose as a Function of Time, TI = 1 Hour

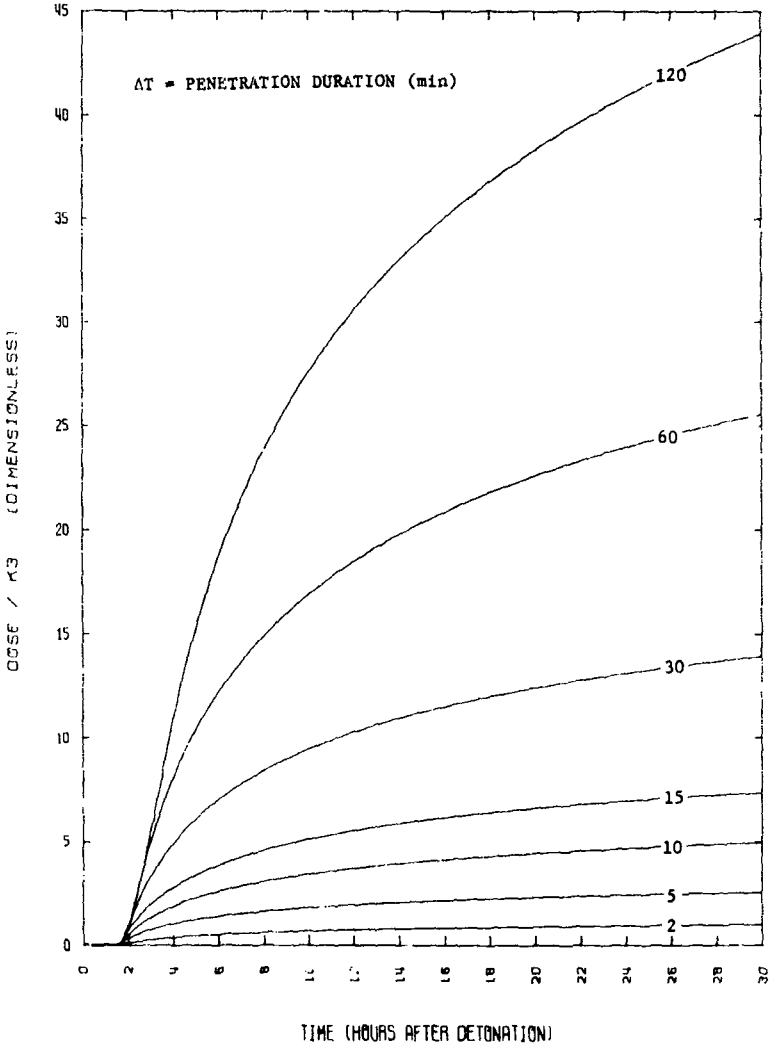

Figure B56. Filter Dose as a Function of Time, TI = 1.5 Hours

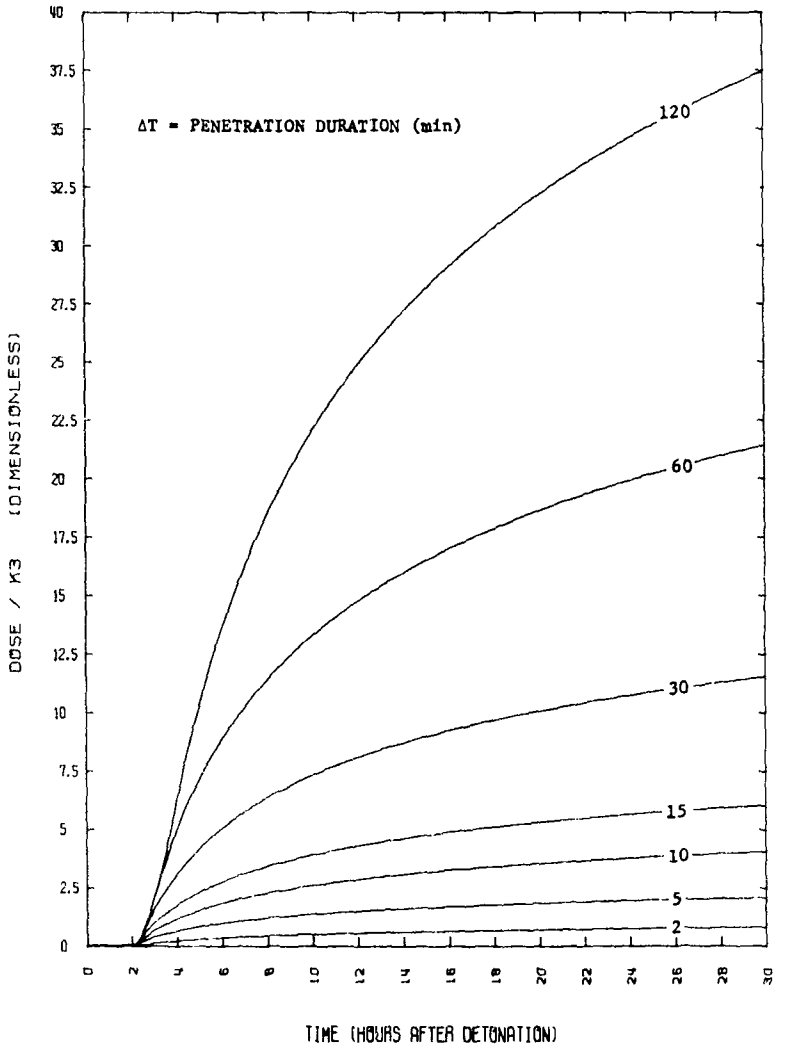

Figure B57. Filter Dose as a Function of Time, TI = 2 Hours

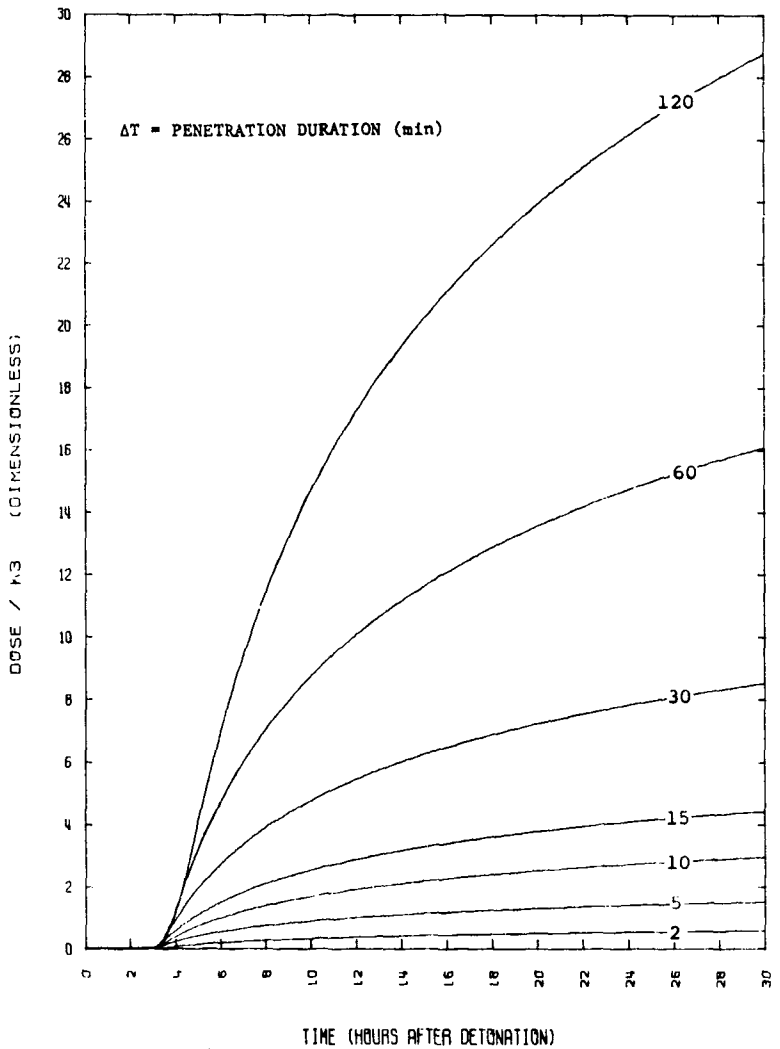

Figure B58. Filter Dose as a Function of Time, TI = 3 Hours

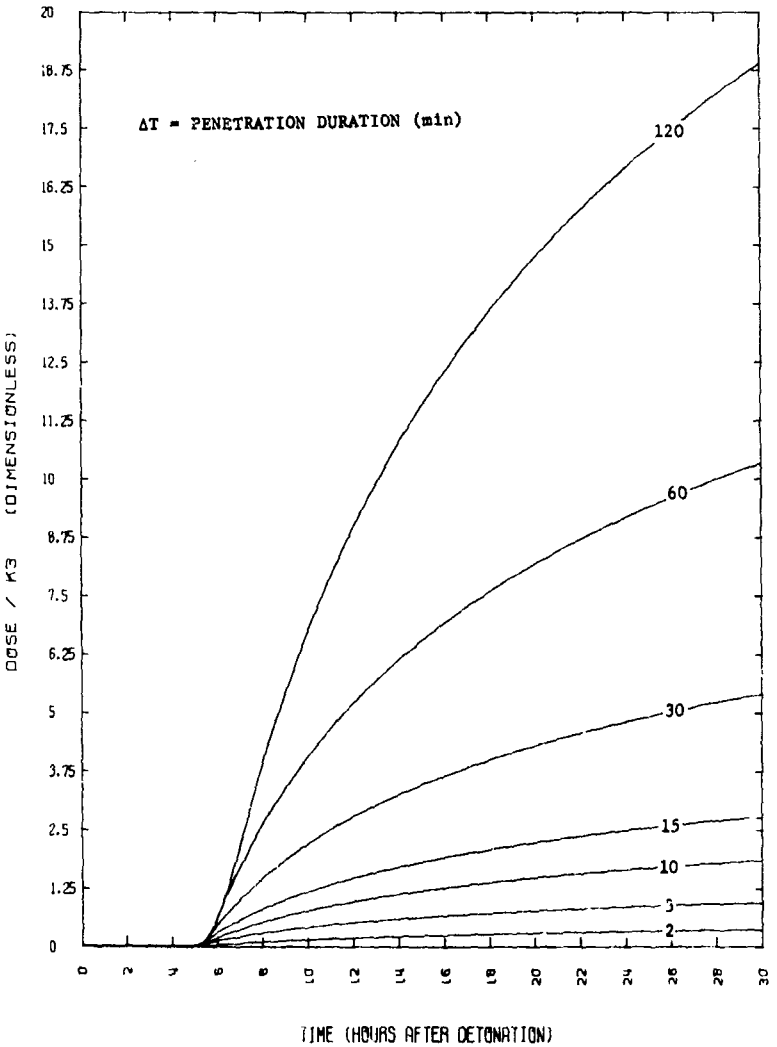

Figure B59. Filter Dose as a Function of Time, TI = 5 Hours

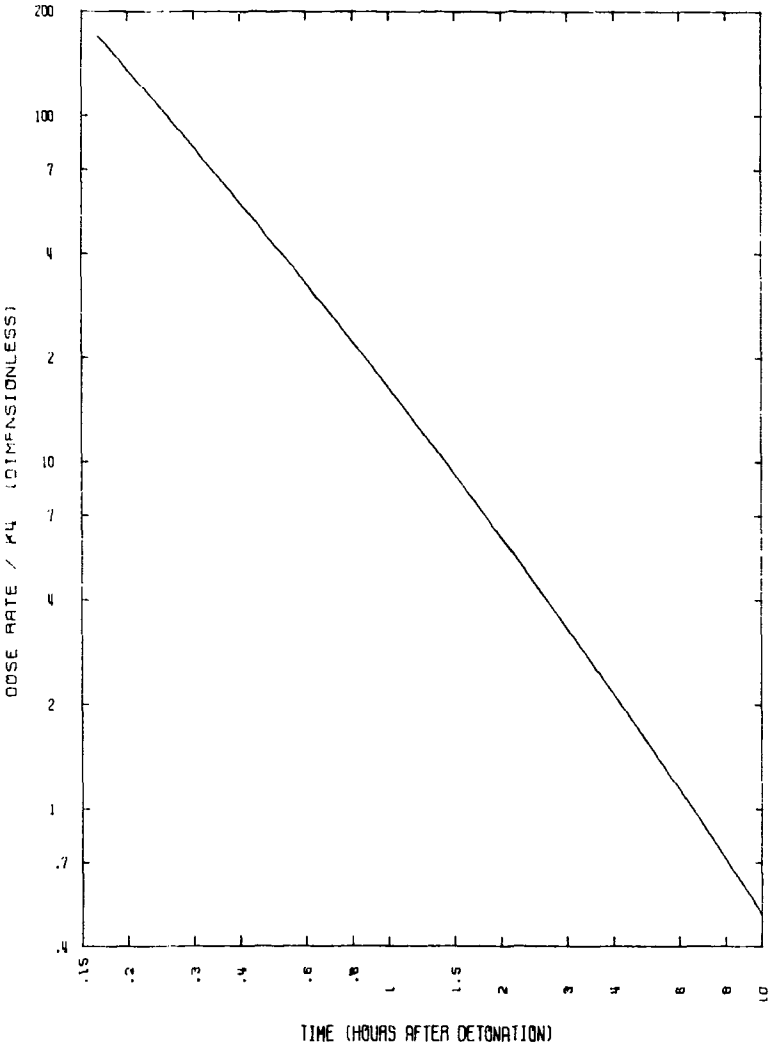

Figure B60. Cloud Immersion Dose Rate

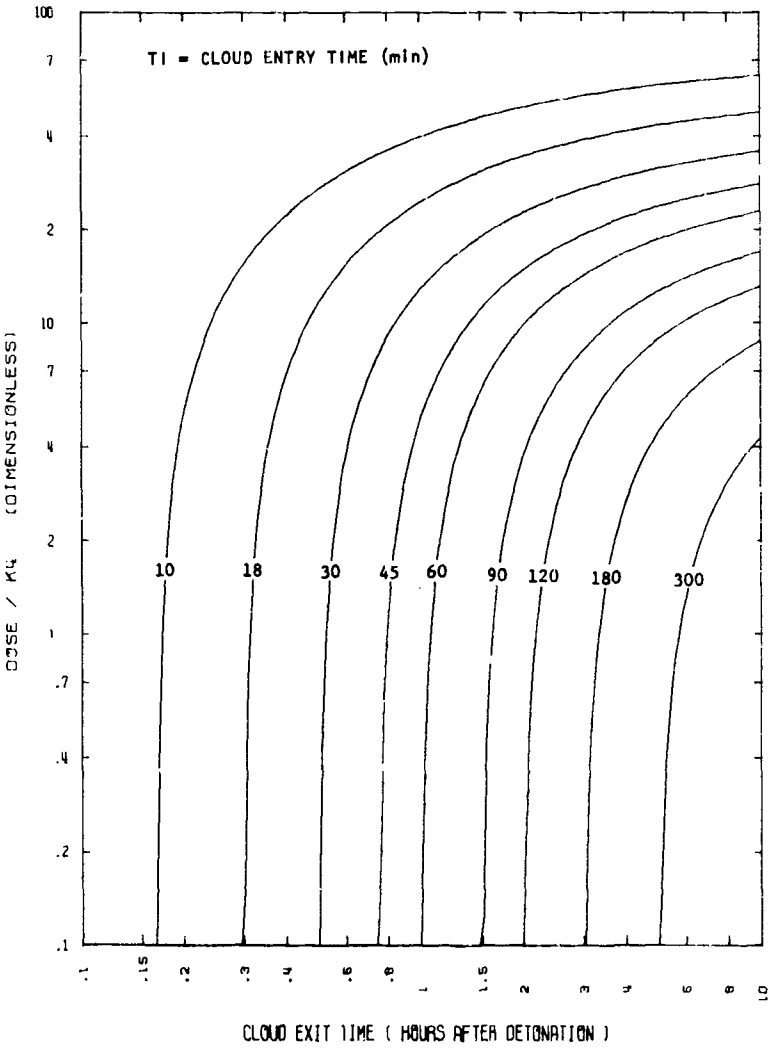

Figure B61. Cloud Immersion Dose

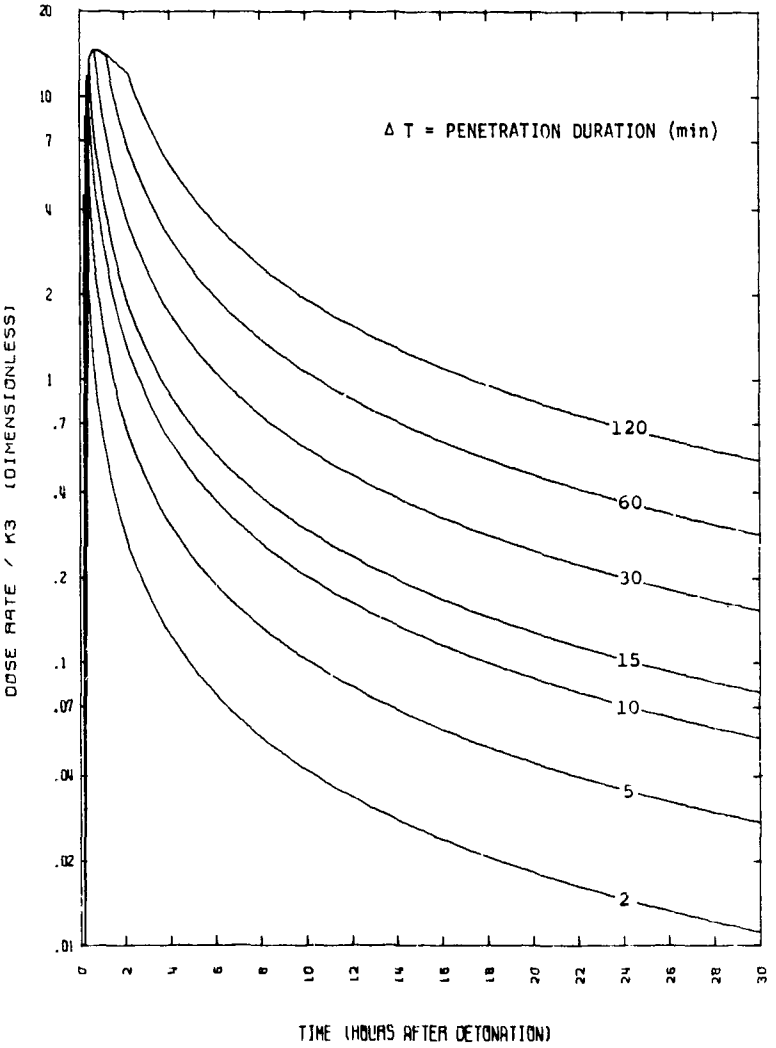

Figure B62. Filter Dust Dose Rate, TI = 10 Minutes

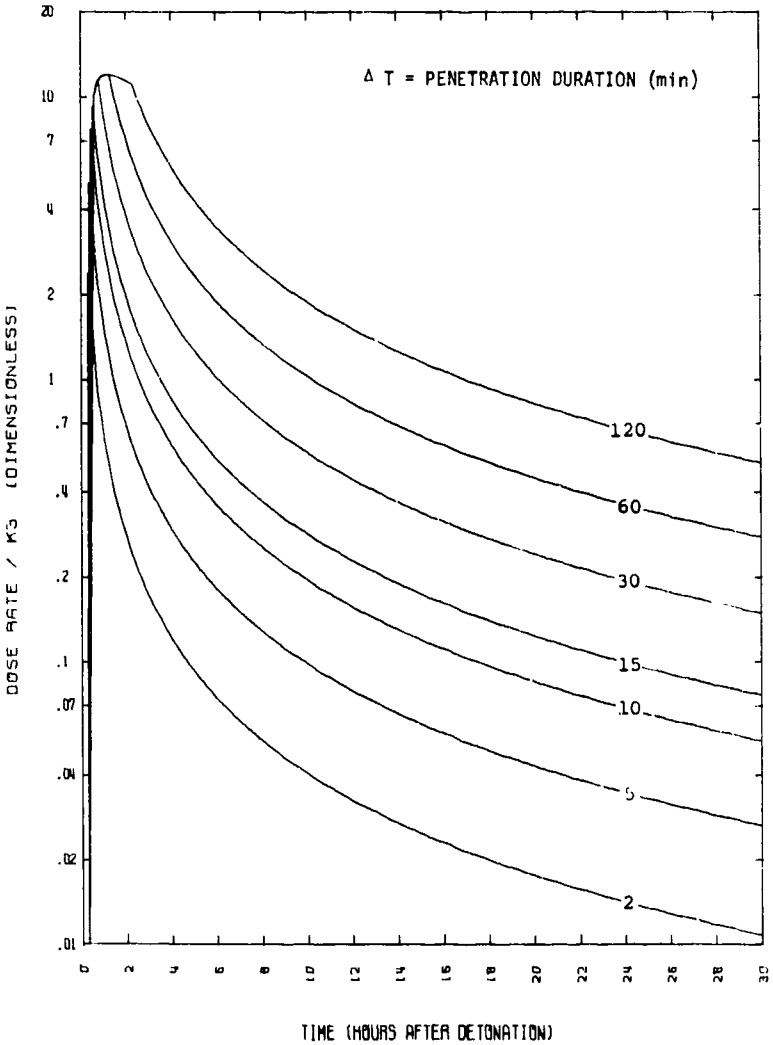

Figure B63. Filter Dust Dose Rate, TI = 18 Minutes

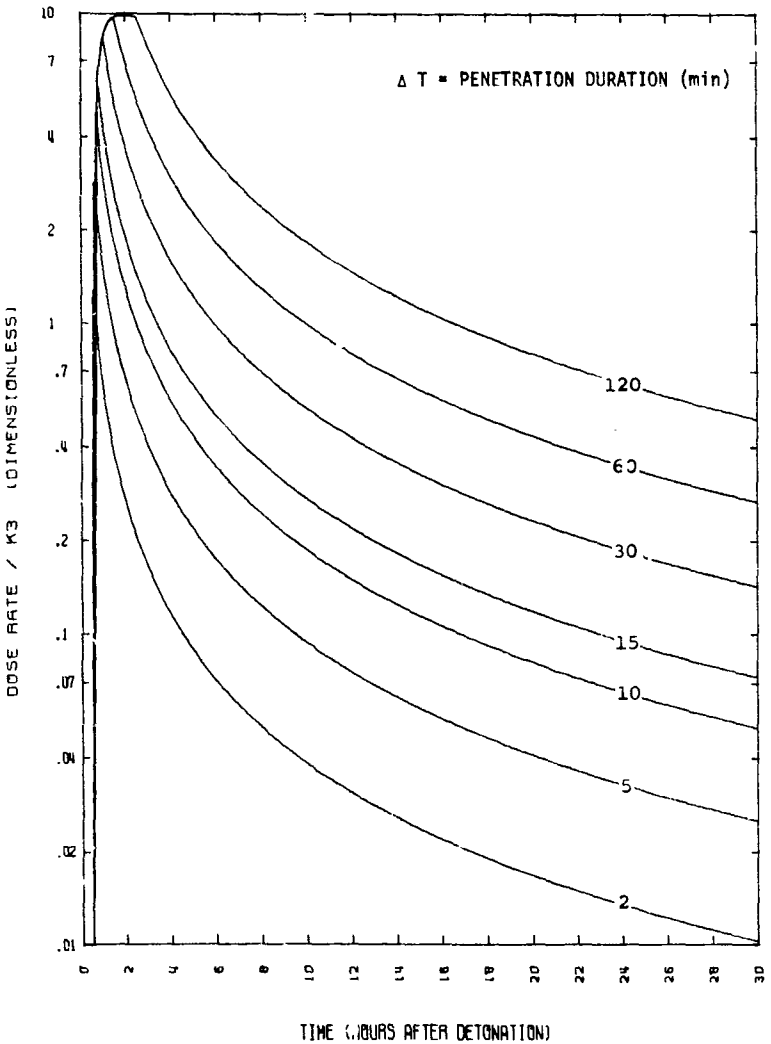

Figure B64. Filter Dust Dose Rate, TI = 30 Minutes

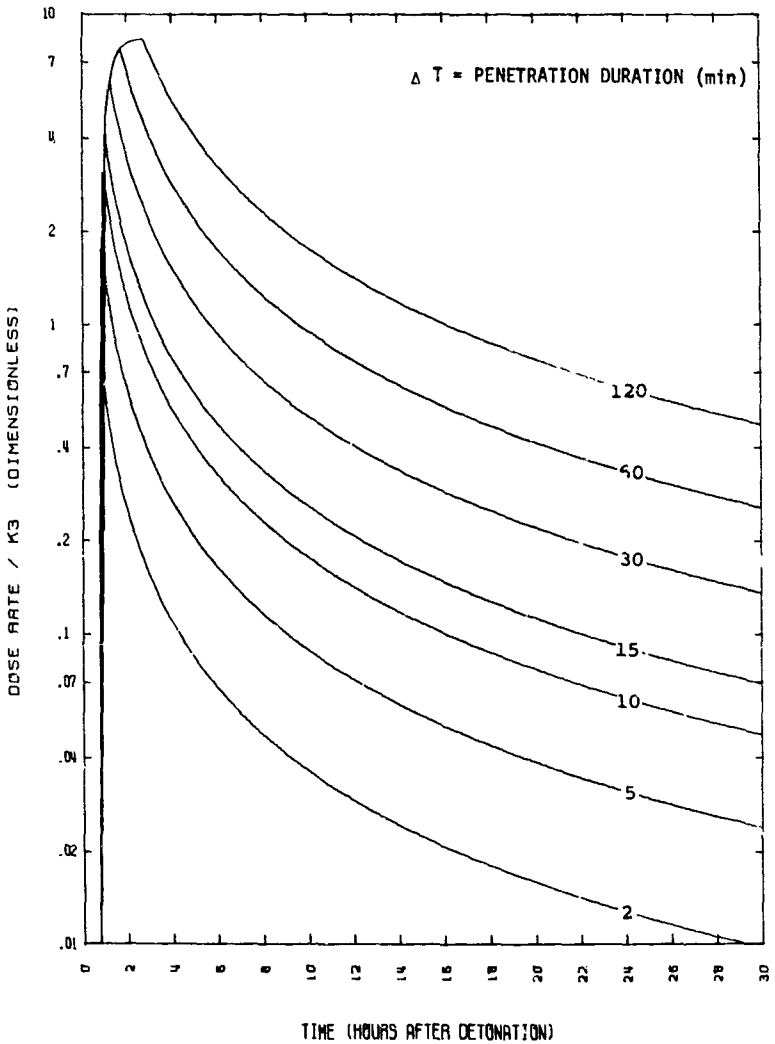

Figure 65. Filter Dust Dose Rate, TI = 45 Minutes

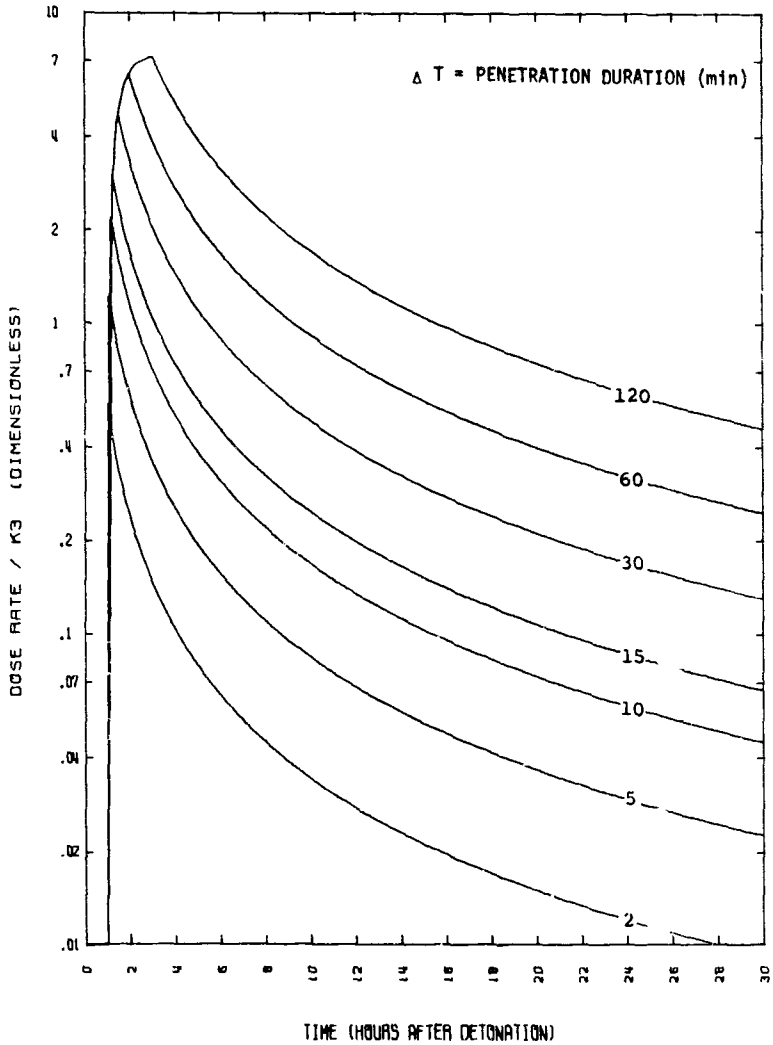

Figure B66. Filter Dust Dose Rate, TI = 1 Hour

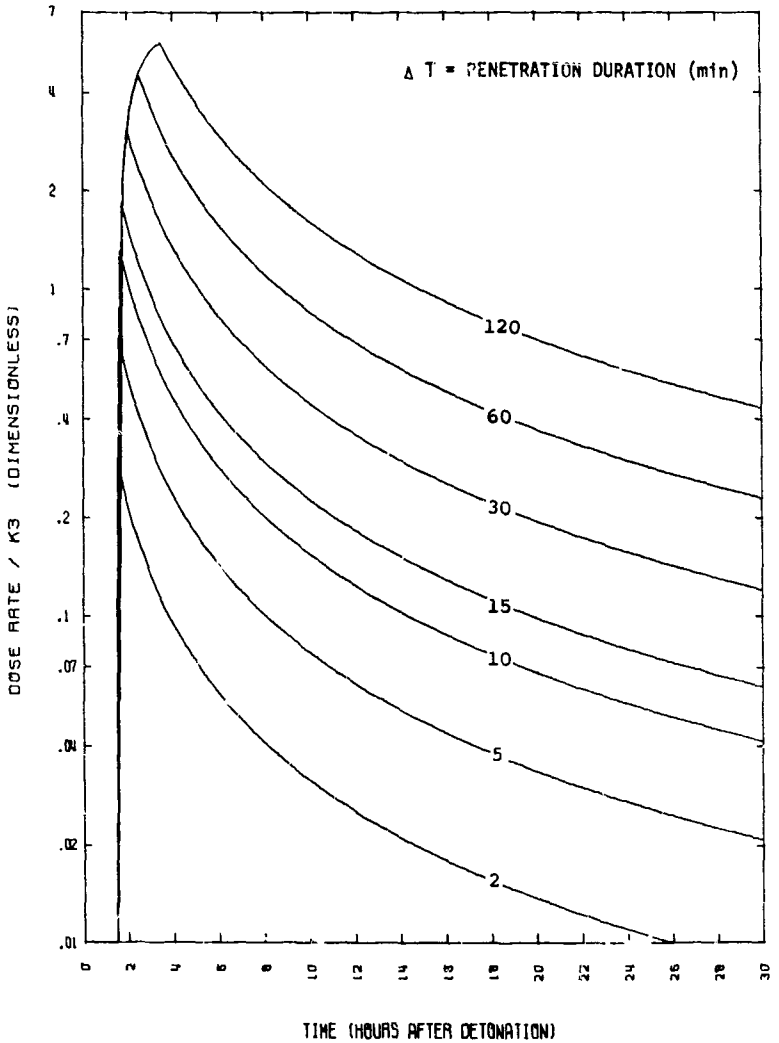

Figure B67. Filter Dust Dose Rate, TI = 1.5 Hours

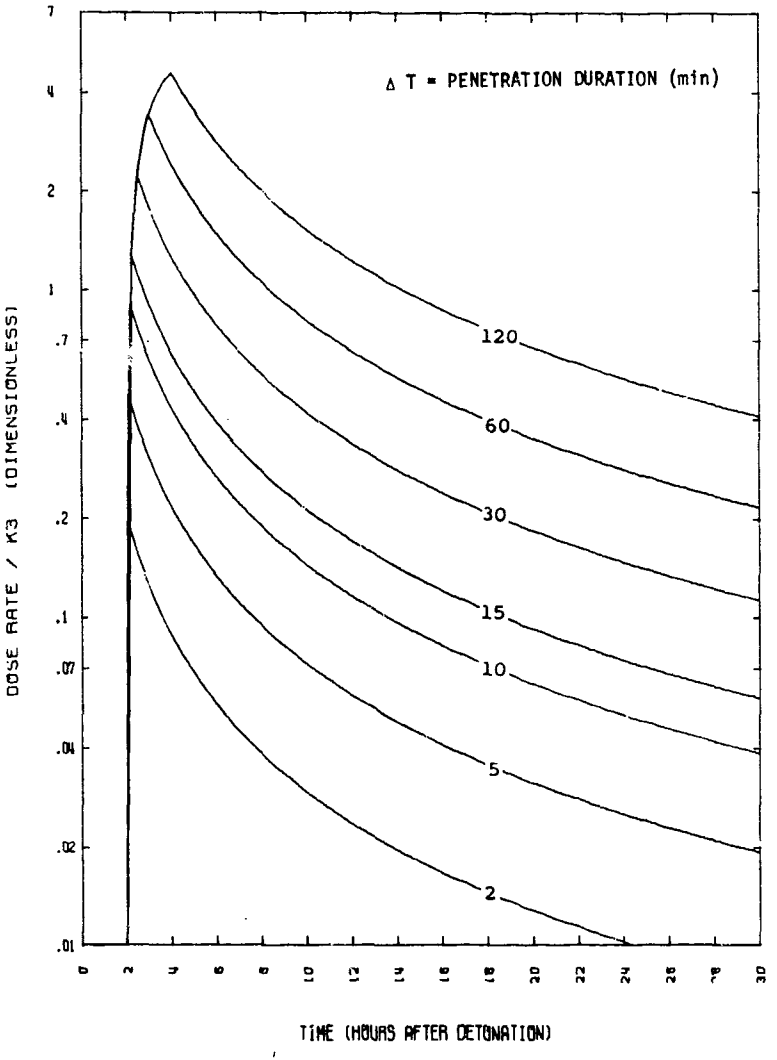

Figure B68. Filter Dust Dose Rate, TI = 2 Hours

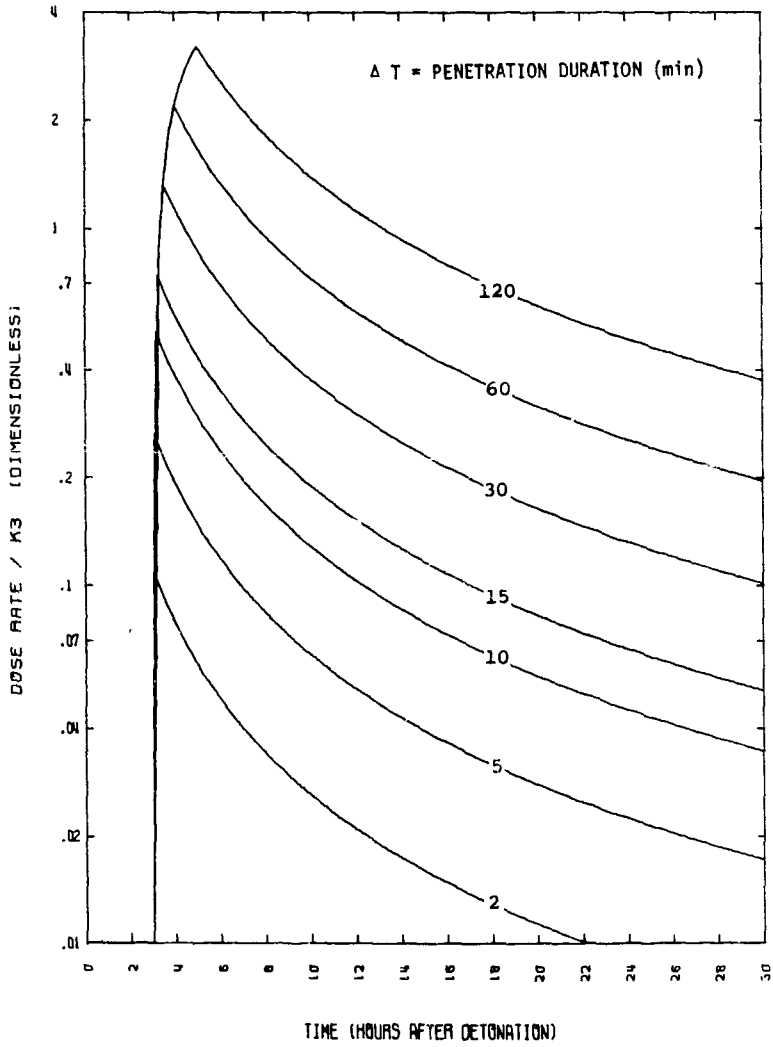

Figure B69. Filter Dust Dose Rate, TI = 3 Hours

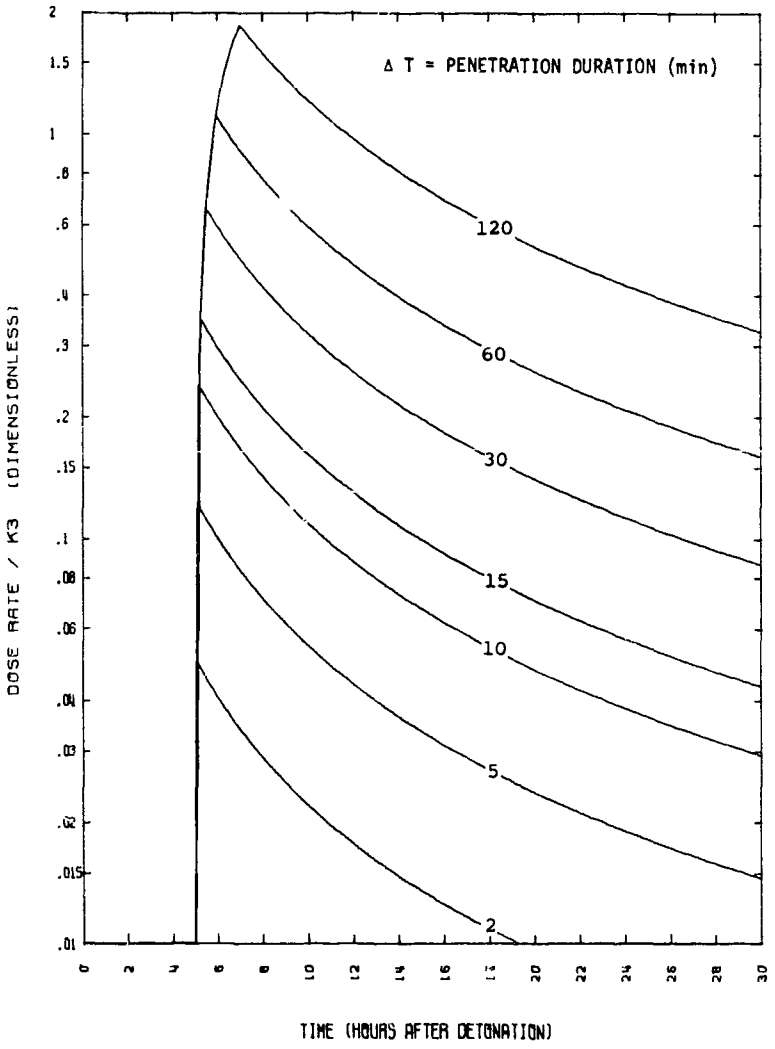

Figure B70. Filter Dust Dose Rate, TI = 5 Hours

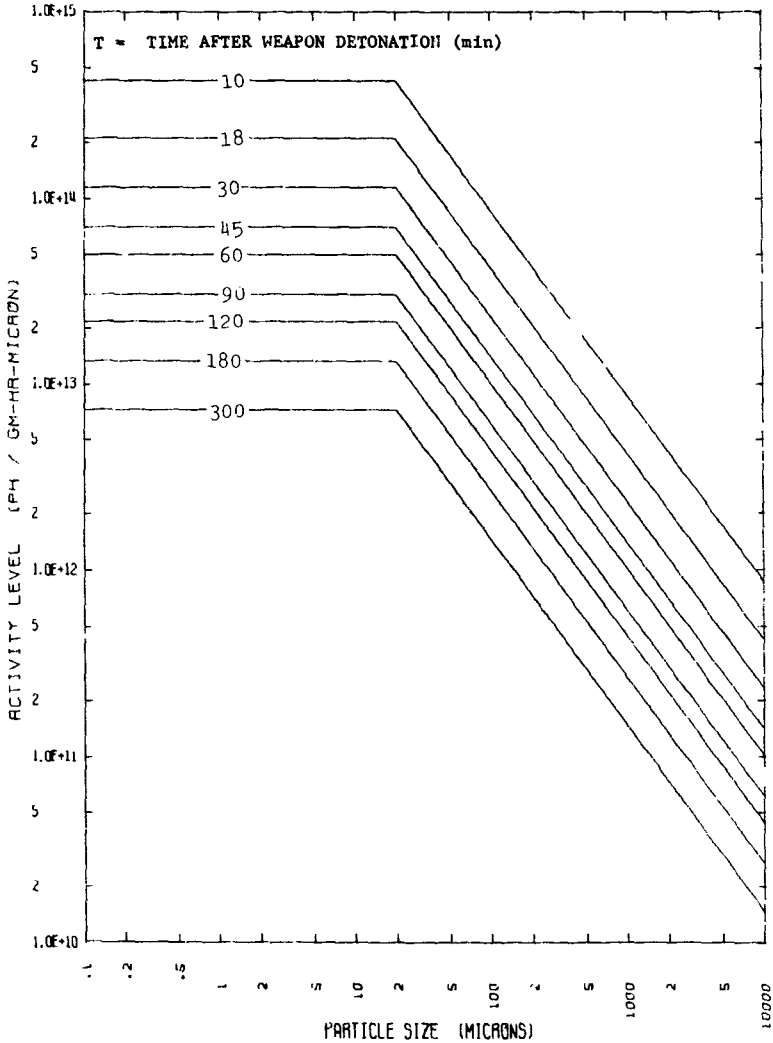

Figure B71. Specific Activity Distribution Function

APPENDIX C

ZERO FALLOUT MODEL

This appendix presents an investigation of the limiting case of a cloud with no fallout. This case is useful because it yields results which are a worst case and which act as a standard of comparison for other cloud models which include fallout. It serves as a check on results of other models to ensure that the general trends and qualitative results are reasonable and realistic.

This limiting case is achieved by "freezing" the 10-minute dust density distribution presented in appendix A, equation (A-1), for all time, i.e., no later fallout is allowed.

$$\rho_d(t) = a_i \left[t^{-1.6} + 1.313\ t^{-0.3} \right] \tag{C-1}$$

$$= a_i \left[(0.167)^{-1.6} + 1.313\ (0.167)^{-0.3} \right] \tag{C-2}$$

$$= 19.83\ a_i \tag{C-3}$$

The same approach used in appendix A yields the relationships below. Note that the only time dependence allowed is that associated with the radioactive decay of the fission products.

$$\frac{\dot{M}_{d_{e/f}}}{K_{1/2}} = 19.83 \qquad t_i \le t \le t_f \tag{C-4}$$

$$\frac{M_{d_{e/f}}(t)}{K_{1/2}} = 19.83\ (t - t_i) \qquad t_i \le t \le t_f \tag{C-5}$$

$$\frac{M_{d_{e/f}}(t)}{K_{1/2}} = 19.83\ (t_f - t_i) \qquad t \geq t_f \qquad \text{(C-6)}$$

$$\frac{\dot{D}_f(t)}{K_3} = 19.83\ (t - t_i)\ t^{-1.2} \qquad t_i \leq t \leq t_f \qquad \text{(C-7)}$$

$$\frac{\dot{D}_f(t)}{K_3} = 19.83\ (t_f - t_i)\ t^{-1.2} \qquad t \geq t_f \qquad \text{(C-8)}$$

$$\frac{D_f(t)}{K_3} = 24.79\ \left(t^{0.8} + 4\ t_i\ t^{-0.2} - 5\ t_i^{\,0.8}\right) \qquad t_i \leq t \leq t_f \qquad \text{(C-9)}$$

$$\frac{D_f(t)}{K_3} = 123.94\left(t_f^{\,0.8} - t_i^{\,0.8} - 0.8(t_f - t_i)\ t^{-0.2}\right) \qquad t \geq t_f \qquad \text{(C-10)}$$

$$\frac{\dot{D}_c(t)}{K_4} = 19.83\ t^{-1.2} \qquad t_i \leq t \leq t_f \qquad \text{(C-11)}$$

$$\frac{D_c(t)}{K_4} = 99.15\ \left(t_i^{-0.2} - t^{-0.2}\right) \qquad t_i \leq t \leq t_f \qquad \text{(C-12)}$$

$$\frac{D_c(t)}{K_4} = 99.15\ \left(t_i^{-0.2} - t_f^{-0.2}\right) \qquad t \geq t_f \qquad \text{(C-13)}$$

where K_1, K_2, K_3, and K_4 are defined in appendix A, equation (A-44).

Figures C1 through C7 present representative graphic solutions of these dose rate, dose, and mass equations. Figure C1 depicts the total mass of dust trapped by the filter during a penetration of indefinite duration for TIs of 10 minutes and 1 hour after detonation. Note that the results are represented

by a simple linear function. There is no fallout to decrease the dust pickup with time. Figures C2 and C3 depict the filter dose rate as a function of time. The decrease with time is much less apparent here because of the zero fallout assumption. The only decrease is caused by radioactive decay. Figures C4 and C5 depict the filter dose as a function of time. The entry times for the figures are self explanatory and the penetration durations are the same as were presented in appendix A. Figure C6 depicts the dose rate due to immersion in the cloud. Note that the time dependence is strictly due to radioactive decay. Figure C7 depicts the cloud immersion dose for TIs of 10 and 60 minutes after detonation. Detailed explanations on the use of similar graphs were presented in appendixes A and B.

With some physical reasoning and heuristic argument, this model could be likened to the cloud resulting from an atmospheric burst. An atmospheric burst does not generate the cloud of dust as does a surface detonation. The fission fragments and neutron activated weapons debris are distributed throughout similar volumes, but there is little or no fallout. The bomb debris consists of condensed particles in the submicron to micron range and tends to remain suspended in the atmosphere. Therefore, this Zero Fallout or "limit case" is similar to an atmospheric burst and should yield similar dose and dose rate results, because in either case the total number of fission fragments are the same and in both cases they remain suspended for extremely long times in the atmosphere. The dose rates and doses are functions of time only through the decay of the fission products.

For an atmospheric detonation, the immersion dose determined from this model is directly applicable. The filter dust mass and dose, however, cannot be so simply determined. In fact, because of the very small particle sizes involved, very little of this radioactive material would be trapped in the aircraft. Most would remain suspended in the air and would be ejected from the aircraft with the air. Therefore, if this model is used to represent the penetration of a cloud generated by an atmospheric detonation, only the cloud immersion dose results of all the results in the above equations would be pertinent.

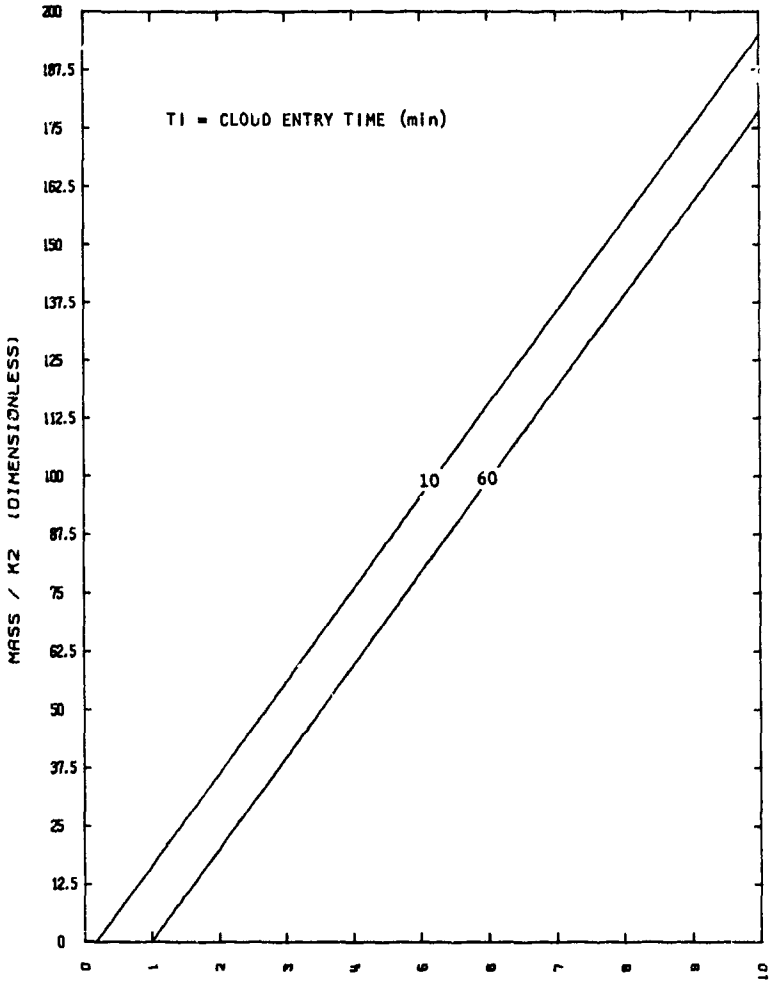

Figure C1. Filter Dust Mass as a Function of Time

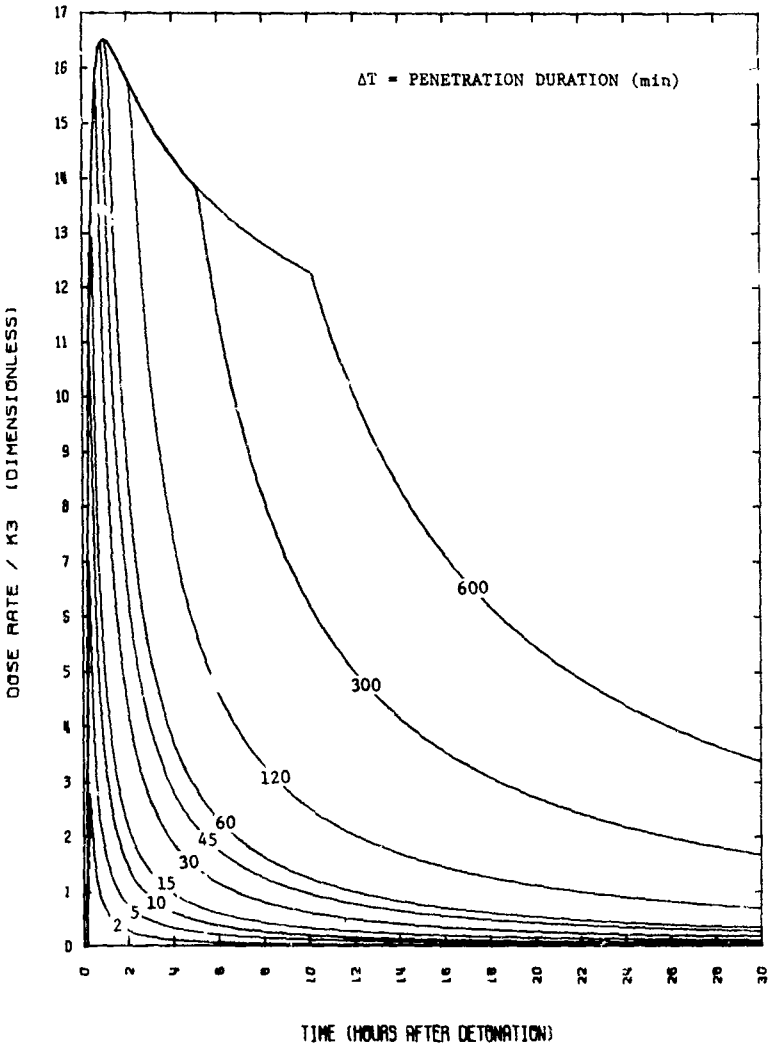

Figure C2. Filter Dose Rate as a Function of Time, TI = 10 Minutes

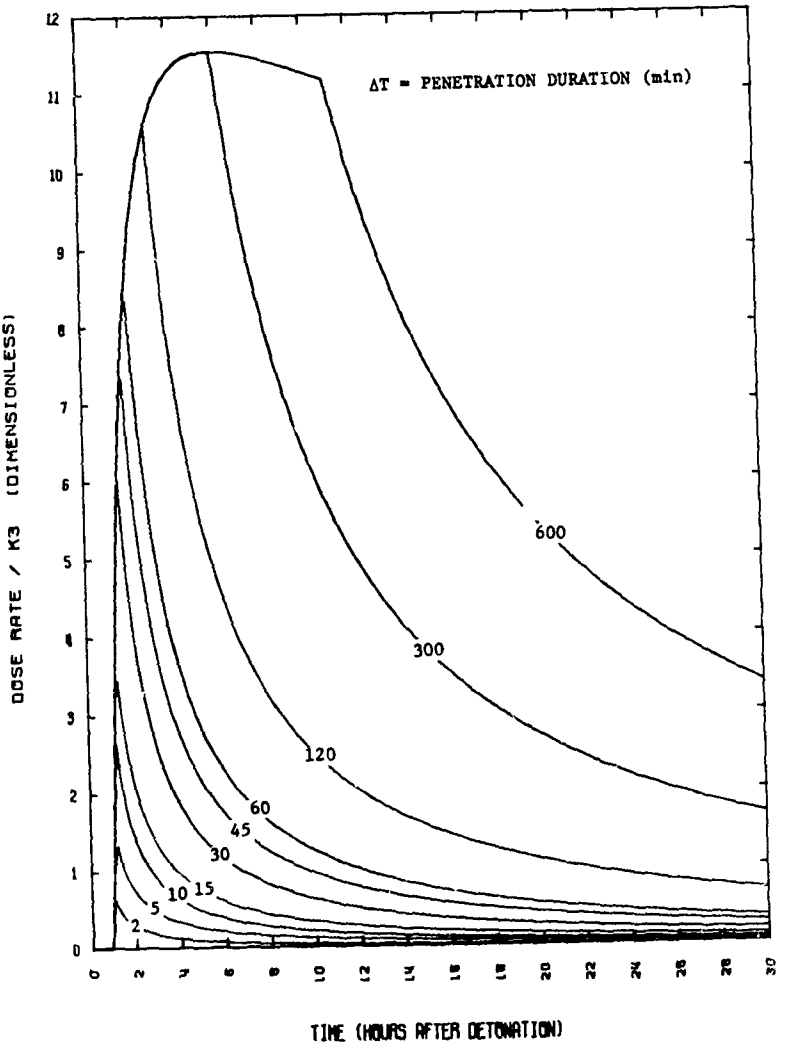

Figure C3. Filter Dose Rate as a Function of Time, TI = 1 Hour

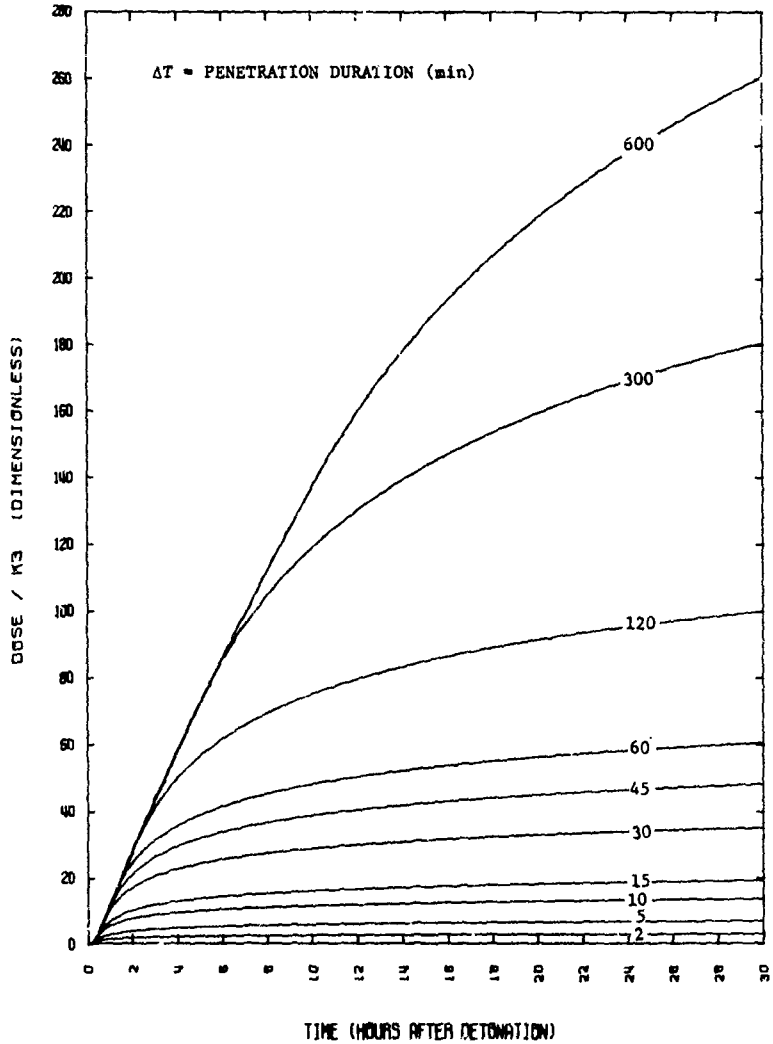

Figure C4. Filter Dose as a Function of Time, TI = 10 Minutes

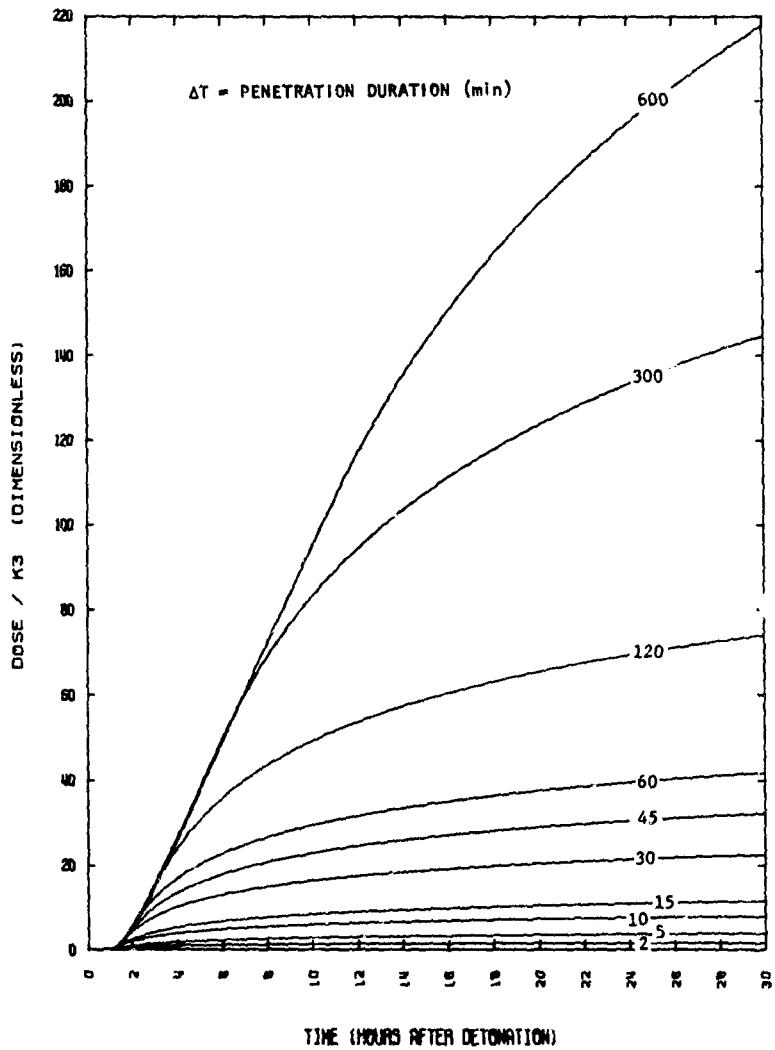

Figure C5. Filter Dose as a Function of Time, TI = 1 Hour

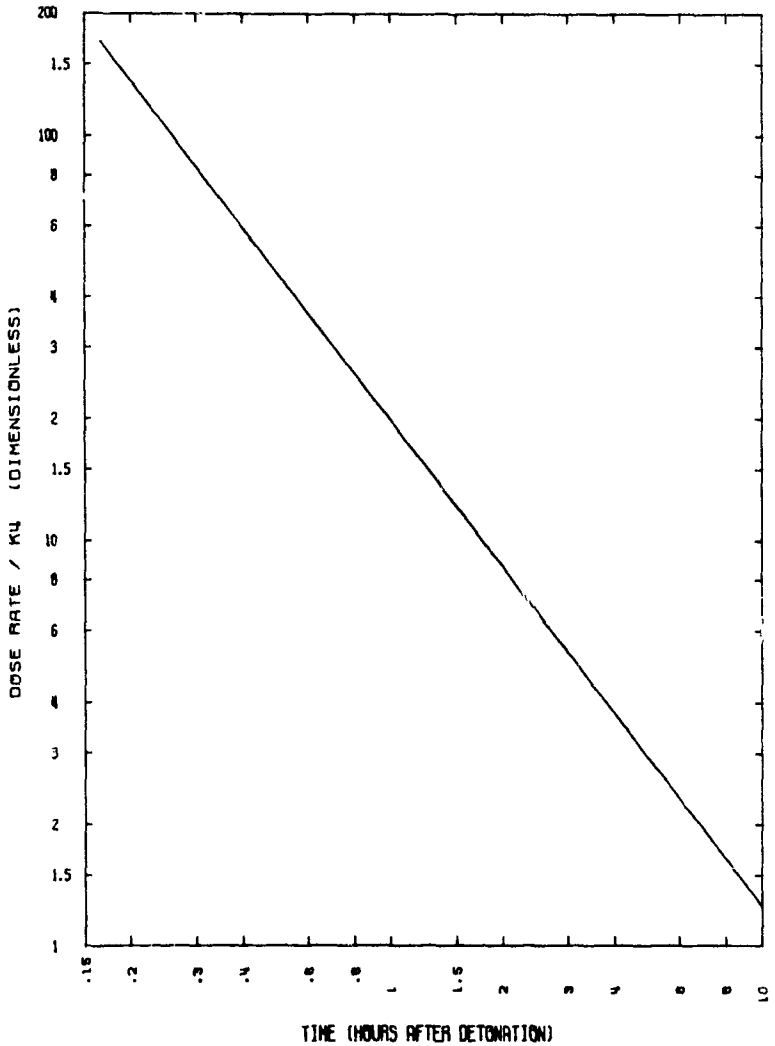

Figure C6. Cloud Immersion Dose Rate

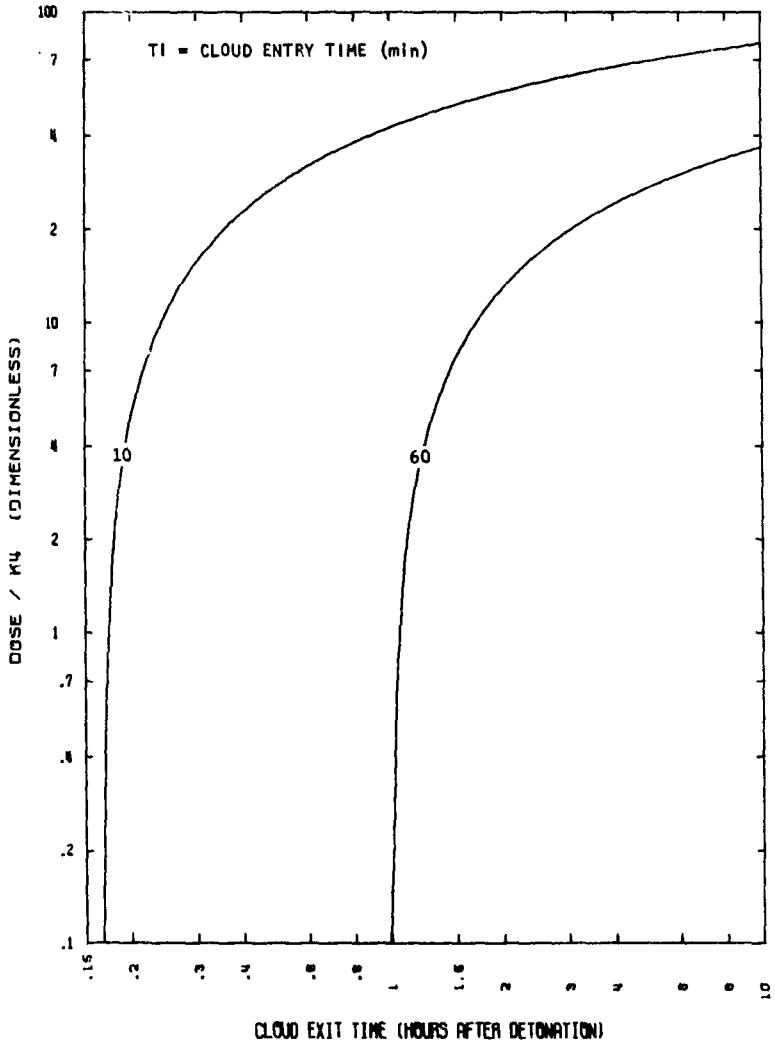

Figure C7. Cloud Immersion Dose

APPENDIX D

COCKPIT MASS AND DOSE MATHEMATICAL DEVELOPMENT

The cockpit mathematical development in this appendix will assume that $FE(r) = 0$. R_c is the critical size and $P_s(r)$ is the probability of settling as determined by the work in section V. The starting point for this development is $\dot{M}_{cp}(r,t)$, the mass rate of flow to the cockpit (settled out). In general,

$$\dot{M}_{cp}(r,t) = \dot{M}_f(r,t)\ P_s(r) \tag{D-1}$$

In particular,

$1 \leq r \leq R_c$

$$\frac{\dot{M}_{cp}(r,t)}{K_2} = 9.946 \times 10^{-2}\ \frac{r^{1.5}}{R_c^{\,2}} \tag{D-2}$$

$R_c \leq r \leq R(t)$

$$\frac{\dot{M}_{cp}(r,t)}{K_2} = 9.946 \times 10^{-2}\ r^{-0.5} \tag{D-3}$$

These equations can be integrated as has been done in earlier sections and $M_{cp}(r)$, $CM_{cp}(r)$, and $M_{cp}(t)$ can be written. Again numerical techniques and integration must be used in some cases, and $r_n = R(t_n)$ and $t_i \leq t_n \leq t_f$. When $R(t_f) > R_c$

$$\frac{M_{cp}(r)}{K_2} = \begin{cases} 9.946 \times 10^{-2} \dfrac{r^{1.5}}{R_c^2} (t_f - t_i) & 1 \le r \le R_c \\ 9.946 \times 10^{-2} r^{-0.5} (t_f - t_i) & R_c \le r \le R(t_f) \\ 9.946 \times 10^{-2} r_n^{-0.5} (t_n - t_i) & R(t_f) \le r_n \le R(t_i) \end{cases} \quad \text{(D-4)}$$

If $R(t_f) < R_c$, then these equations become

$$\frac{M_{cp}(r)}{K_2} = \begin{cases} 9.946 \times 10^{-2} \dfrac{r^{1.5}}{R_c^2} (t_f - t_i) & 1 \le r \le R(t_f) \\ \dfrac{9.946 \times 10^{-2}}{R_c^2} r_n^{1.5} (t_n - t_i) & R(t_f) \le r_n \le R_c \\ 9.946 \times 10^{-2} r_n^{-0.5} (t_n - t_i) & R_c \le r_n \le R(t_i) \end{cases} \quad \text{(D-5)}$$

Integrating the cockpit mass distribution equations above over r, the cumulative mass equations are obtained. For $R(t_f) > R_c$,

$1 \le r \le R_c$

$$\frac{CM_{cp1}(r)}{K_2} = \frac{3.978 \times 10^{-2}}{R_c^2} (t_f - t_i)(r^{2.5} - 1) \quad \text{(D-6)}$$

$R_c \le r \le R(t_f)$

$$\frac{CM_{cp2}(r)}{K_2} = 0.1989 (t_f - t_i)\left(r^{0.5} - R_c^{0.5}\right) + \frac{CM_{cp1}(R_c)}{K_2} \quad \text{(D-7)}$$

$R(t_f) \leq r_n \leq R(t_i)$

$$\frac{CM_{cp3}(r)}{K_2} = \frac{CM_{cp2}\left(R(t_f)\right)}{K_2} + 9.946 \times 10^{-2} \sum_{R(t_f)}^{r_n} r_n^{-0.5} (\tau_n - t_i)\, \Delta r \qquad \text{(D-8)}$$

For $R(t_f) < R_c$, these become

$1 \leq r \leq R(t_f)$

$$\frac{CM_{cp1}(r)}{K_2} = 3.978 \times 10^{-2} \frac{(t_f - t_i)}{R_c^2} (r^{2.5} - 1) \qquad \text{(D-9)}$$

$R(t_f) \leq r_n \leq R_c$

$$\frac{CM_{cp2}(r)}{K_2} = \frac{9.946 \times 10^{-2}}{R_c^2} \sum_{R(t_f)}^{r_n} r_n^{1.5} (t_n - t_i)\, \Delta r + \frac{CM_{cp1}\left(R(t_f)\right)}{K_2} \qquad \text{(D-10)}$$

$R_c \leq r_n \leq R(t_i)$

$$\frac{CM_{cp3}(r)}{K_2} = \frac{CM_{cp2}(R_c)}{K_3} + 9.946 \times 10^{-2} \sum_{R_c}^{r_n} r_n^{-0.5} (t_n - t_i)\, \Delta r \qquad \text{(D-11)}$$

The time function relations also yield two sets of equations. For $R(t) > R_c$,

$$\frac{M_{cp}(t)}{K_2} = (t - t_i)\left(0.1989\, R(t)^{0.5} - 3.978 \times 10^{-2}\, R_c^{-2} - 0.1591\, R_c^{0.5}\right)$$

$$+ 9.946 \times 10^{-2} \sum_{R(t)}^{R(t_i)} r_n^{-0.5} (t_n - t_i)\, \Delta r \qquad \text{(D-12)}$$

When $R(t) < R_c$:

$$\frac{M_{cp}(t)}{k_2} = 3.978 \times 10^{-2} R_c^{-2} (t - t_i) \left(R(t)^{2.5} - 1\right)$$

$$+ 9.946 \times 10^{-2} \left[R_c^{-2} \sum_{4(t)}^{R_c} r_n^{1.5} (t_n - t_i) \Delta r \right.$$

$$\left. + \sum_{R_c}^{R(t_i)} r_n^{-0.5} (t_n - t_i) \Delta r \right] \qquad \text{(D-13)}$$

The cockpit mass equations are plotted in figures D1 through D19.

The development of the dose equations follows a similar technique, except in these equations there are two breakpoints, R_c and 20μ, which R(t) must be allowed to progress through. In addition, provision is made for R_c to be less than, greater than, or equal to 20μ. The basic development stems from the filter dose rates of appendix B multiplied by the cockpit efficiency function of section V, i.e.,

$$\dot{D}_{cp}(r,t) = \dot{D}_f(r,t)\ P_s(r) \qquad \text{(D-14)}$$

The conditions noted above lead to the necessity of writing a set of equations for each set of conditions in each of the $D_{cp}(r)$, $CD_{cp}(r)$, and the $D_{cp}(t)$ functions. These will be stated below with little explanation other than the conditions to which the equations apply. Again $r_n = R(t_n)$, where $t_i \leq t_n \leq t_f$, as before.

The cockpit dose as a function of r will be stated first. For convenience, let $T(t) = 1.25\left(t^{0.8} - t_i^{0.8}\right) + T_{mc}^{-0.2} (t_i - t)$. When $R_c \geq 20$,

$20 \leq R_c \leq R(t_f)$

$$\frac{D_{cp}(r)}{K_3} = \begin{cases} \frac{17.645}{R_c^2} r^{1.5} T(t_f) & 1 \leq r \leq 20 \\ \frac{352.9}{R_c^2} r^{0.5} T(t_f) & 20 \leq r \leq R_c \\ 352.9\, r^{-1.5} T(t_f) & R_c \leq r \leq R(t_f) \\ 352.9\, r_n^{-1.5} T(t_n) & R(t_f) \leq r_n \leq R(t_i) \end{cases} \qquad \text{(D-15)}$$

$20\mu \leq R(t_f) \leq R_c$

$$\frac{D_{cp}(r)}{K_3} = \begin{cases} \frac{17.645}{R_c^2} r^{1.5} T(t_f) & 1 \leq r \leq 20 \\ \frac{352.9}{R_c^2} r^{0.5} T(t_f) & 20 \leq r \leq R(t_f) \\ \frac{352.9}{R_c^2} r_n^{0.5} T(t_n) & R(t_f) \leq r_n \leq R_c \\ 352.9\, r_n^{-1.5} T(t_n) & R_c \leq r_n \leq R(t_i) \end{cases} \qquad \text{(D-16)}$$

$R(t_f) \leq 20\mu \leq R_c$

$$\frac{D_{cp}(r)}{K_3} = \begin{cases} \frac{17.645}{R_c^2} r^{1.5} T(t_f) & 1 \leq r \leq R(t_f) \\ \frac{17.645}{R_c^2} r_n^{1.5} T(t_n) & R(t_f) \leq r_n \leq 20 \\ \frac{352.9}{R_c^2} r_n^{0.5} T(t_n) & 20 \leq r_n \leq R_c \\ 352.9\, r_n^{-1.5} T(t_n) & R_c \leq r_n \leq R(t_i) \end{cases} \qquad \text{(D-17)}$$

If $R_c < 20\mu$, the following set is generated.

$R_c < 20 < R(t_f)$

$$\frac{D_{cp}(r)}{K_3} = \begin{cases} \frac{17.645}{R_c^2} r^{1.5} T(t_f) & 1 \le r \le R_c \\ 17.645\, r^{-0.5} T(t_f) & R_c \le r \le 20 \\ 352.9\, r^{-1.5} T(t_f) & 20 \le r \le R(t_f) \\ 352.9\, r_n^{-1.5} T(t_n) & R(t_f) \le r_n \le R(t_i) \end{cases} \quad \text{(D-18)}$$

$R_c < R(t_f) < 20$

$$\frac{D_{cp}(r)}{K_3} = \begin{cases} \frac{17.645}{R_c^2} r^{1.5} T(t_f) & 1 \le r \le R_c \\ 17.645\, r^{-0.5} T(t_f) & R_c \le r \le R(t_f) \\ 17.645\, r_n^{-0.5} T(t_n) & R(t_f) \le r_n \le 20 \\ 352.9\, r_n^{-1.5} T(t_n) & 20 \le r_n \le R(t_i) \end{cases} \quad \text{(D-19)}$$

$R(t_f) < R_c < 20$

$$\frac{D_{cp}(r)}{K_3} = \begin{cases} \frac{17.645}{R_c^2} r^{1.5} T(t_f) & 1 \le r \le R(t_f) \\ \frac{17.645}{R_c^2} r_n^{1.5} T(t_n) & R(t_f) \le r_n \le R_c \\ 17.645\, r_n^{-0.5} T(t_n) & R_c \le r_n \le 20 \\ 352.9\, r_n^{-1.5} T(t_n) & 20 \le r_n \le R(t_i) \end{cases} \quad \text{(D-20)}$$

To completely define the cumulative dose function the foregoing equations must be integrated over r resulting in several conditional sets of equations as before. When $R_c \geq 20$,

$20 \leq R_c \leq R(t_f)$

$$\frac{CD_{cp1}(r)}{K_3} = \frac{7.058}{R_c^2} T(t_f) \left(r^{2.5} - 1\right) \qquad 1 \leq r \leq 20 \qquad \text{(D-21)}$$

$$\frac{CD_{cp2}(r)}{K_3} = \frac{CD_{cp1}(20)}{K_3} + \frac{235.27}{R_c^2} T(t_f) \left(r^{1.5} - 89.443\right) \qquad 20 \leq r \leq R_c \qquad \text{(D-22)}$$

$$\frac{CD_{cp3}(r)}{K_3} = \frac{CD_{cp2}(R_c)}{K_3} + 705.8\, T(t_f) \left(R_c^{-0.5} - r^{-0.5}\right) \qquad R_c \leq r \leq R(t_f) \qquad \text{(D-23)}$$

$$\frac{CD_{cp4}(r)}{K_3} = \frac{CD_{cp3}\left(R(t_f)\right)}{K_3} + 352.9 \sum_{R(t_f)}^{r_n} r_n^{-1.5}\, T(t_n)\, \Delta r \qquad R(t_f) \leq r_n \leq R(t_i) \qquad \text{(D-24)}$$

$20 \leq R(t_f) \leq R_c$

$$\frac{CD_{cp1}(r)}{K_3} = \frac{7.058}{R_c^2} T(t_f) \left(r^{2.5} - 1\right) \qquad 1 \leq r \leq 20 \qquad \text{(D-25)}$$

$$\frac{CD_{cp2}(r)}{K_3} = \frac{CD_{cp1}(20)}{K_3} + \frac{235.27}{R_c^2} T(t_f) \left(r^{1.5} - 89.443\right) \qquad 20 \leq r \leq R(t_f) \qquad \text{(D-26)}$$

$$\frac{CD_{cp3}(r)}{K_3} = \frac{CD_{cp2}\left(R(t_f)\right)}{K_3} + \frac{352.9}{R_c^2} \sum_{R(t_f)}^{r_n} r_n^{0.5}\, T(t_n)\, \Delta r \qquad R(t_f) \leq r_n \leq R_c \qquad \text{(D-27)}$$

$$\frac{CD_{cp4}(r)}{K_3} = \frac{CD_{cp3}(R_c)}{K_3} + 352.9 \sum_{R_c}^{r_n} r_n^{-1.5}\, T(t_n)\, \Delta r \qquad R_c \leq r_n \leq R(t_i) \qquad \text{(D-28)}$$

$R(t_f) \leq 20 \leq R_c$

$$\frac{CD_{cp1}(r)}{K_3} = \frac{7.058}{R_c^2} T(t_f) \left(r^{2.5} - 1\right) \qquad 1 \leq r \leq R(t_f) \quad \text{(D-29)}$$

$$\frac{CD_{cp2}(r)}{K_3} = \frac{CD_{cp1}\left(R(t_f)\right)}{K_3} + \frac{17.645}{R_c^2} \sum_{R(t_f)}^{r_n} r_n^{1.5} T(t_n) \Delta r \qquad R(t_f) \leq r_n \leq 20 \quad \text{(D-30)}$$

$$\frac{CD_{cp3}(r)}{K_3} = \frac{CD_{cp2}(20)}{K_3} + \frac{352.9}{R_c^2} \sum_{20}^{r_n} r_n^{0.5} T(t_n) \Delta r \qquad 20 \leq r_n \leq R_c \quad \text{(D-31)}$$

$$\frac{CD_{cp4}(r)}{K_3} = \frac{CD_{cp3}(R_c)}{K_3} + 352.9 \sum_{R_c}^{r_n} r_n^{-1.5} T(t_n) \Delta r \qquad R_c \leq r_n \leq R(t_i) \quad \text{(D-32)}$$

The last set of equations results when $R_c < 20$.

$R_c \leq 20 \leq R(t_f)$

$$\frac{CD_{cp1}(r)}{K_3} = \frac{7.058}{R_c^2} T(t_f) \left(r^{2.5} - 1\right) \qquad 1 \leq r \leq R_c \quad \text{(D-33)}$$

$$\frac{CD_{cp2}(r)}{K_3} = \frac{CD_{cp1}(R_c)}{K_3} + 35.29\, T(t_f) \left(r^{0.5} - R_c^{0.5}\right) \qquad R_c \leq r \leq 20 \quad \text{(D-34)}$$

$$\frac{CD_{cp3}(r)}{K_3} = \frac{CD_{cp2}(20)}{K_3} + 705.8\, T(t_f) \left(0.2236 - r^{-0.5}\right) \qquad 20 \leq r \leq R(t_f) \quad \text{(D-35)}$$

$$\frac{CD_{cp4}(r)}{K_3} = \frac{CD_{cp3}\left(R(t_f)\right)}{K_3} + 352.9 \sum_{R(t_f)}^{r_n} r_n^{-1.5} T(t_n) \Delta r \qquad R(t_f) \leq r_n \leq R(t_i) \quad \text{(D-36)}$$

$R_c \leq R(t_f) \leq 20$

$$\frac{CD_{cp1}(r)}{K_3} = \frac{7.058}{R_c^2} T(t_f) \left(r^{2.5} - 1\right) \qquad 1 \leq r \leq R_c \qquad \text{(D-37)}$$

$$\frac{CD_{cp2}(r)}{K_3} = \frac{CD_{cp1}(R_c)}{K_3} + 35.29\, T(t_f) \left(r^{0.5} - R_c^{0.5}\right) \qquad R_c \leq r \leq R(t_f) \qquad \text{(D-38)}$$

$$\frac{CD_{cp3}(r)}{K_3} = \frac{CD_{cp2}\left(R(t_f)\right)}{K_3} + 17.645 \sum_{R(t_f)}^{r_n} r_n^{-0.5}\, T(t_n)\Delta r \qquad R(t_f) \leq r_n \leq 20 \qquad \text{(D-39)}$$

$$\frac{CD_{cp4}(r)}{K_3} = \frac{CD_{cp3}(20)}{K_3} + 352.9 \sum_{20}^{r_n} r_n^{-1.5}\, T(t_n)\Delta r \qquad 20 \leq r_n \leq R(t_i) \qquad \text{(D-40)}$$

$R(t_f) \leq R_c \leq 20$

$$\frac{CD_{cp1}(r)}{K_3} = \frac{7.058}{R_c^2} T(t_f) \left(r^{2.5} - 1\right) \qquad 1 \leq r \leq R(t_f) \qquad \text{(D-41)}$$

$$\frac{CD_{cp2}(r)}{K_3} = \frac{CD_{cp1}\left(R(t_f)\right)}{K_3} + \frac{17.645}{R_c^2} \sum_{R(t_f)}^{r_n} r_n^{1.5}\, T(t_n)\Delta r \qquad R(t_f) \leq r_n \leq R_c \qquad \text{(D-42)}$$

$$\frac{CD_{cp3}(r)}{K_3} = \frac{CD_{cp2}(R_c)}{K_3} + 17.645 \sum_{R_c}^{r_n} r_n^{-0.5}\, T(t_n)\Delta r \qquad R_c \leq r_n \leq 20 \qquad \text{(D-43)}$$

$$\frac{CD_{cp4}(r)}{K_3} = \frac{CD_{cp3}(20)}{K_3} + 352.9 \sum_{20}^{r_n} r_n^{-1.5}\, T(t_n)\Delta r \qquad 20 \leq r_n \leq R(t_i) \qquad \text{(D-44)}$$

To complete the cockpit dose development, the dose as a function of time must be determined. This development again results in sets of conditional equations with some numerical integration. For convenience, let $TT(t) = 0.25\, t^{0.8} - 1.25\, t_i^{0.8} + t_i\, t^{-0.2}$. For $t_i \leq t \leq t_f$,

$20 \leq R_c \leq R(t)$

$$\frac{D_{cp1}(t)}{K_3} = \left(4201.535\ R_c^{-2} + 799.907\ R_c^{-0.5} - 705.8\ R(t)^{-0.5}\right) TT(t) + 352.9\left(t_i^{-0.2} - t^{-0.2}\right) \sum_{R(t)}^{R(t_i)} r_n^{-1.5}\,(t_n - t_i)\Delta r \qquad \text{(D-45)}$$

$20 \leq R(t) \leq R_c$

$$\frac{D_{cp2}(t)}{K_3} = R_c^{-2}\left(4201.535 + 94.107\ R(t)^{1.5}\right) TT(t) + 352.9\left(t_i^{-0.2} - t^{-0.2}\right)\left[R_c^{-2}\sum_{R(t)}^{R_c} r_n^{0.5}\,(t_n - t_i)\Delta r + \sum_{R_c}^{R(t_i)} r_n^{-1.5}\,(t_n - t_i)\Delta r\right] \qquad \text{(D-46)}$$

$R(t) \leq 20 \leq R_c$

$$\frac{D_{cp3}(t)}{K_3} = 7.058\ R_c^{-2}\left(R(t)^{2.5} - 1\right) TT(t) + \left(t_i^{-0.2} - t^{-0.2}\right)\left[17.645\ R_c^{-2}\sum_{R(t)}^{20} r_n^{1.5}\,(t_n - t_i)\Delta r + 352.9\ R_c^{-2}\sum_{20}^{R_c} r_n^{0.5}\,(t_n - t_i)\Delta r + 352.9\sum_{R_c}^{R(t_i)} r_n^{-1.5}\,(t_n - t_i)\Delta r\right] \qquad \text{(D-47)}$$

For the region where $t > t_f$,

$20 \leq R_c \leq R(t_f)$

$$\frac{D_{cp}(t)}{K_3} = \left(t_f^{-0.2} - t^{-0.2}\right)\left[\left(4201.535\ R_c^{-2} + 799.907\ R_c^{-0.5} - 705.8\ R(t_f)^{-0.5}\right)(t_f - t_i) + 352.9 \sum_{R(t_f)}^{R(t_i)} r_n^{-1.5}\,(t_n - t_i)\Delta r\right] + \frac{D_{cp1}(t_f)}{K_3} \qquad \text{(D-48)}$$

$20 \leq R(t_f) \leq R_c$

$$\frac{D_{cp}(t)}{K_3} = \left(t_f^{-0.2} - t^{-0.2}\right)\left[\left(4201.535 + 94.107\ R(t_f)^{1.5}\right)\left(R_c^{-2}\right)(t_f - t_i) + 352.9\left(R_c^{-2}\sum_{R(t_f)}^{R_c} r_n^{0.5}\,(t_n - t_i)\Delta r + \sum_{R_c}^{R(t_i)} r_n^{-1.5}\,(t_n - t_i)\Delta r\right)\right] + \frac{D_{cp2}(t_f)}{K_3} \qquad \text{(D-49)}$$

$R(t_f) \leq 20 \leq R_c$

$$\frac{D_{cp}(t)}{K_3} = \left(t_f^{-0.2} - t^{-0.2}\right)\left[7.058\ R_c^{-2}\left(R(t_f)^{2.5} - 1\right)(t_f - t_i) + 17.645\ R_c^{-2}\sum_{R(t_f)}^{20} r_n^{1.5}\,(t_n - t_i)\Delta r + 352.9\ R_c^{-2}\sum_{20}^{R_c} r_n^{0.5}\,(t_n - t_i)\Delta r + 352.9 \sum_{R_c}^{R(t_i)} r_n^{-1.5}\,(t_n - t_i)\Delta r\right] + \frac{D_{cp3}(t_f)}{K_3} \qquad \text{(D-50)}$$

Finally, when $R_c < 20$, and $t_i \leq t \leq t_f$,

$R_c \leq 20 \leq R(t)$

$$\frac{D_{cp4}(t)}{k_3} = \left(315.634 - 28.232\ R_c^{0.5} - 7.058\ R_c^{-2} - 705.8\ R(t)^{-0.5}\right) TT(t)$$
$$+ 352.9\ \left(t_i^{-0.2} - t^{-0.2}\right) \sum_{R(t)}^{R(t_i)} r_n^{-1.5}\ (t_n - t_i)\Delta r \qquad \text{(D-51)}$$

$R_c \leq R(t) \leq 20$

$$\frac{D_{cp5}(t)}{k_3} = \left(35.29\ R(t)^{0.5} - 7.058\ R_c^{-2} - 28.232\ R_c^{0.5}\right) TT(t)$$
$$+ \left(t_i^{-0.2} - t^{-0.2}\right) \left[17.645 \sum_{R(t)}^{20} r_n^{-0.5}\ (t_n - t_i)\Delta r\right.$$
$$\left. + 352.9 \sum_{20}^{R(t_i)} r_n^{-1.5}\ (t_n - t_i)\Delta r\right] \qquad \text{(D-52)}$$

$R(t) \leq R_c \leq 20$

$$\frac{D_{cp6}(t)}{k_3} = 7.058\ R_c^{-2}\ \left(R(t)^{2.5} - 1\right)\ TT(t)$$
$$+ \left(t_i^{-0.2} - t^{-0.2}\right) \left[17.645\ R_c^{-2} \sum_{R(t)}^{R_c} r_n^{1.5}\ (t_n - t_i)\Delta r\right.$$
$$+ 17.645 \sum_{R_c}^{20} r_n^{-0.5}\ (t_n - t_i)\Delta r$$
$$\left. + 352.9 \sum_{20}^{R(t_i)} r_n^{-1.5}\ (t_n - t_i)\Delta r\right] \qquad \text{(D-53)}$$

When $t > t_f$,

$R_c \leq 20 \leq R(t_f)$

$$\frac{D_{cp}(t)}{K_3} = \left(t_f^{-0.2} - t^{-0.2}\right) \left[\left(315.634 - 28.232\ R_c^{0.5} - 7.058\ R_c^{-2} - 705.8\ R(t_f)^{-0.5}\right)(t_f - t_i) + 352.9 \sum_{R(t_f)}^{R(t_i)} r_n^{-1.5}\,(t_n - t_i)\Delta r\right] + \frac{D_{cp4}(t_f)}{K_3} \qquad \text{(D-54)}$$

$R_c \leq R(t_f) \leq 20$

$$\frac{D_{cp}(t)}{K_3} = \left(t_f^{-0.2} - t^{-0.2}\right) \left[\left(35.29\ R(t_f)^{0.5} - 7.058\ R_c^{-2} - 28.232\ R_c^{0.5}\right)(t_f - t_i) + 17.645 \sum_{R(t_f)}^{20} r_n^{-0.5}\,(t_n - t_i)\Delta r + 352.9 \sum_{20}^{R(t_i)} r_n^{-1.5}\,(t_n - t_i)\Delta r\right] + \frac{D_{cp5}(t_f)}{K_3} \qquad \text{(D-55)}$$

$R(t_f) \leq R_c \leq 20$

$$\frac{D_{cp}(t)}{K_3} = \left(t_f^{-0.2} - t^{-0.2}\right) \left[7.058\ R_c^{-2}\left(R(t_f)^{2.5} - 1\right)(t_f - t_i) + 17.645\ R_c^{-2} \sum_{R(t_f)}^{R_c} r_n^{1.5}\,(t_n - t_i)\Delta r + 17.645 \sum_{R_c}^{20} r_n^{-0.5}\,(t_n - t_i)\Delta r + 352.9 \sum_{20}^{R(t_i)} r_n^{-1.5}\,(t_n - t_i)\Delta r\right] + \frac{D_{cp6}(t_f)}{K_3} \qquad \text{(D-56)}$$

The dose equations are plotted in figures D20 through D46. The cockpit dose rate equations are plotted in figures D47 through D55.

This completes the mathematical development of the mass and dose equation sets for the cockpit model.

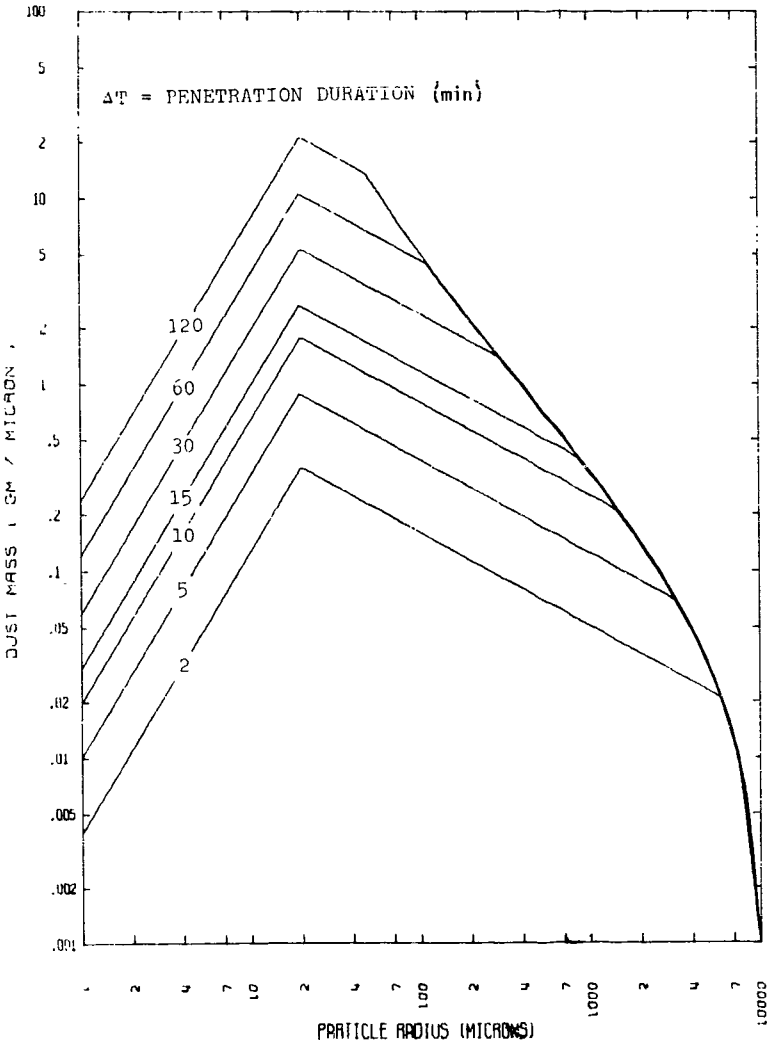

Figure D1. Cockpit Dust Mass Distribution Function, TI = 10 Minutes

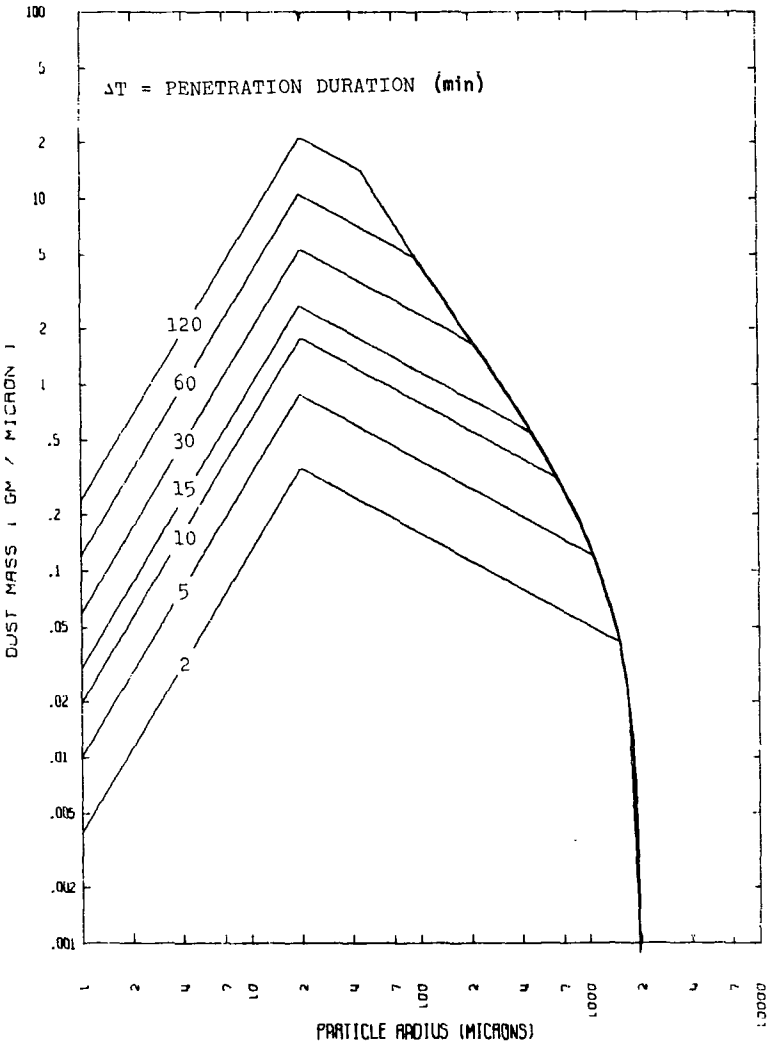

Figure D2. Cockpit Dust Mass Distribution Function, TI = 18 Minutes

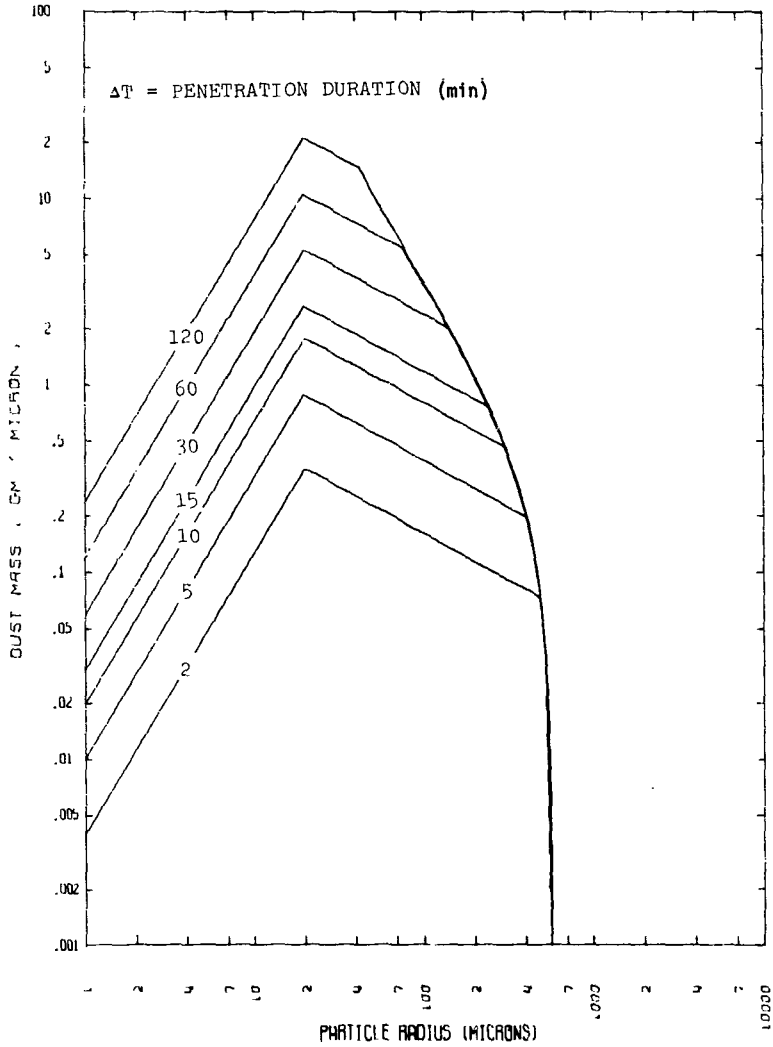

Figure D3. Cockpit Dust Mass Distribution Function, TI = 30 Minutes

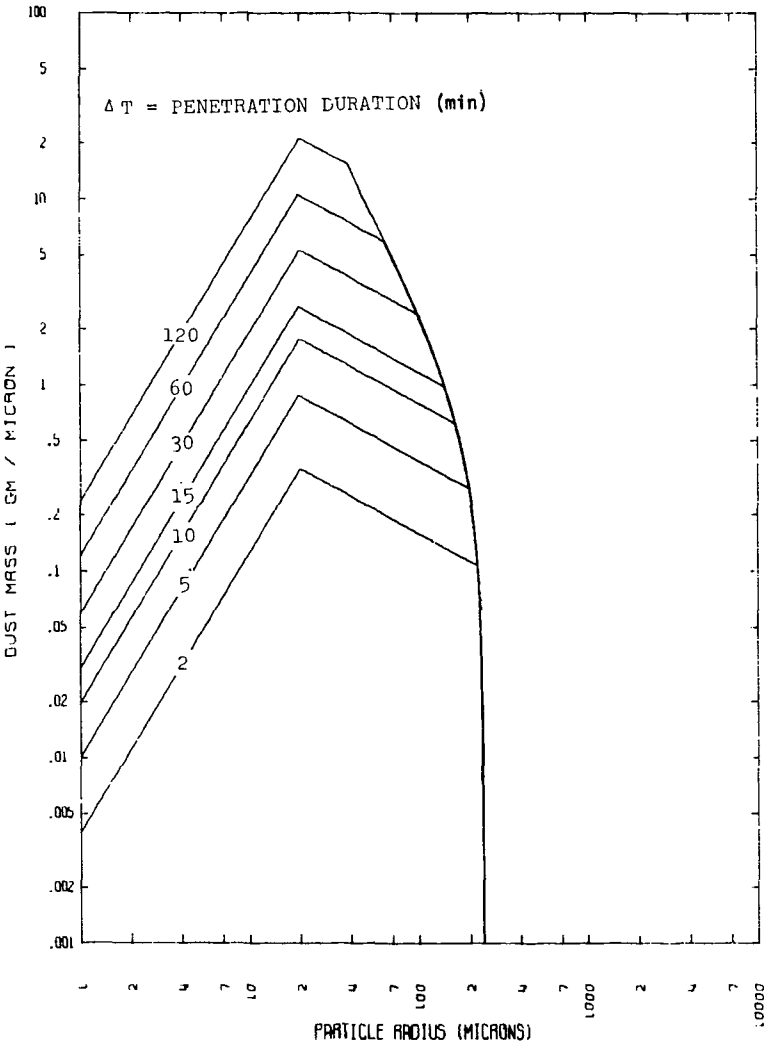

Figure D4. Cockpit Dust Mass Distribution Function, TI = 45 Minutes

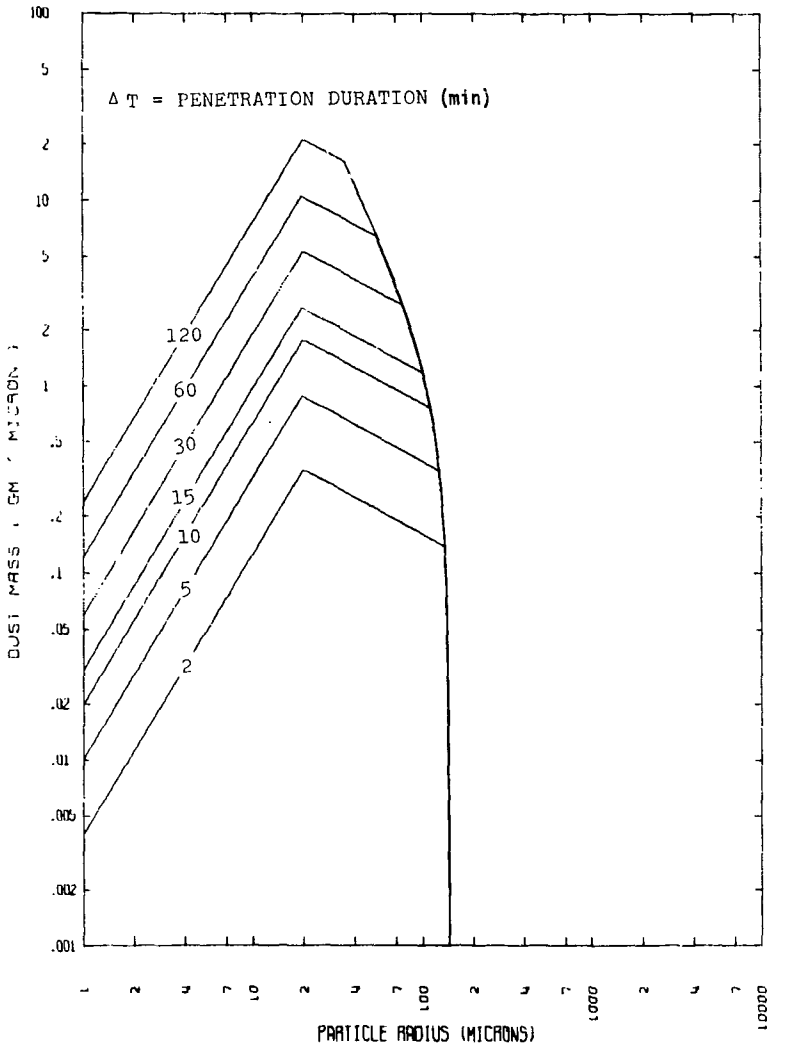

Figure D5. Cockpit Dust Mass Distribution Function, TI = 1 Hour

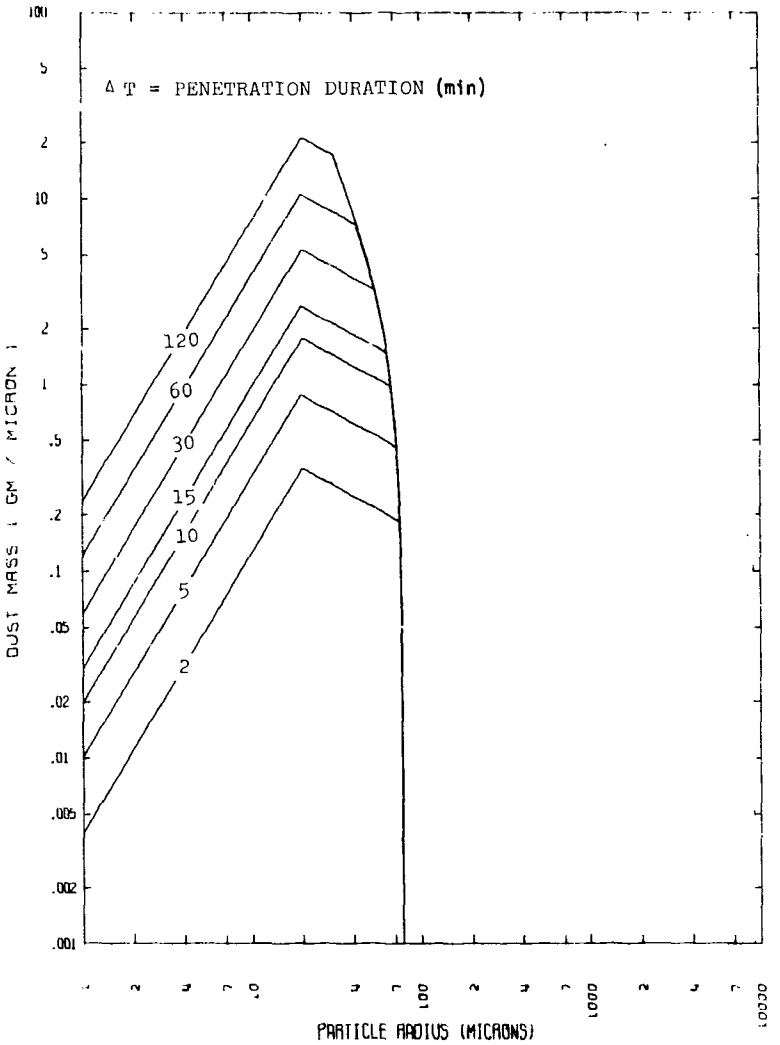

Figure D6. Cockpit Dust Mass Distribution Function, TI = 1.5 Hours

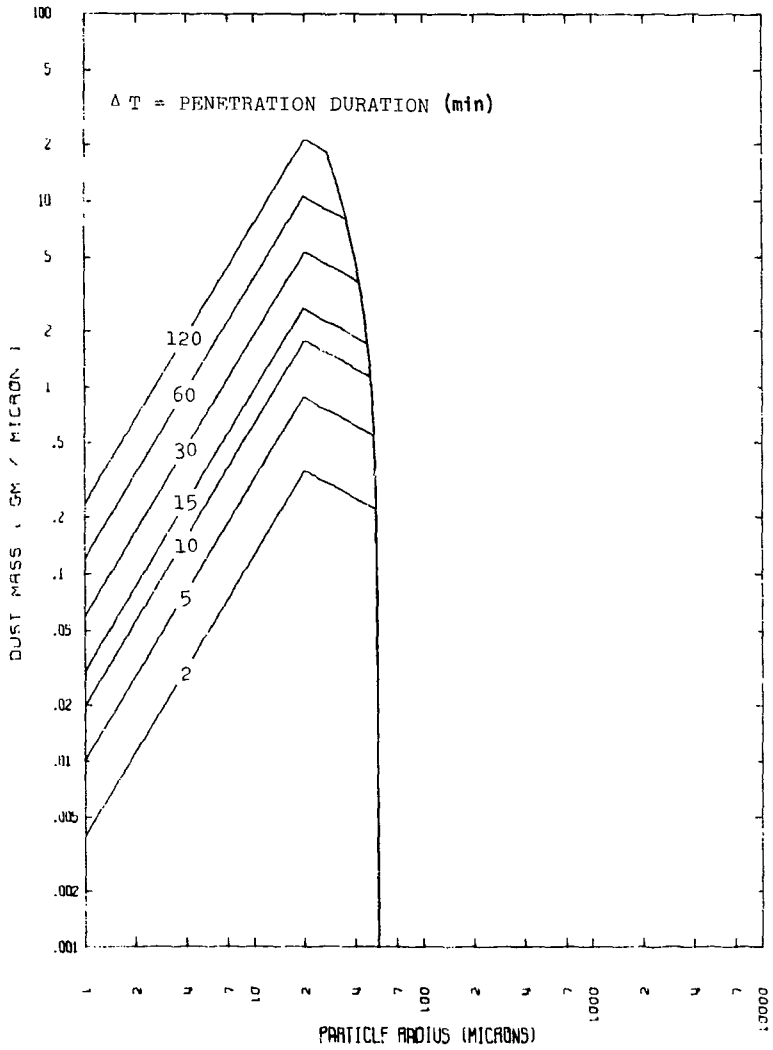

Figure D7. Cockpit Dust Mass Distribution Function, TI = 2 Hours

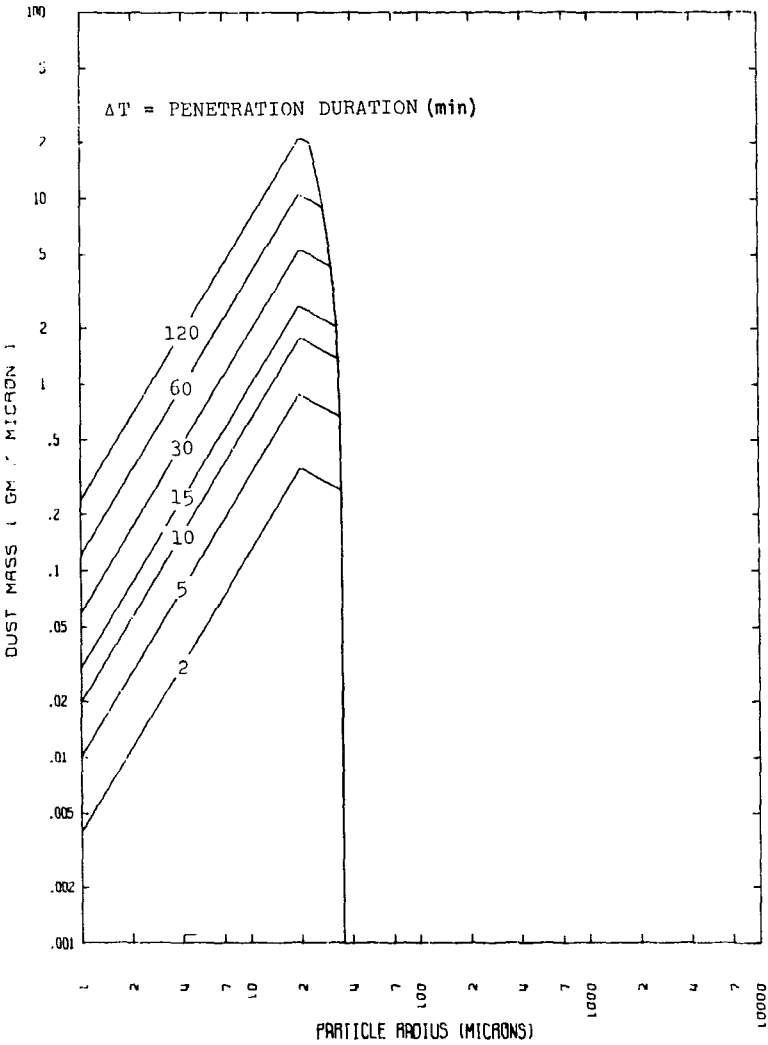

Figure D8. Cockpit Dust Mass Distribution Function, TI = 3 Hours

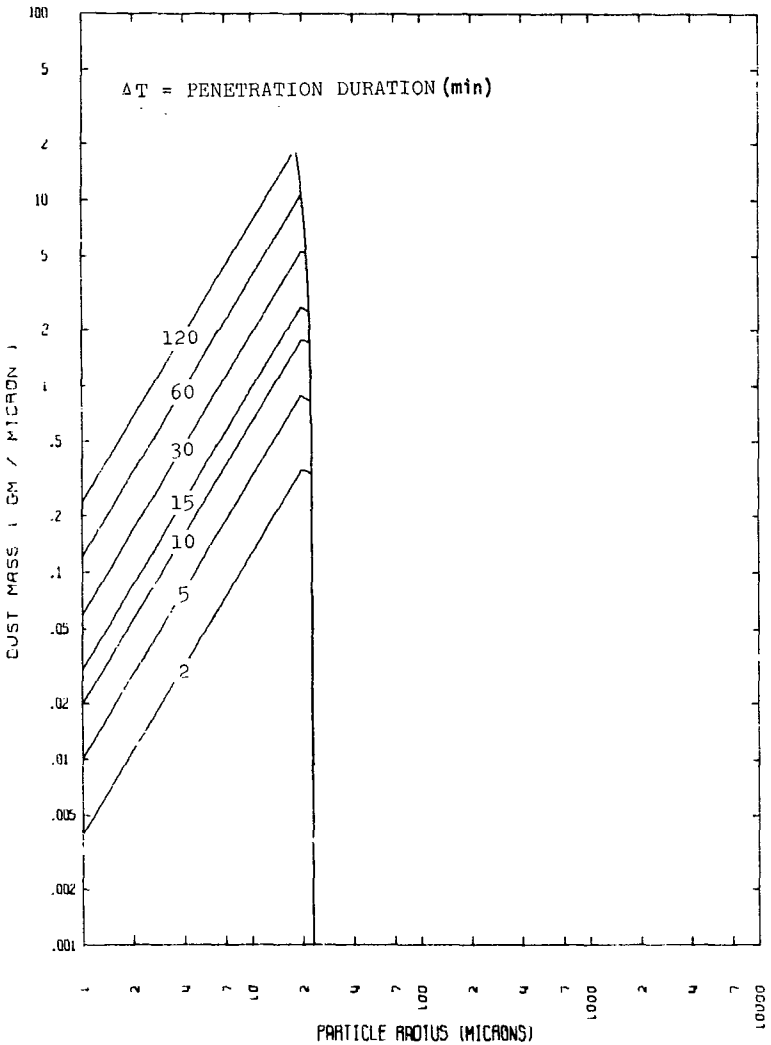

Figure D9. Cockpit Dust Mass Distribution Function, TI = 5 Hours

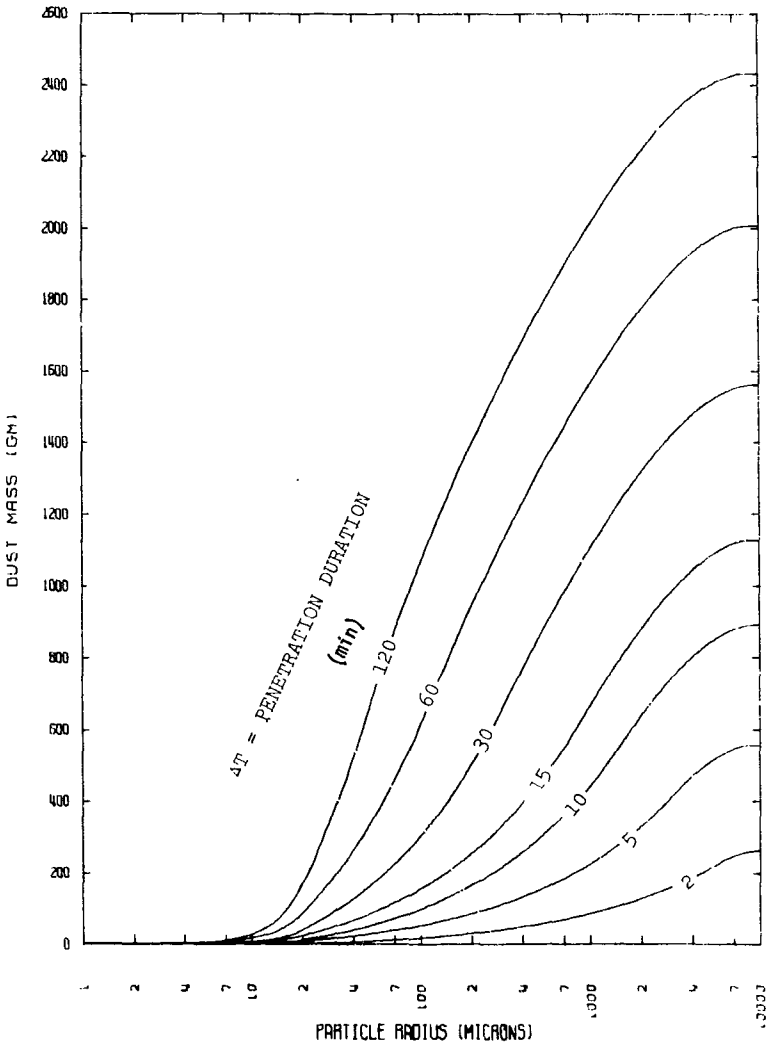

Figure D10. Cumulative Dust Mass in Cockpit, TI = 10 Minutes

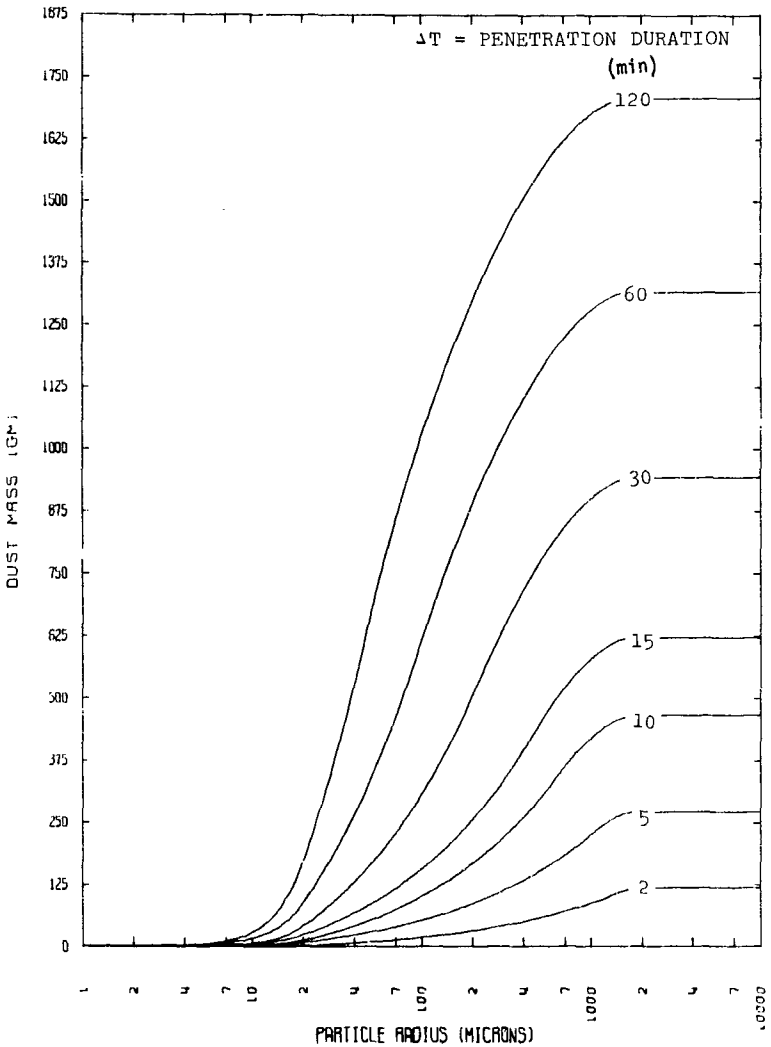

Figure D1i. Cumulative Dust Mass in Cockpit, TI = 18 Minutes

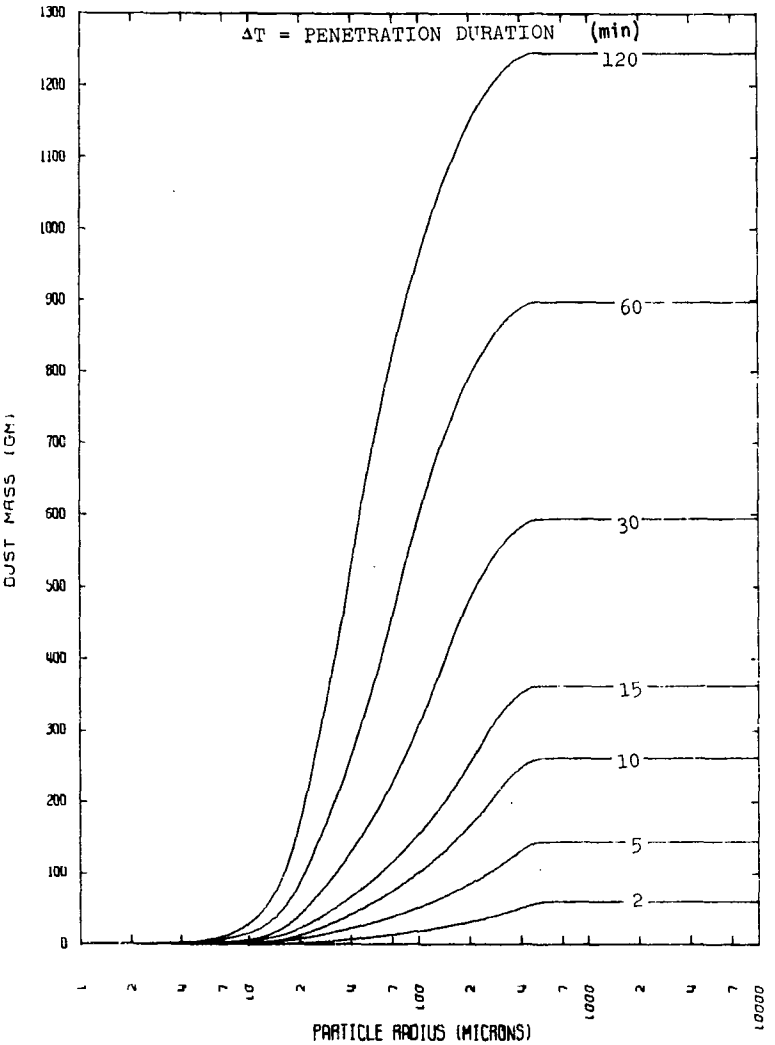

Figure D12. Cumulative Dust Mass in Cockpit, TI = 30 Minutes

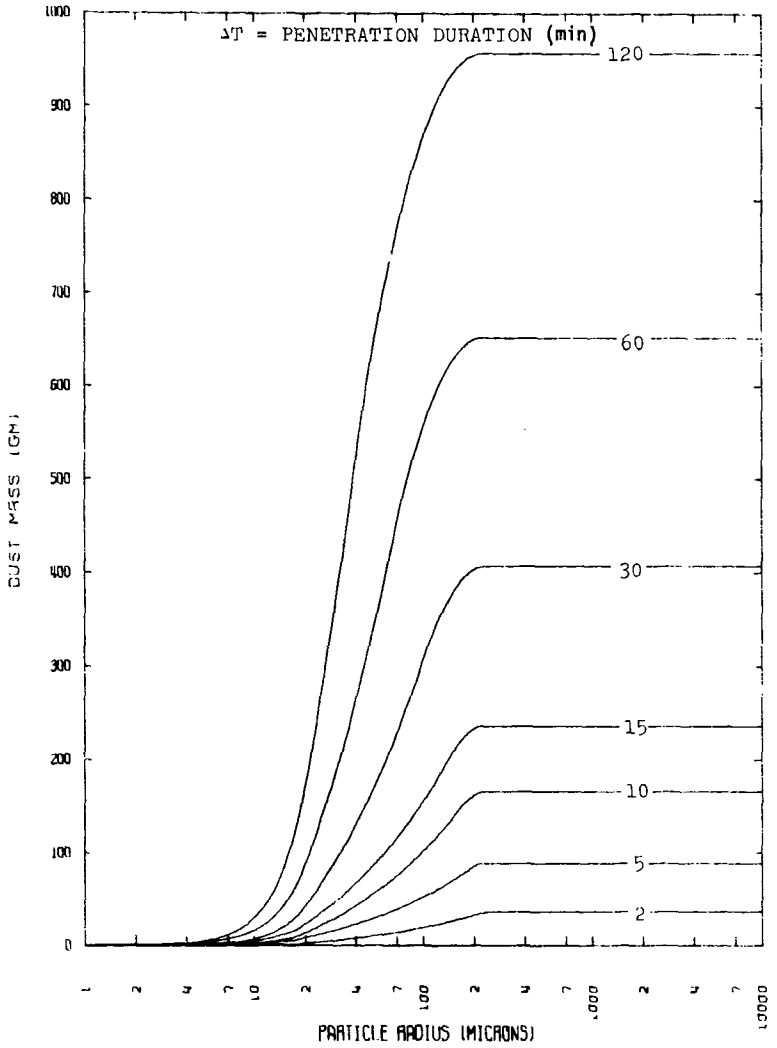

Figure D13. Cumulative Dust Mass in Cockpit, TI = 45 Minutes

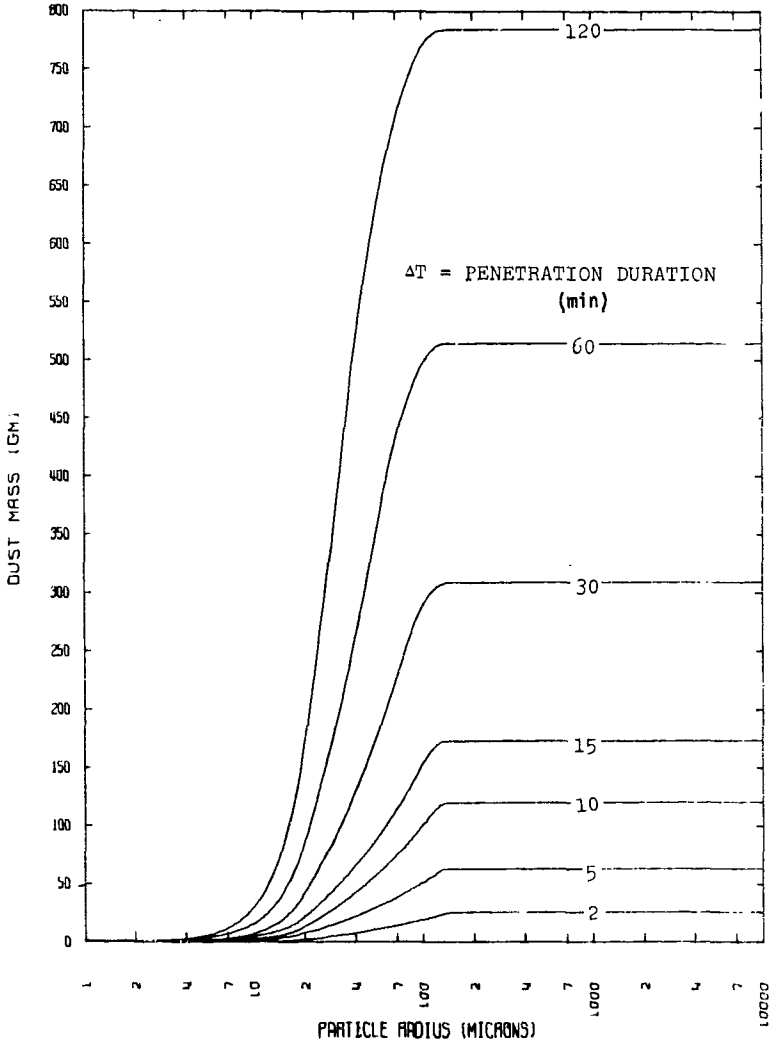

Figure D14. Cumulative Dust Mass in Cockpit, TI = 1 Hour

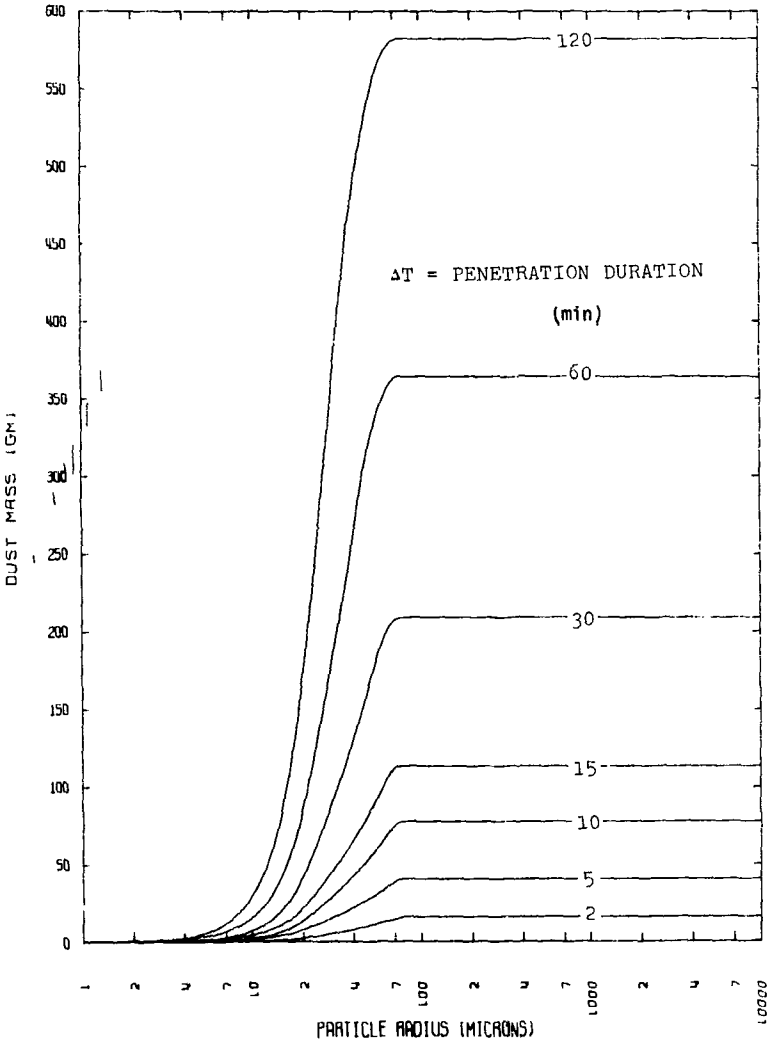

Figure D15. Cumulative Dust Mass in Cockpit, TI = 1.5 Hours

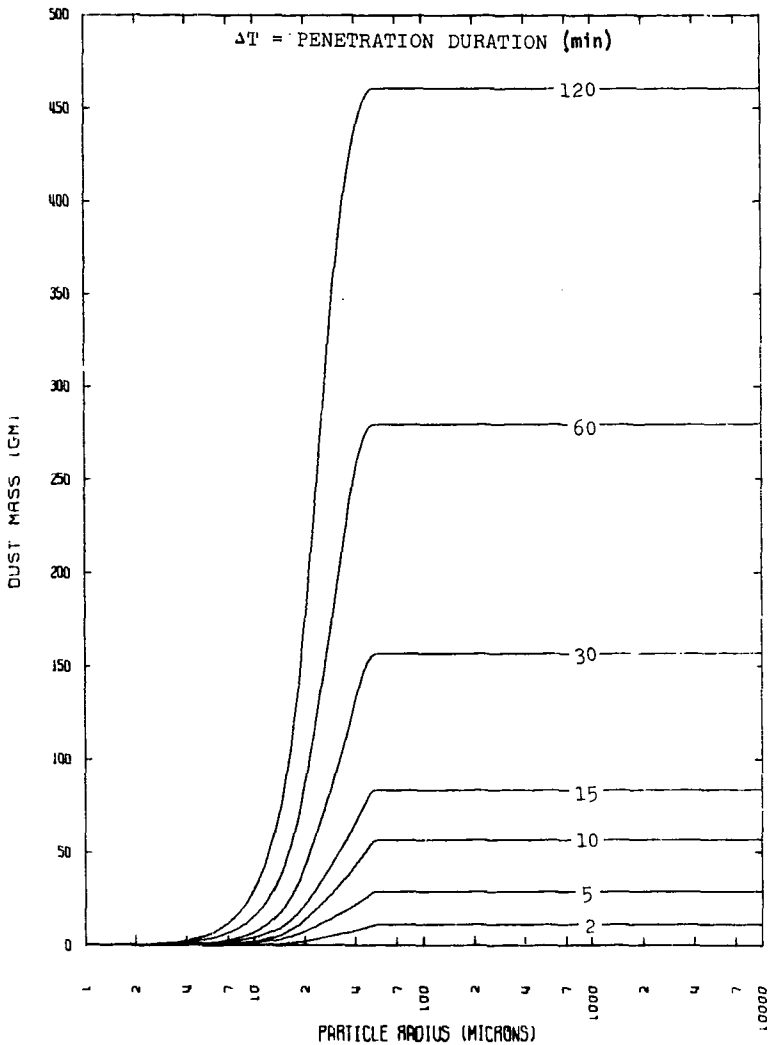

Figure D16. Cumulative Dust Mass in Cockpit, TI = 2 Hours

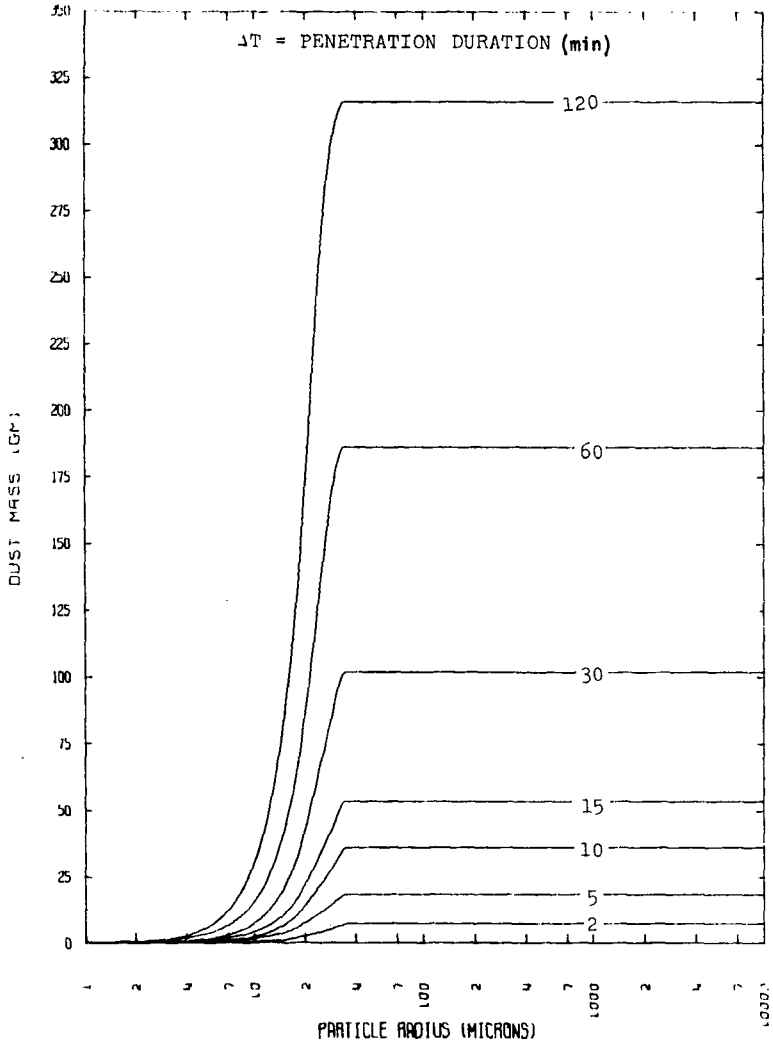

Figure D17. Cumulative Dust Mass for Cockpit, TI = 3 Hours

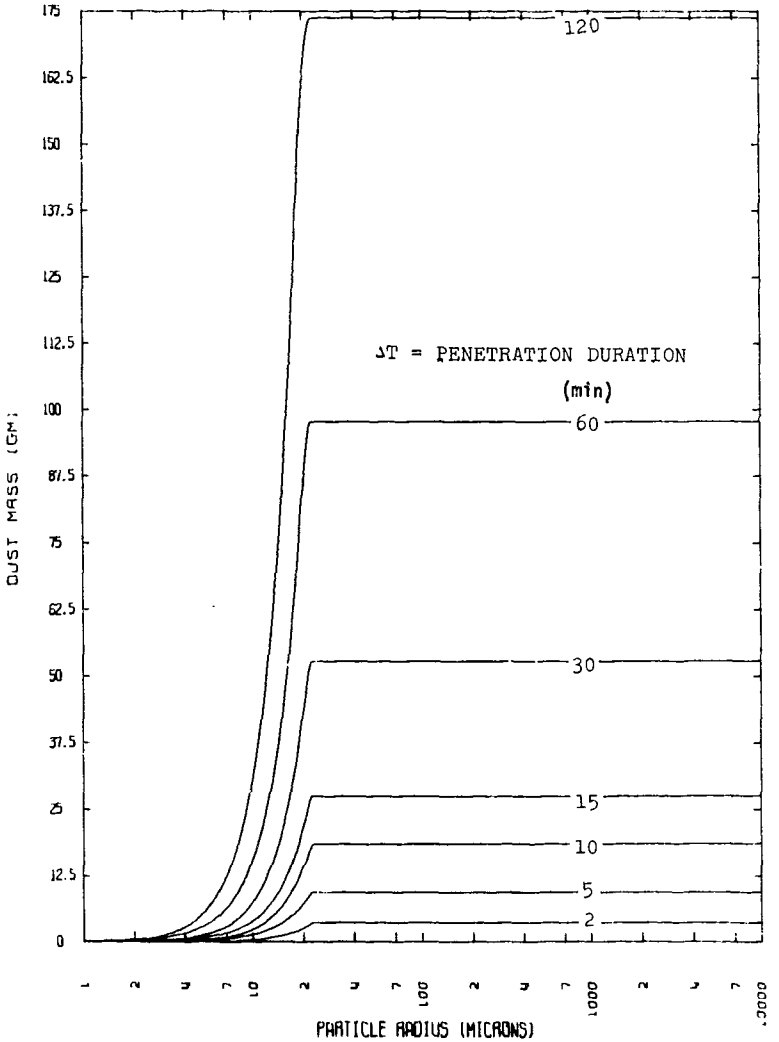

Figure D18. Cumulative Dust Mass for Cockpit, TI = 5 Hours

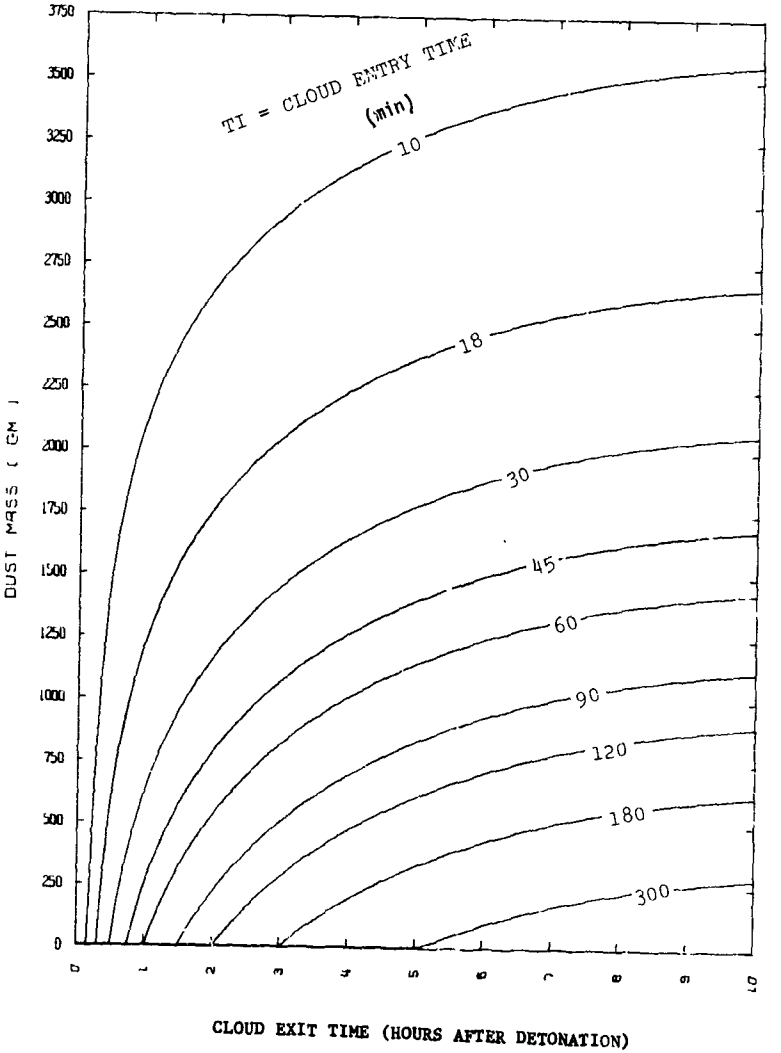

Figure D19. Dust Mass Collected in the Cockpit

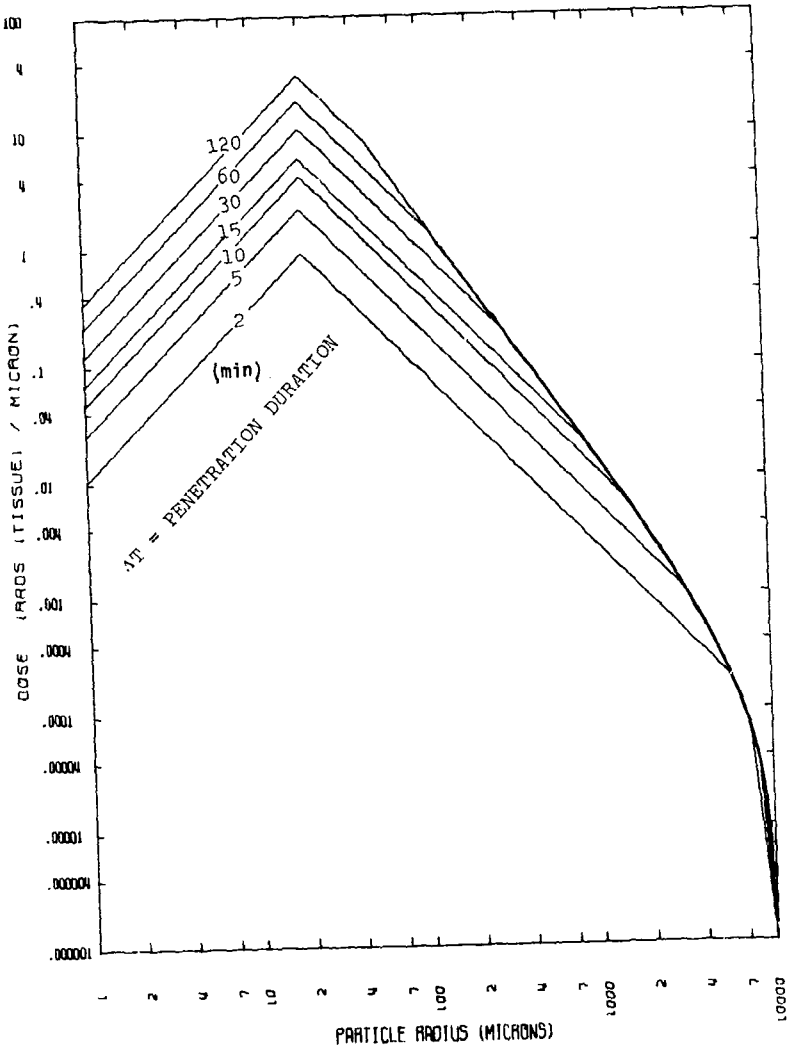

Figure D20. Cockpit Dust Dose Distribution at 30 Hours, TI = 10 Minutes

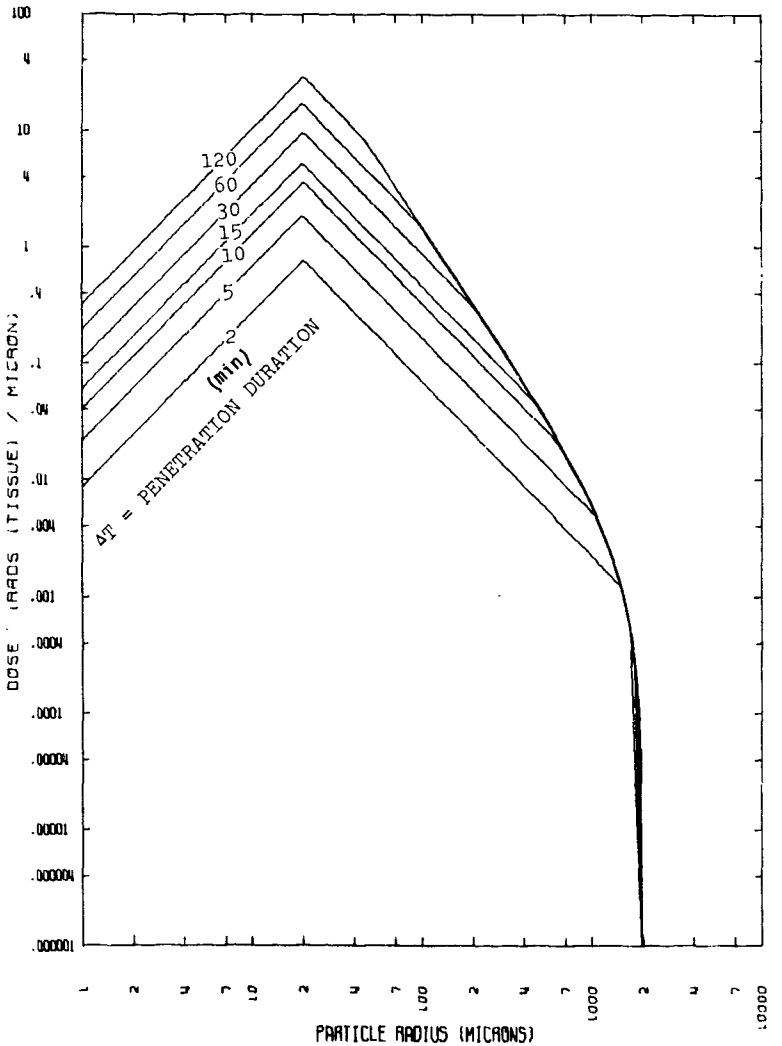

Figure D21. Cockpit Dust Dose Distribution at 30 Hours, TI = 18 Minutes

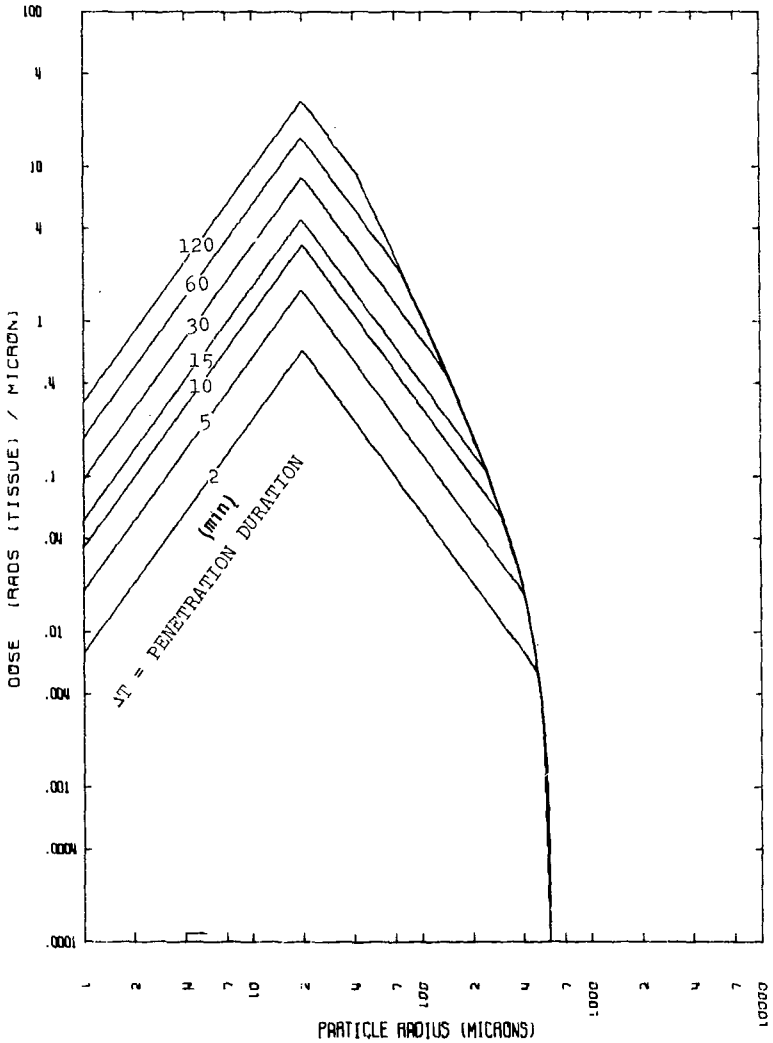

Figure D22. Cockpit Dust Dose Distribution at 30 Hours, TI = 30 Minutes

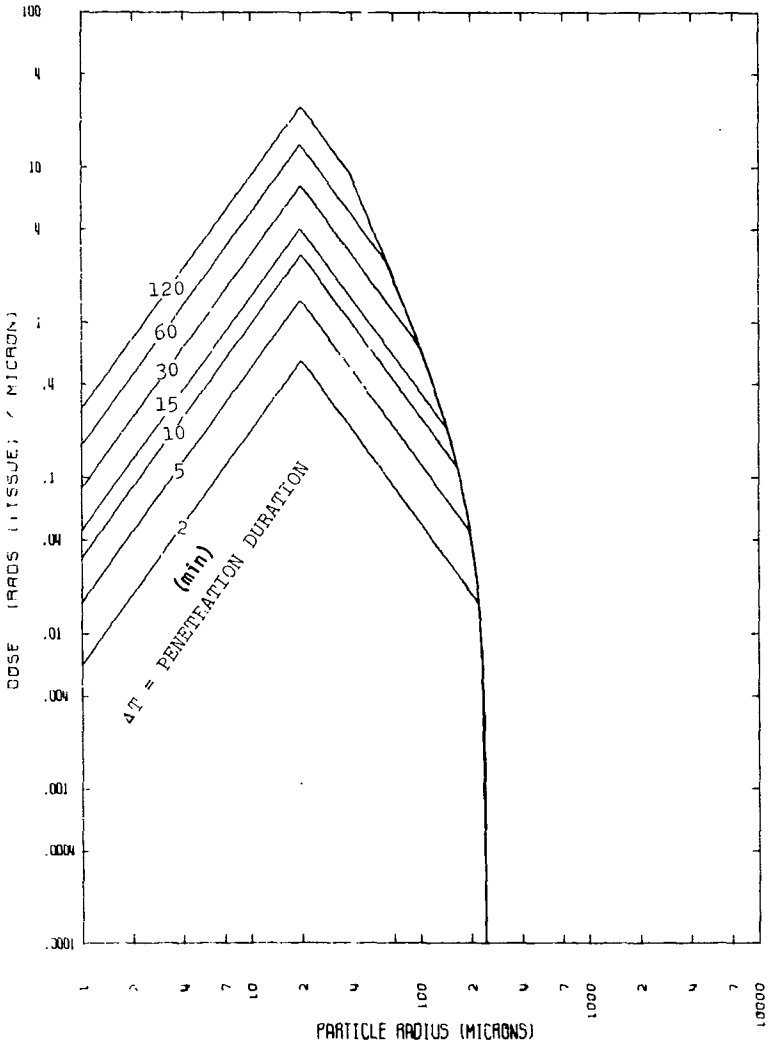

Figure D23. Cockpit Dust Dose Distribution at 30 Hours, TI = 45 Minutes

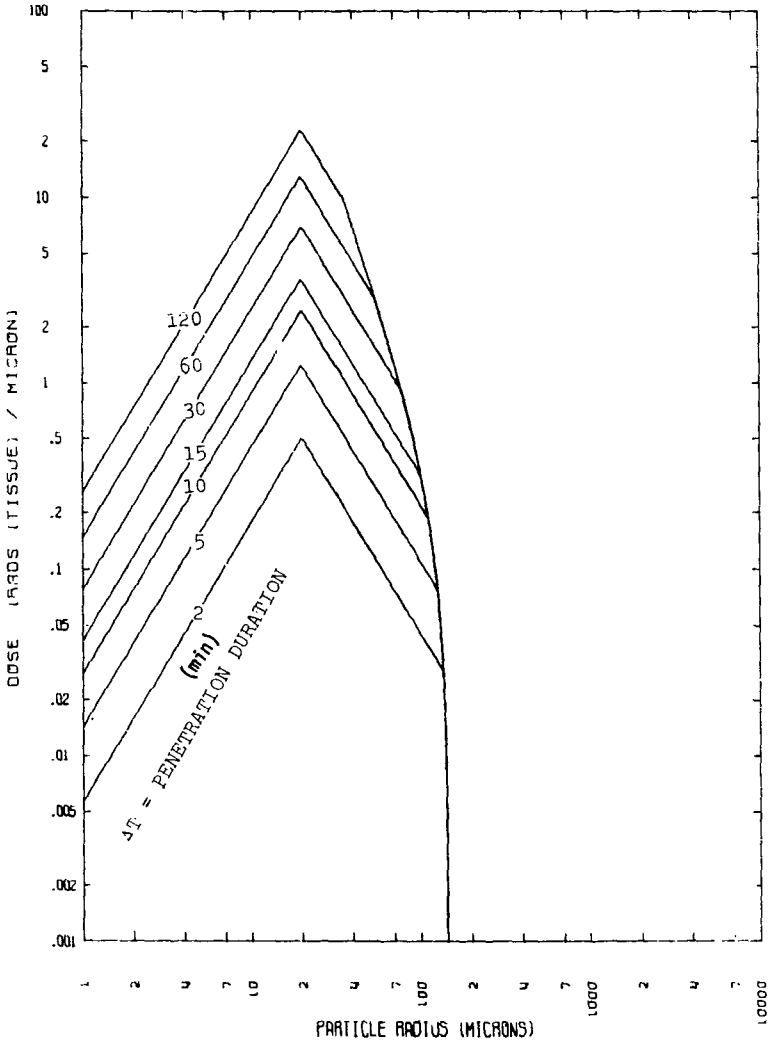

Figure D24. Cockpit Dust Dose Distribution at 30 Hours, TI = 1 Hour

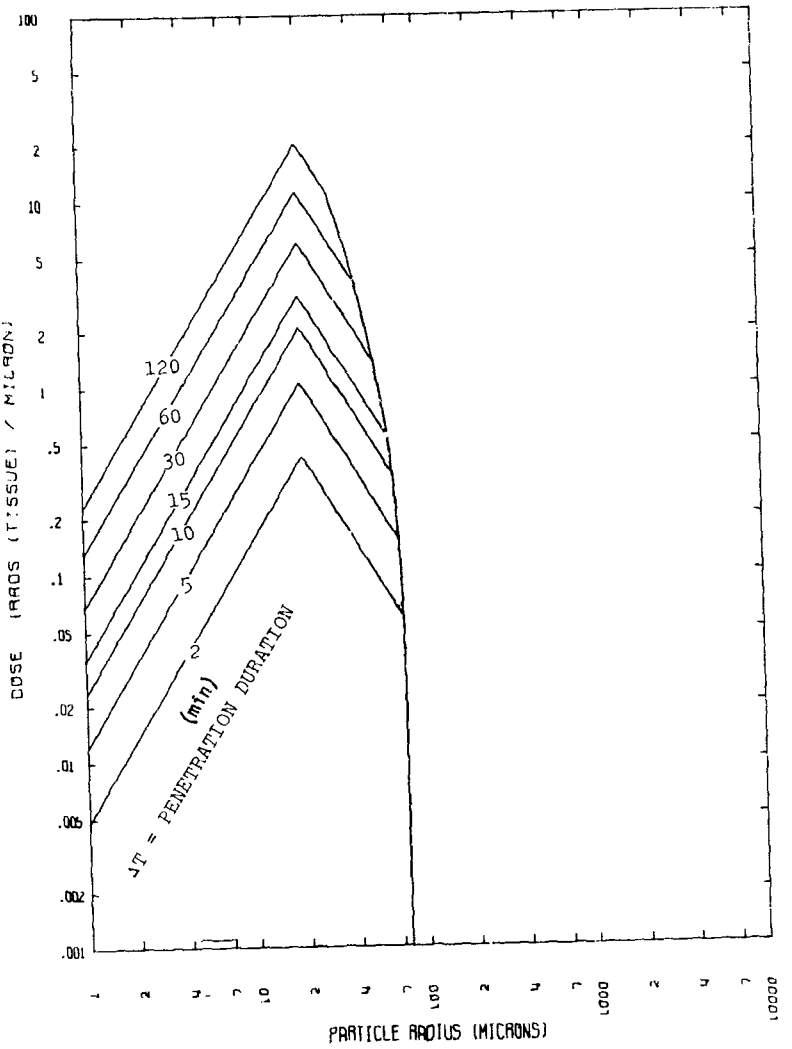

Figure D25. Cockpit Dust Dose Distribution at 30 Hours, TI = 1.5 Hours

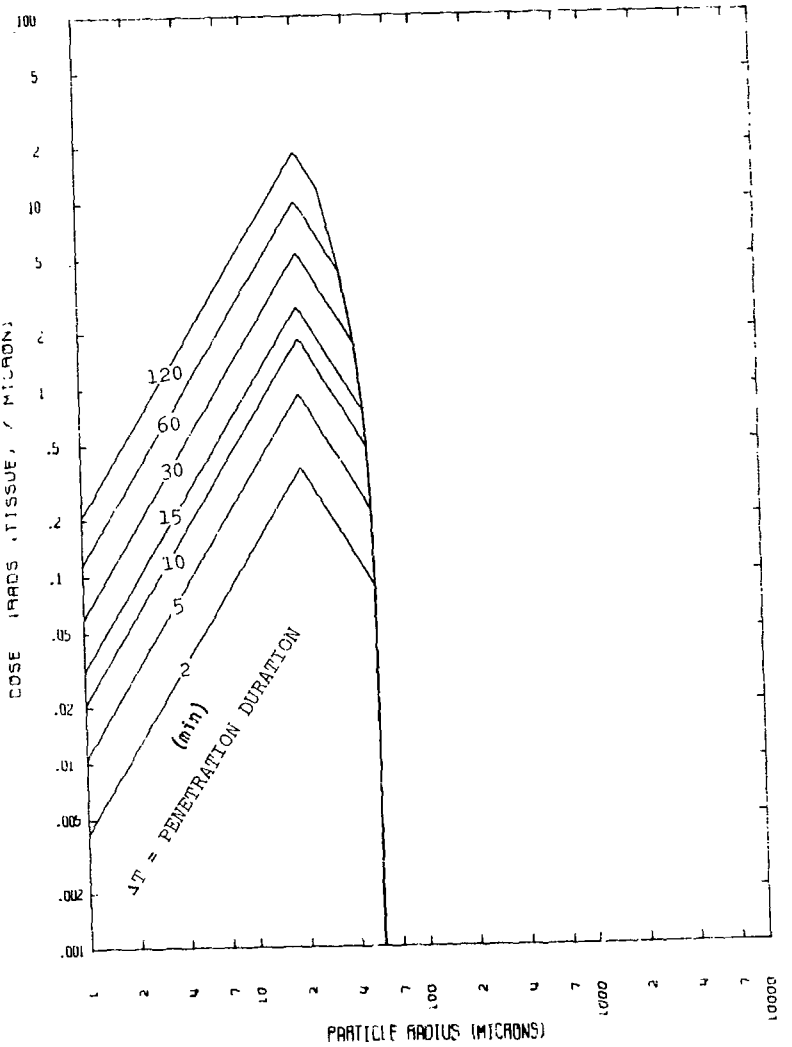

Figure D26. Cockpit Dust Dose Distribution at 30 Hours, TI = 2 Hours

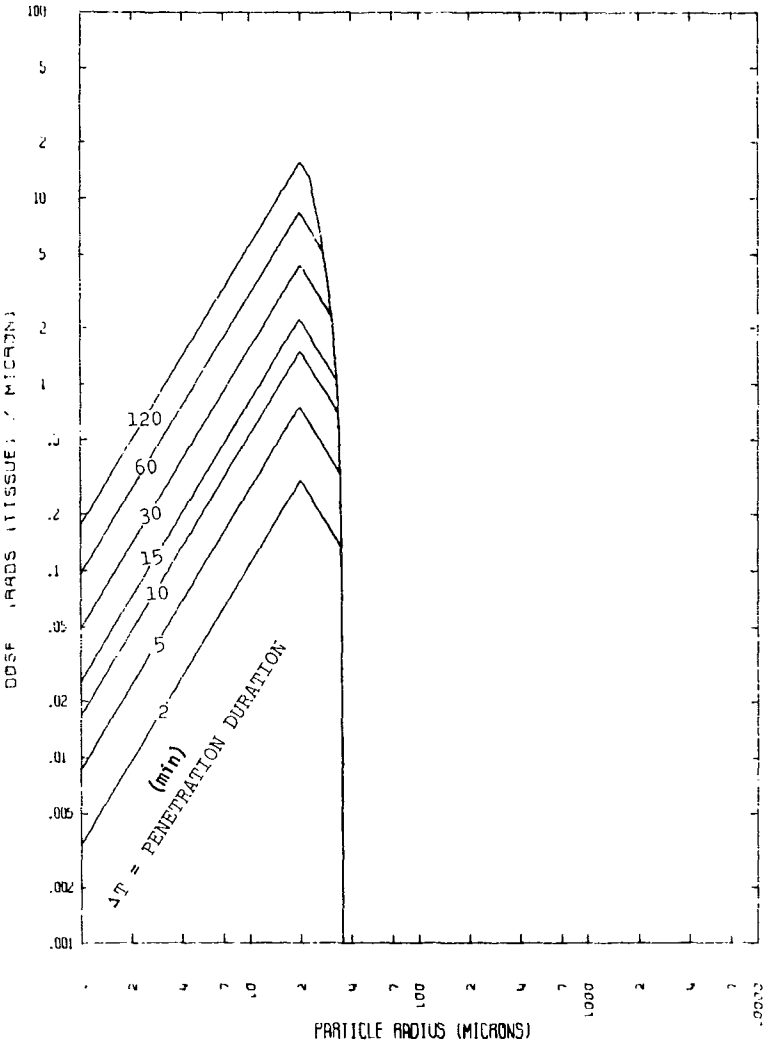

Figure D27. Cockpit Dust Dose Distribution at 30 Hours, TI = 3 Hours

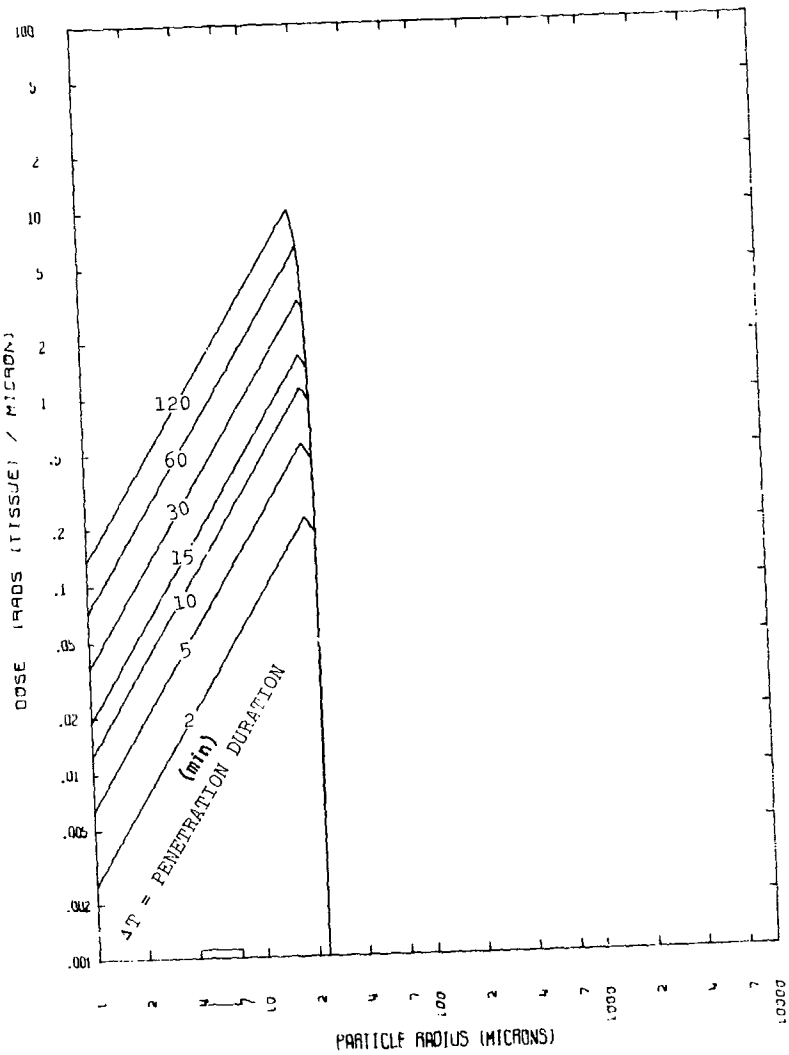

Figure D28. Cockpit Dust Dose Distribution at 30 Hours, TI = 5 Hours

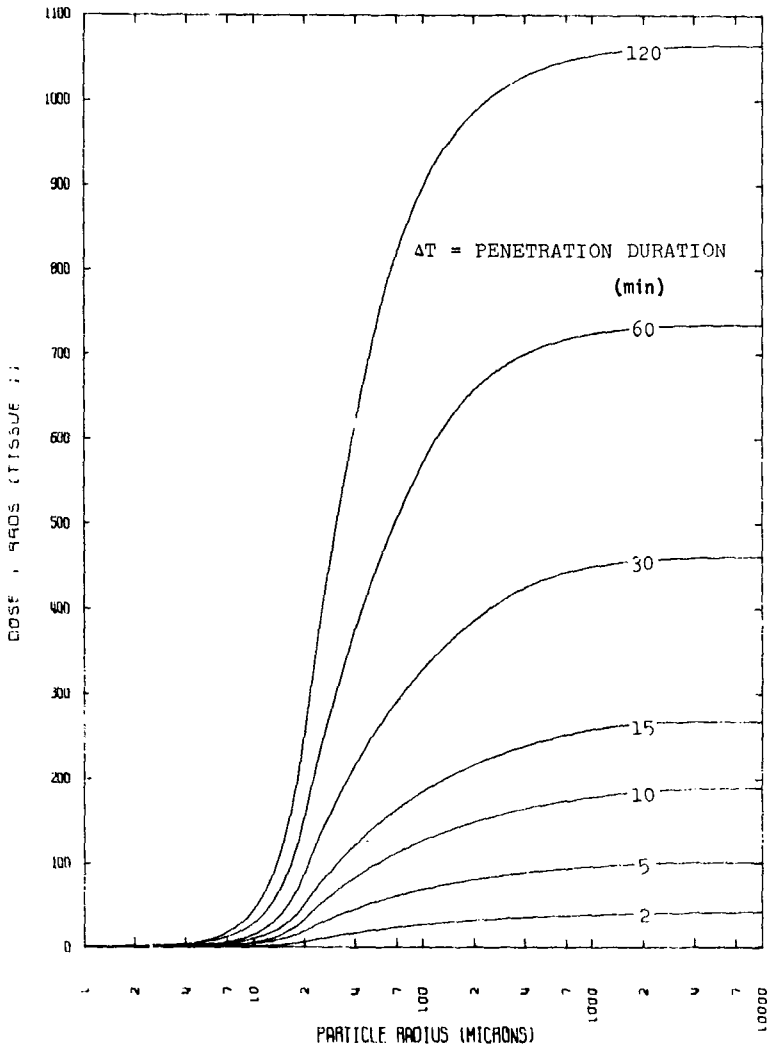

Figure D29. Cumulative Cockpit Dose at 30 Hours, TI = 10 Minutes

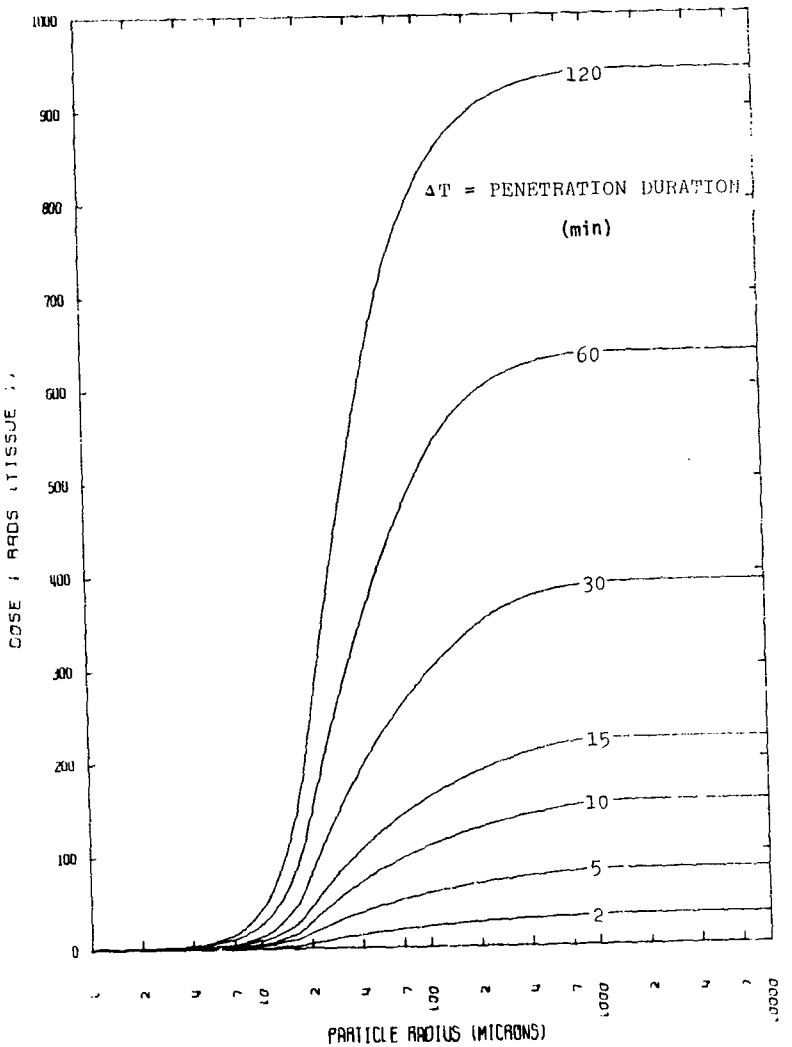

Figure D30. Cumulative Cockpit Dose at 30 Hours, T1 = 18 Minutes

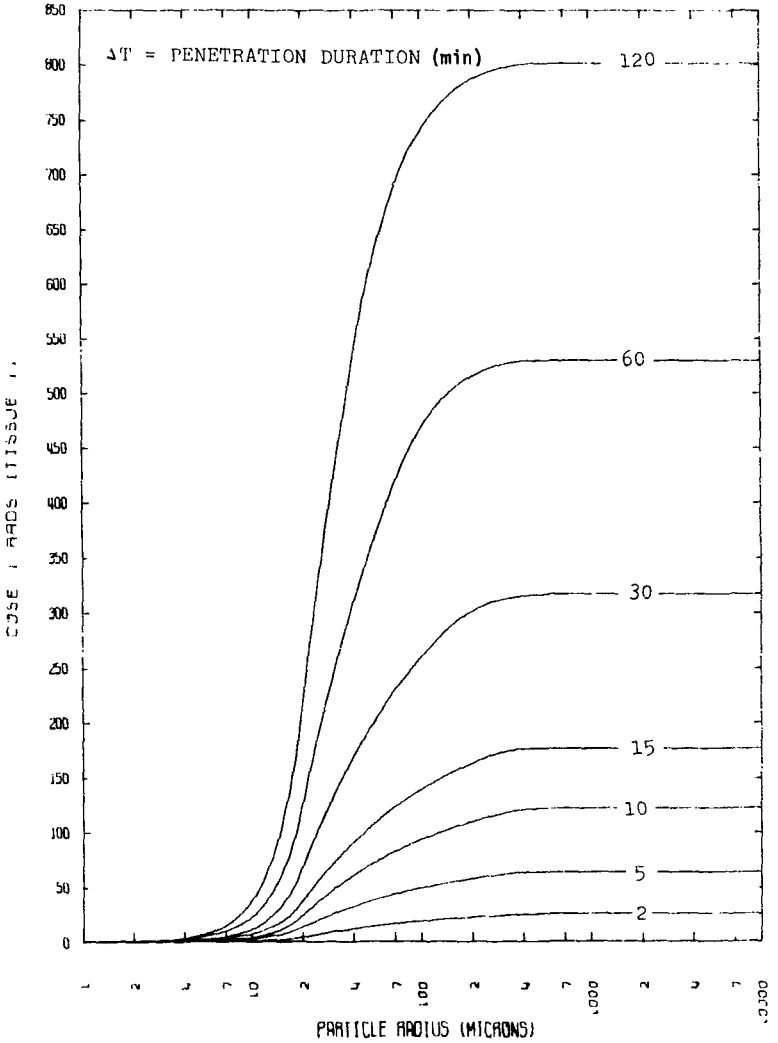

Figure D31. Cumulative Cockpit Dose at 30 Hours, TI = 30 Minutes

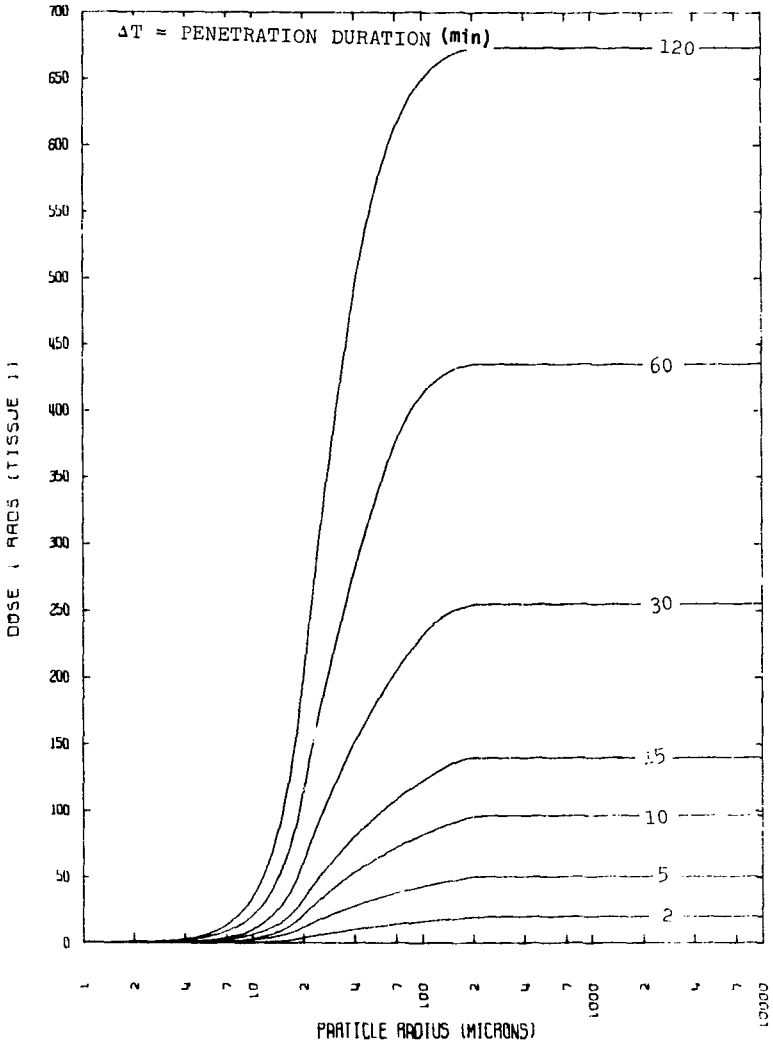

Figure D32. Cumulative Cockpit Dose at 30 Hours, TI = 45 Minutes

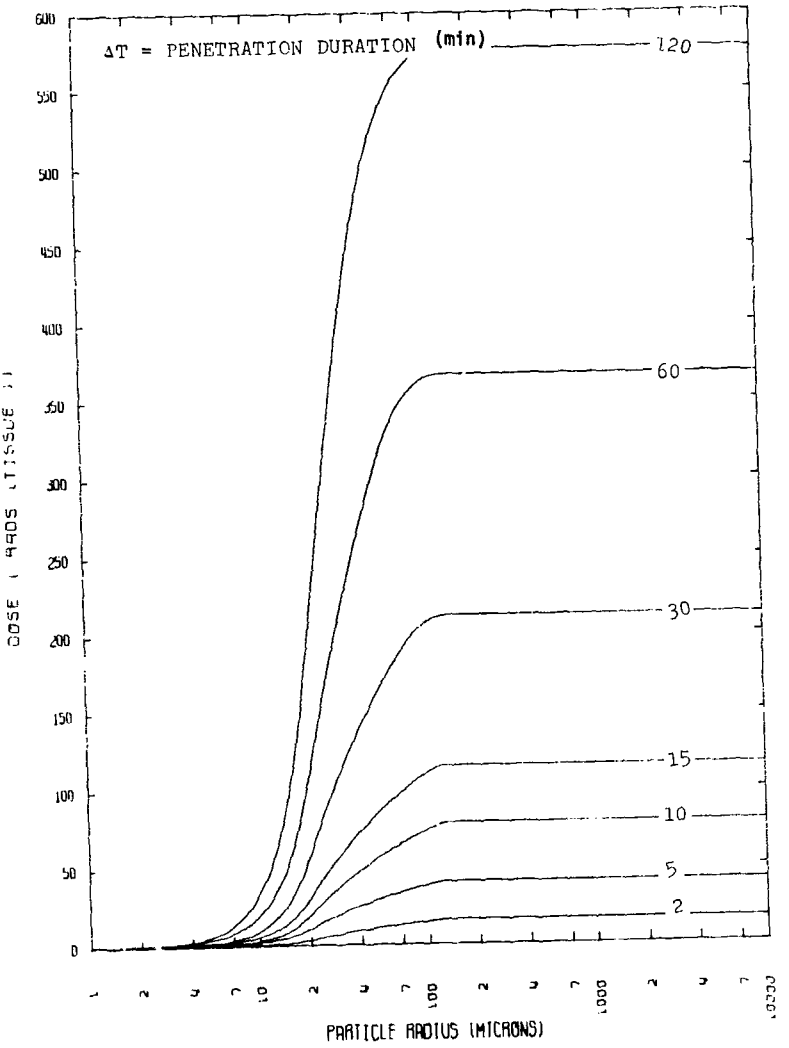

Figure D33. Cumulative Cockpit Dose at 30 Hours, TI = 1 Hour

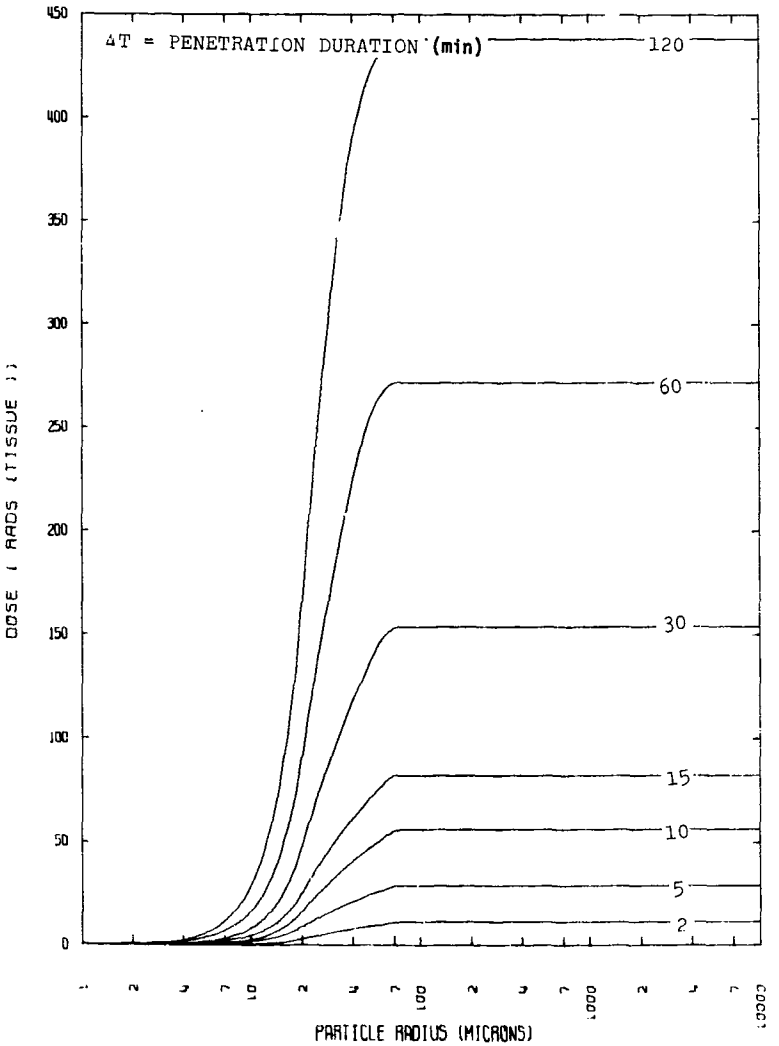

Figure D34. Cumulative Cockpit Dose at 30 Hours, TI = 1.5 Hours

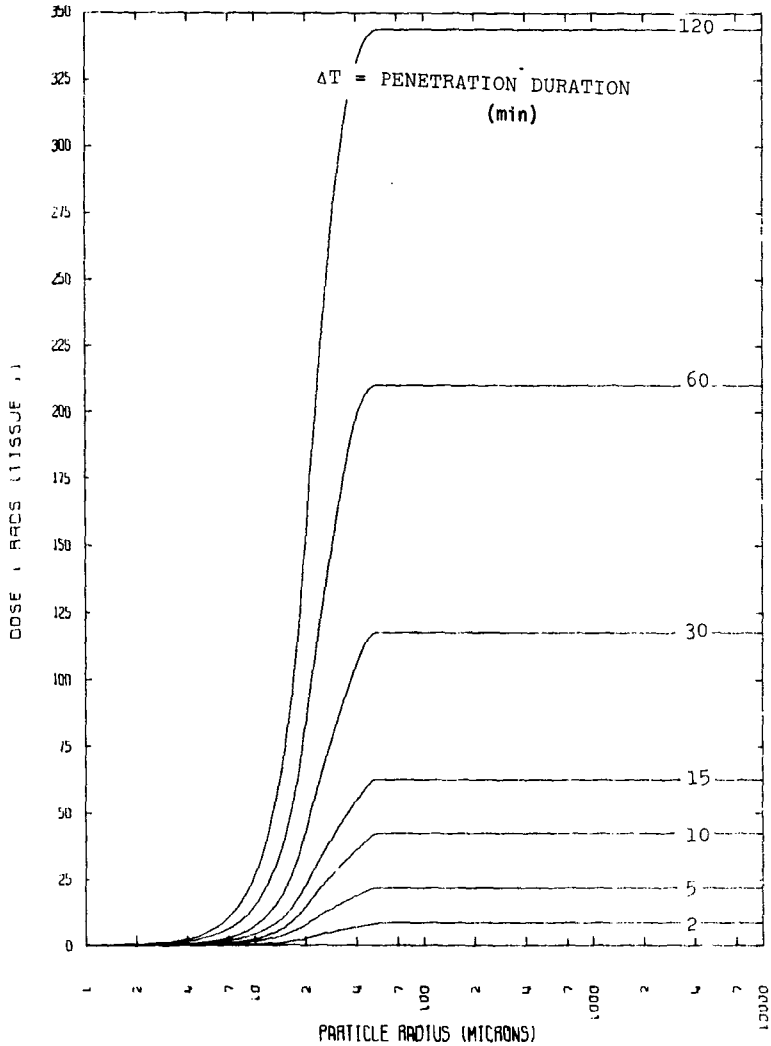

Figure D35. Cumulative Cockpit Dose at 30 Hours, TI = 2 Hours

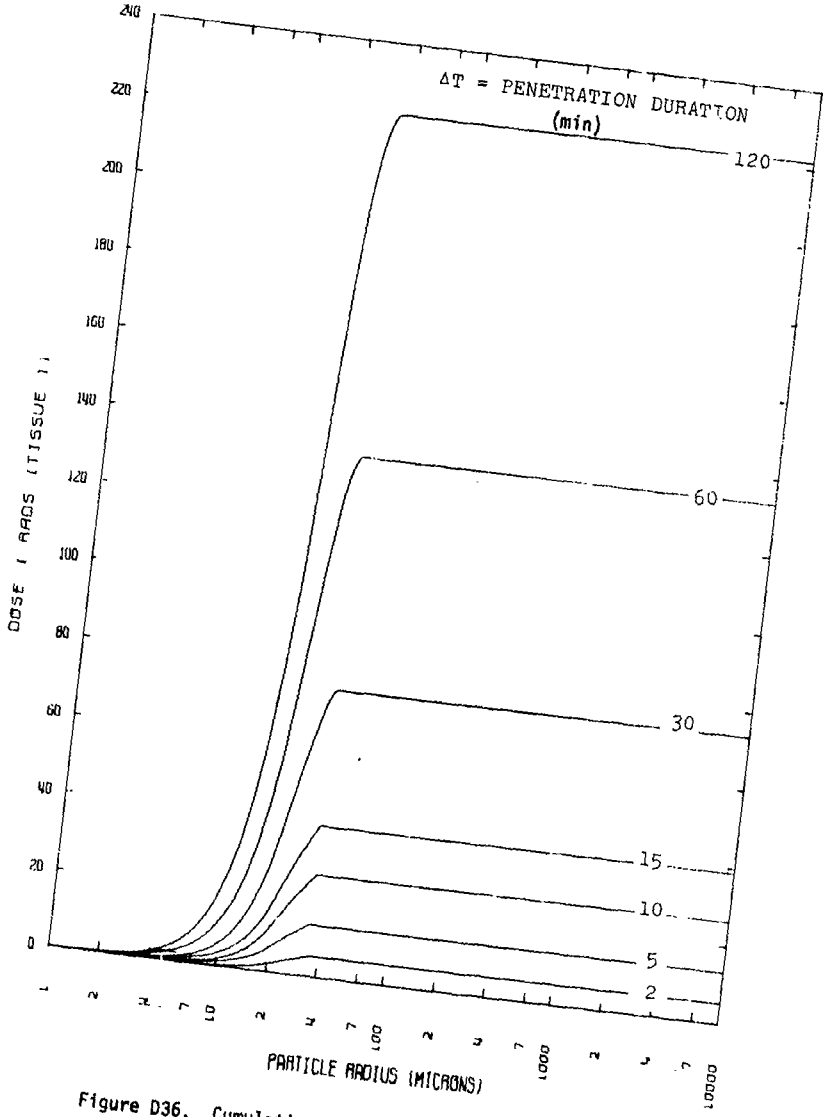

Figure D36. Cumulative Cockpit Dose at 30 Hours, TI = 3 Hours

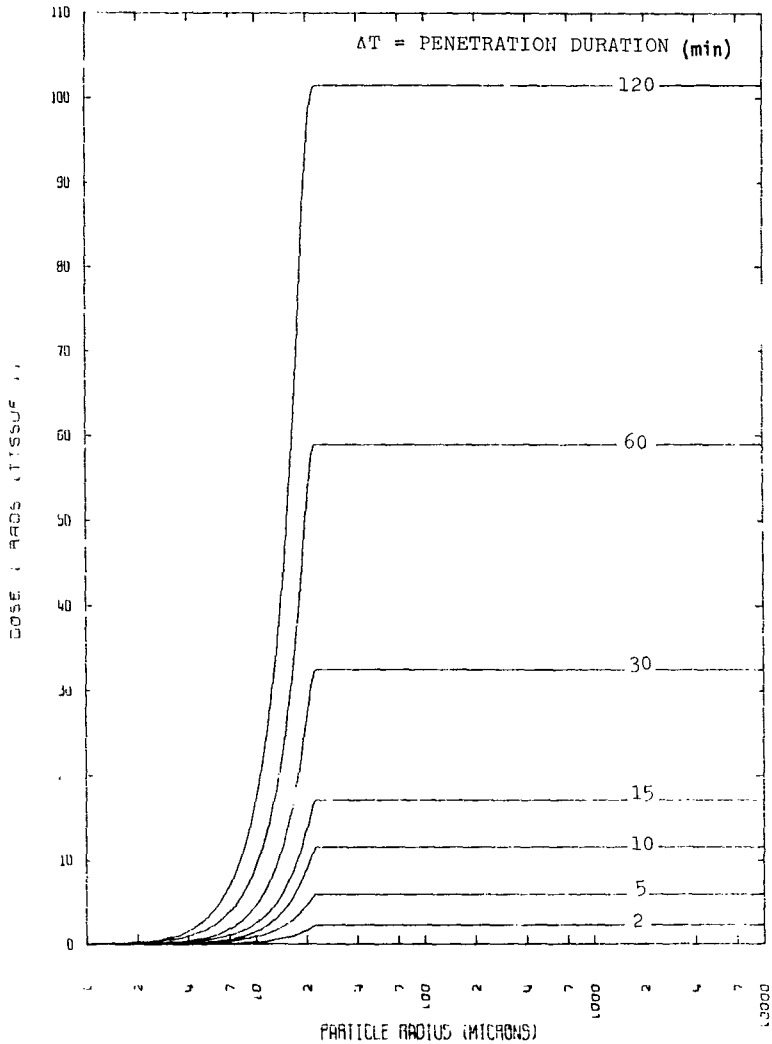

Figure D37. Cumulative Cockpit Dose at 30 Hours, TI = 5 Hours

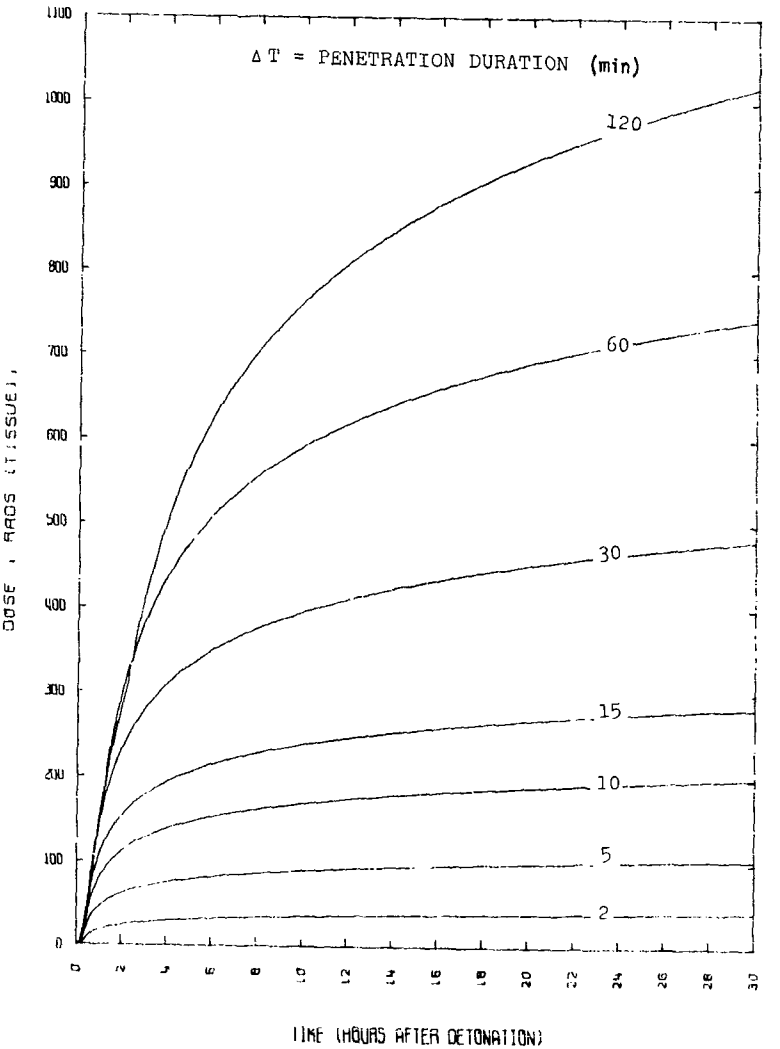

Figure D38. Cockpit Dust Dose,
TI = 10 Minutes

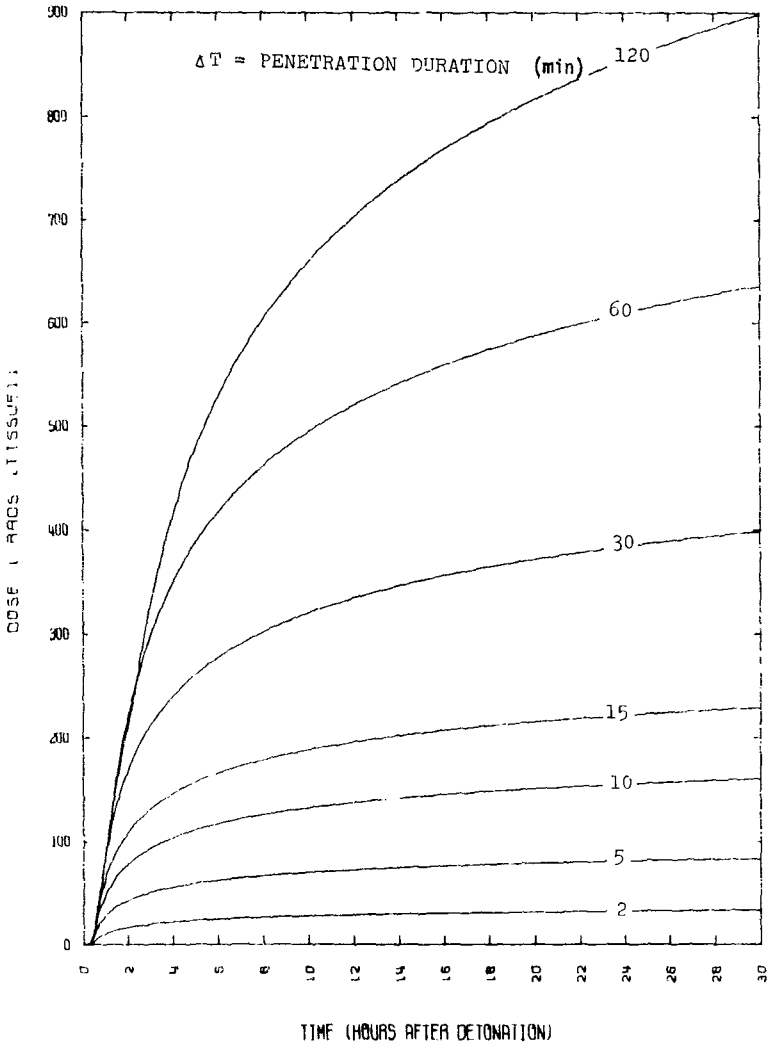

Figure D39. Cockpit Dust Dose,
TI = 18 Minutes

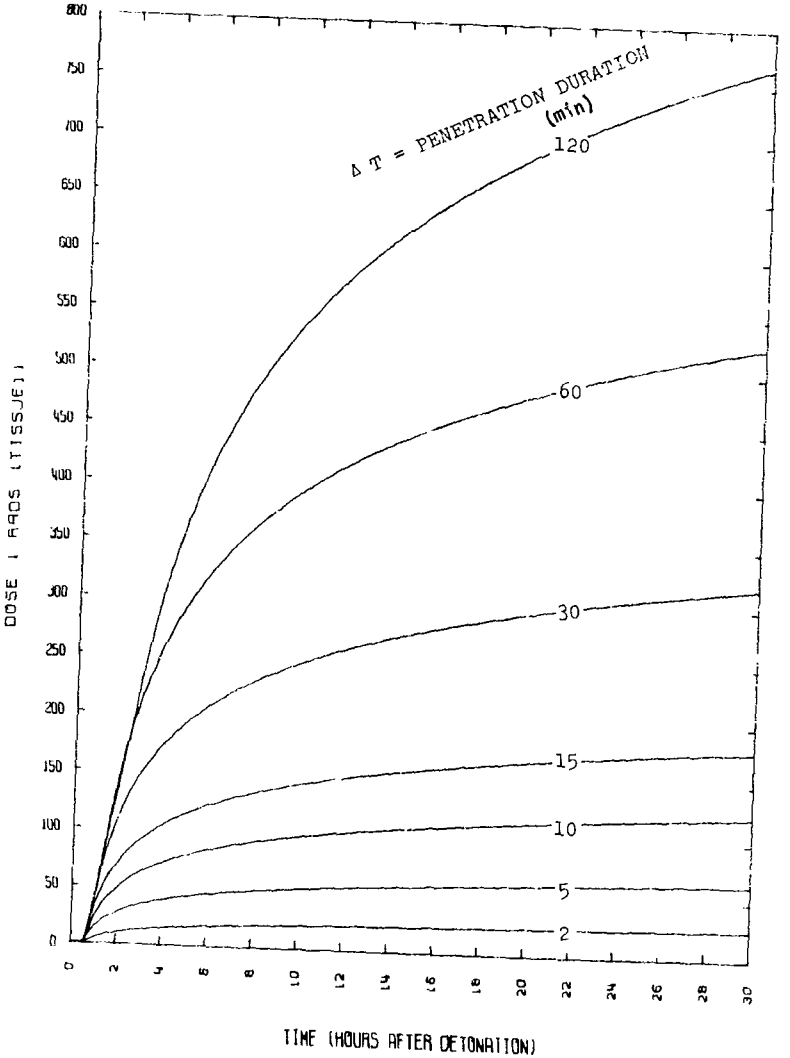

Figure D40. Cockpit Dust Dose,
TI = 30 Minutes

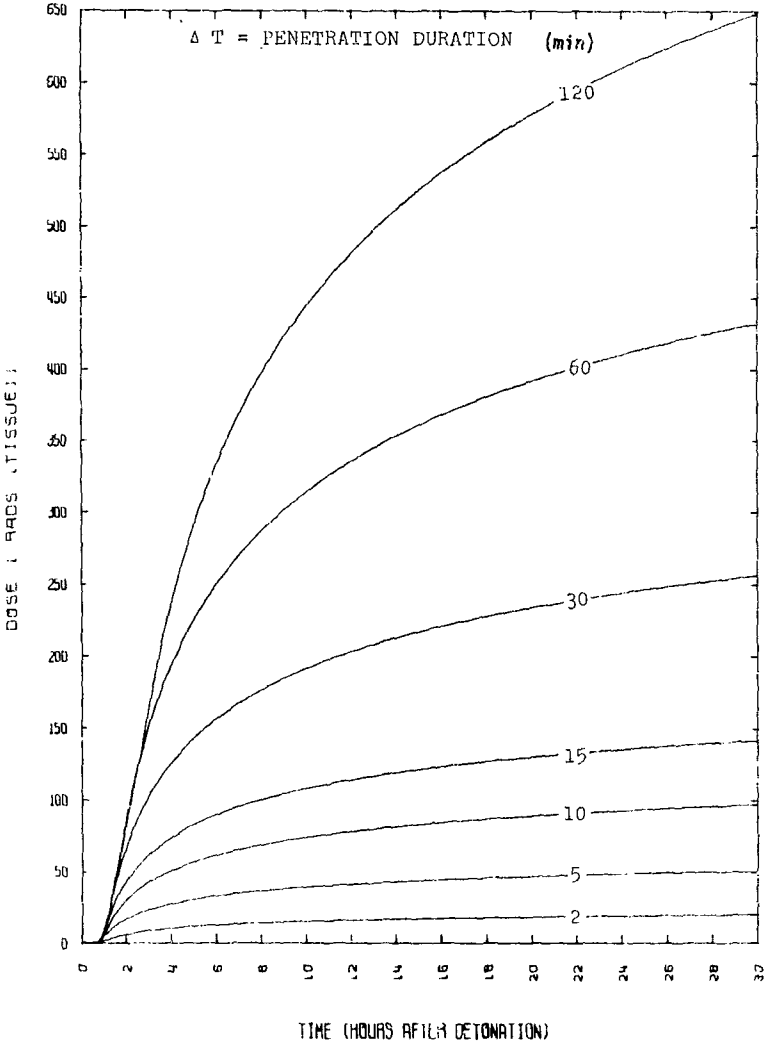

Figure D41. Cockpit Dust Dose,
TI = 45 Minutes

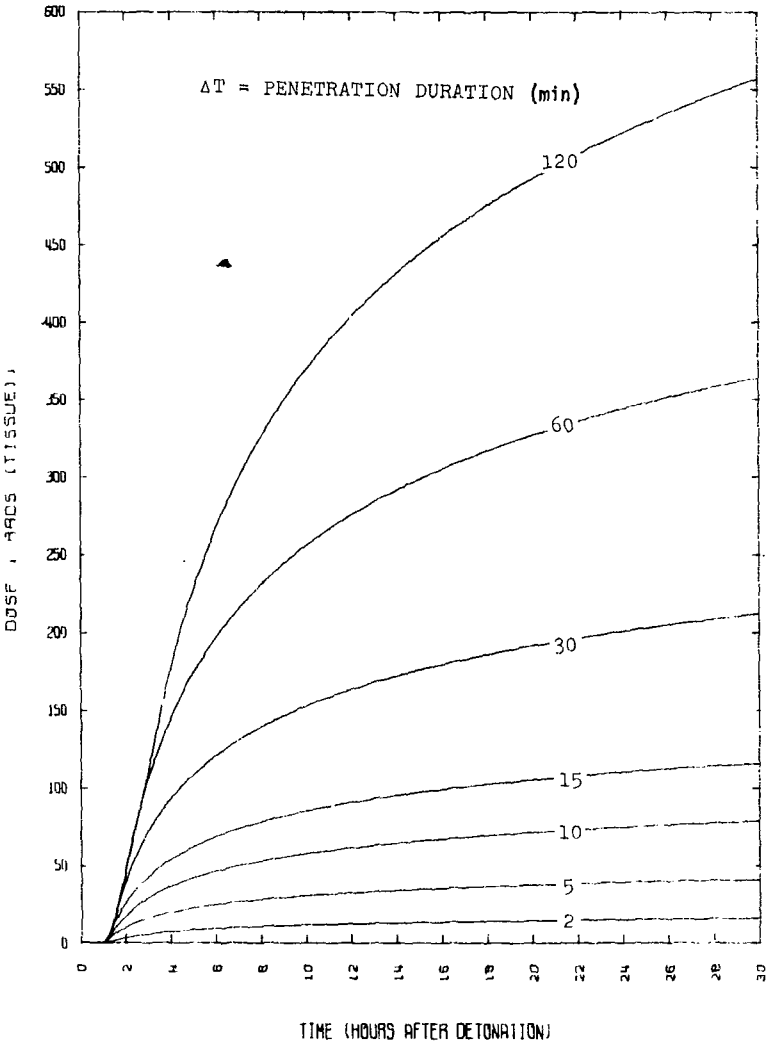

Figure D42. Cockpit Dust Dose, TI = 1 Hour

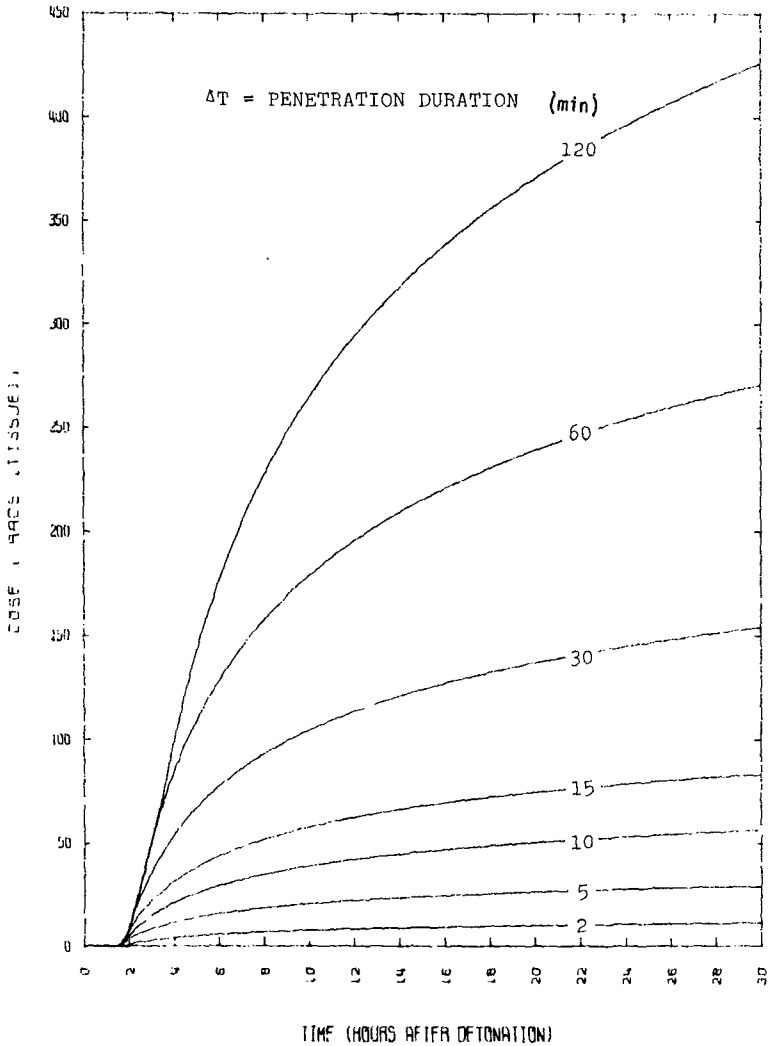

Figure D43. Cockpit Dust Dose,
TI = 1.5 Hours

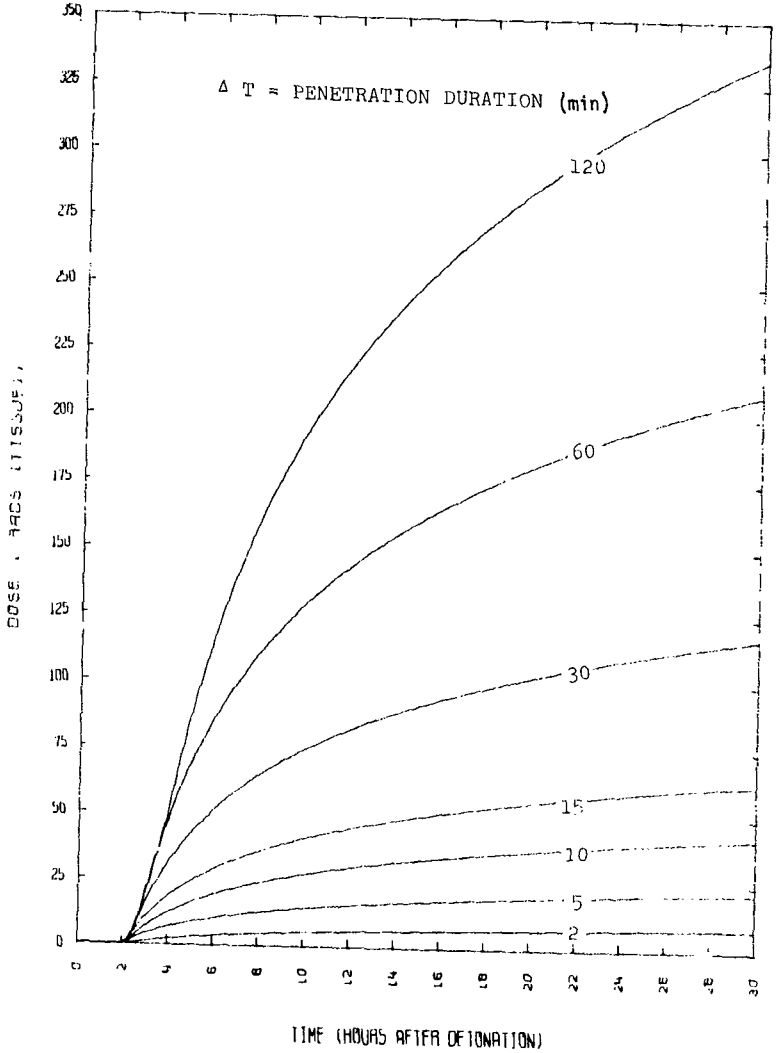

Figure D44. Cockpit Dust Dose,
TI = 2 Hours

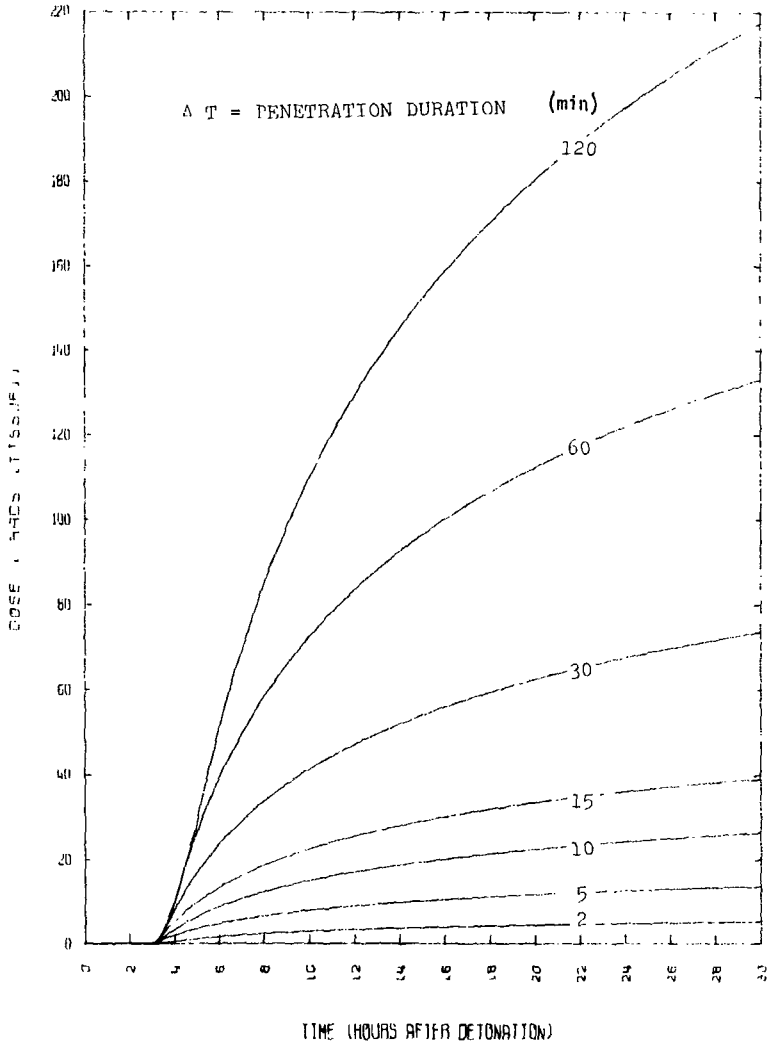

Figure D45. Cockpit Dust Dose,
TI - 3 Hours

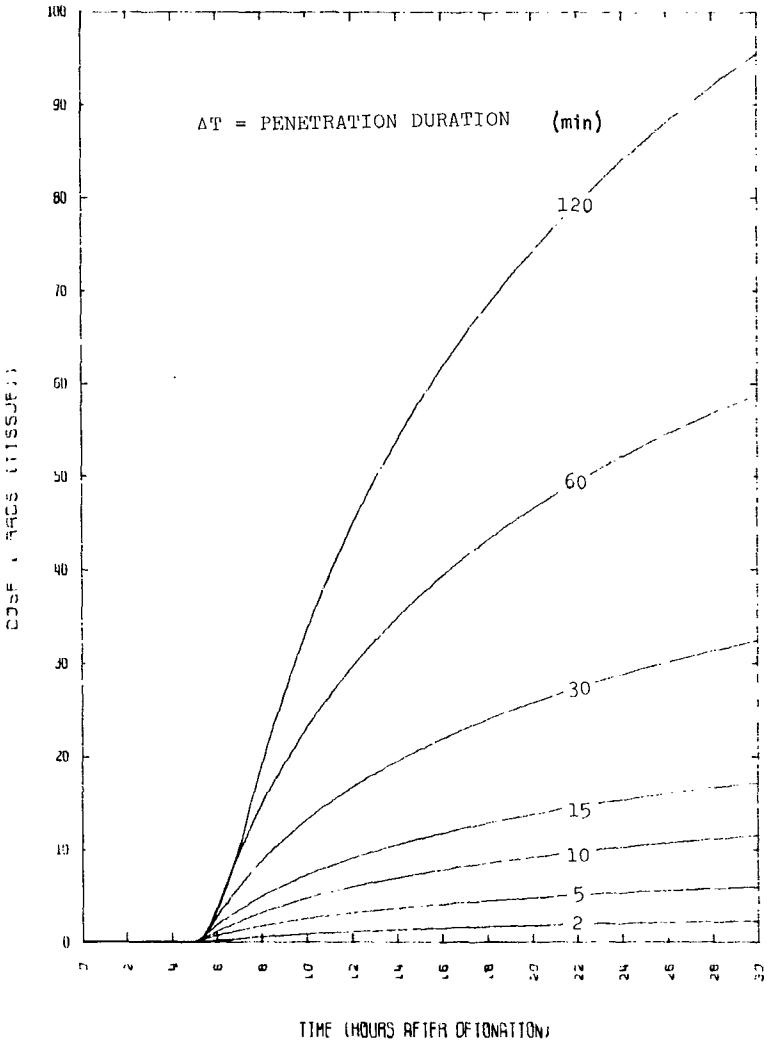

Figure D46. Cockpit Dust Dose,
TI = 5 Hours

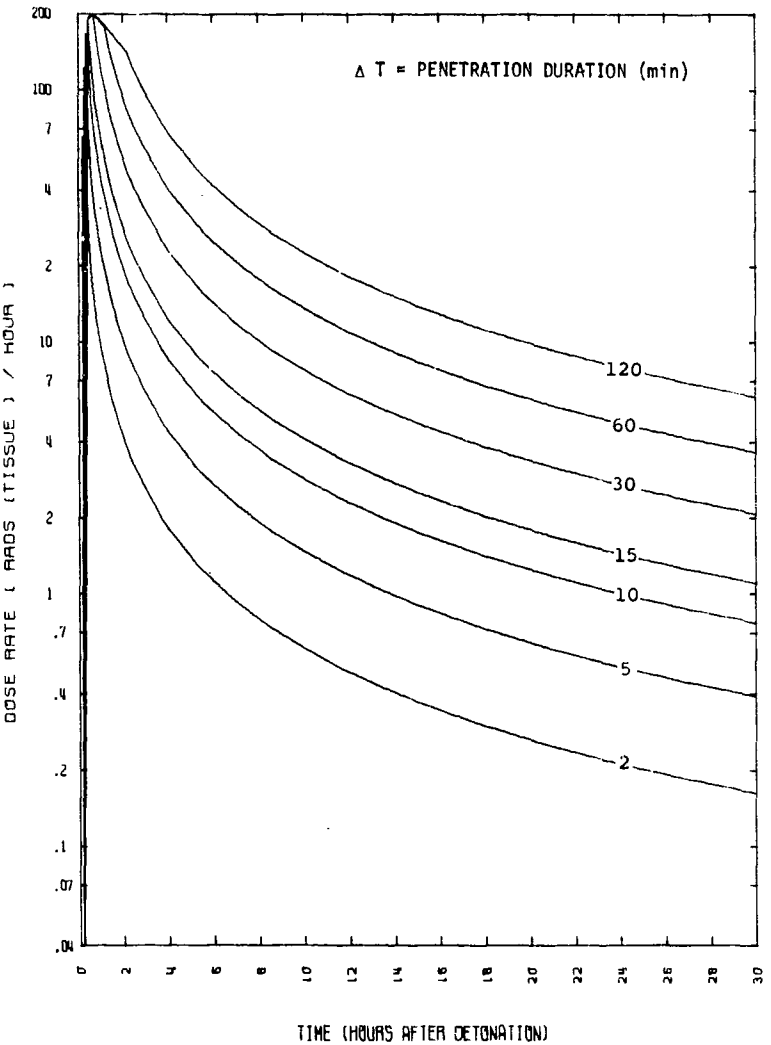

Figure D47. Cockpit Dust Dose Rate, TI = 10 Minutes

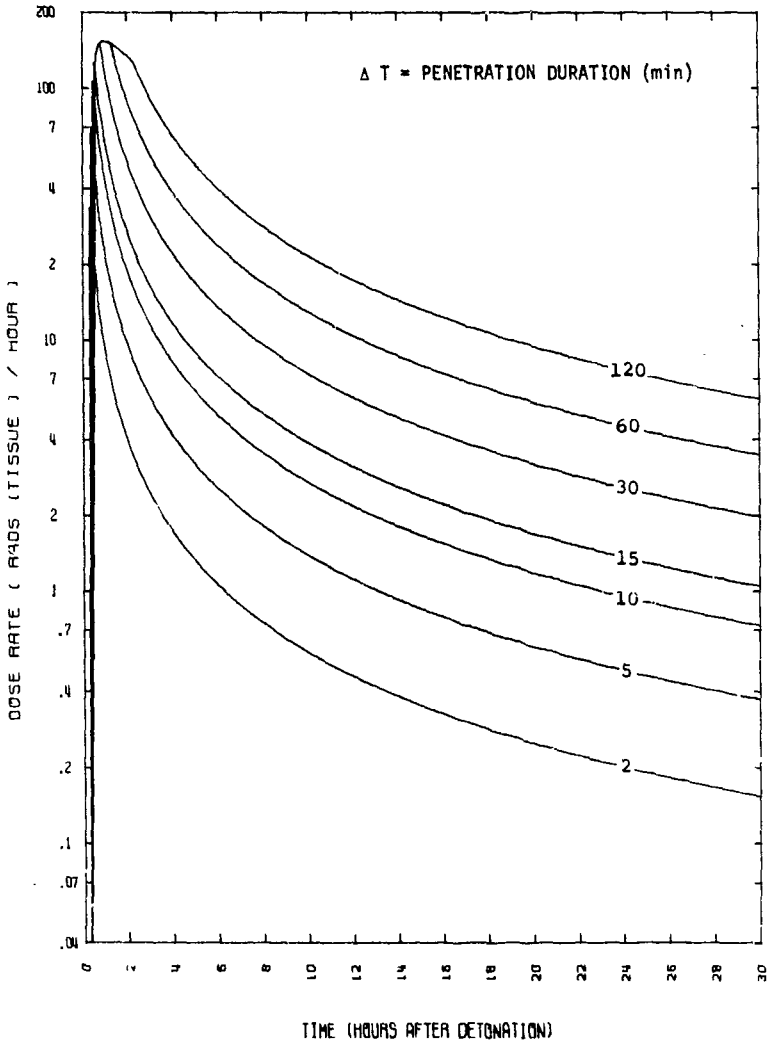

Figure D48. Cockpit Dust Dose Rate, TI = 18 Minutes

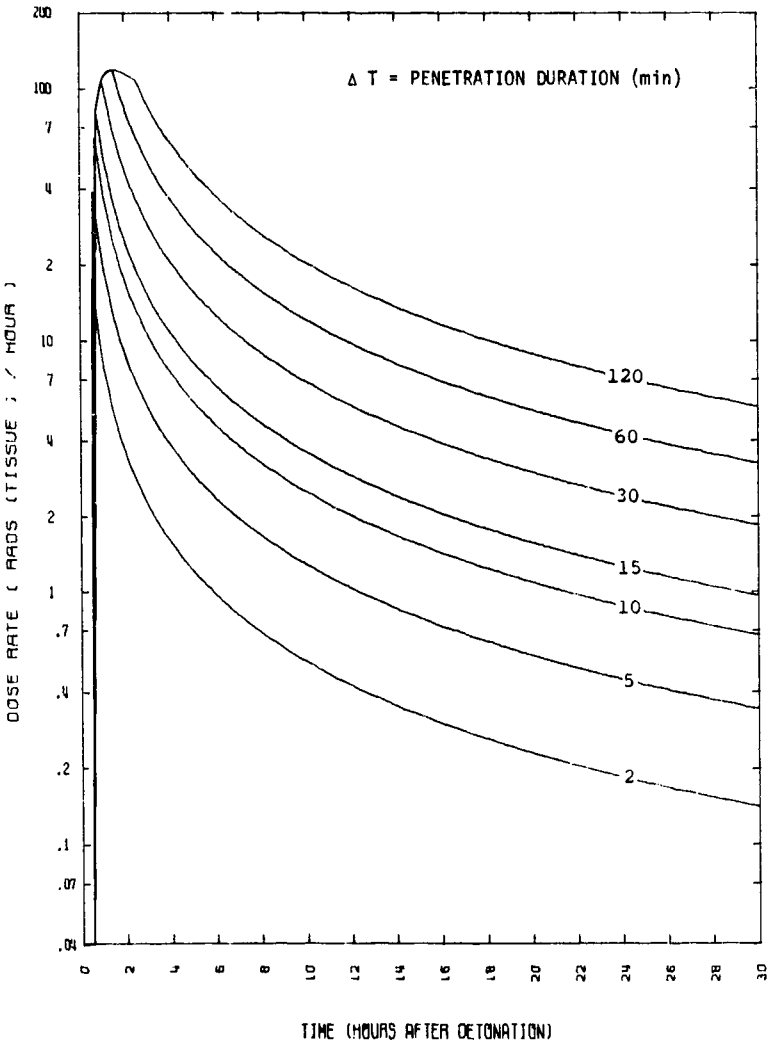

Figure D49. Cockpit Dust Dose Rate, TI = 30 Minutes

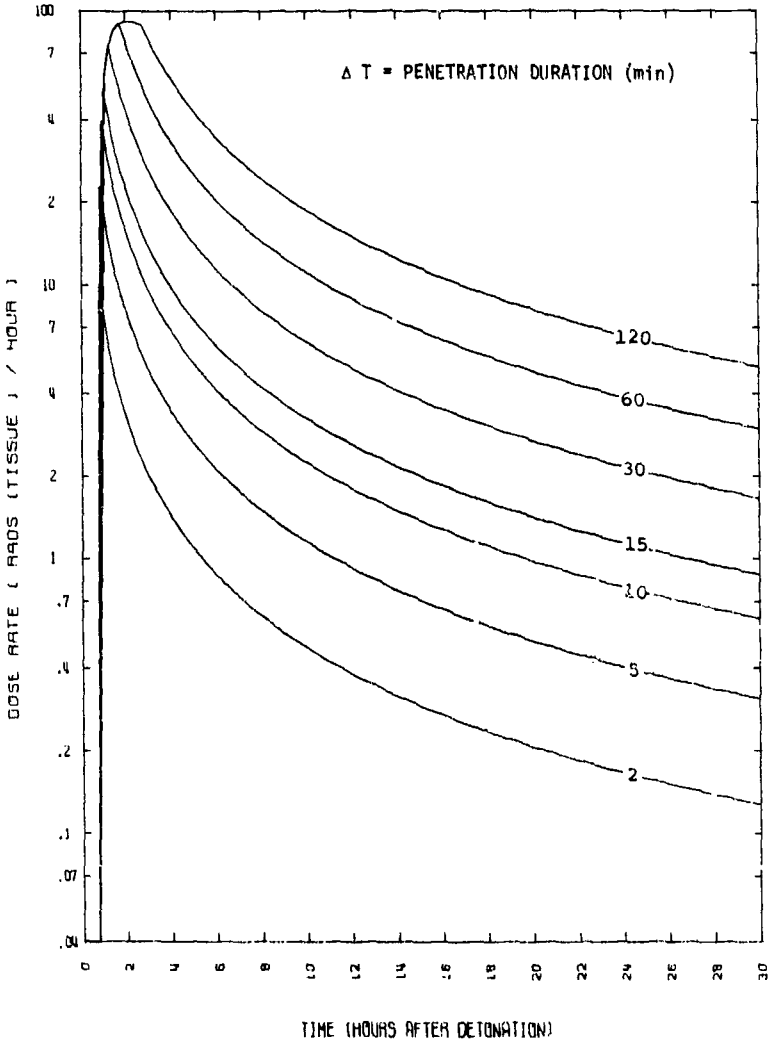

Figure D50. Cockpit Dust Dose Rate,
TI = 45 Minutes

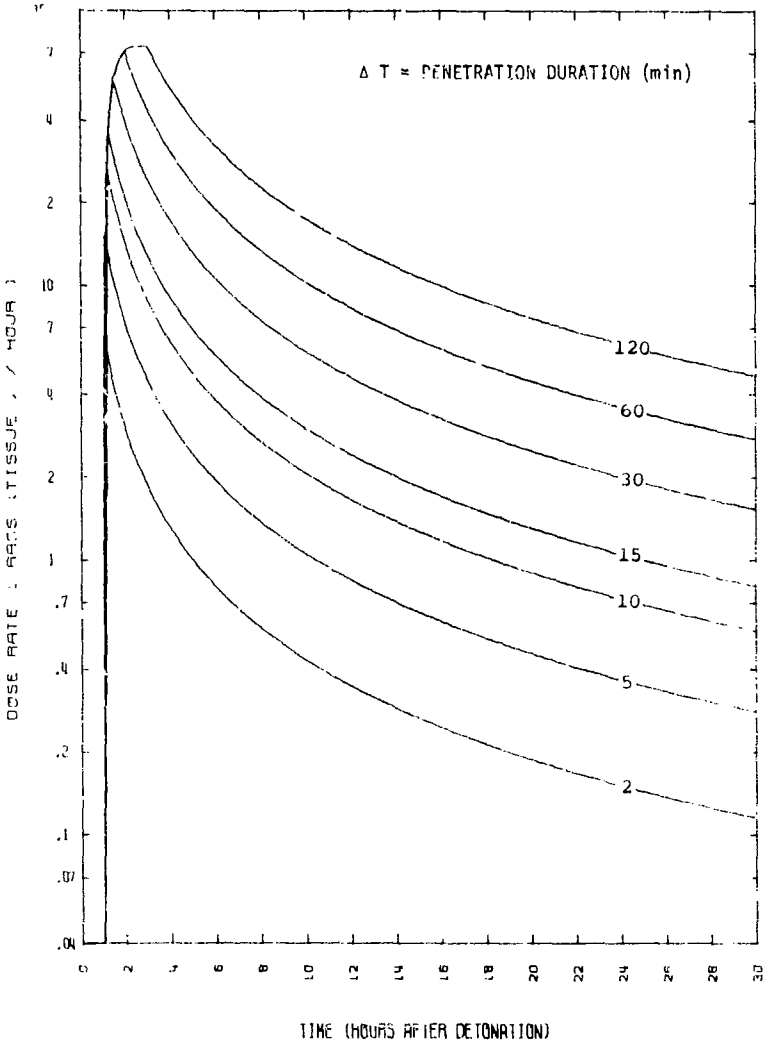

Figure D51. Cockpit Dust Dose Rate, TI = 1 Hour

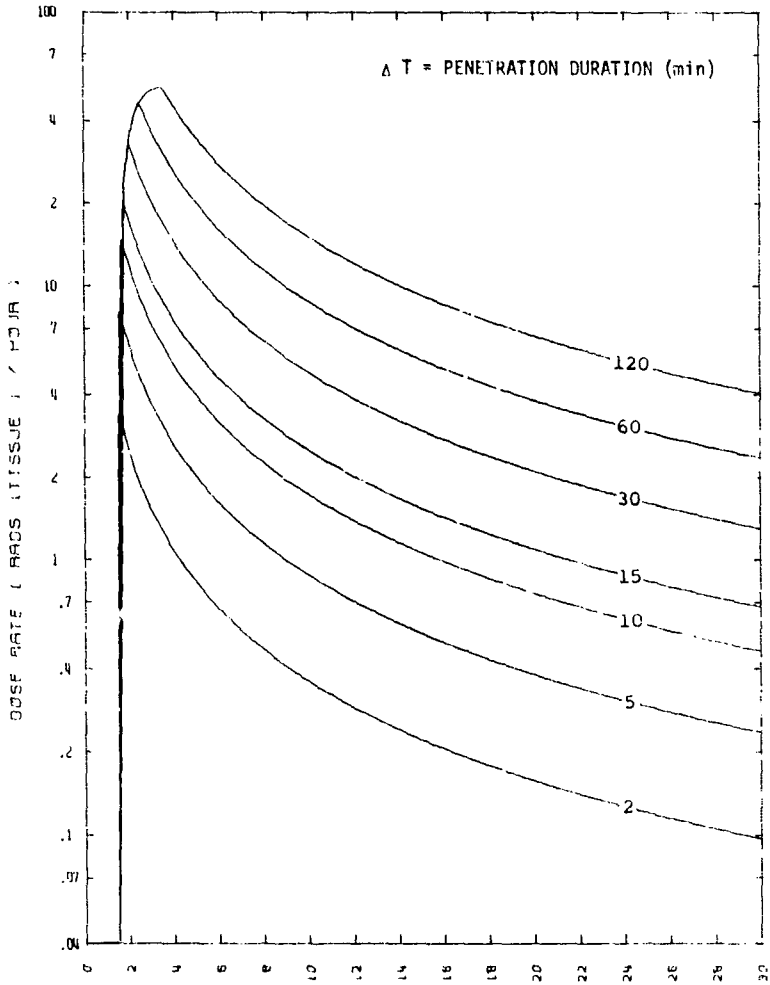

TIME (HOURS AFTER DETONATION)

Figure D52. Cockpit Dust Dose Rate, TI = 1.5 Hours

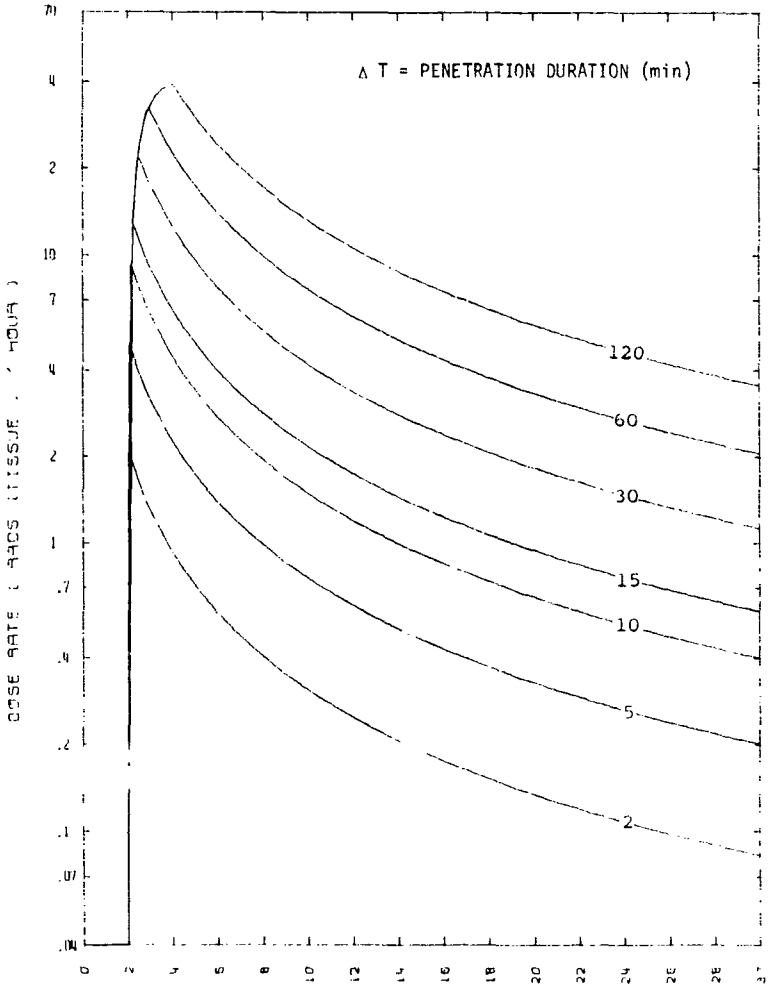

Figure D53. Cockpit Dust Dose Rate, TI = 2 Hours

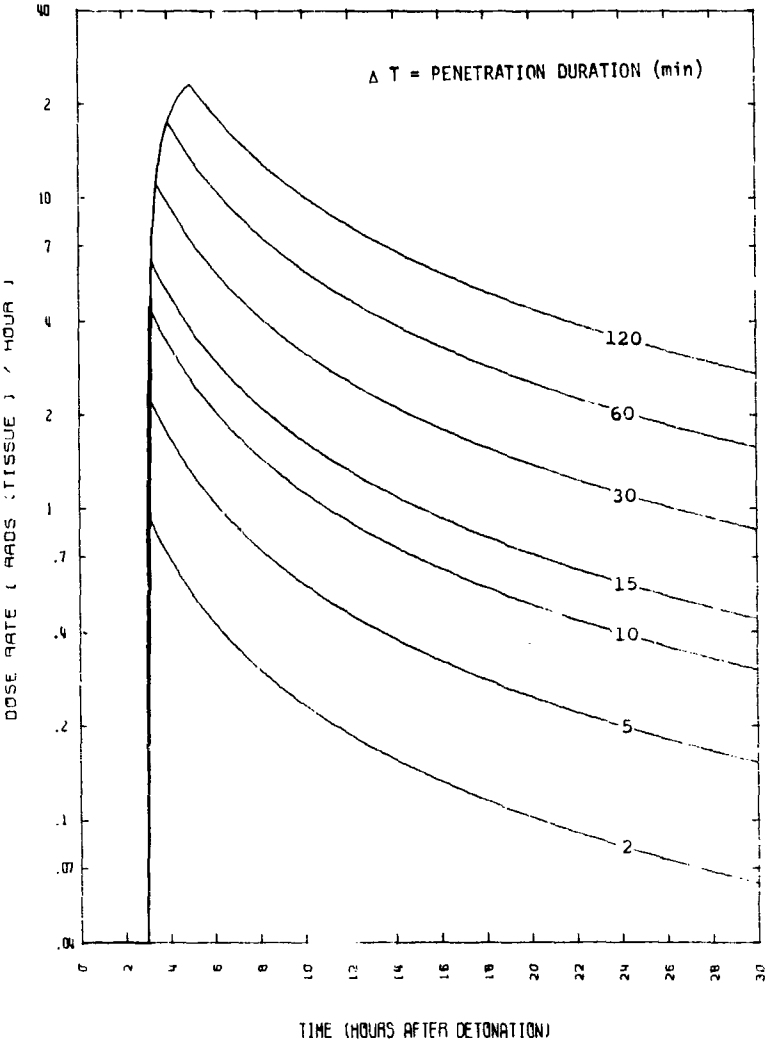

Figure D54. Cockpit Dust Dose Rate, TI = 3 Hours

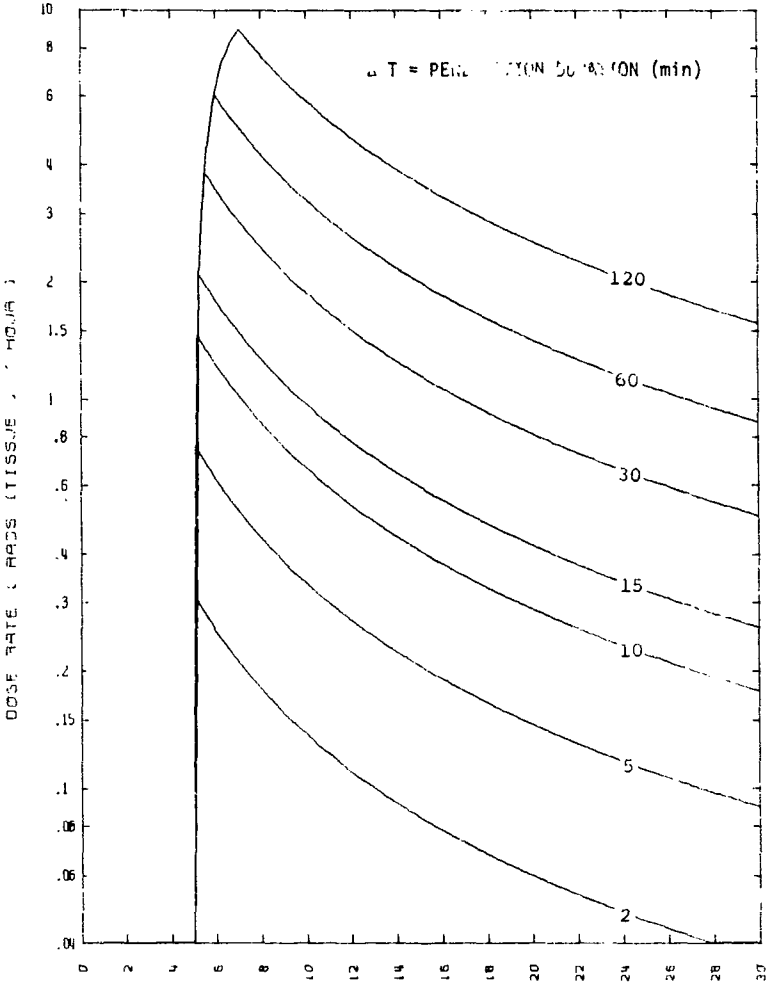

Figure D55. Cockpit Dust Dose Rate,
TI = 5 Hours

REFERENCES

1. Whitaker, W., Personal Communication.

2. Glasstone, Samuel, The Effects of Nuclear Weapons, US Atomic Energy Commission, February 1964.

3. Langham, W. H., ed., Radiobiological Factors in Manned Space Flight, Publication No. 1487, National Academy of Sciences, National Research Council, Washington, DC, pp. 8-84, 1967.

4. Patrick, R. P., Arnett, G. D., and Yingling, W. A., Cockpit Air Filtration Requirements of the B-1 in a Nuclear Dust Environment, AFWL-TR-73-83, Air Force Weapons Laboratory, Kirtland AFB, NM, July 1973.

5. Task Group on Lung Dynamics, "Deposition and Retention of the Human Respiratory Tract," Health Physics, V. 12, pp. 173-207, 1966.

6. Hobbs, C. H. et al., "Toxicity of Inhaled 90_Y Fused Clay in Beagle Dogs, III," Contained in reference 7, pp. 145-150.

7. Staff of the Fission Product Inhalation Program, Fission Product Inhalation Program Annual Report, 1970-1971, US Atomic Energy Commission, Division of Biology and Medicine, November 1971.

8. Radiological Health Handbook, PB 121784R, US Dept of Health, Education, and Welfare, Public Health Service, Bureau of State Services, Division of Radiological Health, Washington, DC, September 1960.

9. Lamb, Horrace, Hydrodynamics, 6th Edition, Dover Publications, New York, 1932.

10. Handbook on Aerosols, US Atomic Energy Commission, 1963.

11. Schlichting, Hermann, Boundary Layer Theory, McGraw-Hill, 1960.